UiT The Arctic University of Norway

Faculty of Health Sciences

Role of CALCOCO1 in scaling down endoplasmic reticulum and Golgi by autophagy

Thaddaeus Mutugi Nthiga

A dissertation for the degree of Philosophiae Doctor, November 2019

Role of CALCOCO1 in scaling down endoplasmic reticulum and Golgi by autophagy

By

Thaddaeus Mutugi Nthiga

A dissertation for the degree of Philosophiae Doctor

UiT The Arctic University of Norway

Faculty of Health Sciences

Department of Medical Biology

Molecular Cancer Research Group

November 2019

Everywhere nature works true to scale, and everything has its proper size accordingly

D'Arcy Thompson

Acknowledgements

The completion of my PhD journey would not have been achieved without the support and contributions by people to whom I wish to register my appreciation.

Foremost, I express my gratitude to the group leader Terje Johansen for according me the opportunity to be here. I greatly appreciate your support, patience, co-supervision and inputs. I appreciate the boundless freedom to explore without which the completion of this work would not have been realised.

I would like to thank my supervisor Trond Lamark for the help throughout the duration of this work. I am greatly indebted to your support, time and the many discussions. Your contribution during the preparation of the manuscripts is highly appreciated

I wish to acknowledge the co-supervision and the support by Eva Sjøttem. I gratefully regard your material contribution to this work.

I thankfully appreciate the technical assistance by Aud, Gry, Hanne, Jack, Kenneth and Toril. Thanks for your helping hands.

Many thanks to my colleagues in the lab. In no particular order, I acknowledge Birendra, Anthimi, Juncal, Mireia, Mads, Pradip, Yakubu, Nikoline, Katrine, Hallvard and Steingrim; it was pleasure working alongside you guys. Special thanks to Birendra for your timely microscopy imaging; it made all the difference.

Special regards to Gry and Hanne for picking me at the airport on my arrival in Tromsø. I am greatly indebted to your kindness and thanks for easing my arrival.

Lastly and importantly, I wish to recognize and appreciate the immense moral support from my family. Special thanks to my wife Kawira and our children Mukami and Munene. Thanks for your understanding.

Mutugi Nthiga

November 2019, Tromsø

Table of Contents

Abbreviations

ATG	AuTophaGy related
ARF4	ADP-ribosylation factor 4
ATF4	Cyclic AMP-dependent transcription factor ATF-4
ATF6	Cyclic AMP-dependent transcription factor ATF-6
ATL3	Atlastin-3
CALCOCO1	Calcium binding and coiled-coil domain-containing protein 1
CCPG1	Cell cycle progression protein 1
CHOP	C/EBP homologous protein
CREB3	Cyclic AMP-responsive element-binding protein 3
CRISPR	Clustered Regularly Interspaced Short Palindromic Repeats
ER	Endoplasmic reticulum
ERAD	ER-associated degradation
FFAT	two phenylalanines (FF) in an Acidic Tract
FAM134B	Family with Sequence Similarity 134, Member B
GADD34	Growth Arrest And DNA-Damage-Inducible 34
GM130	130 KDa Cis-Golgi Matrix Protein
GCP60	Golgi complex Associated Protein 1, 60kDa
HSP47	Heat Shock Protein, 47kDa
IRE1	Inositol-Requiring Enzyme 1
LDS	LIR-docking site
LIR	LC3-interaction region
MCs	membrane contact sites
NAP1	Nucleosome assembly protein 1

NDP52	Nuclear Dot Protein 52
ORP1L	Oxysterol Binding Protein-Like 1A
ORP3	Oxysterol Binding Protein (OSBP)-related protein 3
OSBP	Oxysterol Binding Protein
PERK	PKR-Like Endoplasmic Reticulum Kinase
RTN3	Reticulon 3
SINTBAD	similar to NAP1 TBK1 adaptor
SQSTM1	Sequestosome 1
STARD11	StAR-Related Lipid Transfer Protein 11
TAX1BP1	Tax1 Binding Protein 1
TBK1	TANK Binding Kinase 1
TEX264	Testis-Expressed Protein 264
TFE3	Transcription Factor E3
WIPI	WD-repeat protein interacting with phosphoinositides
XBP1	X-Box Binding Protein 1
zDABM	zDHHC AR-binding motif
DHHC13	Zinc Finger DHHC-Type Containing 13
ZDHHC17	Zinc Finger DHHC-Type Containing 17
UIR	UIM-interacting region
ULK1/2	Unc-51-Like Kinase
UDS	UIM docking site
UPR	unfolded protein response
VAPA	VAMP Associated Protein A
VAPB	VAMP Associated Protein B

List of papers

Paper I

Thaddaeus Mutugi Nthiga, Birendra Kumar Shrestha, Eva Sjøttem, Jack-Ansgar Bruun, Kenneth Bowitz Larsen, Trond Lamark and Terje Johansen

CALCOCO1 acts with VAMP-Associated proteins to mediate ER-phagy. *The EMBO Journal.* In revision

Paper II

Thaddaeus Mutugi Nthiga, Birendra Kumar Shrestha, Jack-Ansgar Bruun, Kenneth Bowitz Larsen, Terje Johansen and Trond Lamark

Regulation of Golgi turnover by CALCOCO1-mediated selective autophagy. *Manuscript*

Summary

Endoplasmic reticulum (ER) and Golgi apparatus are key organelles in the synthesis, modification and trafficking of proteins in eukaryotic cells. In response to stress stimuli such as nutrients deprivation, accumulation of misfolded proteins or exposure to chemicals, the ER increases in size through increased synthesis of its components to counteract the stress. Similarly, Golgi response to stress increases synthesis of its components to augment its functions. The excess ER components are scaled down by ER-phagy to restore the physiological size. ER-phagy is a form of autophagy that targets specific portions of the ER for degradation in the lysosome. The degradation is mediated by adaptor molecules called ER-phagy receptors, which connect the ER to the autophagy machinery. Previous studies have identified different ER-phagy receptors. The involvement of autophagy in the degradation of Golgi however, has not been demonstrated.

This thesis present detailed studies of CALCOCO1, and show that it is an autophagy receptor for the degradation of the ER and Golgi apparatus. In the first paper, it is shown that CALCOCO1 is homomeric and that a proportion of the protein localizes in the Golgi apparatus. Functional studies revealed CALCOCO1 is a soluble ER-phagy receptor for the degradation of tubular ER in response to proteotoxic- and starvation-induced stress. On the ER membrane, CALCOCO1 interacts with VAMP-associated proteins VAPA and VAPB via an evolutionary conserved FFAT-like motif and recruits autophagy machinery by binding directly to ATG8 proteins via LIR and UDS interacting region (UIR) motifs acting co-dependently. Depletion of CALCOCO1 caused expansion of the ER and inefficient basal autophagy.

In the second paper, involvement of autophagy in the degradation of Golgi apparatus is, for the first time, demonstrated and CALCOCO1 is revealed to be the selective autophagy receptor for the degradation in response to nutrients deprivation. CALCOCO1 interaction with Golgi membrane occurs by binding to the cytoplasmic Ankyrin repeats (AR) domains of membrane-bound Golgi-resident palmitoyltransferases ZDHHC17 and ZDHHC13 via an evolutionary conserved zDHHC-AR-binding motif (zDABM) located at the C-terminal half of the protein. The zDABM motif was also identified and validated in the C-terminal region of the CALCOCO1 paralog, TAX1BP1. Inhibition of autophagy or depletion of CALCOCO1 caused expansion of the Golgi and accumulation of its structural and transmembrane proteins.

1. Introduction

Maintenance of organellar quality and quantity is crucial for cellular health, function and adaptation to environmental conditions. The amount and size of each organelle in a eukaryotic cell is appropriately regulated based on the size of the cell and physiological demands. As the cell grows, the functional needs for organelles increases, so, the organelles grow as well in order to meet the increased requirements for their functions. When a cell divide into two for instance, the amount of each organelle is doubled so as to keep the amounts in daughter cells constant (Rafelski and Marshall, 2008).

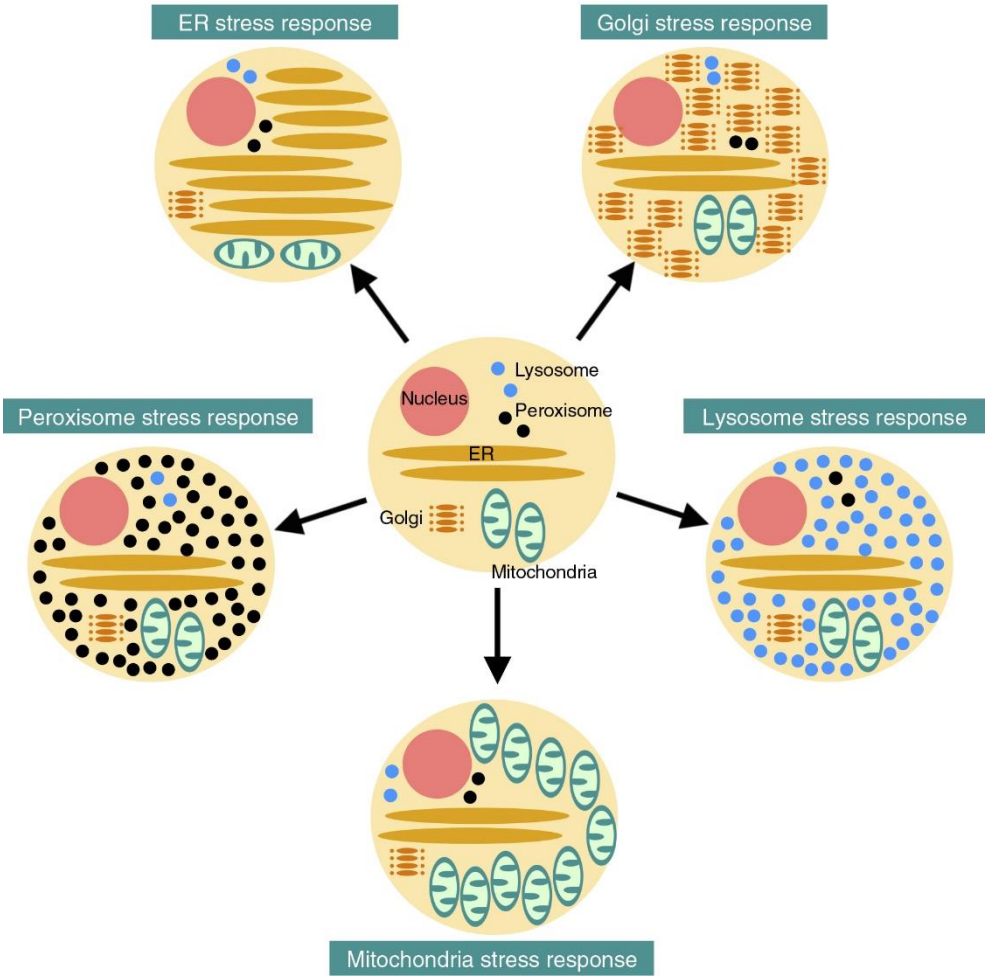

Figure 1. Regulation of organelles. Organelle response pathways regulate the capacity of each organelle (ER, Golgi, lysosome, mitochondria, peroxisome, and nucleus) in accordance with cellular cellular physiological requirements. Figure is adapted with permission from (Taniguchi and Yoshida, 2017).

Similarly, when the function of a specific organelle is insufficient in the cell, hence causing stress, the amount of the organelle is scaled up to increase the capacity of the organelle to perform the functions for which it is responsible. For instance, when the function of the ER becomes insufficient during toxic insults, pathogen attacks or proteins and lipid demands, the ER becomes increased in size through an upregulated synthesis of its components by a mechanism called the ER stress response or unfolded protein response (UPR), a signalling pathway that monitors proper ER function (Karagöz et al., 2019, Nunnari and Walter, 1996, Rafelski and Marshall, 2008) (Figure 1). Likewise, the Golgi stress response increases the amount of the Golgi by upregulating the synthesis of Golgi structural proteins (Oku et al., 2011, Taniguchi and Yoshida, 2017). Thus, the scaling up of organelles in eukaryotic cells requires regulated synthesis of new components.

Conversely, exceeding the threshold amounts of specific organelles or upon resolution of the stress and stress response, the cell triggers destruction mechanisms for scaling down the amount of organelles to their pre-stress state. This generally involves dismantling, removal and degradation of the damaged organelles or the excess components generated during the stress response phase (Anding and Baehrecke, 2017, Bernales et al., 2006, Okamoto, 2014). The organelles therefore are in a constant dynamic state of expansion and reduction as dictated by physiological demands and autoregulation mechanisms. Emerging evidence from studies in recent years has demonstrated that autophagy scales down the amount of organelles through selective targeting of excess organelles and organelle components for degradation.

The autophagy pathways selective for organelles, collectively called organellophagy, are classified depending on the organelle being targeted. Thus, mitophagy, lysophagy, pexophagy, nucleophagy, ER-phagy and ribophagy refers to autophagy pathways for the degradation of the mitochondria, lysosome, peroxisome, nucleus, ER and ribosomes respectively (Kirkin and Rogov, 2019, Okamoto, 2014, Zaffagnini and Martens, 2016, Anding and Baehrecke, 2017). This places autophagy as a major factor in the maintenance of organellar homeostasis and cellular adaptation to varying environmental cues and stresses. In fact, defects in several organellophagy pathways are associated with several human disorders, including neurodegeneration, obesity, atherosclerosis and cancer, underscoring the physiological significance of organellophagy in health and disease (Mizushima and Komatsu, 2011).

The degradation of organelles by organellophagy requires an initiating signal to trigger the process and specific molecules that connect the organelle or parts of the organelle to the autophagy machinery for degradation. These molecules are called autophagy receptors and they perform their function either by recognizing specific labels on organelles or by being part of the targeted organelle. Previous studies have identified different receptors for the degradation of the ER (Wilkinson, 2019c). The involvement of autophagy in the degradation of Golgi however, has not been demonstrated. This thesis present detailed studies of CALCOCO1, an hitherto poorly characterized protein, and show that it is an autophagy receptor for the degradation of the ER and Golgi apparatus when the initiating signal is nutrients deprivation. The studies are presented as manuscripts. To frame the studies in context, the insights into the ER, the Golgi, and autophagy are reviewed below.

2. Structure and Function of endoplasmic reticulum

The endoplasmic reticulum is the largest membrane-bound organelle in eukaryotic cells and forms a continuous, membranous compartment that extends from the nuclear envelope to the outer periphery of cells. The term endoplasmic reticulum (ER) was coined by Keith Porter and Frances Kallman in 1952 to describe the observation of preferential concentration of reticular vesicular elements in the perinuclear region of the cytoplasm, known as endoplasm, and their absence in the exoplasmic periphery of the cytoplasm (Palade, 1956, Porter and Kallman, 1952). Functionally, the ER plays critical roles in diverse processes in metabolism, signalling and intracellular organization. The ER serves many functions including:

a) Synthesis, folding, modification and transport of proteins
b) Synthesis and distribution of phospholipids and steroids and
c) Storage of calcium ions within its lumen and their regulated release into the cytoplasm (Chen et al., 2013, Schröder, 2008, Schwarz and Blower, 2016, Voeltz et al., 2002)

Broadly, the ER consists of two domains: the nuclear envelope (NE) and a cytoplasmic peripheral ER made up of sac-like sheets and polygonal array of tubules (Chen et al., 2013). The two domains form a contiguous membrane network with a common luminal space. The NE encloses the nucleus and consists of a double membrane enclosing a lumen, with the two membranes connected only at the nuclear pores. The NE controls the flow of information from the cytoplasm to the nucleus and acts as a scaffold for chromatin organization.

The distribution of ER sheets and tubules of the peripheral ER is tightly regulated and can vary substantially in different cell types or in response to growth cues and conditions. Some cells therefore exhibit special ER arrangements. In mammalian cells, the peripheral ER extends from the NE to the entire cell. In yeast and plant cells however, it is located beneath the plasma membrane, the cortex region, only linked by a few tubules to the NE. Muscle cells contain a mainly tubular ER called sarcoplasmic reticulum (SR), specialized for calcium storage for myofibre contractions (Voeltz et al., 2006).

Ultrastructurally, the peripheral ER is divided into two interconnected compartments, namely, the rough endoplasmic reticulum (RER) and the smooth endoplasmic reticulum (SER). The RER is sheet-like in morphology and is characterised by the presence of ribosomes associated with the biosynthesis of membrane and secretory proteins. The SER is devoid of ribosomes and is more tubular in structure with greater numbers of branch points (Chen et al., 2013, English et al., 2009). The SER is involved in the generation of steroid hormones, detoxification of xenobiotics, protein transport and carbohydrate metabolism. The RER and SER are present in different proportions in different cell lineages depending on the functional specialization. Cells that secrete large amounts of proteins are rich in RER while steroid-producing cells have rich composition of SER. Thus, the ER of digestive enzyme-secreting exocrine cells such as pancreatic acinar cells, is predominantly RER. Conversely, the ER of steroid hormones producing cells in the adrenal cortex and endocrine glands or xenobiotics metabolising cells in the liver is predominantly SER. In cells, the RER and SER do not usually occupy spatially segregated regions. However, in some cell types, such as hepatocytes and neurons, the RER and the SER occupy different cellular areas (Borgese et al., 2006, Wilkinson, 2019a).

The morphology of the peripheral ER is dynamic depending on the physiological conditions. Distinct proteins maintain the shape and structure of the ER sheets and tubules. Reticulon (RTN) and REEP protein families promote the membrane curvature of ER tubules via scaffolding and hydrophobic wedging and their depletion leads to loss of tubules. Members of both families are ubiquitously expressed in eukaryotic cells and are enriched in the ER tubules and the curved edges of the ER sheets (Chen et al., 2013, Shibata et al., 2010). Members of the atlastin (ATL) family of dynamin-related guanosine triphosphatases (GTPases) are thought to mediate the formation of tubular three-way junctions, giving rise to the characteristic polygonal tubular network (Goyal and Blackstone, 2013). An alternative complement of proteins regulate the structure of ER sheets, with p180, kinectin and CLIMP63

being proposed to play a role in shaping and luminal spacing. Mutations in ER-shaping proteins are associated with neurologic disorders such as hereditary spastic paraplegias and amyotrophic lateral sclerosis (Goyal and Blackstone, 2013, Chen et al., 2013).

2.1 ER connects to other organelles at membrane contact sites

The peripheral ER network of sheets and tubules extends throughout the cytoplasm making contacts with most of the organelles, including the Golgi, plasma membrane, mitochondria, endosomes, autophagosomes, lipid droplets and peroxisomes with its cytoplasmic surface at membrane contact sites (MCs). Many ER peripheral membrane proteins are also localized on its cytoplasmic surface. The membrane contact sites facilitate non-vesicular communication between organelles and their formation is dynamic, depending on the functional demands of the contacts, which may include calcium exchange, organelle movement, fission and morphological rearrangement (Zhang and Hu, 2016). The formation of MCs generally requires either protein-protein or protein-lipid interactions between proteins on the cytoplasmic surface of the ER and those anchored on other organelles. Below, the insights into VAMP-associated proteins (VAPs), which are involved in many contacts between the ER and other organelles, are outlined.

2.2 VAPs connect ER to other organelles

Most of the described molecular bridges (MCs) between the ER and other organelles involve VAMP-associated proteins (VAPs) on the ER, type II integral ER membrane proteins conserved in all eukaryotes. In vertebrates, there are two VAPs, VAPA and VAPB. The two VAPs share high sequence identity and similar domain organization consisting of a cytosolic N-terminal major sperm protein (MSP) domain, a central coiled-coil domain and a C-terminal transmembrane domain containing a dimerization motif. VAPs interact with proteins bearing a short motif named FFAT (two phenylalanines in an acidic tract) using their MSP domain. So far, it is the only known mechanism by which peripheral proteins are recruited to the cytoplasmic surface of the ER (Murphy and Levine, 2016). Recently however, a novel FFAT-binding ER membrane protein, motile sperm domain-containing protein-2 (MOSPD2), was found to interact with many VAP-binding proteins, implying that it also recruits peripheral proteins to the ER surface (Di Mattia et al., 2018).

The core amino acid sequence of the FFAT motif is EFFDAxE, where x is any amino acid. The core sequence is supplemented by flanking regions, especially upstream, of mostly acidic residues (Loewen et al., 2003a). The binding of the FFAT motif to the MSP domain is initiated by the acidic tract and then cemented by the core motif (Furuita et al., 2010). FFAT motifs are found in a wide variety of proteins localized mostly at MCs where they anchor other organelles to the ER via interaction with VAPs. MCs are built by VAPs interacting either with other membrane-anchored proteins such as STARD3 and STARD3NL or with soluble proteins that can also bind to other organelles such as STARD11, PTPIP51, OSBP, ORP1L and ORP3. MCs formed by VAPs and their interacting proteins are involved in diverse biological functions including calcium trafficking, lipid transport, endosome dynamics, cytoskeletal organization, peroxisome growth and autophagy (Murphy and Levine, 2016).

Two recent reports have demonstrated the role of VAPs in promoting autophagy by augmenting endosomal pathway and autophagosome biogenesis. The first report demonstrated that VAPs interact with FIP200 and ULK1 through their FFAT motifs to stabilize the ULK1/FIP200 complex and with WIP12 to enhance the tethering of the isolation membrane (IM) to the ER. These interactions therefore modulate the formation of autophagosomes (Zhao et al., 2018). The MCs formed by the VAPs between the ER and the Golgi mediate the transfer of phosphatidylinositol-4-phosphate (PtdIns4P) from the Golgi to the ER. The second report demonstrated that failure to tether the ER to the Golgi when VAPs are lost led to an increase in Golgi PtdIns4P levels and an expansion of endosomal pool derived from the Golgi. Fusion of these endosomes with lysosomes led to an increase in lysosomes with aberrant acidity, contents and shape, leading to a defective autophagolysosomal degradation (Mao et al., 2019).

2.3 Misfolded proteins cause ER stress

One of the main functions of the ER is synthesis of proteins for the secretory pathway. To gain activity and traffic to their final destinations, the proteins are folded by ER chaperones to acquire the appropriate conformations. The folding in the ER is also guided by posttranslational modifications including N-glycosylation, disulphide bonds formation and lipidation. Despite this dedicated folding mechanism, an accumulation of unfolded or misfolded proteins in the ER lumen can occur under conditions that interfere with the

physiological functions and functional capacity of the ER. The accumulation of unfolded proteins in the lumen of the ER generate a state known as *ER stress* (Schröder, 2008).

ER stress is observed in physiological and pathological conditions that perturb the ER homeostasis and proper functioning such as during differentiation of type B lymphocytes into plasma cells, protein folding defects, redox imbalance, calcium imbalance, cellular ATP imbalance, viral infections, nutrient deprivation and environmental toxins. Unfolded proteins are harmful to cells because they display non-native hydrophobic patches that interact and inhibit the functions of other proteins. Thus, accumulation of unfolded proteins may disrupt calcium gradients across membranes or could interfere with chaperone and degradation systems. For this reason, restoration of the ER homeostasis is critical for cell survival (Bravo et al., 2013, Schröder, 2008).

2.4 The unfolded protein response is ER's answer to stress

The cellular response to ER stress is known as the unfolded protein response (UPR). The purpose of the UPR is to counteract the ER stress and restore the normal function of the ER. It is a signalling pathway that monitors proper ER function and adjust protein synthesis, chaperone levels and the activity of protein degradation pathways accordingly. The UPR responses may act in parallel or in series and include:

(i) Increased expression of chaperones to increase the folding capacity of the ER

(ii) Temporary inhibition of general translation and transcription of secretory proteins in order to decrease the unfolded protein load of the ER

(iii) Stimulation of phospholipids and other membrane lipids biosynthesis to increase the size of the ER through generation of sheets and tubules. This increases the capacity of the ER to accommodate the increases in unfolded protein load

(iv) Induction of an antioxidant response to counteract ROS formed during repetitive oxidative protein folding attempts in the ER-stressed cells

(v) Transcriptional stimulation of degradative quality control of the unfolded and misfolded proteins. Two degradation routes are activated: ER-associated degradation (ERAD) in which proteins are retrotranslocated to the cytosol, ubiquitinated and degraded in the proteasome and ER-phagy, a form of autophagy in which parts of the ER and misfolded proteins in the ER are targeted to the lysosome for degradation

(vi) Cell fate regulation through co-ordination of apoptotic and antiapoptotic signals. If the proper ER function cannot be restored due to severe impairment, apoptosis programme is initiated, leading to demise of the cell (Karagöz et al., 2019, Schröder, 2008).

2.5 Three UPR response pathways and activation mechanisms

The gene targets of UPR depend on the tissue and nature of the physiological trigger of the ER stress (Rutkowski and Hegde, 2010). The UPR consists of three response pathways that are defined by three ER sensor proteins: IRE1 (inositol-requiring protein 1), PERK (protein kinase R-like ER kinase) and ATF6 (activating transcription factor) (Figure 2). The IRE1 is the most conserved sensor because it exists from yeast to mammals while PERK and ATF6 are found only in metazoan cells (Mori, 2009).

The three sensors harbour luminal, transmembrane and cytoplasmic domains. They sense the presence of unfolded proteins through their luminal domains and transduce the signal to the nucleus via the cytosol to trigger compensatory responses for restoring homeostasis. Under normal physiological conditions, the three protein sensors are bound and inhibited by the glucose-regulated protein 78kDa (GRP78, also known as BiP) in the ER lumen. Accumulation of unfolded and misfolded proteins bind and recruits GRP78 away from the three sensors, thereby activating the sensors to transduce information about protein folding status to the nucleus via distinct transducers: ATF4 for PERK, cleaved ATF6 for ATF6 and XBP1 for IRE1. Direct binding of the misfolded proteins to the sensor proteins has also been proposed as a model of activation of UPR (Karagöz et al., 2019, Walter and Ron, 2011, Yoshida, 2007).

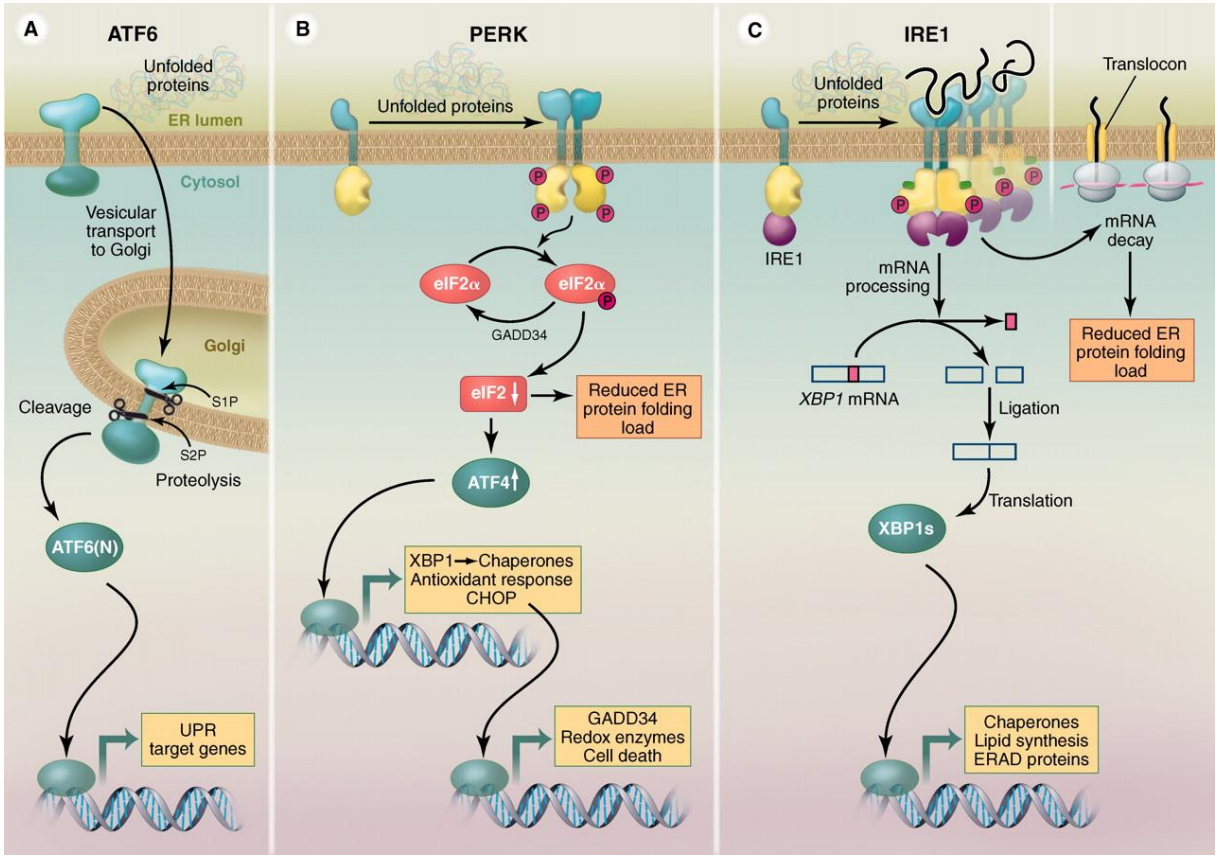

Figure 2. The three branches of the UPR. Three ER stress sensors (ATF6, PERK, and IRE1) monitor the protein-folding conditions in the ER lumen and transmit that information to drive UPR response. Each sensor uses a unique signal transduction pathway to activate specialized transcription factors that drive the transcription of the target genes that alleviate ER stress. The PERK and IRE1 pathways also reduce the folding load of the ER by negatively regulating translation and degrading ER-targeted mRNAs respectively. Figure adapted with permission from (Walter and Ron, 2011).

2.5.1 IRE1 pathway

IRE1 is a type 1 ER transmembrane protein with a cytoplasmic portion that contains a serine/threonine kinase domain and an endonuclease activity, hence IRE1 is a bifunctional enzyme. In response to the accumulation of unfolded proteins and ER stress, IRE1 oligomerizes and trans-autophosphorylates the kinase domains. The oligomerization is triggered either by binding of the unfolded proteins to the luminal domain of IRE1 or when it is released from the inhibitory interaction with GRP78 due to competition from unfolded proteins (Karagöz et al., 2019, Walter and Ron, 2011). In mammalian cells, there are two IRE1 paralogs, IRE1α and IRE1β, sharing structural similarity but performing different functions. IRE1α exerts its function through two downstream pathways, namely unconventional splicing of the X-box-binding protein-1 (XBP1) and IRE1-depedent decay

(RIDD). Surprisingly, IRE1α also regulates its expression by cleaving its own mRNA (Hollien et al., 2009, Tirasophon et al., 2000). IRE1β mediates site-specific cleavage of 28S rRNA to attenuate translation (Tirasophon et al., 1998).

Once activated, the endonuclease activity of IRE1α excise a 26-nucleotide intron from the XBP1 mRNA by unconventional splicing to produce a spliced XBP1 (XBP1s), a potent transcription factor. In metazoans, both the unspliced XBP1 (XBP1u) and the spliced XBP1 are translated but play different functions. The XBP1s induces expression of chaperones, glycosylation enzymes, ERAD components, autophagy components, lipid biogenesis enzymes and redox components. Upregulation of chaperones increases the capacity of the ER to deal with unfolded protein load (Bravo et al., 2013, Karagöz et al., 2019, Ron and Walter, 2007). The XBP1u on the other hand functions as a negative feedback regulator of XBP1s by sequestering the protein from the nucleus and promoting its degradation by the proteasome (Yoshida et al., 2006).

In addition to the non-canonical splicing of XBP1 mRNA, the nuclease activity of IRE1α target a sub-set of ER-associated mRNAs for cleavage in a process known as IRE1α-dependent decay (RIDD) in order to reduce the translational load on the ER by removing mRNAs that could otherwise be translated. IRE1α signalling is attenuated after prolonged ER stress and this is characterized by IRE1α cluster dissolution, dephosphorylation and decline in endonuclease activity (Li et al., 2010, Rubio et al., 2011).

2.5.2 PERK pathway

PERK is a type 1 transmembrane kinase that resembles IRE1 structurally. The cytoplasmic portion of PERK also contain a serine/threonine kinase domain which undergoes activating trans-autophosphorylation by homodimerization once released from GRP78 in ER-stressed cells. The activated PERK phosphorylates eukaryotic translation initiation factor 2, subunit 1α (EIF2α) at serine 51 which reduces formation of translation initiation complexes leading to general translation attenuation and hence reducing the protein load on the ER. Paradoxically, the phosphorylation of EIF2α allows translation of a subset of mRNAs which have a short open reading frame in their 5’ untranslated region, therefore enabling cap-independent translation. Among them is the mRNA encoding for transcription factor ATF4. ATF4 upregulates expression of genes encoding the ER chaperones (GRP78 and GRP94), macroautophagy, protein secretion and anti-oxidant response.

Two important target genes driven by ATF4 are CHOP (C/EBP homologous protein) and GADD34 (growth arrest and DNA damage–inducible 34). CHOP is a transcription factor that controls genes encoding components involved in apoptosis, depending on the magnitude of stress stimuli. ATF4 and CHOP have been implicated in the regulation of many autophagy related genes. Thus, PERK pathway is protective at modest levels of stress but contribute to cell death pathways under prolonged stress. PERK activation is rapidly reversible when ER homeostasis is restored. GADD34 plays a role in terminating PERK signalling by dephosphorylating EIF2α in a negative feedback manner. The dephosphorylation of EIF2α is also done by CReP (constitutive repressor of EIF2α phosphorylation), a constitutively expressed phosphatase (Bravo et al., 2013, Walter and Ron, 2011, Karagöz et al., 2019).

The PERK pathway also buffers against the ER stress through nuclear factor erythroid 2-like 2 (NRF2/NFE2L2) transcription factor. In unstressed cells, NRF2 is sequestered in the cytoplasm by KEAP1. Activated PERK during stress phosphorylates NRF2 which triggers its dissociation from KEAP1 and translocation to the nucleus where it induces expression of genes involved in antioxidant responses and autophagy (Cullinan et al., 2003, B'Chir et al., 2013). In addition to PERK, preferential translation of ATF4 is induced by other EIF2α kinases in responses to diverse stress conditions. These kinases include GCN2 (General Control Nonderepressible 2), HRI (Heme Regulated Initiation Factor 2 Alpha Kinase) and PKR (Protein Kinase RNA-Activated) and they are activated by nutrient deprivation, heme and oxidative stress and viral infection respectively. Because ATF4 is a common downstream target of all the EIF2α kinases, EIF2α-P/ATF4 pathway has been referred to as the integrated stress response (ISR) (Harding et al., 2003, Sonenberg and Hinnebusch, 2009, Wek and Cavener, 2007).

2.5.3 ATF6 pathway

ATF6 is a single-pass type 2 transmembrane ER protein and serves as both a sensor of ER stress and a transcriptional activator of UPR target genes. There are two stress responsive isoforms, ATF6α and ATF6β, with ATF6α being the predominant activator of UPR target genes. The ATF6β transcriptionally represses the ATFα signal by blocking its binding to promoter sequences and therefore serves as a negative regulator of this arm of UPR. The C-terminus of ATF6 bears Golgi localization sequences and is luminal in the ER while the N-terminus, which bears the transcriptional activity, is cytosolic (Shen et al., 2002, Thuerauf et al., 2007, Thuerauf et al., 2004).

During ER stress, ATF6 is released from the GRP78 sequestration, thereby exposing the Golgi localization signals, which facilitate its anterograde transport from the ER to the Golgi in COP-II vesicles. In the Golgi, it undergoes sequential cleavage by site-1 protease (S1P) and site-2 protease (S2P) to release the transcriptionally active N-terminus portion, ATF6(N), which then translocates to the nucleus where it binds ER stress response elements (ERSE) associated with promoters of UPR targeted genes. ATF6 upregulates the expression of ER chaperones such as GRP78 and GRP94, transcription factors XBP1 and CHOP, ERAD components and disulphide isomerases (Bravo et al., 2013, Haze et al., 1999, Schindler and Schekman, 2009, Walter and Ron, 2011). ATF6α is only transiently active because the increase in its transcriptional activity in response to unfolded proteins increases its own degradation by the proteasome (Thuerauf et al., 2002).

2.5.4 Cross talk between different UPR branches

Although ER stress sensors use different mechanisms and effectors to activate UPR, studies have shown that they connect to generate integrated responses to stress. For instance, there is a close relationship between the IRE1 and ATF6 pathways. ATF6 controls the transcription of XBP1 while on the other hand, XBP1u targets the active ATF6 to the proteasome for degradation. ATF6 also heterodimerizes with XBP1 to promote the degradation of ERAD components (Yamamoto et al., 2007, Yoshida et al., 2001, Yoshida et al., 2009). A dominant negative form of PERK has been shown to activate both ATF6 and XBP1 (Yamaguchi et al., 2008). The PERK pathway also facilitates both the synthesis of ATF6 and trafficking of ATF6 from the ER to the Golgi for intramembrane proteolysis and activation (Teske et al., 2011). It is not known how each UPR branch contributes to the final biological effect but studies have shown that differential activation of different pathways could determine either cell adaptation or cell death. For instance, persistent ER stress attenuates the activities of IRE1 and ATF6 but not PERK. Sustained PERK signalling impairs cell proliferation and promotes apoptosis while sustained IRE1 signalling enhances cell proliferation without promoting cell death (Lin et al., 2007, Lin et al., 2009).

2.6 ERAD quality control mechanism removes misfolded proteins from ER

Membrane and secretory proteins are synthesized and folded in the ER before their release into the secretory pathway. It is estimated that about one-third of all eukaryotic proteins, including all cell-surface and secretory proteins and proteins located in compartments along

the exocytic or endocytic pathways, are folded and matured in the ER before trafficking to their final destinations (van Anken and Braakman, 2005). The folding is facilitated by ER-resident chaperones in a process that is guided by posttranslational modifications of nascent polypeptide chains (Braakman and Hebert, 2013, Cherepanova et al., 2016). Despite these enormous resources, protein misfolding occurs frequently and especially during conditions that perturb ER functions or if the proteins harbour disease-causing mutations that compromise biogenesis (Schröder, 2008, Tao and Conn, 2018).

The ER however, has a quality control mechanism that ensures only the correctly folded proteins exit the ER for their destinations while the incompletely folded proteins are retained in the ER to undergo further rounds of folding. Calnexin and calreticulin play essential roles as chaperones in the ER quality control process by trapping partially folded or unfolded proteins in the ER (Hebert et al., 1995). Incorrectly folded or terminally misfolded proteins are targeted for degradation to maintain ER homeostasis. Failure to adequately degrade the misfolded proteins lead to their accumulation in the intracellular or extracellular spaces, causing pathological conditions. For instance, mutations in α_1-antitrypsin (AAT) cause the mutant proteins to polymerize and accumulate in the ER of hepatocytes, leading to chronic liver disease (Perlmutter and Silverman, 2011).

Terminally misfolded proteins in the ER are targeted for degradation through two different pathways, namely ER-associated degradation (ERAD) and ER-phagy (Meusser et al., 2005, Wilkinson, 2019a) (Figure 3). These degradative pathways occur in parallel to UPR but each of them is also regulated by UPR through regulation of protein synthesis, chaperone levels and the activity of the degradative components (Karagöz et al., 2019, Preissler and Ron, 2019, Sun and Brodsky, 2019). In ERAD pathway, the misfolded proteins are retro-translocated across the ER membrane into the cytoplasm where they are polyubiquitinated and targeted for degradation in the proteasome (Meusser et al., 2005). ERAD is considered as the main pathway through which most of the misfolded proteins are degraded. The diameter of the pore in the retro-translocon however, may exclude misfolded oligomeric or aggregated proteins from being exported from the ER to the cytoplasm. These proteins are instead targeted for degradation by ER-phagy, a form of autophagy that engulfs specific portions of the ER and targets them for degradation in the lysosome. ER-phagy is also involved in the degradation of the excess ER components and membranes produced during UPR (Wilkinson, 2019a, Bernales et al., 2006). Detailed insights into ER-phagy will be outlined in section 4.6.

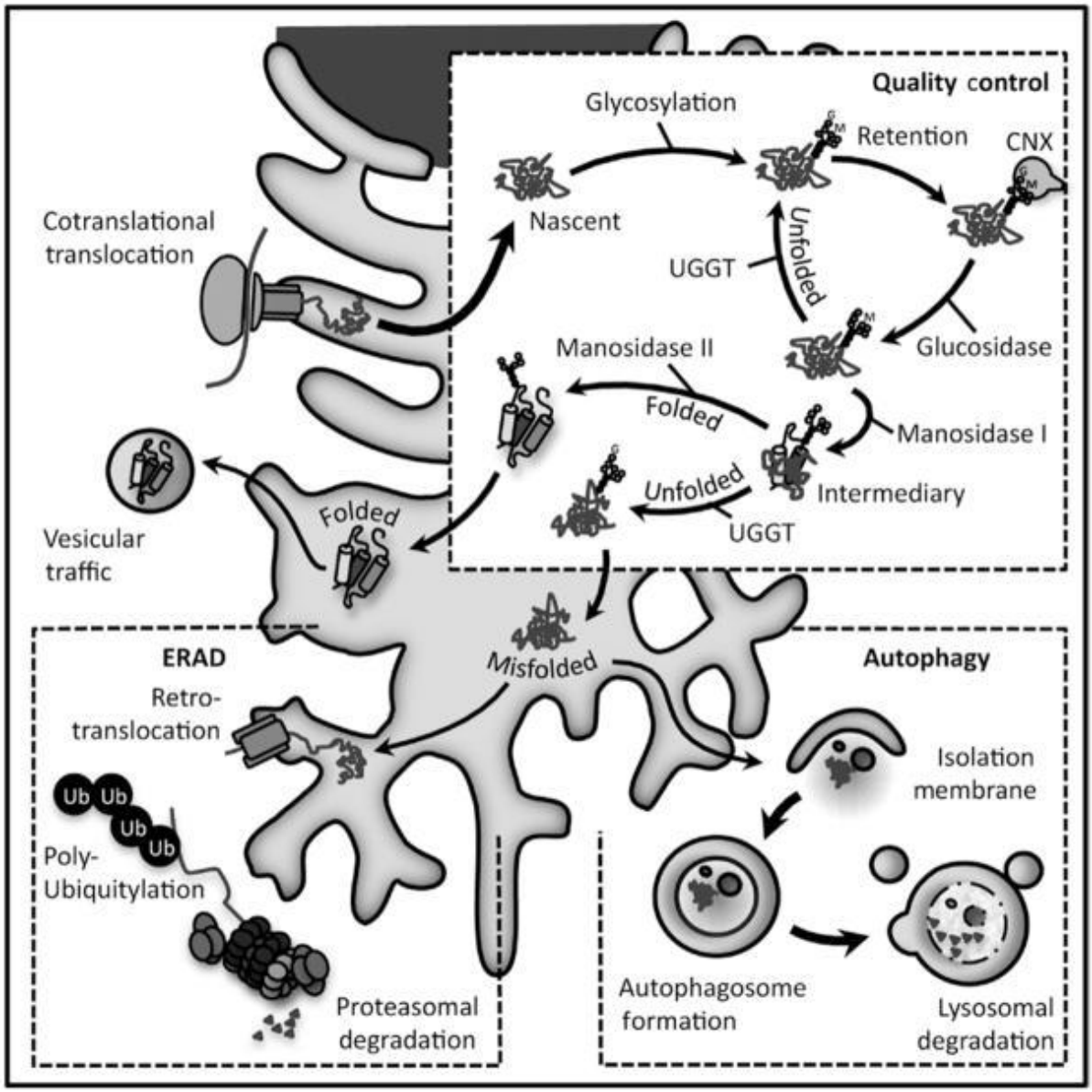

Figure 3. The ER quality control system: Newly synthesized proteins are glycosylated and retained in the lumen of the ER by calnexin and calreticulin for folding cycles. The correctly folded proteins are exported from the ER by vesicle trafficking while the improperly folded proteins are retained for more folding cycles. Terminally misfolded proteins are degraded through ubiquitin-proteasome pathway or autophagy. Figure adapted with permission from (Bravo et al., 2013).

3. Structure and function of Golgi apparatus

The Golgi complex is a key membrane-bound organelle in the secretory pathway downstream of the ER. The existence of the Golgi apparatus was described in 1898 by Camillo Golgi when he published his observations of an internal reticular complex that surrounded the nucleus of Purkinje cells in the barn owl cerebellum (Golgi and Lipsky, 1989). The primary and widely accepted roles of the Golgi complex are the biosynthesis of some lipids such as glycolipids and sphingomyelin and the modification, sorting, packaging and recycling of the secretory proteins and lipids downstream of the ER. It is at the Golgi that proteins are modified and selected for traffic to the endocytic organelles, to the cell surface for secretion or presentation, or for retrieval back to the ER (Klute et al., 2011). The modifications include glycosylation, phosphorylation, sulphation and proteolysis. In addition, the Golgi apparatus plays important roles in diverse cellular processes including division, migration morphogenesis, growth, apoptosis, autophagy and stress response (Rasika et al., 2019).

In higher eukaryotes, the Golgi complex consists of multiple flattened cisternal membranes arranged in close apposition to each other to form stacks (Hicks and Machamer, 2005). The stacks are polarized, consisting of a cis-side, called cis-Golgi network (CGN), a medial Golgi area of disc-shaped flattened cisternae, and a trans-side, called trans-Golgi network (TGN). The cis-side and trans-side face the ER and away from the ER, respectively, and are associated with tubular reticular network of membranes. In mammalian cells, the individual Golgi stacks are interconnected laterally with equivalent cisternae of different stacks by tubular structures to form a ribbon structure that is localized in the perinuclear region. A mammalian cell typically contains about 40-100 Golgi stacks interconnected with each other into a continuous ribbon-like structure in this manner. The formation and maintenance of the Golgi ribbon relies on the microtubule cytoskeleton originating from the perinuclear centrosome (Wang and Seemann, 2011).

Although the most common characteristics of the Golgi in higher eukaryotes is that of multiple flattened cisternal membranes closely aligned to form stacks, some species and specialized cell types show variations in the number and morphological organization of the stacks. In some eukaryotic species, for example the yeast *S. cerevisiae*, the Golgi membranes do not form stacks but are distributed throughout the cytoplasm (Dacks et al., 2003). In insect cells, Golgi cisternae form stacks but the stacks are usually dispersed throughout the cytoplasm (Hicks and Machamer, 2005). In some unicellular eukaryotes, including

Trypanasoma brucei (He et al., 2004), *Toxoplasma gondii* (Hager et al., 1999) and the green algae, *Ostreococus tauri* (Henderson et al., 2007), each cell contains only a single Golgi stack. The lack of stacks in yeast has been interpreted to mean that stacking is not required for Golgi functioning. Nevertheless, the complex organization in higher eukaryotes has been suggested to have important functional consequences (Wang and Seemann, 2011).

Some eukaryotic species such as *Giardia intestinalis,* lack Golgi structures. However, despite having no Golgi-type organelles, these Golgi-lacking organisms contain genes homologous to those encoding for Golgi-related functions in mammals, implying that all extant eukaryotes have some conserved Golgi function. This is evolutionary significant because it implies that Golgi bodies were present in the last common eukaryotic ancestor. The Golgi therefore is a fundamental feature of the eukaryotic membrane trafficking system and the variations in architecture and complexity between different eukaryotic lineages evolved after eukaryogenesis and are likely a product of an evolutionary process of gene duplication and coevolution of specificity encoding membrane trafficking proteins (Dacks et al., 2003, Klute et al., 2011).

The steady-state structure of the Golgi stacks is partly maintained by the balance between the anterograde and retrograde transport through the Golgi. Inhibition of ER-Golgi traffic by either physiological conditions such as osmotic stress or drugs causes the Golgi to collapse into the ER due to unbalanced retrograde traffic (Dinter and Berger, 1998, Lee and Linstedt, 1999). Conversely, temperature blocks that inhibit exit from either the cis-Golgi or trans-Golgi networks cause significant swelling due to the accumulation of the anterograde cargo in the CGN or TGN (Griffiths et al., 1985, Ladinsky et al., 2002, Matlin and Simons, 1983). The structure of the Golgi and the formation and maintenance of Golgi stacks and ribbons also depend on Golgi matrix proteins and intact microtubule network. More particularly, microtubules facilitate Golgi ribbon formation by maintaining stacks in close proximity and in the pericentrosomal region. On the other hand, connections between cisternae into stacks are formed and maintained by the Golgi matrix proteins which include Golgi stacking proteins (GRASPs) and membrane tether proteins such as GM130. Besides the membrane traffic and Golgi matrix proteins, the Golgi structure also depends on SNAREs, kinases, methyltransferases and GTPases (Barr and Short, 2003, De Matteis and Morrow, 2000, Li et al., 2019). These observations underscore the sensitivity of the Golgi structure to dynamic equilibrium of membrane traffic and the integrity of Golgi-associated proteins.

3.1 Golgi stress and Golgi stress response

The Golgi apparatus modifies secretory and membrane proteins and sort them for transport by vesicular pathway to their final destinations. The structure and function of the Golgi however can be impaired by stress conditions such nutrient deprivation, excess secretory proteins from the ER, changes in Golgi pH or ion content, disruption of protein modifications and viral assembly and budding at the Golgi membranes. Golgi stress causes disruption and insufficiency of the Golgi function and therefore cells activate Golgi stress response mechanism to restore homeostasis and Golgi function. The amount and structure of the Golgi apparatus therefore is dynamically regulated in accordance with physiological and pathological conditions.

For instance, the amount of the Golgi apparatus is dynamically changed in prolactin cells of the pituitary glands and in acinar cells of the mammary glands of female mice in response to the suckling stimulus, which enhances secretion of prolactin and milk proteins. Whereas in lactating female mice the Golgi is expanded, the size is decreased when the female is separated from her pups. When the female is re-united with her pups, the size of the Golgi increases again (Clermont et al., 1993, Rambourg et al., 1993). Another example is the fragmentation of the Golgi apparatus caused by huge influx of viral glycoproteins when cells are infected with viruses (Campadelli et al., 1993). Furthermore, disruption of the Golgi function with pharmacological agents such as monesin causes swelling of the Golgi cisternae (Oku et al., 2011). These observations suggest that, similar to the ER stress signalling, the Golgi apparatus, in response to Golgi stress, may initiate stress response signalling to regulate its functional capacity accordingly and buffer against the stress conditions.

3.2 Three Golgi stress response pathways

From studies of ER stress response, it is already established that an organelle stress response mechanisms involve three key components, namely, a sensor that detects insufficiency of organelle function, a transcription factor that increases transcription of genes involved in organelle function, and an enhancer element to which the transcription factor binds. In the case of the mammalian ER stress response, there are three response pathways. The sensor, transcription factor, and enhancer of the IRE1 pathway are IRE1, pXBP1(S), and UPRE, respectively, for the PERK pathway are PERK, ATF4, and AARE and those of the ATF6 pathway are ATF6, ATF6(N) and ERSE. The molecular mechanisms of the Golgi stress

response however are currently not as well known but recent studies have identified three Golgi response pathways, namely the TFE3, HSP47 and CREB3 pathways (Taniguchi and Yoshida, 2017).

3.2.1 TFE3 pathway

TFE3 pathway was revealed in the studies of Oku et al and Taniguchi et al in which TFE3, a basic-helix-loop type transcription factor, is the key regulator (Oku et al., 2011, Taniguchi et al., 2015). Under normal conditions, TFE3 is phosphorylated at Ser108 and retained in the cytoplasm. When glycosylation or sialic acid modification in the Golgi is impaired, either by genetic mutations, knockdown or inhibitors, TFE3 is dephosphorylated, translocates to the nucleus and binds to Golgi apparatus stress response element (GASE) to activate transcription of genes encoding Golgi structural proteins (GM130, GCP60, and Giantin), glysosylation enzymes (sialyltransferase 4A, sialyltransferase 10, and fucosyltransferase) and vesicular transport components (syntaxin 3A).

3.2.2 HSP47 pathway

HSP47 is an ER localized chaperone for the folding of collagens (Nagata et al., 1988). Surprisingly, the expression of HSP47 is increased when cells are treated with Benzyl-*N*-acetyl-α-galactosaminide (benzylGalNAc), a chemical that inhibits mucin O-glycans glycosylation (Miyata et al., 2013). The first sugar to be conjugated to mucin core proteins is *N*-acetylgalactosamine (GalNAc). BenzylGalNAc competitively inhibits O-glycosylation because it is structurally similar to GalNAc. When expression of HSP47 was suppressed by siRNA, benzylGalNac treatment resulted in fragmentation of the Golgi and apoptosis. When HSP47 was overexpressed however, benzylGalNAc-induced apoptosis was attenuated. These observations suggested that HSP47 is induced by Golgi stress to protect cells from Golgi stress-induced apoptosis. The molecular sensors as well as the transcription factors involved in this pathway are not known. More intriguing is how an ER localized chaperone is able to protect cells from Golgi stress.

3.2.3 CREB3-ARF4 pathway

CREB3 is a basic leucine zipper ER membrane-bound transcription factor closely related to ATF6, one of the three ER stress transducers, and with a similar mechanism of activation. ARF4 is a member of the small GTPase family and is localized in the Golgi membrane where it regulates Golgi to ER vesicular transport. The CREB3 pathway induces collapse of the

Golgi apparatus and apoptosis in response to Golgi stress through transcriptional upregulation of ARF4 (Reiling et al., 2013). Upon induction of Golgi stress by inducers such as brefeldin (BFA), CREB3 is transported from the ER to the Golgi where it is cleaved by site-1 (S1P) and site-2 (S2P) proteases to liberate the cytoplasmic domain which then translocates to the nucleus to activate ARF4 transcription, leading to Golgi stress-induced apoptosis. Like TFE3 and HSP47 pathways, the molecular sensor for CREB3-ARF4 Golgi stress response pathway is not known. Regardless, it is part of a signalling cascade from the Golgi that is set in motion by Golgi stress.

In summary, Golgi fragmentation and disassembly are pathological features of several neurodegenerative conditions as well as several bacterial and viral infections (Gonatas et al., 2006). It is conceivable that these morphological changes are linked to Golgi stress induction. Elucidating the molecular mechanisms of the Golgi stress response therefore might be critical in identifying treatment and management options for these conditions.

3.3 Palmitoyltransferases ZDHHC17 and ZDHHC13 modify proteins at the Golgi

S-acylation is a reversible post-translational attachment of fatty acids onto cysteine residues of proteins. This post-translational modification (PTM) is commonly referred to as palmitoylation, reflecting the fact that palmitic acid is the predominant amino acid added to proteins this way (Muszbek et al., 1999). Palmitoylation serves specific functions on the modified proteins, including facilitating membrane attachment of soluble proteins, regulating protein sorting to specific intracellular compartments, modulating protein folding and stability and regulating distribution of proteins in membranes. The proteins modified by palmitoylation are diverse and includes both soluble and transmembrane proteins. For soluble proteins, a major function of S-acylation is to provide a stable membrane anchor, thus it is essential for membrane association of signalling molecules (Blaskovic et al., 2014, Fukata and Fukata, 2010, Lemonidis et al., 2017b, Lemonidis et al., 2015b). It is estimated that about 10% of the mammalian proteome is modified by palmitoylation and about 500 proteins in human have been identified as substrates (Martin and Cravatt, 2009, Tate et al., 2015).

In mammals, palmitoylation reactions are mediated by a family of 24 acyltransferase enzymes (Fukata et al., 2004). These enzymes share a conserved membrane topology with four to six transmembrane domains and a catalytic Asp-His-His-Cys motif (DHHC) in a cysteine-rich 51- amino acid zinc finger-like domain (zDHHC-CR). Most of these enzymes are associated

with the endoplasmic reticulum and Golgi with the catalytic zDHHC motif facing the cytoplasm, but some have also been reported to associate dynamically with the plasma membrane and endosomes (Ernst et al., 2018, Mitchell et al., 2006, Ohno et al., 2006, Politis et al., 2005). Because zDHHC enzymes are membrane associated, S-acylation reactions occur at the cytosolic face of intracellular membranes. This distinguishes S-acylation from other lipid modifications such as myristoylation and prenylation which occur in the cytosol (Resh, 2006). Palmitoylation by DHHC enzymes is thought to occur in a two-step reaction mechanism in which the fatty acid is first attached to the cysteine of the DHHC motif of the enzyme to form an acyl-enzyme intermediate, a process known as autoacylation, followed by the transfer of the acyl group (palmitate) to a cysteine residue on the target protein (Jennings and Linder, 2012, Mitchell et al., 2010). Except for ZDHHC17 and ZDHHC13, it is not well known how the other DHHC enzymes engage their substrates.

ZDHHC17 and ZDHHC13 are also known as Huntingtin-interacting protein 14 (HIP14) and 14-like (HIP14L) respectively. These two are ubiquitously expressed (Ohno et al., 2006) and differ from the other DHHC enzymes by having N-terminal ankyrin repeats (AR) domains. AR domains act as substrate-recruiting modules for S-acylation reactions but may also participate in S-acylation-independent functions such as the activation of c-Jun N terminus kinase (JNK) (Harada et al., 2003, Yang and Cynader, 2011) and suppression of heterotrimeric G-protein signalling (Hemsley and Grierson, 2011). For interaction, the AR domains of ZDHHC17 and ZDHHC13 recognize specific evolutionary conserved or a closely related sequence in the interacting proteins that conforms to [VIAP][VIT]XXQP consensus, where X is any amino acid. The sequence motif has been called zDHHC-AR-binding motif (zDABM) and a screen of human proteins based on this motif identified over 90 proteins as interactors of zDHHC17 (Lemonidis et al., 2017a, Lemonidis et al., 2015a). To date, ZDHHC17 has been shown to bind and mediates S-acylation of Huntingtin (HTT), JNK3α2, CSPα and SNAP25b (Huang et al., 2011, Jennings and Linder, 2012, Lemonidis et al., 2014, Yang et al., 2013). Both ZDHHC17 and ZDHHC13 are localized in the Golgi (Ernst et al., 2018), but a separate study reported localization of ZDHHC13 in the endoplasmic reticulum (Ohno et al., 2006). Loss of ZDHHC17/13 in mice produces Huntingtin-like phenotypes (Milnerwood et al., 2013, Singaraja et al., 2011, Sutton et al., 2013), underscoring the critical physiological roles of these enzymes.

4. Cellular health and function are maintained by autophagy

Eukaryotic cells maintain their function, health and survival by removing surplus, broken or dangerous components such as proteins aggregates, surplus or damaged organelles and intracellular pathogens (Mizushima and Komatsu, 2011). Failure to control the accumulation of any of these types of components can lead to diseases in humans such as neurodegeneration, cancer and infectious diseases (Dikic and Elazar, 2018, Mizushima and Komatsu, 2011). The molecular mechanism for degrading these components is autophagy, an evolutionary conserved catabolic process that shuttles cytoplasmic materials or foreign agents to the lysosome for degradation. Under basal conditions, autophagy facilitates the constitutive turnover of cytoplasmic components to maintain homeostasis. During nutrients starvation, autophagy is induced to degrade cellular macromolecules such as lipids, carbohydrates and proteins to recycle nutrients and generate energy. Based on how the cargo material is delivered to the lysosome, autophagy is classified as either microautophagy, chaperone-mediated autophagy (CMA) or macroautophagy (Levine and Klionsky, 2004, Maria Cuervo, 2004, Ohsumi, 2014, Feng et al., 2014) (Figure 4).

4.1 Microautophagy

Microautophagy is a form of autophagy in which the cytoplasmic cargo destined for degradation is directly engulfed by invagination of the lysosomal membrane (vacuole in yeast and plants) (Galluzzi et al., 2017). The lysosomal membrane invagination to trap cytosolic components was originally observed in rat liver cells (Mortimore et al., 1988, Saito and Ogawa, 1974), but later studies in yeast *Pichia pastoris* showed use of a similar process to sequester peroxisomes for degradation when yeast cells were shifted from methanol to glucose medium (Tuttle and Dunn, 1995, Yuan et al., 1997). Subsequent studies done in several yeast species and the ability to reconstitute yeast microautophagy *in vitro* with isolated vacuoles led to the discovery of the molecular machiney involved in the process and the realisation that some of the involved genes were shared with macroautopahgy (Kunz et al., 2004, Leão-Helder et al., 2004, Mijaljica et al., 2011, Sakai et al., 1998, Uttenweiler et al., 2007). The microautophagy process in yeast is either nonselective, in which intracellular proteins and organelles are indiscriminately engulfed by the vacuole, or selective, in which specific intracellular components are targeted for degradation. Thus, several forms of selective microautophagy in yeast have been described: micropexophagy (for peroxisomes)

(Sakai et al., 1998, Yuan et al., 1997), micromitophagy (for mitochondria) (Lemasters, 2014), microlipophagy (for lipid droplets) (Seo et al., 2017) and piecemeal microautophagy (for portions of the nucleus) (Roberts et al., 2003).

The study of microautophagy in mammalian cells has been slower relative to the studies in yeast partly because of difficulties in detecting an invagination-like process in secondary lysosomes and also because the essential genes for yeast microautophagy have no conserved function in mammals (Tekirdag and Cuervo, 2018). Recent studies however have demonstrated a degradation process in mammalian cells and *Drosophila* with similar characteristics to yeast microautophagy. The process, termed endosomal microautophagy, occurs in the late endosomes or multivesicular bodies and not lysosomes and relies on multiple endosomal sorting complexes required for transport (ESCRT) systems for the formation of the vesicles in which the cytosolic cargo is internalized. The endosomal microautophagy degrades cytosolic proteins either in bulk or selectively. The selective cargo is for proteins bearing KFERQ-like motif that is recognized by heat shock cognate 70 KDa chaperone (HSC70). Upon cargo binding, HSC70 electrostatically interacts directly with phosphatidylserine on the endosomal membrane and then internalized along with the substrate in ESCRT-mediated microvesicles (Mukherjee et al., 2016, Sahu et al., 2011, Uytterhoeven et al., 2015, Mejlvang et al., 2018).

4.2 Chaperone-mediated autophagy (CMA)

CMA is a multistep process in which intracellular soluble proteins bearing KFERQ-like motif are selectively recognized by the cytosolic heat shock cognate chaperone of 70 kDa (HSC70) and delivered to the lysosome for degradation. About 40% of proteins in the mammalian proteome contain a canonical KFERQ-like motif, thus CMA may play major cellular regulatory functions (Chiang and Dice, 1988, Chiang et al., 1989, Kaushik and Cuervo, 2018). Binding of HSC70 targets the substrate proteins to the lysosomal membranes of CMA-competent lysosomes via binding to the cytosolic tail of monomeric lysosome-associated membrane protein type-2A (LAMP2A). Upon binding, the substrates are unfolded and LAMP-2A multimerizes to form CMA translocation complex through which the substrate proteins translocate across the lysosomal membrane one-by-one in a process mediated by an intralysosomal HCS70 (lys-HSC70). The translocated proteins are then rapidly degraded in the lysosomal lumen into their constitutive amino acids (Agarraberes et al., 1997,

Bandyopadhyay et al., 2008, Cuervo and Dice, 1996, Cuervo et al., 1997, Salvador et al., 2000). CMA occurs at basal level in most cells but maximal activation occurs during stress conditions such as nutrient deprivation (Cuervo et al., 1995), oxidative stress (Finn and Dice, 2005, Kiffin et al., 2004), DNA damage (Park et al., 2015), proteotoxic stress (Cuervo et al., 1999), hypoxia (Hubbi et al., 2013, Vasco Ferreira et al., 2015) and lipid overload (Kaushik and Cuervo, 2015, Rodriguez-Navarro et al., 2012).

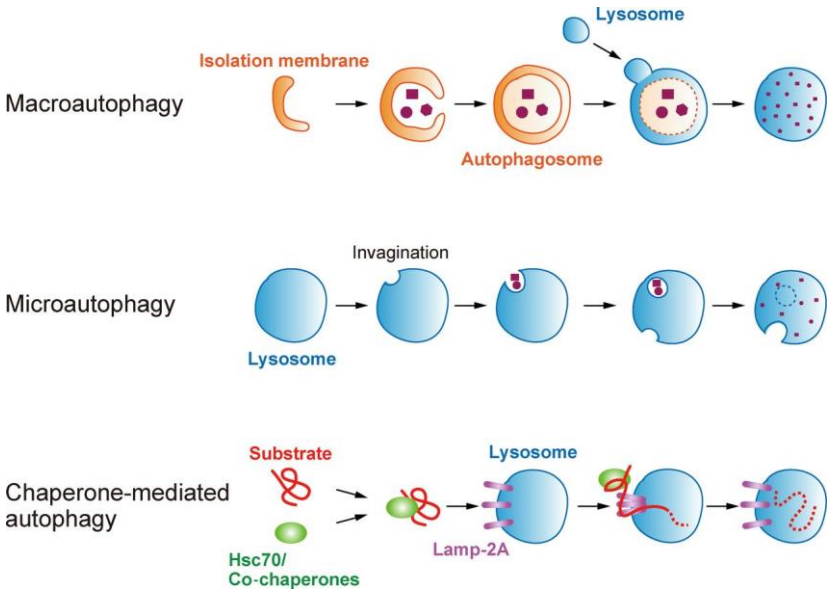

Figure 4. Three types of autophagy. In macroautophagy, cup-shaped double membrane structures called phagophores (isolation membranes) expand to engulf cytoplasmic material. The autophagosome is formed by a closure of the growing phagophore, and it fuses with lysosomes to degrade its contents. In microautophagy, cytosolic proteins and organelles are sequestered by an invagination of the lysosomal membrane. In CMA, specific proteins are recognized by HSC70 and translocated by the lysosomal membrane protein LAMP2A into the lysosome where it is degraded. Figure adapted with permission from (Okamoto, 2014).

4.3 Macroautophagy

Macroautophagy is the best characterized form of autophagy and therefore the universal connotation of autophagy. Thus, in the rest of this section it will be referred simply as autophagy. It involves sequestration of the cytoplasmic material into double-membraned vesicles called autophagosomes, which then fuse with the lysosomes to degrade their contents. The formation of the autophagosome involves multiple membrane remodelling processes, including initiation and nucleation of cup-shaped isolation membrane called phagophore and its subsequent fusion and closure (Ohsumi, 2014, Feng et al., 2014). The autophagosomes have considerable sequestering capacity and therefore this form of autophagy is the main mechanism in eukaryotic cells for degrading bulk or selective cargoes that are larger than individual proteins. Selective autophagy removes or recycles harmful or unneeded materials from the cell to maintain homeostasis and requires adaptor molecules to link the cargo to the autophagy machinery. These materials include protein aggregates, excess or damaged organelles and intracellular pathogens (Kirkin, 2019, Zaffagnini and Martens, 2016, Gatica et al., 2018). Bulky autophagy is triggered by nutrients starvation to degrade cellular macromolecules such as lipids, carbohydrates and proteins to recycle biosynthetic precursors and generate energy (Johansen and Lamark, 2011, Turco et al., 2019a, Galluzzi et al., 2017).

4.4 Autophagosome formation is regulated by evolutionary conserved proteins

The molecular mechanisms underlying the formation and degradation of the autophagosome and the identification of autophagy-related (ATG) genes regulating the process were first elucidated in yeast but are mainly conserved in higher eukaryotes (Ohsumi, 2014). These proteins functionally assemble into temporal hierarchical complexes to initiate the formation, expansion, and closure of phagophores around the cargo to form the autophagosomes. According to current understanding, the ULK1 complex, composed of the ULK1 or ULK2 kinase and scaffolding subunits ATG13, RB1-inducible coiled-coil protein 1 (FIP200/RB1CC1) and ATG101; and the class-III PI3K (PI3KC3) complex, composed of the catalytic subunit vacuolar protein sorting 34 (VPS34), vesicular transport factor p115 (VPS15/PIK3R4), Beclin-1 and ATG14 are required for the initiation and nucleation of the phagophores (Dikic and Elazar, 2018, Yu et al., 2018, Zhao and Zhang, 2019) (Figure 5).

In a widely accepted model, phagophores in mammalian cells are initiated and formed on the ER membrane domains. Under basal conditions ULK1 complex and hence autophagy, is inhibited by the mammalian target of rapamycin (mTOR) through direct binding and phosphorylation of ULK1 and ATG13. Under nutrients starvation, mTOR activity is inhibited leading to the activation of ULK1 complex and recruitment of the complex to phosphatidylinositol 3-phosphate (PI3P)-enriched membrane subdomains of the ER called omegasomes that are also marked by PI3P-binding protein zinc-finger FYVE domain-containing protein 1 (DFCP1) and ATG9 vesicles (Mancias and Kimmelman, 2016, Yu et al., 2018, Bento et al., 2016). The mechanism of how ULK1 complex translocates to the phagophore formation sites on the omegasomes is not well understood but it has been shown to be mediated by the Rab1 effector C9orf72 (Webster et al., 2016). After recruitment, the ULK1 complex is stabilized by membrane association properties of ULK1 and ATG13 (Galluzzi et al., 2017, Bento et al., 2016)and direct interaction of ULK1 and FIP200 with ER contact proteins VAPA and VAPB (Zhao et al., 2018). The ULK1 complex recruits class-III PI3K (PI3KC3) complex to the phagophore initiation sites through interaction of ATG14L with ATG13, and activates it through phosphorylation of VPS34 and Beclin-1 by ULK1 (Galluzzi et al., 2017, Dikic and Elazar, 2018).

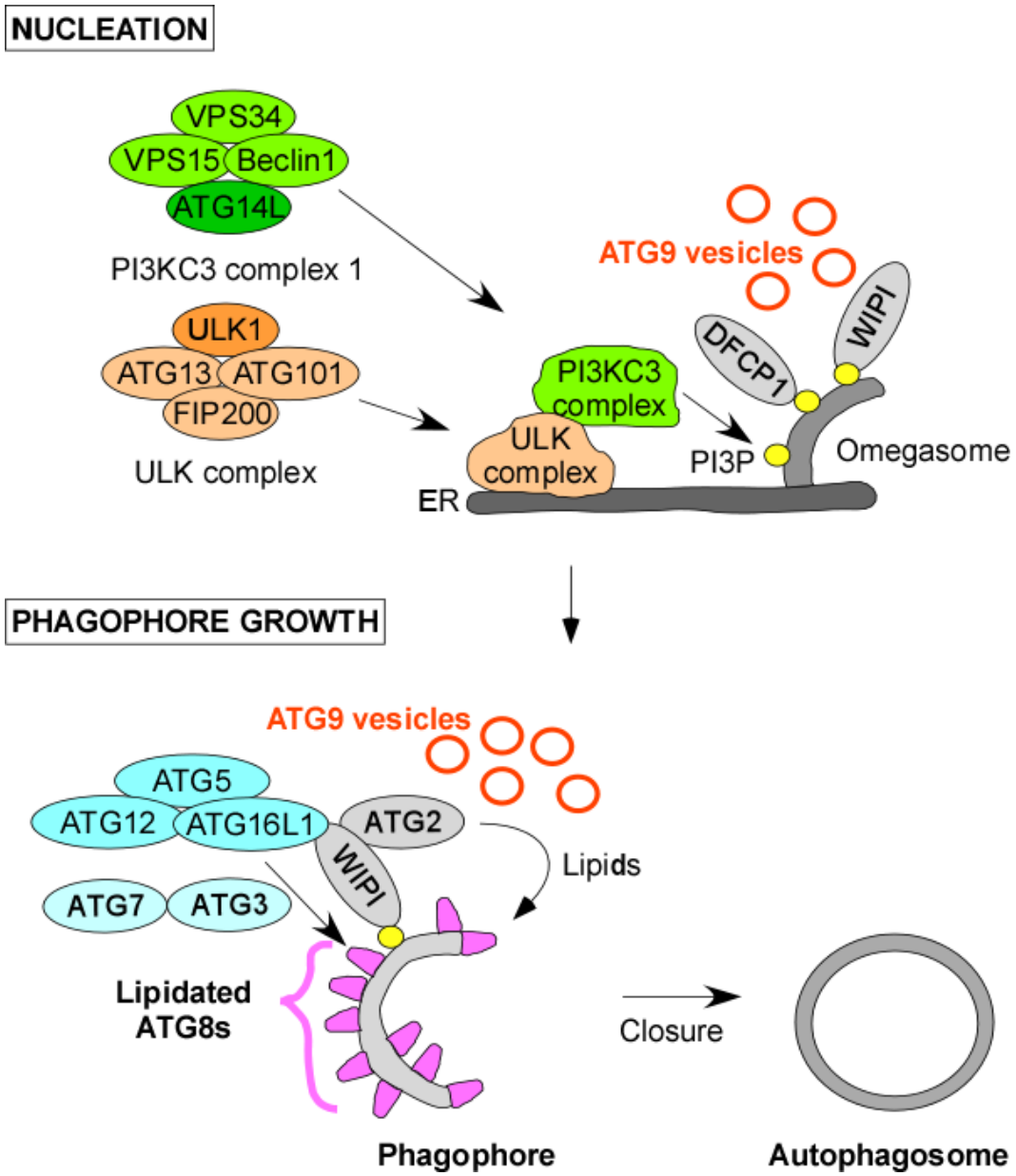

Figure 5. Basal autophagy proteins mediating autophagosome formation. Autophagosome formation (nucleation) is initiated at the ER membrane by the ULK1 kinase complex (ULK1/2, FIP200, ATG13, ATG101) and the class-III PI3K complex 1 (VPS34, VPS15, Beclin-1, ATG14). Local PI3P production at an ER structure called omegasome then recruits PI3P binding proteins like the WIPI proteins and DFCP1. Phagophore growth is then initiated by WIPI dependent recruitment of ATG2 and the ATG12-ATG5:ATG16L1 complex. The ATG12-ATG5:ATG16L1 complex acting with the E1 ligase ATG7 and the E2 ligase ATG3, mediate lipidation of ATG8 proteins to phosphatidylethanolamine (PE) on the phagophore. ATG2 together with ATG9 vesicles, are essential for the transfer of lipids or membrane material to the growing phagophore. ATG8s act as a scaffold for the recruitment of cargos or autophagy proteins essential for phagophore growth or closure (not illustrated).

The activated VPS34 phosphorylates phosphatidylinositol (PI) to generate phosphatidylinositol-3-phosphate (PI3P) which nucleates the location of phagophore formation. The PI3P recruits WD repeat domain phosphoinositide interacting (WIPI) proteins (WIPI1–4) which in turn recruit ATG2 to promote phagophore expansion and closure. ATG2 is a lipid-binding and transfer protein and the ATG2-WIPI complex has been shown to support phagophore expansion by tethering it to the ER and subsequently transferring lipids from the ER, ATG9-containing vesicles and COPII vesicles (Graef, 2018, Maeda et al., 2019, Osawa et al., 2019, Otomo et al., 2018, Otomo and Maeda, 2019, Tang et al., 2019a, Tang et al., 2019b, Valverde et al., 2019). The WIPI proteins also function together with FIP200 to recruit ATG16L1 which act in complex with ATG12-ATG5 conjugate to facilitate conjugation of ATG8 family proteins to the nucleated phagophore membranes (Dikic and Elazar, 2018).

The attachment of ATG8 to the phagophore membrane is a culmination of two parallel ubiquitin-like conjugation systems: the ATG12 and ATG8 conjugation systems. In the first system, ubiquitin-like protein ATG12 is conjugated to ATG5 (ATG12-ATG5) in a series of reactions catalysed by ATG7 acting as E1-like enzyme and ATG10 acting as E2-like enzyme. Mechanistically, the ATG12 is activated by ATG7 and transferred to ATG10 which then covalently links it to ATG5. ATG16L1 then noncovalently binds ATG5 to form ATG12-ATG5:ATG16L1 complex. The ATG12-ATG5:ATG16L1 associates with the phagophore membranes and assist in the recruitment of ATG8 by mediating the final step of the ATG8 conjugation system (Bento et al., 2016, Weidberg et al., 2011, Matsuzawa-Ishimoto et al., 2018, Mancias and Kimmelman, 2016).

The ATG8 conjugation system covalently attaches ubiquitin-like ATG8 family proteins to membrane-resident phosphatidylethanolamine (PE). But before this can happen, precursor ATG8 proteins are processed by cysteine proteases (ATG4A, B, C and D), which cleave the C-terminus of the ATG8 to expose the glycine residue (ATG8-I form). The cleavage is crucial for the ATG8-I conjugation to the PE in a mechanism dependent on ATG7, ATG3 and ATG12-ATG5:ATG16L1 acting as E1-like, E2-like and E3-like enzymes respectively, leading to its attachment to the PE. This reaction is generally called lipidation and results in a tight association of the ATG8 with phagophore membrane (Turco et al., 2019a, Mancias and Kimmelman, 2016, Yu et al., 2018). Note that there are six ATG8 family proteins in mammals, divided further into two subfamilies; microtubule-associated proteins 1 A/1B light chain 3 (LC3) subfamily comprising LC3A, LC3B and LC3C proteins; and the γ-

aminobutyric acid receptor-associated protein (GABARAP) subfamily comprising GABARAP, GABARAPL1, GATE-16/GABARAPL2 proteins. The lipidated ATG8 proteins recruit LIR-containing proteins to the growing phagophore including members of ULK1/2 and PI3KC3 complexes and ATG4 proteases (Alemu et al., 2012, Skytte Rasmussen et al., 2017, Birgisdottir et al., 2019). Lipidated ATG8 proteins also recruit autophagy receptors to the inner (concave) surface of the growing phagophores (Rogov et al., 2014, Johansen and Lamark, 2011, Johansen and Lamark, 2019). The ATG8 proteins also recruit fusion factors to aid in the maturation of autophagosomes as discussed below and (Figure 6).

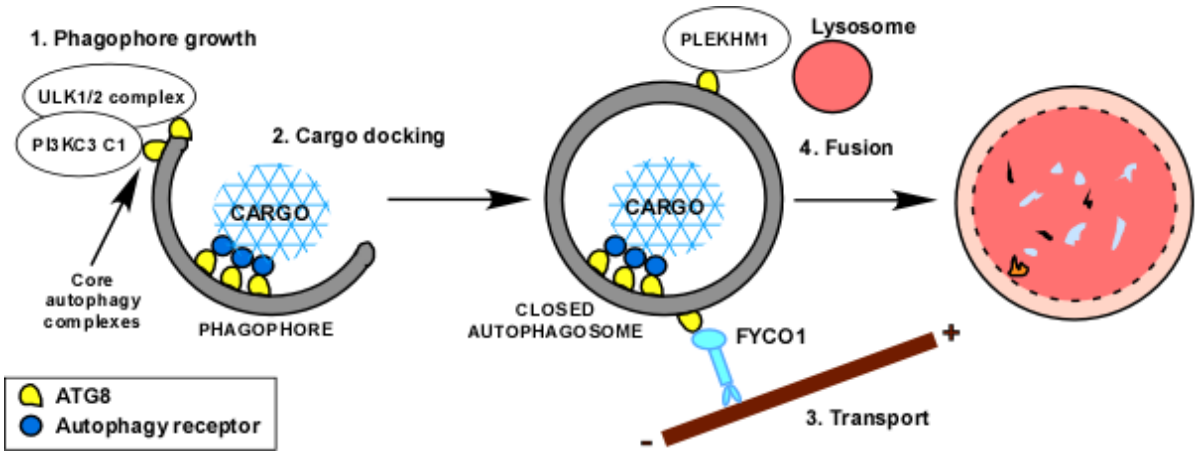

Figure 6. Main functions of lipidated ATG8 proteins. Lipidation of GABARAPs to the rim of the growing phagophore facilitates phagophore growth by recruiting LIR-containing basal autophagy proteins like ULK1 and ATG14 (1). Lipidation of ATG8s to the inner surface of the growing phagophore is essential in selective autophagy, since it is necessary for the docking of cargos to the phagophore. (2). Lipidation of ATG8s to closed autophagosomes promote maturation by recruiting proteins involved in transport of autophagosomes (3) or fusion of autophagosomes with lysosomes (4).

The closure of the phagophore to form an autophagosome is completed by membrane abscission mediated by the endosomal complex required for transport (ESCRT). Following closure, the autophagosome undergoes maturation, which involves fusion with lysosomes or late endosomes to from autolysosome in a poorly understood process. The fusion machinery involves SNARE proteins including syntaxin 17 (STX17) and synaptosomal-associated protein 29 (SNAP29) on the autophagosome; and vesicle-associated membrane protein 8 (VAMP8) on the lysosome. The homotypic fusion and protein sorting (HOPS) complex mediates membrane tethering to support the SNARE-mediated sorting and is recruited by

ATG8. Fusion is followed by degradation of the contents (Dikic and Elazar, 2018, Matsuzawa-Ishimoto et al., 2018, Yu et al., 2018).

4.5 Selective macroautophagy is initiated by cargo

The selectivity in autophagy is mediated by selective autophagy receptors (SARs), which link the cargo material to the phagophore membranes (Gatica et al., 2018, Johansen and Lamark, 2011, Johansen and Lamark, 2019, Kirkin, 2019, Stolz et al., 2014). The linkage involves SAR binding to the cargo on one hand and to the ATG8 family proteins on the phagophore membrane on the other (Birgisdottir et al., 2013, Johansen and Lamark, 2019, Pankiv et al., 2007, Rogov et al., 2014). In the classical model of mammalian selective autophagy, the cargo receptors act downstream of the autophagy machinery to tether the cargo to the ATG8-family proteins on the autophagosome membrane. While this model may be correct in the case of starvation-induced autophagy where some cargoes are selectively degraded (Turco et al., 2019a, Zaffagnini and Martens, 2016), it has emerged from recent studies that the cargo receptors also act upstream by promoting autophagosome formation around the cargo material destined for degradation by recruiting the autophagy machinery including ULK1/2 kinase complex and ATG8 proteins. This has been termed “cargo-induced selective” autophagy to reflect the fact that it is the presence of the cargo that induces autophagy (Fracchiolla et al., 2016, Kamber et al., 2015, Lazarou et al., 2015, Ravenhill et al., 2019, Smith et al., 2018, Turco et al., 2019a, Turco et al., 2019b, Vargas et al., 2019).

The interaction of SARs with ATG8 family proteins is mediated by a LIR (LC3 interacting region) motif, which has a core sequence of [W/F/Y]xx[L/V/I], but also contains negatively charged residues inside or adjacent to the core motif. This motif interacts with a LIR docking site (LDS) in the ATG8 family protein, consisting of two hydrophobic pockets mediating the interaction with the core motif and adjacent positively charged side chains forming electrostatic interactions (Johansen and Lamark, 2019, Wirth et al., 2019). Recently, it has emerged that ATG8 family proteins may also recognize ubiquitin-interacting motif (UIM)-like sequences present on some receptors, like RPN10, to recruit cargo-receptor complexes to the phagophore membranes (Marshall et al., 2019a). The binding site for UIM-like motifs is called UIM-docking site (UDS) and is on the opposite side of the ATG8 molecule relative to the LDS.

4.6 ER-phagy monitors ER quantity and protein quality

ER-phagy is a form of autophagy that engulfs specific portions of the ER and targets them for degradation in the lysosome (Figure 7). In response to pathological or physiological conditions such as nutrients deprivation, accumulation of misfolded proteins, or exposure to chemicals, the ER increases in size through increased synthesis of ER resident proteins to augment its functions and restore homeostasis (Bernales et al., 2006, Wilkinson, 2019b). ER-phagy targets the misfolded proteins for degradation and during recovery, it also sequesters the excess ER components for degradation to restore the physiological size. Thus, ER-phagy can be viewed both as an ER protein quality control mechanism and as an ER scaling down mechanism.

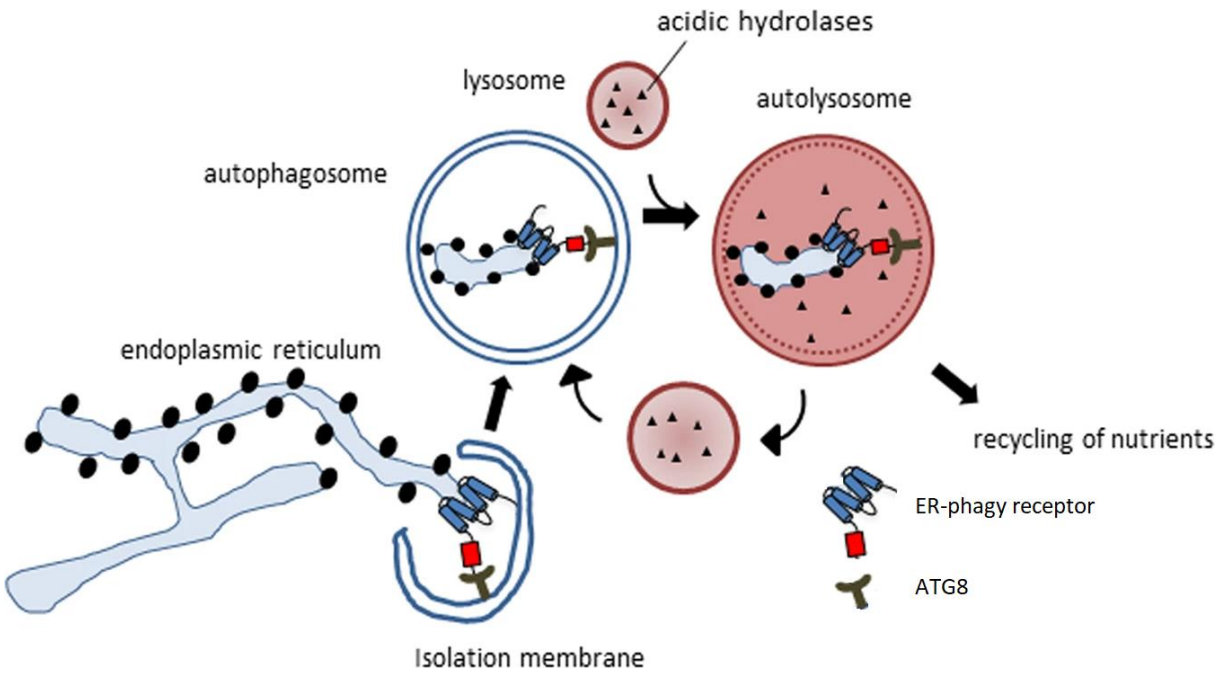

Figure 7. The process of ER-phagy. ER-phagy receptors recruit autophagy machinery to the ER fragments by binding to ATG8 proteins. This allows formation of autophagosomes around the portions which are then delivered to the lysosome for degradation. Figure adapted with permission from (Hübner and Dikic, 2019).

ER-phagy uses cargo receptors to target specific ER subdomains and sub-compositions for degradation. ER-phagy in yeast is mediated by two receptors, Atg39 and Atg40 (Mochida et al., 2015). In mammals, seven ER-phagy receptors, targeting different ER subdomains for degradation, have so far been identified: FAM134B, RTN3L, SEC62, CCPG1, ATL3, TEX264 and p62 (An et al., 2019a, Chen et al., 2019, Chino et al., 2019, Fumagalli et al., 2016, Grumati et al., 2017a, Khaminets et al., 2015, Smith et al., 2018) (Figure 8). FAM134B mediates starvation-induced ER-phagy in mammalian cells and localizes at the curved edges of ER sheets via a reticulon homology domain (RHD). The RHD is thought to be involved in promoting membrane curvature during autophagosome formation (Khaminets et al., 2015). Misfolded protein aggregates formed by Niemann–Pick type C disease protein and mutant type I procollagen (PC1) have also been identified as FAM134B ER cargoes (Forrester et al., 2019, Schultz et al., 2018).

The ER-phagy receptors RTN3L and ATL3 mediate starvation-induced degradation of ER tubules. Similar to FAM134B, RTN3 contains a reticulon homology domain (Chen et al., 2019, Grumati et al., 2017b). SEC62 is a component of the translocation machinery in the ER. It acts as an ER-phagy receptor for the degradation of excess intraluminal cargo resulting from activation of UPR. This role is independent of its function in the translocation complex (Fumagalli et al., 2016). CCPG1 is an ER transmembrane protein which is up-regulated during ER stress to mediate removal of portions of the peripheral ER that contain insoluble protein aggregates (Smith et al., 2018). TEX264 ER-phagy receptor functions at the three-way junctions and was found responsible for the turnover of a large number of ER proteins during nutrient starvation (An et al., 2019b, Chino et al., 2019). SQSTM1/p62 is the only soluble ER-phagy receptor identified so far. It acts with the ER transmembrane E3 ligase TRIM13 to mediate proteotoxic stress-induced ER-phagy via the N-degron pathway (Ji et al., 2019). This ER-phagy process is activated by the binding of p62 to N-terminally arginylated proteins and is important in ER protein quality control. The involvement of p62 in this ER-phagy shows that resident ER proteins and soluble SARs may co-operate in ER-phagy processes. It is not known whether the receptors co-operate to promote degradation of the ER and how such co-operation could be regulated. Loss of the known receptors does not block ER-phagy completely and the effects of their loss appears to be tissue-restricted (Wilkinson, 2019b), suggesting existence of yet unidentified receptors.

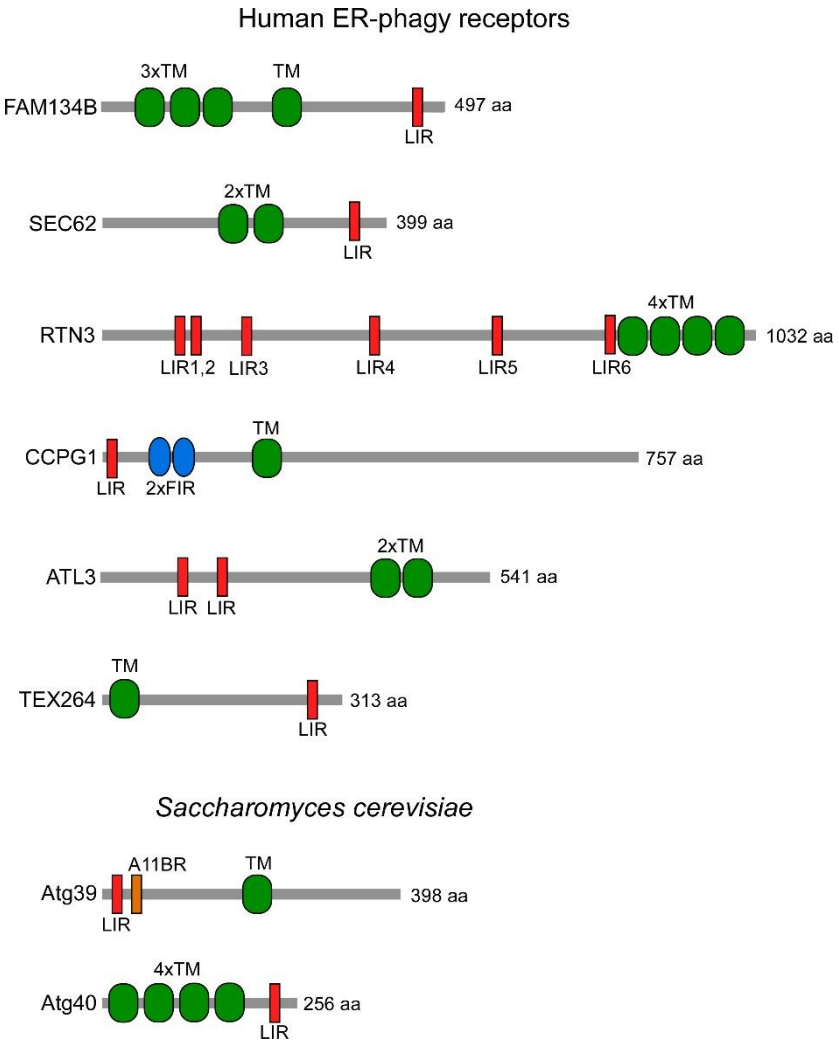

Fig 8. ER-phagy cargo receptors in human and yeast. Abbreviations: LIR, LC3-interacting region; FIR, FIP200-interacting region; A11BR, Atg11-binding region; TM, transmembrane.

5. CALCOCO1 start journey to autophagy

CALCOCO1 is an evolutionary conserved protein and a paralog to TAX1BP1 and NDP52, two well-known selective autophagy receptor proteins. The three proteins form a small protein family with substantial similarity and identity with a similar domain structure composed of an N-terminal SKICH domain, middle coil-coil regions (CC) and varying carboxy terminal (CT) regions that contain one or two zinc finger domains. In addition, they contain an atypical LIR (CLIR) motif (LVV) in the linker region between the SKICH domain and the coiled-coil domain (Tumbarello et al., 2015, von Muhlinen et al., 2012). An important difference between CALCOCO1 and its paralogs is the presence of ubiquitin-binding zinc

fingers in NDP52 and TAX1BP1. However, although CALCOCO1 contains a C-terminal zinc finger domain too, it does not bind to ubiquitin (Thurston et al., 2009). The C-terminus of NDP52 also interacts with galectins to mediate xenophagy (Thurston et al., 2012). This ability of TAX1BP1 and NDP52 to bind ubiquitin and, for NDP52, galectins, coupled with their ability to interact with ATG8 proteins, mediate their functions as autophagy receptors (Tumbarello et al., 2012, von Muhlinen et al., 2013, Whang et al., 2017). Interaction of CALCOCO1 with ATG8 proteins has not been characterized. However, two recent studies have associated CALCOCO1 with autophagy. In a quantitative proteomics study aimed at identifying novel and known autophagosome-enriched proteins in human cells, CALCOCO1 was found to be enriched in autophagosomes from pancreatic cancer cell lines (Mancias et al., 2014). CALCOCO1 was also one of the top hits in another quantitative proteomics study of proteins that were stabilized in ATG16L1 KO murine bone marrow-derived macrophages relative to WT controls (Samie et al., 2018). Previous studies have suggested CALCOCO1 function in transcriptional co-activation, glucose metabolism and calcium signalling and determined that CALCOCO1 mRNA is highly expressed in the rat brain (Kim et al., 2003, Takahashi et al., 2004).

6. Aims and objectives of the study

CALCOCO1 is a paralog to TAX1BP1 and NDP52, two well characterized autophagy receptors for the degradation of ubiquitinated cargoes and pathogenic bacteria in eukaryotic cells. The three proteins share substantial similarity and identity and have a similar domain structure composed of an N-terminal SKICH domain, middle coiled-coil regions and a C-terminal region that contains one or two zinc finger domains. Despite the similarity however, whether CALCOCO1 performs an autophagy-related function has hitherto not been known. The aim of the study therefore was to clarify role of CALCOCO1 in autophagy. Arising from this goal, the objectives of the study were thus defined:

i) Define whether CALCOCO1 is an autophagy substrate and clarify its interaction with ATG8 proteins.
ii) Determine protein interacting partners of CALCOCO1.
iii) Investigate the functional significance of the identified interactions and establish their relevance to the autophagy process.

7. Summary of papers

Paper I

CALCOCO1 acts with VAMP-Associated Proteins to mediate ER-phagy

Thaddaeus Mutugi Nthiga, Birendra Kumar Shrestha, Eva Sjøttem, Jack-Ansgar Bruun, Kenneth Bowitz Larsen, Trond Lamark and Terje Johansen

This study established that CALCOCO1 is homomeric and a proportion of the protein is localized in the Golgi apparatus. Functional studies revealed that CALCOCO1 is a soluble ER-phagy receptor for the degradation of tubular endoplasmic reticulum in response to proteotoxic and starvation-induced stress. On the ER membrane, CALCOCO1 interacts with VAMP-associated proteins VAPA and VAPB via an evolutionary conserved FFAT-like motif and recruits autophagy machinery by binding directly to ATG8 proteins via LIR and UDS interacting region (UIR) motifs acting co-dependently. Depletion of CALCOCO1 caused expansion of the ER and inefficient basal autophagy flux.

Paper II

Regulation of Golgi turnover by CALCOCO1-mediated selective autophagy

Thaddaeus Mutugi Nthiga, Birendra Kumar Shrestha, Jack-Ansgar Bruun, Kenneth Bowitz Larsen, Terje Johansen and Trond Lamark

Involvement of autophagy in the degradation of Golgi apparatus is, for the first time, demonstrated in this study and CALCOCO1 is revealed to be the selective autophagy receptor for the degradation in response to nutrients deprivation. CALCOCO1 interaction with the Golgi membrane occurs by binding to the cytoplasmic Ankyrin repeats (AR) domains of cis-Golgi localized palmitoyltransferases ZDHHC17 and ZDHHC13 via an evolutionary conserved zDHHC-AR-binding motif (zDABM) located at the C-terminal half of the protein. The zDABM motif was also identified and validated in the C-terminal region of TAX1BP1. Golgi stress response signalling increases the amount of Golgi components including structural proteins and enzymes and autophagy degrades the excess components to scale down the Golgi to pre-stress status. Inhibition of autophagy or depletion of CALCOCO1 caused expansion of the Golgi and accumulation of its structural and transmembrane proteins.

8. Discussion

The studies in this thesis have characterized new biochemical, molecular and interaction features of CALCOCO1 and in the process uncovered its function as a selective ER-phagy and Golgiphagy receptor. While cytoplasmic localization of CALCOCO1 was previously reported (Stadler et al., 2013, Wiemann et al., 2004, Yang et al., 2006), this study revealed extensive co-localization of CALCOCO1 with Golgi apparatus and the endoplasmic reticulum. The discovery of Golgi and ER localization means that CALCOCO1 performs functions that have not been imagined previously. About 30% of proteins in a CALCOCO1 interactome, generated by affinity purification mass spectrometry-based screen, were associated with either the Golgi or ER, suggesting that CALCOCO1 is a component of protein complexes formed by Golgi- and ER-associated proteins.

The SKICH domain, atypical LIR motif, LVV, and coiled-coil domain are extremely well conserved features of the CALCOCO protein family with most variations occurring at the C-termini (Figure 9). Whereas the coiled-coil domains of CALCOCO1 paralogs, TAX1BP1 and NDP52, have previously been shown to mediate homodimerization and heterodimerization with each other (Ling and Goeddel, 2000, Morriswood et al., 2007b, Sternsdorf et al., 1997), the character of the coiled-coil domain of CALCOCO1 has hitherto not been known. The studies in paper I reveal that the coiled-coil domain of CALCOCO1 mediates homomerization, but unexpectedly, CALCOCO1 heterodimerizes with neither TAX1BP1 nor NDP52.

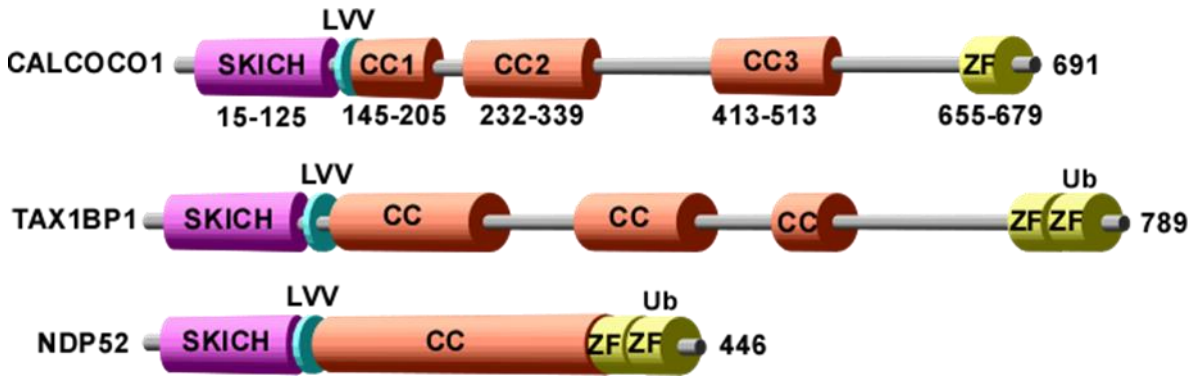

Figure 9. Domain organization of CALCOCO protein family. CC, coiled-coil; ZF, zinc finger; Ub, ubiquitin.

LIR motifs connect autophagy receptors to the autophagy machinery by interacting with LDS sites on ATG8 family proteins (Johansen and Lamark, 2019). Recently, a novel docking site on ATG8 family proteins for ubiquitin interacting motif (UIM)-like sequences present in some autophagy receptors was also reported. This UIM-docking site (UDS) is located on the opposite side of the ATG8 proteins relative to the LDS. This makes it possible for ATG8 proteins to simultaneously recruit both LIR- and UIM-containing proteins (Marshall et al., 2019b). The atypical LIR motif, so called because it engages only one LDS hydrophobic pocket instead of two, was first described in NDP52 and shown to be an LC3C-only interacting motif, hence was termed CLIR (von Muhlinen et al., 2012). In this study however, we show that NDP52 also interacts strongly with GABARAP via the atypical LIR motif, suggesting that LVV is not an LC3C-only interacting motif.

CALCOCO1 preferentially interacts with GABARAP, GABARAPL1 and GABARAPL2. The mode of interaction however differs from that of NDP52 because in addition to the atypical LIR motif, we show that CALCOCO1 also interacts through a C-terminal region that binds to the UDS site of ATG8 proteins. We called this region of CALCOCO1 UDS interacting region (UIR) because it did not have homology to UIM-like sequences as described in some proteins (Marshall et al., 2019b). Both LIR and UIR of CALCOCO1 were required for strong interaction with ATG8 proteins and for efficient degradation by autophagy. TAX1BP1 also has a C-terminal UIR that binds to the UDS site of GABARAP, but comparison of the primary structures shows no sequence conservation between this region and the UIR of CALCOCO1, implying a convergent evolution of the binding function.

The SKICH and zinc finger domains of TAX1BP1 and NDP52 mediate important interactions that enable their functions as selective autophagy receptors. The SKICH domains of TAX1BP1 and NDP52 interact with ULK1 complex scaffolding protein FIP200 and TBK1 adaptor proteins NAP1 and SINTBAD, while the zinc finger domains bind ubiquitin (Ravenhill et al., 2019, Thurston et al., 2009). The C-terminal region of NDP52 and, as shown in paper I, TAX1BP1, also interacts with galectin-8, a protein which binds exposed host glycans on damaged *Salmonella*-containing vacuoles (Thurston et al., 2012). These interactions are critical for TAX1BP1 and NDP52 functions as autophagy receptors. The interaction with FIP200 and TBK1 adaptors mediates recruitment of the upstream core autophagy machinery to initiate autophagosome formation in the vicinity of microbe-containing vacuoles and ubiquitinated cargoes (Ravenhill et al., 2019). In contrast, CALCOCO1 binds neither FIP200, TBK1 adaptors, ubiquitin nor, as shown in paper I,

galectins. This may clarify why CALCOCO1 has not been associated with autophagy receptor functions similar to its paralogs. However, we show in this thesis that CALCOCO1 has evolved alternative biochemical interaction features to mediate autophagy.

The C-terminal region of CALCOCO1, in addition to the UDS-interacting region (UIR) described above, also contains evolutionary conserved FFAT-like motif and zDHHC-AR-binding motif (zDABM) (Figure 10). The FFAT motif targets proteins to the cytoplasmic face of the endoplasmic reticulum by binding to the cytoplasmic MSP domains of VAP protein family. The consensus amino acid sequence of the core FFAT motif is EFFDAxE, where x is any amino acid. The core motif is supplemented by an upstream acidic tract region (Loewen et al., 2003b). The FFAT-like motif in CALCOCO1 encompasses 680-FFFSTQD-686 core sequence and differs from the canonical FFAT motif at positions 1, 2, 4 and 7, consistent with other FFAT-like motifs (Mikitova and Levine, 2012). The FFAT motif interaction with VAP involves both the acidic tract and the core FFAT motif (Furuita et al., 2010). The upstream acidic tract in CALCOCO1 overlaps with its zinc finger domain. This shows a divergent evolution of a function within the zinc finger region, different from the ubiquitin binding of the TAX1BP1 and NDP52 zinc finger domains (Thurston et al., 2009).

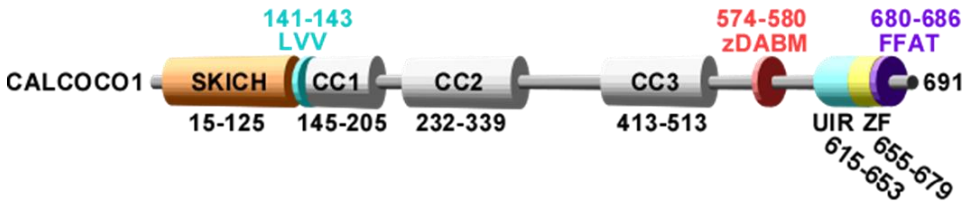

Figure 10. CALCOCO1 domain organization showing the locations of FFAT-like and zDABM motifs.

VAP proteins are predominantly located in the tubular subdomains of the peripheral endoplasmic reticulum (Wang et al., 2017). In response to ER stress, the cell engages an autoregulatory mechanism called unfolded proteins response (UPR) (Schröder, 2008). One of the consequences of UPR is increase in size of the peripheral ER through generation of sheets and tubules. Following UPR, the cell engages autophagy to degrade the excess portions of the ER (Bernales et al., 2006, Fumagalli et al., 2016). Our studies in paper I revealed that VAPA and VAPB recruit CALCOCO1 during proteotoxic and starvation-induced stress to mediate

degradation of the excess tubular ER. Therefore, we identified CALCOCO1 as a soluble ER-phagy receptor.

Most of the other identified ER-phagy receptors are ER-resident membrane proteins bearing ATG8-binding LIR motifs and include FAM134B, RTN3L, SEC62, CCPG1, ATL3, TEX264 (An et al., 2019b, Chen et al., 2019, Chino et al., 2019, Fumagalli et al., 2016, Grumati et al., 2017b, Khaminets et al., 2015, Smith et al., 2018). However, through binding to ER transmembrane E3 ligase TRIM13, p62 was recently identified as a mediator of proteotoxic stress-induced ER-phagy via the N-degron pathway (Ji et al., 2019). For CALCOCO1, we suggest a model where CALCOCO1 bound to VAPs, recruits the core autophagy machinery, via the ATG8 family proteins, to specific ER subdomains to initiate autophagosome biogenesis and capture of the degradable cargo.

The mechanism of the ER fragmentation and packaging into autophagosomes is not known but it is thought to require recognition by the autophagy machinery and morphological rearrangement of ER membrane by remodelling activities (Grumati et al., 2017b, Wilkinson, 2019c) . It is plausible to envisage that the autophagy machinery is assembled on extrusions that have been generated by either the remodelling activities or ER damage. In this case, the rate limiting step in ER-phagy, presumably, is the recruitment of the autophagy machinery to the extrusions to mediate autophagosome biogenesis. We postulate that CALCOCO1 mediates recognition of specific VAP-rich tubular ER portions by the autophagy machinery via ATG8 family proteins. This in turn initiates autophagosome biogenesis in the vicinity of those regions for engulfment and degradation, consistent with the emerging notion from recent studies that receptors act upstream of the autophagy machinery (Turco et al., 2019a, Kirkin, 2019). The co-localization of early phagophore markers WIPI2 and ATG13 with CALCOCO1 puncta during starvation in this study and with VAPA/B in a previous study (Zhao et al., 2018), supports this proposition.

CALCOCO1-VAP coupling has the capacity for generating and targeting ER tubular extrusions for degradation by autophagy. This proposistion is supported by ours and other studies as well. Our study shows that VAPs are stabilized during starvation-induced stress, suggesting readily availability on portions of the ER that may need to be degraded. The proposition is also supported by the fact that overexpression of VAPA/B causes ER punctuation. Interaction of VAP with FFAT motif-containing proteins may also regulate ER morphology (Kaiser et al., 2005). A recent study identified VAPs in interactomes of ER

reshaping RTN protein family (Grumati et al., 2017b), implying presence of VAPs in extrusions generated by membrane reshaping activities of RTN proteins.

Another driver of ER membrane rearrangement and packaging into autophagosomes is protein-protein interactions and self-interaction among receptors (Wilkinson, 2019a). Consistent with this notion, VAP interacts with itself via its coiled-coil domain to form homodimers and with other ER proteins via either the coiled-coil domain or the transmembrane domain to form oligomeric chains. In addition, dimerization could occur between two FFAT motifs already bound to the VAP (Kaiser et al., 2005, Kim et al., 2010). Because CALCOCO1 is dimeric according to this study, bivalent interaction with VAP dimers or oligomeric chains could target the ER membrane more tightly and recruit increased amounts of autophagy machinery proteins, resulting in increased morphological changes and fragmentation.

VAP-FFAT interactions have been associated with cytoskeletal organization, membrane trafficking, calcium signalling, ERAD, membrane contact sites and autophagosome biogenesis (Murphy and Levine, 2016, Zhao et al., 2018). An important question for future investigation is whether, apart from ER-phagy, CALCOCO1 is involved in any of these VAP-associated cellular functions. It is already reported that CALCOCO1 binds calcium via the C-terminal region (Takahashi et al., 2004), implying possible involvement in calcium metabolism. It would also be interesting to find out whether CALCOCO1 is part of membrane contact sites formed by VAPs between the ER and other organelles.

In paper II, we show for the first time that autophagy is involved in the degradation of Golgi apparatus. We also show that CALCOCO1 is a selective autophagy receptor for the degradation of Golgi membranes during nutrients starvation. CALCOCO1 interaction with the Golgi membrane occurs by binding to the cytoplasmic Ankyrin repeats (AR) domains of Golgi-localized palmitoyltransferases ZDHHC17 and ZDHHC13 via an evolutionary conserved zDHHC-AR-binding motif (zDABM). The zDABM motifs or closely related sequences have been identified in over 90 proteins and are characterized by VIAP)(VIT)XXQP core consensus sequence (Lemonidis et al., 2017a, Lemonidis et al., 2015a).

The zDABM motif in CALCOCO1 encompasses the core 574-VVISQP-580 sequence at the C-terminal half of the protein. The motif was also identified and validated in the C-terminal region of TAX1BP1, encompassing 673-VVCSQP-679 core sequence. However, the motif is

not conserved in NDP52. This suggest that, similar to CALCOCO1, TAX1BP1 could serve as a selective autophagy receptor for the degradation of Golgi membranes. Palmitoyltransferases, also called S-acyltransferases, are transmembrane enzymes which catalyse the reversible addition of fatty acids, typically palmitate, to cysteine residues of proteins. Mammals have 24 of these enzymes which typically are characterized by a cytoplasmic conserved catalytic Asp-His-His-Cys (DHHC) motif. Among the 24 palmitoyltransferases, only ZDHHC17 and ZDHHC13 contain AR domains, which typically recruit substrates but may also serve palmitoylation-independent functions (Lemonidis et al., 2015a). In this study, we show that the interaction of the AR domains of ZDHHC17/C13 with CALCOCO1 mediate starvation-induced degradation of Golgi membranes. To the extent that CALCOCO1 is not a palmitoylation substrate (Blanc et al., 2015), obviously this is a palmitoylation-independent function.

The results from this study suggest that under basal conditions, CALCOCO1 is anchored on the Golgi by ZDHHC17/13. Nutrients starvation induces fragmentation of the Golgi and delivery of those fragments to the autophagosomes in the cytoplasm. We suggest that the delivery of the fragments to the autophagosomes is mediated by CALCOCO1 (and TAX1BP1) interaction with the autophagy machinery. In this case, CALCOCO1 bound to ZDHHC17/13-enriched Golgi fragments or subdomains, recruit autophagy machinery via interaction with ATG8 family proteins to initiate autophagosome biogenesis and subsequent degradation of those portions of the Golgi. This proposition is consistent with the notion that autophagy receptors act upstream of the core autophagy machinery (Turco et al., 2019a). This view is firmed in the study by the showing that during starvation, the absence of CALCOCO1 or expression of CALCOCO1 lacking ATG8-binding LIR and UIR motifs, stabilized ZDHHC17/C13 and a subset of Golgi structural and membrane proteins including GM130 and TMEM165.

Because the zDABM motif has been identified in a large number of proteins (Lemonidis et al., 2017a), it is expected that the interaction of CALCOCO1 or TAX1BP1 with ZDHHC17/13 is transient under normal conditions. The recruitment of the autophagy machinery therefore could be what buttresses the interactions to form stable entities necessary for Golgi deformation, punctation and engulfment into autophagosomes. This is consistent with the already established notion that many cellular multi-component complexes do not exist as strong, stable entities, but instead, are assembled in a more stochastic manner with

transient encounter complexes being progressively buttressed by the combinatorial addition of further elements or ligands (Morriswood et al., 2007a, Tang et al., 2006).

Similar to the degradation of other organelles by autophagy, we presume that Golgi degradation is prompted by damage or the need to scale down the amount of Golgi following stress response. It has been shown previously that the Golgi apparatus is fragmented in response to pathological and physiological conditions such as bacterial and viral infections, neurodegenerative diseases and nutrient starvation (Campadelli et al., 1993, Takahashi et al., 2011, Gonatas et al., 2006). In addition, Golgi stress response increases the amount of Golgi by increasing synthesis of Golgi structural proteins such as GM130, GCP60 and giantin; glycosyltransferases and vesicular transport components (Sasaki and Yoshida, 2015). The involvement of CALCOCO1 in the selective degradation of Golgi membranes implies that it is involved in scaling down the amount of Golgi following stress response and potentially, in immunity. We demonstrate this in our study by showing that Golgi-resident proteins are degraded in a CALCOCO1-dependent manner.

The results from our study also suggest that CALCOCO1-ZDHHC17/13 interaction could be involved in trafficking to and from the Golgi. Overexpression of CALCOCO1 lacking the zDABM motif caused a fragmented Golgi phenotype. Previous studies show that overexpression of mutant forms of proteins that are involved in vesicular trafficking between the ER and the Golgi cause a similar phenotype of disassembled Golgi stacks (Wilson et al., 1994, Dascher and Balch, 1994). The disassembly of the Golgi stacks by the expression of mutant CALCOCO1 lacking the zDABM motif therefore suggest a disruption of trafficking to and from the Golgi, probably due to a dominant negative effect of the overexpressed mutant CALCOCO1. It is plausible to speculate that the interaction of CALCOCO1 with ZDHHC17/C13 play some role in vesicular trafficking to and from the Golgi, especially because CALCOCO1 is also bound via VAPs to ER tubes which typically are in close apposition to cis-Golgi (Venditti et al., 2019). The interactome of CALCOCO1 generated in this study identified proteins involved in the endocytic pathway as putative interactors, implying that the trafficking role could also be between the Golgi and other components of the endocytic pathway other than the ER. However, further investigations are needed to firm such a conclusion.

In conclusion, the studies uncovered CALCOCO1 as a common node in the degradation of the ER and Golgi components. The ER and the Golgi are functionally linked as constituents

of the secretory pathway and physically linked through protein complexes (Kawano et al., 2006) and play key roles in the pathogenesis of various human diseases (Gonatas et al., 2006, Mizushima and Komatsu, 2011, Rasika et al., 2019, Yoshida, 2007). For example, the ER and Golgi are exploited by bacteria and viruses during their infection cycles (Campadelli et al., 1993, Grumati et al., 2018, Junjhon et al., 2014, Welsch et al., 2009). ER-phagy is thought to be an active defense mechanism of the host cell in eliminating proliferating bacteria and viruses in the ER compartments (Chiramel and Best, 2018, Chiramel et al., 2016, Grumati et al., 2018, Lennemann and Coyne, 2017, Wu et al., 2014). Since Golgiphagy degrades Golgi membranes, it is plausible to postulate that it could play a role in eliminating viruses contained in the Golgi compartments. The role of CALCOCO1 in mediating ER-phagy and Golgiphagy therefore, has potential prognostic roles in multiple human pathologies associated with the ER and Golgi, including aging, cancer, neurodegenerative and infectious diseases.

9.0 Methodological considerations

9.1 Immunoprecipitation-based Mass spectrometry

Immunoprecipitation in combination with mass spectrometry (IP-MS) was used to identify protein interactors of CALCOCO1. In IP-MS, a target protein-specific antibody bound to a solid support is used to co-immunoprecipitate, from a complex mixture, proteins that are bound to the target protein. Following immunoprecipitation, proteins trapped on the antibody on the solid support are washed and eluted to obtain purified target and proteins bound to it. The co-immunoprecipitated proteins are then identified by mass spectrometry analysis and subsequently validated for direct interaction (Dunham et al., 2012). In this study EGFP-CALCOCO1 was immunoprecipitated from lysate of HEK 293 cells stably expressing EGFP-CALCOCO1 using anti-GFP antibody coupled to magnetic beads. The co-immunoprecipitated proteins were then identified by mass spectrometry. A negative control experiment using lysate from cells expressing EGFP only was carried out in parallel in order to filter for proteins that were non-specifically interacting with the antibody and beads.

While IP-MS is a powerful technique for identifying physiologically relevant protein-protein interactions, breakage of cells to prepare lysates causes proteins that are normally separated by membranes to come into contact leading to identification of physiologically irrelevant interactors. Despite negative control experiment to filter out nonspecific interactors, some nonspecific interactors of the IP reagents end up being identified as interactors (Dunham et al., 2012). The interactions of the identified proteins with the target protein are therefore tested by in vitro interaction assays using purified proteins. Accordingly, the interactions of CALCOCO1 with VAPA, VAPB and ZDHHC17 were validated by *in vitro* pulldown assays. Functional relevance of the interactions were validated successfully in cell-based studies such as microscopy and loss of function effects.

9.2 In vitro GST-pulldown assay

GST-pulldown assay was used to confirm interactions of CALCOCO1 with the putative interactor proteins identified in the IP-MS and to demarcate specific domains that were mediating those interactions. The assay involves mixing a GST-tagged protein that is immobilized on glutathione sepharose beads with a second protein that has been *in vitro* translated in the presence of radioactive methionine (^{35}S-methionine). After incubating in a

rotor to allow for binding, the beads are washed and the protein complexes then eluted from the beads by boiling in sample buffer and finally resolved by SDS-PAGE. The SDS-PAGE gels are dried and subsequently analysed by autoradiography for the presence or absence of interactions (Sambrook and Russell, 2006).

For the studies in this thesis, CALCOCO1 or the target protein was either tagged with GST and immobilized on glutathione sepharose beads or in vitro-translated from a T7 promoter-containing vector in the presence of ^{35}S-methionine using TNT T7 reticulocyte Lysate system. Although in vitro pulldown assay is a powerful technique for validating direct protein-protein interactions, it can generate false positive and false negative interactions with the false positives being physiologically irrelevant. In cells, proteins are folded and posttrnslationally modified to acquire their native conformations, the form with which they interact with other proteins. In vitro-translated proteins may fail to acquire the correct folding leading to proteins that could otherwise interact in cells not interacting. In vitro pulldown assay brings together proteins that in cells are normally in different organelles or membranes, thereby enabling interactions that are physiologically irrelevant. This is especially common if the proteins involved have unfolded or flexible regions, which are relatively sticky and therefore binds non-specifically to other proteins (Wissmueller et al., 2011).

Integral membrane proteins are highly hydrophobic and tend to form aggregates in solution. For this reason, they are difficult to purify from bacteria or to *in vitro*-translate. Pull down assays therefore could not be carried out with several putative interactors of CALCOCO1 because it was not possible to *in vitro*-translate them or purify them from bacteria.

9.3 CRISPR/Cas9 technology

CRISPR/Cas9 technique was used in this study to generate CALCOCO1 knock out (KO) cells. CRISPR (Clustered Regularly Interspaced Short Palindromic Repeats) are DNA sequences that form part of bacterial defense system and the basis for CRISPR-Cas9 genome editing technology. CRISPR consists of repeating sequences of bacterial DNA interspaced by spacer sequences which are remnants of viral DNA from past viral invasions (Wright et al., 2016, Lander, 2016). The spacer sequences act as genetic memory that guide the bacteria to detect and destroy the virus when repeat invasions occur. The guidance mechanism is that the CRISPR sequences are transcribed into short RNA sequences which fuse with and guide Cas nucleases to matching DNA sequences which they then cut, hence destroying the virus. There

are many Cas enzymes in bacteria, the one that has been commonly used in CRISPR technology is Cas9. CRISPR/Cas9 technology is used to permanently edit or modify genes in living cells. It involves co-expression of CRISPR Cas9 nuclease and a guide RNA (gRNA) that is complementary to a target DNA sequence, into a cell. The target sequence must be immediately adjacent to a Protospacer Adjacent Motif (PAM). PAM sequences serves as the binding signal for Cas9 nuclease. Once expressed, the Cas9 protein and the gRNA form a complex and when the target DNA is found by the gRNA, Cas9 binds at the PAM sequence and cuts the target DNA sequence which then undergo mutations such as deletions and insertions as it is repaired by DNA repair mechanisms (Sternberg and Doudna, 2015, Anders and Jinek, 2014).

This study used wild type Cas9, which cuts DNA strands at the same place leaving blunt ends that often undergo mutations as they are rejoined. The gRNA can potentially bind to non-target genes leading to off-target effects by generating mutations at random sites. Because the wild type Cas9 nuclease was used in generating CALCOCO1 KO cells in this study, there was possibility of producing off-target effects. One of the effects observed in CALCOCO1 KO cells was decreased autophagy flux as evidenced by accumulation of autophagy receptors p62, NDP52 and NBR1. When the cells were reconstituted with wild type EGFP-CALCOCO1 however, the autophagy flux was restored, suggesting that the decreased autophagy flux was specific to CALCOCO1 KO and not a consequence of off-target effects.

9.4 Stable expression of proteins

Stable expression of EGFP-CALCOCO1/VAPs/ZDHHC17/ZDHHC13 were made using the Flp-In T-Rex system. The system is based on tetracycline-inducible expression of a gene of interest. For all the cells made in this study, the expression of the gene was under the control of tetracycline-inducible CMV promoter. Thus the level of expression is not equal or regulated as the endogenous protein. This has the potential consequence of producing detrimental effects or artefacts depending on whether the expression is too high or too low. The stable expression of tagged proteins in this study were necessitated by either lack of good anti-body for detecting the endogenous protein especially for microscopy or the need to reconstitute CALCOCO1 KO cells in order to reverse the effects of knocking out the protein.

Expression of tagged proteins also has the potential to mislocalize proteins in cells. For the experiments in this study, both a small tag like Myc and a big tag like EGFP produced similar

localization pattern in cells and it was therefore concluded that the tag did not affect CALCOCO1 localization.

9.5 Western blotting

Western blotting (WB) was extensively used in this study to detect and characterize the quantities of the studied target proteins that were present in cell extracts. The technique was developed in 1979 (Towbin et al., 1979) and involves separation of proteins in a complex mixture according to their masses by sodium dodecyl sulphate–polyacrylamide gel electrophoresis (SDS-PAGE), transfer of the separated proteins to a protein-binding membrane, probing for the target protein on the membrane by a primary anti-body specific to the protein and subsequently visualizing the protein by incubating the membrane with a secondary antibody coupled, commonly, to a chemiluminescence substrate. Despite its widespread use in molecular biology and biochemistry research, a sample readings of the published literature show lack of a unified WB protocol in terms of sample preparation, buffers used and interpretation of obtained results. This makes reproducibility of results between different research groups, and even different researchers, difficult. Another problem of western blotting is variation in transfer efficiencies between different experiments and sometimes between different parts of the same membrane. This makes relative comparison of results deceptive. This is particularly concerning because of the emerging trend of presenting western blotting results not as absolute certainties of biological phenomena but as statistical variables that can be determined by averages of dosimetrical data from several experiments. It is not difficult to see how one deceptive result, obtained because of the above stated reasons, can tilt the average to the desired or deceptive conclusion.

Relative comparison of target protein amounts in different samples is normally derived by normalising against a housekeeping protein loading control. The potential limitation of this is that when the protein of interest is expressed at low levels in a biological sample and a need arises to load more of the sample in order to be able to detect the protein. While the protein of interest may be in the dynamic range of the biological material being investigated, the amount of the housekeeping proteins, usually expressed at high levels, are not linear at high protein concentrations (Dittmer and Dittmer, 2006), that is, beyond certain amounts, antibodies are not able to detect differences in the amounts. As a result, there will be an appearance of equal loading while in reality it is a façade. As at present, there are no guidelines as to beyond what

amount should a housekeeping protein not be used as a loading control or, as a minimum, not be used as the basis for relative comparison of specific protein amounts in different samples.

In this study, various approaches were used to address these problems in the experiments. First, we believe that proper relative comparisons of proteins amounts should be within the same gel or membrane and the certainty of the results obtained should be based on reproducibility after repeated immunoblotting experiments of the same sample or different samples. Thus, the relative protein amounts between samples are presented within the same gel and not as averages of dosimetrical data from several experiments. This was done after validating the data by repeated western blotting experiments. At all times, an attempt was made to load the minimum amount of the sample that was needed to detect the target protein. When there was a need to load more of the sample in order to detect the protein of interest, that particular loading was not used for loading control comparisons. Instead, a separate immunoblotting for the housing keeping protein with lower amounts of protein loading was used.

10. References

Agarraberes, F. A., Terlecky, S. R. & Dice, J. F. 1997. An Intralysosomal hsp70 Is Required for a Selective Pathway of Lysosomal Protein Degradation. *The Journal of Cell Biology,* 137**,** 825.

Alemu, E. A., Lamark, T., Torgersen, K. M., Birgisdottir, A. B., Larsen, K. B., Jain, A., Olsvik, H., Overvatn, A., Kirkin, V. & Johansen, T. 2012. ATG8 family proteins act as scaffolds for assembly of the ULK complex: sequence requirements for LC3-interacting region (LIR) motifs. *J Biol Chem,* 287**,** 39275-90.

An, H., Ordureau, A., Paulo, J. A., Shoemaker, C. J., Denic, V. & Harper, J. W. 2019a. TEX264 Is an Endoplasmic Reticulum-Resident ATG8-Interacting Protein Critical for ER Remodeling during Nutrient Stress. *Mol Cell,* 74**,** 891-908.

An, H., Ordureau, A., Paulo, J. A., Shoemaker, C. J., Denic, V. & Harper, J. W. 2019b. TEX264 Is an Endoplasmic Reticulum-Resident ATG8-Interacting Protein Critical for ER Remodeling during Nutrient Stress. *Mol Cell*.

Anders, C. & Jinek, M. 2014. Chapter One - In Vitro Enzymology of Cas9. *In:* DOUDNA, J. A. & SONTHEIMER, E. J. (eds.) *Methods in Enzymology.* Academic Press.

Anding, A. L. & Baehrecke, E. H. 2017. Cleaning House: Selective Autophagy of Organelles. *Developmental Cell,* 41**,** 10-22.

B'chir, W., Maurin, A. C., Carraro, V., Averous, J., Jousse, C., Muranishi, Y., Parry, L., Stepien, G., Fafournoux, P. & Bruhat, A. 2013. The eIF2alpha/ATF4 pathway is essential for stress-induced autophagy gene expression. *Nucleic Acids Res,* 41**,** 7683-99.

Bandyopadhyay, U., Kaushik, S., Varticovski, L. & Cuervo, A. M. 2008. The Chaperone-Mediated Autophagy Receptor Organizes in Dynamic Protein Complexes at the Lysosomal Membrane. *Molecular and Cellular Biology,* 28**,** 5747.

Barr, F. A. & Short, B. 2003. Golgins in the structure and dynamics of the Golgi apparatus. *Current Opinion in Cell Biology,* 15**,** 405-413.

Bento, C. F., Renna, M., Ghislat, G., Puri, C., Ashkenazi, A., Vicinanza, M., Menzies, F. M. & Rubinsztein, D. C. 2016. Mammalian Autophagy: How Does It Work? *Annual Review of Biochemistry,* 85**,** 685-713.

Bernales, S., Mcdonald, K. L. & Walter, P. 2006. Autophagy Counterbalances Endoplasmic Reticulum Expansion during the Unfolded Protein Response. *PLOS Biology,* 4**,** e423.

Birgisdottir, A. B., Lamark, T. & Johansen, T. 2013. The LIR motif - crucial for selective autophagy. *J Cell Sci,* 126**,** 3237-47.

Birgisdottir, A. B., Mouilleron, S., Bhujabal, Z., Wirth, M., Sjottem, E., Evjen, G., Zhang, W., Lee, R., O'reilly, N., Tooze, S. A., Lamark, T. & Johansen, T. 2019. Members of the autophagy class III phosphatidylinositol 3-kinase complex I interact with GABARAP and GABARAPL1 via LIR motifs. *Autophagy,* 15**,** 1333-1355.

Blanc, M., David, F., Abrami, L., Migliozzi, D., Armand, F., Burgi, J. & Van Der Goot, F. G. 2015. SwissPalm: Protein Palmitoylation database. *F1000Res,* 4**,** 261.

Blaskovic, S., Adibekian, A., Blanc, M. & Van Der Goot, G. F. 2014. Mechanistic effects of protein palmitoylation and the cellular consequences thereof. *Chemistry and Physics of Lipids,* 180**,** 44-52.

Borgese, N., Francolini, M. & Snapp, E. 2006. Endoplasmic reticulum architecture: structures in flux. *Curr Opin Cell Biol,* 18**,** 358-64.

Braakman, I. & Hebert, D. N. 2013. Protein Folding in the Endoplasmic Reticulum. *Cold Spring Harbor Perspectives in Biology,* 5.

Bravo, R., Parra, V., Gatica, D., Rodriguez, A. E., Torrealba, N., Paredes, F., Wang, Z. V., Zorzano, A., Hill, J. A., Jaimovich, E., Quest, A. F. G. & Lavandero, S. 2013. Chapter Five - Endoplasmic Reticulum and the Unfolded Protein Response: Dynamics and Metabolic Integration. *In:* JEON, K. W. (ed.) *International Review of Cell and Molecular Biology.* Academic Press.

Campadelli, G., Brandimarti, R., Di Lazzaro, C., Ward, P. L., Roizman, B. & Torrisi, M. R. 1993. Fragmentation and dispersal of Golgi proteins and redistribution of glycoproteins and glycolipids processed through the Golgi apparatus after infection with herpes simplex virus 1. *Proceedings of the National Academy of Sciences,* 90**,** 2798.

Chen, Q., Xiao, Y., Chai, P., Zheng, P., Teng, J. & Chen, J. 2019. ATL3 Is a Tubular ER-Phagy Receptor for GABARAP-Mediated Selective Autophagy. *Current Biology,* 29**,** 846-855.e6.

Chen, S., Novick, P. & Ferro-Novick, S. 2013. ER structure and function. *Current Opinion in Cell Biology,* 25**,** 428-433.

Cherepanova, N., Shrimal, S. & Gilmore, R. 2016. N-linked glycosylation and homeostasis of the endoplasmic reticulum. *Curr Opin Cell Biol,* 41**,** 57-65.

Chiang, H. L. & Dice, J. F. 1988. Peptide sequences that target proteins for enhanced degradation during serum withdrawal. *Journal of Biological Chemistry,* 263**,** 6797-6805.

Chiang, H. L., Terlecky, Plant, C. P. & Dice, J. F. 1989. A role for a 70-kilodalton heat shock protein in lysosomal degradation of intracellular proteins. *Science,* 246**,** 382.

Chino, H., Hatta, T., Natsume, T. & Mizushima, N. 2019. Intrinsically Disordered Protein TEX264 Mediates ER-phagy. *Molecular Cell,* 74**,** 909-921.e6.

Chiramel, A. I. & Best, S. M. 2018. Role of autophagy in Zika virus infection and pathogenesis. *Virus Res,* 254**,** 34-40.

Chiramel, A. I., Dougherty, J. D., Nair, V., Robertson, S. J. & Best, S. M. 2016. FAM134B, the Selective Autophagy Receptor for Endoplasmic Reticulum Turnover, Inhibits Replication of Ebola Virus Strains Makona and Mayinga. *J Infect Dis,* 214**,** S319-s325.

Clermont, Y., Xia, L., Rambourg, A., Turner, J. D. & Hermo, L. 1993. Structure of the Golgi apparatus in stimulated and nonstimulated acinar cells of mammary glands of the rat. *Anat Rec,* 237**,** 308-17.

Cuervo, A. M. & Dice, J. F. 1996. A Receptor for the Selective Uptake and Degradation of Proteins by Lysosomes. *Science,* 273**,** 501.

Cuervo, A. M., Dice, J. F. & Knecht, E. 1997. A Population of Rat Liver Lysosomes Responsible for the Selective Uptake and Degradation of Cytosolic Proteins. *Journal of Biological Chemistry,* 272**,** 5606-5615.

Cuervo, A. M., Hildebrand, H., Bomhard, E. M. & Dice, J. F. 1999. Direct lysosomal uptake of α2-microglobulin contributes to chemically induced nephropathy. *Kidney International,* 55**,** 529-545.

Cuervo, A. M., Knecht, E., Terlecky, S. R. & Dice, J. F. 1995. Activation of a selective pathway of lysosomal proteolysis in rat liver by prolonged starvation. *American Journal of Physiology-Cell Physiology,* 269**,** C1200-C1208.

Cullinan, S. B., Zhang, D., Hannink, M., Arvisais, E., Kaufman, R. J. & Diehl, J. A. 2003. Nrf2 is a direct PERK substrate and effector of PERK-dependent cell survival. *Mol Cell Biol,* 23**,** 7198-209.

Dacks, J. B., Davis, L. a. M., Sjögren, Å. M., Andersson, J. O., Roger, A. J. & Doolittle, W. F. 2003. Evidence for Golgi bodies in proposed 'Golgi-lacking' lineages. *Proceedings of the Royal Society of London. Series B: Biological Sciences,* 270**,** S168-S171.

Dascher, C. & Balch, W. E. 1994. Dominant inhibitory mutants of ARF1 block endoplasmic reticulum to Golgi transport and trigger disassembly of the Golgi apparatus. *J Biol Chem,* 269**,** 1437-48.

De Matteis, M. A. & Morrow, J. S. 2000. Spectrin tethers and mesh in the biosynthetic pathway. *Journal of Cell Science,* 113**,** 2331.

Di Mattia, T., Wilhelm, L. P., Ikhlef, S., Wendling, C., Spehner, D., Nominé, Y., Giordano, F., Mathelin, C., Drin, G., Tomasetto, C. & Alpy, F. 2018. Identification of MOSPD2, a novel scaffold for endoplasmic reticulum membrane contact sites. *EMBO reports,* 19**,** e45453.

Dikic, I. & Elazar, Z. 2018. Mechanism and medical implications of mammalian autophagy. *Nature Reviews Molecular Cell Biology,* 19**,** 349-364.

Dinter, A. & Berger, E. G. 1998. Golgi-disturbing agents. *Histochemistry and Cell Biology,* 109**,** 571-590.

Dittmer, A. & Dittmer, J. 2006. Beta-actin is not a reliable loading control in Western blot analysis. *Electrophoresis,* 27**,** 2844-5.

Dunham, W. H., Mullin, M. & Gingras, A.-C. 2012. Affinity-purification coupled to mass spectrometry: Basic principles and strategies. *PROTEOMICS,* 12**,** 1576-1590.

English, A. R., Zurek, N. & Voeltz, G. K. 2009. Peripheral ER structure and function. *Current Opinion in Cell Biology,* 21**,** 596-602.

Ernst, A. M., Syed, S. A., Zaki, O., Bottanelli, F., Zheng, H., Hacke, M., Xi, Z., Rivera-Molina, F., Graham, M., Rebane, A. A., Björkholm, P., Baddeley, D., Toomre, D., Pincet, F. & Rothman, J. E. 2018. S-Palmitoylation Sorts Membrane Cargo for Anterograde Transport in the Golgi. *Developmental Cell,* 47**,** 479-493.e7.

Feng, Y., He, D., Yao, Z. & Klionsky, D. J. 2014. The machinery of macroautophagy. *Cell Research,* 24**,** 24-41.

Finn, P. F. & Dice, J. F. 2005. Ketone Bodies Stimulate Chaperone-mediated Autophagy. *Journal of Biological Chemistry,* 280**,** 25864-25870.

Forrester, A., De Leonibus, C., Grumati, P., Fasana, E., Piemontese, M., Staiano, L., Fregno, I., Raimondi, A., Marazza, A., Bruno, G., Iavazzo, M., Intartaglia, D., Seczynska, M., Van Anken, E., Conte, I., De Matteis, M. A., Dikic, I., Molinari, M. & Settembre, C. 2019. A selective ER-phagy exerts procollagen quality control via a Calnexin-FAM134B complex. *Embo j,* 38.

Fracchiolla, D., Sawa-Makarska, J., Zens, B., Ruiter, A. D., Zaffagnini, G., Brezovich, A., Romanov, J., Runggatscher, K., Kraft, C., Zagrovic, B. & Martens, S. 2016. Mechanism of cargo-directed Atg8 conjugation during selective autophagy. *eLife,* 5**,** e18544.

Fukata, M., Fukata, Y., Adesnik, H., Nicoll, R. A. & Bredt, D. S. 2004. Identification of PSD-95 Palmitoylating Enzymes. *Neuron,* 44**,** 987-996.

Fukata, Y. & Fukata, M. 2010. Protein palmitoylation in neuronal development and synaptic plasticity. *Nature Reviews Neuroscience,* 11**,** 161.

Fumagalli, F., Noack, J., Bergmann, Timothy j., Cebollero, E., Pisoni, Giorgia b., Fasana, E., Fregno, I., Galli, C., Loi, M., Soldà, T., D'antuono, R., Raimondi, A., Jung, M., Melnyk, A., Schorr, S., Schreiber, A., Simonelli, L., Varani, L., Wilson-Zbinden, C., Zerbe, O., Hofmann, K., Peter, M., Quadroni, M., Zimmermann, R. & Molinari, M. 2016. Translocon component Sec62 acts in endoplasmic reticulum turnover during stress recovery. *Nature Cell Biology,* 18**,** 1173.

Furuita, K., Jee, J., Fukada, H., Mishima, M. & Kojima, C. 2010. Electrostatic Interaction between Oxysterol-binding Protein and VAMP-associated Protein A Revealed by NMR and Mutagenesis Studies. *Journal of Biological Chemistry,* 285**,** 12961-12970.

Galluzzi, L., Baehrecke, E. H., Ballabio, A., Boya, P., Bravo-San Pedro, J. M., Cecconi, F., Choi, A. M., Chu, C. T., Codogno, P., Colombo, M. I., Cuervo, A. M., Debnath, J., Deretic, V., Dikic, I., Eskelinen, E.-L., Fimia, G. M., Fulda, S., Gewirtz, D. A., Green, D. R., Hansen, M., Harper, J. W., Jäättelä, M., Johansen, T., Juhasz, G., Kimmelman, A. C., Kraft, C., Ktistakis, N. T., Kumar, S., Levine, B., Lopez-Otin, C., Madeo, F., Martens, S., Martinez, J., Melendez, A., Mizushima, N., Münz, C., Murphy, L. O., Penninger, J. M., Piacentini, M., Reggiori, F., Rubinsztein, D. C., Ryan, K. M., Santambrogio, L., Scorrano, L., Simon, A. K., Simon, H.-U., Simonsen, A., Tavernarakis, N., Tooze, S. A., Yoshimori, T., Yuan, J., Yue, Z., Zhong, Q. & Kroemer, G. 2017. Molecular definitions of autophagy and related processes. *The EMBO Journal,* 36**,** 1811-1836.

Gatica, D., Lahiri, V. & Klionsky, D. J. 2018. Cargo recognition and degradation by selective autophagy. *Nat Cell Biol,* 20**,** 233-242.

Golgi, C. & Lipsky, N. G. 1989. On the structure of nerve cells1. *Journal of Microscopy,* 155**,** 3-7.

Gonatas, N. K., Stieber, A. & Gonatas, J. O. 2006. Fragmentation of the Golgi apparatus in neurodegenerative diseases and cell death. *J Neurol Sci,* 246**,** 21-30.

Goyal, U. & Blackstone, C. 2013. Untangling the web: Mechanisms underlying ER network formation. *Biochimica et Biophysica Acta (BBA) - Molecular Cell Research,* 1833**,** 2492-2498.

Graef, M. 2018. Membrane tethering by the autophagy ATG2A-WIPI4 complex. *Proceedings of the National Academy of Sciences,* 115**,** 10540.

Griffiths, G., Pfeiffer, S., Simons, K. & Matlin, K. 1985. Exit of newly synthesized membrane proteins from the trans cisterna of the Golgi complex to the plasma membrane. *The Journal of Cell Biology,* 101**,** 949.

Grumati, P., Dikic, I. & Stolz, A. 2018. ER-phagy at a glance. *J Cell Sci,* 131.

Grumati, P., Morozzi, G., Holper, S., Mari, M., Harwardt, M. I., Yan, R., Muller, S., Reggiori, F., Heilemann, M. & Dikic, I. 2017a. Full length RTN3 regulates turnover of tubular endoplasmic reticulum via selective autophagy. *eLife,* 6**,** e25555.

Grumati, P., Morozzi, G., Holper, S., Mari, M., Harwardt, M. I., Yan, R., Muller, S., Reggiori, F., Heilemann, M. & Dikic, I. 2017b. Full length RTN3 regulates turnover of tubular endoplasmic reticulum via selective autophagy. *Elife,* 6.

Hager, K. M., Striepen, B., Tilney, L. G. & Roos, D. S. 1999. The nuclear envelope serves as an intermediary between the ER and Golgi complex in the intracellular parasite Toxoplasma gondii. *J Cell Sci,* 112 (Pt 16)**,** 2631-8.

Harada, T., Matsuzaki, O., Hayashi, H., Sugano, S., Matsuda, A. & Nishida, E. 2003. AKRL1 and AKRL2 activate the JNK pathway. *Genes to Cells,* 8**,** 493-500.

Harding, H. P., Zhang, Y., Zeng, H., Novoa, I., Lu, P. D., Calfon, M., Sadri, N., Yun, C., Popko, B., Paules, R., Stojdl, D. F., Bell, J. C., Hettmann, T., Leiden, J. M. & Ron, D. 2003. An integrated stress response regulates amino acid metabolism and resistance to oxidative stress. *Mol Cell,* 11**,** 619-33.

Haze, K., Yoshida, H., Yanagi, H., Yura, T. & Mori, K. 1999. Mammalian Transcription Factor ATF6 Is Synthesized as a Transmembrane Protein and Activated by Proteolysis in Response to Endoplasmic Reticulum Stress. *Molecular Biology of the Cell,* 10**,** 3787-3799.

He, C. Y., Ho, H. H., Malsam, J., Chalouni, C., West, C. M., Ullu, E., Toomre, D. & Warren, G. 2004. Golgi duplication in Trypanosoma brucei. *J Cell Biol,* 165**,** 313-21.

Hebert, D. N., Foellmer, B. & Helenius, A. 1995. Glucose trimming and reglucosylation determine glycoprotein association with calnexin in the endoplasmic reticulum. *Cell,* 81**,** 425-33.

Hemsley, P. A. & Grierson, C. S. 2011. The Ankyrin Repeats and DHHC S-acyl Transferase Domain of AKR1 Act Independently to Regulate Switching from Vegetative to Mating States in Yeast. *PLOS ONE,* 6**,** e28799.

Henderson, G. P., Gan, L. & Jensen, G. J. 2007. 3-D ultrastructure of O. tauri: electron cryotomography of an entire eukaryotic cell. *PLoS One,* 2**,** e749.

Hicks, S. W. & Machamer, C. E. 2005. Golgi structure in stress sensing and apoptosis. *Biochimica et Biophysica Acta (BBA) - Molecular Cell Research,* 1744**,** 406-414.

Hollien, J., Lin, J. H., Li, H., Stevens, N., Walter, P. & Weissman, J. S. 2009. Regulated Ire1-dependent decay of messenger RNAs in mammalian cells. *The Journal of Cell Biology,* 186**,** 323.

Huang, K., Sanders, S. S., Kang, R., Carroll, J. B., Sutton, L., Wan, J., Singaraja, R., Young, F. B., Liu, L., El-Husseini, A., Davis, N. G. & Hayden, M. R. 2011. Wild-type HTT modulates the enzymatic activity of the neuronal palmitoyl transferase HIP14. *Hum Mol Genet,* 20**,** 3356-65.

Hubbi, M. E., Hu, H., Kshitiz, Ahmed, I., Levchenko, A. & Semenza, G. L. 2013. Chaperone-mediated Autophagy Targets Hypoxia-inducible Factor-1α (HIF-1α) for Lysosomal Degradation. *Journal of Biological Chemistry,* 288**,** 10703-10714.

Hübner, C. A. & Dikic, I. 2019. ER-phagy and human diseases. *Cell Death & Differentiation*.

Jennings, B. C. & Linder, M. E. 2012. DHHC Protein S-Acyltransferases Use Similar Ping-Pong Kinetic Mechanisms but Display Different Acyl-CoA Specificities. *Journal of Biological Chemistry,* 287**,** 7236-7245.

Ji, C. H., Kim, H. Y., Heo, A. J., Lee, S. H., Lee, M. J., Kim, S. B., Srinivasrao, G., Mun, S. R., Cha-Molstad, H., Ciechanover, A., Choi, C. Y., Lee, H. G., Kim, B. Y. & Kwon, Y. T. 2019. The N-Degron Pathway Mediates ER-phagy. *Mol Cell,* 75**,** 1058-1072 e9.

Johansen, T. & Lamark, T. 2011. Selective autophagy mediated by autophagic adapter proteins. *Autophagy,* 7**,** 279-296.

Johansen, T. & Lamark, T. 2019. Selective Autophagy: ATG8 Family Proteins, LIR Motifs and Cargo Receptors. *Journal of Molecular Biology*.

Junjhon, J., Pennington, J. G., Edwards, T. J., Perera, R., Lanman, J. & Kuhn, R. J. 2014. Ultrastructural Characterization and Three-Dimensional Architecture of Replication Sites in Dengue Virus-Infected Mosquito Cells. *Journal of Virology,* 88**,** 4687.

Kaiser, S. E., Brickner, J. H., Reilein, A. R., Fenn, T. D., Walter, P. & Brunger, A. T. 2005. Structural Basis of FFAT Motif-Mediated ER Targeting. *Structure,* 13**,** 1035-1045.

Kamber, Roarke a., Shoemaker, Christopher j. & Denic, V. 2015. Receptor-Bound Targets of Selective Autophagy Use a Scaffold Protein to Activate the Atg1 Kinase. *Molecular Cell,* 59**,** 372-381.

Karagöz, G. E., Acosta-Alvear, D. & Walter, P. 2019. The Unfolded Protein Response: Detecting and Responding to Fluctuations in the Protein-Folding Capacity of the Endoplasmic Reticulum. *Cold Spring Harbor Perspectives in Biology,* 11.

Kaushik, S. & Cuervo, A. M. 2015. Degradation of lipid droplet-associated proteins by chaperone-mediated autophagy facilitates lipolysis. *Nature Cell Biology,* 17**,** 759.

Kaushik, S. & Cuervo, A. M. 2018. The coming of age of chaperone-mediated autophagy. *Nature Reviews Molecular Cell Biology,* 19**,** 365-381.

Kawano, M., Kumagai, K., Nishijima, M. & Hanada, K. 2006. Efficient Trafficking of Ceramide from the Endoplasmic Reticulum to the Golgi Apparatus Requires a VAMP-associated Protein-interacting FFAT Motif of CERT. *Journal of Biological Chemistry,* 281**,** 30279-30288.

Khaminets, A., Heinrich, T., Mari, M., Grumati, P., Huebner, A. K., Akutsu, M., Liebmann, L., Stolz, A., Nietzsche, S., Koch, N., Mauthe, M., Katona, I., Qualmann, B., Weis, J., Reggiori, F., Kurth, I., Hubner, C. A. & Dikic, I. 2015. Regulation of endoplasmic reticulum turnover by selective autophagy. *Nature,* 522**,** 354-8.

Kiffin, R., Christian, C., Knecht, E. & Cuervo, A. M. 2004. Activation of Chaperone-mediated Autophagy during Oxidative Stress. *Molecular Biology of the Cell,* 15**,** 4829-4840.

Kim, J. H., Li, H. & Stallcup, M. R. 2003. CoCoA, a nuclear receptor coactivator which acts through an N-terminal activation domain of p160 coactivators. *Mol Cell,* 12**,** 1537-49.

Kim, S., Leal, S. S., Ben Halevy, D., Gomes, C. M. & Lev, S. 2010. Structural Requirements for VAP-B Oligomerization and Their Implication in Amyotrophic Lateral Sclerosis-associated VAP-B(P56S) Neurotoxicity. *Journal of Biological Chemistry,* 285**,** 13839-13849.

Kirkin, V. 2019. History of the Selective Autophagy Research: How Did It Begin and Where Does It Stand Today? *Journal of Molecular Biology*.

Kirkin, V. & Rogov, V. V. 2019. A Diversity of Selective Autophagy Receptors Determines the Specificity of the Autophagy Pathway. *Molecular Cell,* 76**,** 268-285.

Klute, M. J., Melançon, P. & Dacks, J. B. 2011. Evolution and Diversity of the Golgi. *Cold Spring Harbor Perspectives in Biology,* 3.

Kunz, J. B., Schwarz, H. & Mayer, A. 2004. Determination of Four Sequential Stages during Microautophagy in Vitro. *Journal of Biological Chemistry,* 279**,** 9987-9996.

Ladinsky, M. S., Wu, C. C., Mcintosh, S., Mcintosh, J. R. & Howell, K. E. 2002. Structure of the Golgi and distribution of reporter molecules at 20 degrees C reveals the complexity of the exit compartments. *Mol Biol Cell,* 13**,** 2810-25.

Lander, Eric s. 2016. The Heroes of CRISPR. *Cell,* 164**,** 18-28.

Lazarou, M., Sliter, D. A., Kane, L. A., Sarraf, S. A., Wang, C., Burman, J. L., Sideris, D. P., Fogel, A. I. & Youle, R. J. 2015. The ubiquitin kinase PINK1 recruits autophagy receptors to induce mitophagy. *Nature,* 524**,** 309.

Leão-Helder, A. N., Krikken, A. M., Gellissen, G., Van Der Klei, I. J., Veenhuis, M. & Kiel, J. a. K. W. 2004. Atg21p is essential for macropexophagy and microautophagy in the yeast Hansenula polymorpha. *FEBS Letters,* 577**,** 491-495.

Lee, T. H. & Linstedt, A. D. 1999. Osmotically Induced Cell Volume Changes Alter Anterograde and Retrograde Transport, Golgi Structure, and COPI Dissociation. *Molecular Biology of the Cell,* 10**,** 1445-1462.

Lemasters, J. J. 2014. Variants of mitochondrial autophagy: Types 1 and 2 mitophagy and micromitophagy (Type 3). *Redox Biology,* 2**,** 749-754.

Lemonidis, K., Gorleku, O. A., Sanchez-Perez, M. C., Grefen, C. & Chamberlain, L. H. 2014. The Golgi S-acylation machinery comprises zDHHC enzymes with major differences in substrate affinity and S-acylation activity. *Molecular Biology of the Cell,* 25**,** 3870-3883.

Lemonidis, K., Macleod, R., Baillie, G. S. & Chamberlain, L. H. 2017a. Peptide array-based screening reveals a large number of proteins interacting with the ankyrin-repeat domain of the zDHHC17 S-acyltransferase. *Journal of Biological Chemistry,* 292**,** 17190-17202.

Lemonidis, K., Salaun, C., Kouskou, M., Diez-Ardanuy, C., Chamberlain, L. H. & Greaves, J. 2017b. Substrate selectivity in the zDHHC family of S-acyltransferases. *Biochemical Society Transactions,* 45**,** 751-758.

Lemonidis, K., Sanchez-Perez, M. C. & Chamberlain, L. H. 2015a. Identification of a Novel Sequence Motif Recognized by the Ankyrin Repeat Domain of zDHHC17/13 S-Acyltransferases. *Journal of Biological Chemistry,* 290**,** 21939-21950.

Lemonidis, K., Werno, M. W., Greaves, J., Diez-Ardanuy, C., Sanchez-Perez, M. C., Salaun, C., Thomson, D. M. & Chamberlain, L. H. 2015b. The zDHHC family of S-acyltransferases. *Biochem Soc Trans,* 43**,** 217-21.

Lennemann, N. J. & Coyne, C. B. 2017. Dengue and Zika viruses subvert reticulophagy by NS2B3-mediated cleavage of FAM134B. *Autophagy,* 13**,** 322-332.

Levine, B. & Klionsky, D. J. 2004. Development by self-digestion: molecular mechanisms and biological functions of autophagy. *Dev Cell,* 6**,** 463-77.

Li, H., Korennykh, A. V., Behrman, S. L. & Walter, P. 2010. Mammalian endoplasmic reticulum stress sensor IRE1 signals by dynamic clustering. *Proc Natl Acad Sci U S A,* 107**,** 16113-8.

Li, J., Ahat, E. & Wang, Y. 2019. Golgi Structure and Function in Health, Stress, and Diseases. *In:* KLOC, M. (ed.) *The Golgi Apparatus and Centriole: Functions, Interactions and Role in Disease.* Cham: Springer International Publishing.

Lin, J. H., Li, H., Yasumura, D., Cohen, H. R., Zhang, C., Panning, B., Shokat, K. M., Lavail, M. M. & Walter, P. 2007. IRE1 signaling affects cell fate during the unfolded protein response. *Science,* 318**,** 944-9.

Lin, J. H., Li, H., Zhang, Y., Ron, D. & Walter, P. 2009. Divergent effects of PERK and IRE1 signaling on cell viability. *PLoS One,* 4**,** e4170.

Ling, L. & Goeddel, D. V. 2000. T6BP, a TRAF6-interacting protein involved in IL-1 signaling. *Proc Natl Acad Sci U S A,* 97**,** 9567-72.

Loewen, C. J. R., Roy, A. & Levine, T. P. 2003a. A conserved ER targeting motif in three families of lipid binding proteins and in Opi1p binds VAP. *The EMBO Journal,* 22**,** 2025-2035.

Loewen, C. J. R., Roy, A. & Levine, T. P. 2003b. A conserved ER targeting motif in three families of lipid binding proteins and in Opi1p binds VAP. *EMBO J,* 22**,** 2025-2035.

Maeda, S., Otomo, C. & Otomo, T. 2019. The autophagic membrane tether ATG2A transfers lipids between membranes. *Elife,* 8.

Mancias, J. D. & Kimmelman, A. C. 2016. Mechanisms of Selective Autophagy in Normal Physiology and Cancer. *J Mol Biol,* 428**,** 1659-80.

Mancias, J. D., Wang, X., Gygi, S. P., Harper, J. W. & Kimmelman, A. C. 2014. Quantitative proteomics identifies NCOA4 as the cargo receptor mediating ferritinophagy. *Nature,* 509**,** 105.

Mao, D., Lin, G., Tepe, B., Zuo, Z., Tan, K. L., Senturk, M., Zhang, S., Arenkiel, B. R., Sardiello, M. & Bellen, H. J. 2019. VAMP associated proteins are required for autophagic and lysosomal degradation by promoting a PtdIns4P-mediated endosomal pathway. *Autophagy,* 15**,** 1214-1233.

Maria Cuervo, A. 2004. Autophagy: in sickness and in health. *Trends in Cell Biology,* 14**,** 70-77.

Marshall, R. S., Hua, Z., Mali, S., Mcloughlin, F. & Vierstra, R. D. 2019a. ATG8-Binding UIM Proteins Define a New Class of Autophagy Adaptors and Receptors. *Cell,* 177**,** 766-781.e24.

Marshall, R. S., Hua, Z., Mali, S., Mcloughlin, F. & Vierstra, R. D. 2019b. ATG8-Binding UIM Proteins Define a New Class of Autophagy Adaptors and Receptors. *Cell*.

Martin, B. R. & Cravatt, B. F. 2009. Large-scale profiling of protein palmitoylation in mammalian cells. *Nature Methods,* 6**,** 135-138.

Matlin, K. S. & Simons, K. 1983. Reduced temperature prevents transfer of a membrane glycoprotein to the cell surface but does not prevent terminal glycosylation. *Cell,* 34**,** 233-243.

Matsuzawa-Ishimoto, Y., Hwang, S. & Cadwell, K. 2018. Autophagy and Inflammation. *Annual Review of Immunology,* 36**,** 73-101.

Mejlvang, J., Olsvik, H., Svenning, S., Bruun, J.-A., Abudu, Y. P., Larsen, K. B., Brech, A., Hansen, T. E., Brenne, H., Hansen, T., Stenmark, H. & Johansen, T. 2018. Starvation induces rapid degradation of selective autophagy receptors by endosomal microautophagy. *The Journal of Cell Biology,* 217**,** 3640.

Meusser, B., Hirsch, C., Jarosch, E. & Sommer, T. 2005. ERAD: the long road to destruction. *Nature Cell Biology,* 7**,** 766-772.

Mijaljica, D., Prescott, M. & Devenish, R. J. 2011. Microautophagy in mammalian cells: Revisiting a 40-year-old conundrum. *Autophagy,* 7**,** 673-682.

Mikitova, V. & Levine, T. P. 2012. Analysis of the Key Elements of FFAT-Like Motifs Identifies New Proteins That Potentially Bind VAP on the ER, Including Two AKAPs and FAPP2. *PLOS ONE,* 7**,** e30455.

Milnerwood, A. J., Parsons, M. P., Young, F. B., Singaraja, R. R., Franciosi, S., Volta, M., Bergeron, S., Hayden, M. R. & Raymond, L. A. 2013. Memory and synaptic deficits in Hip14/DHHC17 knockout mice. *Proceedings of the National Academy of Sciences,* 110**,** 20296.

Mitchell, D. A., Mitchell, G., Ling, Y., Budde, C. & Deschenes, R. J. 2010. Mutational Analysis of Saccharomyces cerevisiae Erf2 Reveals a Two-step Reaction Mechanism for Protein Palmitoylation by DHHC Enzymes. *Journal of Biological Chemistry,* 285**,** 38104-38114.

Mitchell, D. A., Vasudevan, A., Linder, M. E. & Deschenes, R. J. 2006. Protein palmitoylation by a family of DHHC protein S-acyltransferases. *J Lipid Res,* 47**,** 1118-27.

Miyata, S., Mizuno, T., Koyama, Y., Katayama, T. & Tohyama, M. 2013. The endoplasmic reticulum-resident chaperone heat shock protein 47 protects the Golgi apparatus from the effects of O-glycosylation inhibition. *PLoS One,* 8**,** e69732.

Mizushima, N. & Komatsu, M. 2011. Autophagy: Renovation of Cells and Tissues. *Cell,* 147**,** 728-741.

Mochida, K., Oikawa, Y., Kimura, Y., Kirisako, H., Hirano, H., Ohsumi, Y. & Nakatogawa, H. 2015. Receptor-mediated selective autophagy degrades the endoplasmic reticulum and the nucleus. *Nature,* 522**,** 359.

Mori, K. 2009. Signalling Pathways in the Unfolded Protein Response: Development from Yeast to Mammals. *The Journal of Biochemistry,* 146**,** 743-750.

Morriswood, B., Ryzhakov, G., Puri, C., Arden, S. D., Roberts, R., Dendrou, C., Kendrick-Jones, J. & Buss, F. 2007a. T6BP and NDP52 are myosin VI binding partners with potential roles in cytokine signalling and cell adhesion. *J Cell Sci,* 120**,** 2574-85.

Morriswood, B., Ryzhakov, G., Puri, C., Arden, S. D., Roberts, R., Dendrou, C., Kendrick-Jones, J. & Buss, F. 2007b. T6BP and NDP52 are myosin VI binding partners with potential roles in cytokine signalling and cell adhesion. *Journal of Cell Science,* 120**,** 2574.

Mortimore, G. E., Lardeux, B. R. & Adams, C. E. 1988. Regulation of microautophagy and basal protein turnover in rat liver. Effects of short-term starvation. *Journal of Biological Chemistry,* 263**,** 2506-2512.

Mukherjee, A., Patel, B., Koga, H., Cuervo, A. M. & Jenny, A. 2016. Selective endosomal microautophagy is starvation-inducible in Drosophila. *Autophagy,* 12**,** 1984-1999.

Murphy, S. E. & Levine, T. P. 2016. VAP, a Versatile Access Point for the Endoplasmic Reticulum: Review and analysis of FFAT-like motifs in the VAPome. *Biochimica et Biophysica Acta (BBA) - Molecular and Cell Biology of Lipids,* 1861**,** 952-961.

Muszbek, L., Haramura, G., Cluette-Brown, J. E., Van Cott, E. M. & Laposata, M. 1999. The pool of fatty acids covalently bound to platelet proteins by thioester linkages can be altered by exogenously supplied fatty acids. *Lipids,* 34 Suppl**,** S331-7.

Nagata, K., Hirayoshi, K., Obara, M., Saga, S. & Yamada, K. M. 1988. Biosynthesis of a novel transformation-sensitive heat-shock protein that binds to collagen. Regulation by mRNA levels and in vitro synthesis of a functional precursor. *J Biol Chem,* 263**,** 8344-9.

Nunnari, J. & Walter, P. 1996. Regulation of Organelle Biogenesis. *Cell,* 84**,** 389-394.

Ohno, Y., Kihara, A., Sano, T. & Igarashi, Y. 2006. Intracellular localization and tissue-specific distribution of human and yeast DHHC cysteine-rich domain-containing proteins. *Biochim Biophys Acta,* 1761**,** 474-83.

Ohsumi, Y. 2014. Historical landmarks of autophagy research. *Cell Research,* 24**,** 9-23.

Okamoto, K. 2014. Organellophagy: Eliminating cellular building blocks via selective autophagy. *The Journal of Cell Biology,* 205**,** 435.

Oku, M., Tanakura, S., Uemura, A., Sohda, M., Misumi, Y., Taniguchi, M., Wakabayashi, S. & Yoshida, H. 2011. Novel Cis-acting Element GASE Regulates Transcriptional Induction by the Golgi Stress Response. *Cell Structure and Function,* 36**,** 1-12.

Osawa, T., Kotani, T., Kawaoka, T., Hirata, E., Suzuki, K., Nakatogawa, H., Ohsumi, Y. & Noda, N. N. 2019. Atg2 mediates direct lipid transfer between membranes for autophagosome formation. *Nature Structural & Molecular Biology,* 26**,** 281-288.

Otomo, T., Chowdhury, S. & Lander, G. C. 2018. The rod-shaped ATG2A-WIPI4 complex tethers membranes in vitro. *Contact (Thousand Oaks),* 1.

Otomo, T. & Maeda, S. 2019. ATG2A transfers lipids between membranes in vitro. *Autophagy,* 15**,** 2031-2032.

Palade, G. E. 1956. The endoplasmic reticulum. *The Journal of biophysical and biochemical cytology,* 2**,** 85-98.

Pankiv, S., Clausen, T. H., Lamark, T., Brech, A., Bruun, J.-A., Outzen, H., Øvervatn, A., Bjørkøy, G. & Johansen, T. 2007. p62/SQSTM1 Binds Directly to Atg8/LC3 to Facilitate Degradation of Ubiquitinated Protein Aggregates by Autophagy. *Journal of Biological Chemistry,* 282**,** 24131-24145.

Park, C., Suh, Y. & Cuervo, A. M. 2015. Regulated degradation of Chk1 by chaperone-mediated autophagy in response to DNA damage. *Nature Communications,* 6**,** 6823.

Perlmutter, D. H. & Silverman, G. A. 2011. Hepatic Fibrosis and Carcinogenesis in α1-Antitrypsin Deficiency: A Prototype for Chronic Tissue Damage in Gain-of-Function Disorders. *Cold Spring Harbor Perspectives in Biology,* 3.

Politis, E. G., Roth, A. F. & Davis, N. G. 2005. Transmembrane topology of the protein palmitoyl transferase Akr1. *J Biol Chem,* 280**,** 10156-63.

Porter, K. R. & Kallman, F. L. 1952. SIGNIFICANCE OF CELL PARTICULATES AS SEEN BY ELECTRON MICROSCOPY. *Annals of the New York Academy of Sciences,* 54**,** 882-891.

Preissler, S. & Ron, D. 2019. Early Events in the Endoplasmic Reticulum Unfolded Protein Response. *Cold Spring Harbor Perspectives in Biology,* 11.

Rafelski, S. M. & Marshall, W. F. 2008. Building the cell: design principles of cellular architecture. *Nature Reviews Molecular Cell Biology,* 9**,** 593-602.

Rambourg, A., Clermont, Y., Chretien, M. & Olivier, L. 1993. Modulation of the Golgi apparatus in stimulated and nonstimulated prolactin cells of female rats. *Anat Rec,* 235**,** 353-62.

Rasika, S., Passemard, S., Verloes, A., Gressens, P. & El ghouzzi, V. 2019. Golgipathies in Neurodevelopment: A New View of Old Defects. *Developmental Neuroscience*.

Ravenhill, B. J., Boyle, K. B., Von Muhlinen, N., Ellison, C. J., Masson, G. R., Otten, E. G., Foeglein, A., Williams, R. & Randow, F. 2019. The Cargo Receptor NDP52 Initiates Selective Autophagy by Recruiting the ULK Complex to Cytosol-Invading Bacteria. *Molecular Cell,* 74**,** 320-329.e6.

Reiling, J. H., Olive, A. J., Sanyal, S., Carette, J. E., Brummelkamp, T. R., Ploegh, H. L., Starnbach, M. N. & Sabatini, D. M. 2013. A CREB3–ARF4 signalling pathway mediates the response to Golgi stress and susceptibility to pathogens. *Nature Cell Biology,* 15**,** 1473.

Resh, M. D. 2006. Trafficking and signaling by fatty-acylated and prenylated proteins. *Nat Chem Biol,* 2**,** 584-90.

Roberts, P., Moshitch-Moshkovitz, S., Kvam, E., O'toole, E., Winey, M. & Goldfarb, D. S. 2003. Piecemeal Microautophagy of Nucleus in Saccharomyces cerevisiae. *Molecular Biology of the Cell,* 14**,** 129-141.

Rodriguez-Navarro, J. A., Kaushik, S., Koga, H., Dall, Armi, C., Shui, G., Wenk, M. R., Di Paolo, G. & Cuervo, A. M. 2012. Inhibitory effect of dietary lipids on chaperone-mediated autophagy. *Proceedings of the National Academy of Sciences,* 109**,** E705.

Rogov, V., Dötsch, V., Johansen, T. & Kirkin, V. 2014. Interactions between Autophagy Receptors and Ubiquitin-like Proteins Form the Molecular Basis for Selective Autophagy. *Molecular Cell,* 53**,** 167-178.

Ron, D. & Walter, P. 2007. Signal integration in the endoplasmic reticulum unfolded protein response. *Nat Rev Mol Cell Biol,* 8**,** 519-29.

Rubio, C., Pincus, D., Korennykh, A., Schuck, S., El-Samad, H. & Walter, P. 2011. Homeostatic adaptation to endoplasmic reticulum stress depends on Ire1 kinase activity. *J Cell Biol,* 193**,** 171-84.

Rutkowski, D. T. & Hegde, R. S. 2010. Regulation of basal cellular physiology by the homeostatic unfolded protein response. *The Journal of Cell Biology,* 189**,** 783.

Sahu, R., Kaushik, S., Clement, C. C., Cannizzo, E. S., Scharf, B., Follenzi, A., Potolicchio, I., Nieves, E., Cuervo, A. M. & Santambrogio, L. 2011. Microautophagy of Cytosolic Proteins by Late Endosomes. *Developmental Cell,* 20**,** 131-139.

Saito, T. & Ogawa, K. 1974. LYSOSOMAL CHANGES IN RAT HEPATIC PARENCHYMAL CELLS AFTER GLUCAGON ADMINISTRATIONI. *Acta Histochemica et Cytochemica,* 7**,** 1-18.

Sakai, Y., Koller, A., Rangell, L. K., Keller, G. A. & Subramani, S. 1998. Peroxisome Degradation by Microautophagy in Pichia pastoris: Identification of Specific Steps and Morphological Intermediates. *The Journal of Cell Biology,* 141**,** 625.

Salvador, N., Aguado, C., Horst, M. & Knecht, E. 2000. Import of a Cytosolic Protein into Lysosomes by Chaperone-mediated Autophagy Depends on Its Folding State. *Journal of Biological Chemistry,* 275**,** 27447-27456.

Sambrook, J. & Russell, D. W. 2006. Detection of Protein-Protein Interactions Using the GST Fusion Protein Pulldown Technique. *CSH Protoc,* 2006.

Samie, M., Lim, J., Verschueren, E., Baughman, J. M., Peng, I., Wong, A., Kwon, Y., Senbabaoglu, Y., Hackney, J. A., Keir, M., Mckenzie, B., Kirkpatrick, D. S., Van Lookeren Campagne, M. & Murthy, A. 2018. Selective autophagy of the adaptor TRIF regulates innate inflammatory signaling. *Nature Immunology,* 19**,** 246-254.

Sasaki, K. & Yoshida, H. 2015. Organelle autoregulation—stress responses in the ER, Golgi, mitochondria and lysosome. *The Journal of Biochemistry,* 157**,** 185-195.

Schindler, A. J. & Schekman, R. 2009. In vitro reconstitution of ER-stress induced ATF6 transport in COPII vesicles. *Proceedings of the National Academy of Sciences,* 106**,** 17775.

Schröder, M. 2008. Endoplasmic reticulum stress responses. *Cellular and Molecular Life Sciences,* 65**,** 862-894.

Schultz, M. L., Krus, K. L., Kaushik, S., Dang, D., Chopra, R., Qi, L., Shakkottai, V. G., Cuervo, A. M. & Lieberman, A. P. 2018. Coordinate regulation of mutant NPC1 degradation by selective ER autophagy and MARCH6-dependent ERAD. *Nat Commun,* 9**,** 3671.

Schwarz, D. S. & Blower, M. D. 2016. The endoplasmic reticulum: structure, function and response to cellular signaling. *Cellular and Molecular Life Sciences,* 73**,** 79-94.

Seo, A. Y., Lau, P. W., Feliciano, D., Sengupta, P., Gros, M. a. L., Cinquin, B., Larabell, C. A. & Lippincott-Schwartz, J. 2017. AMPK and vacuole-associated Atg14p orchestrate mu-lipophagy for energy production and long-term survival under glucose starvation. *Elife,* 6.

Shen, J., Chen, X., Hendershot, L. & Prywes, R. 2002. ER stress regulation of ATF6 localization by dissociation of BiP/GRP78 binding and unmasking of Golgi localization signals. *Dev Cell,* 3**,** 99-111.

Shibata, Y., Shemesh, T., Prinz, W. A., Palazzo, A. F., Kozlov, M. M. & Rapoport, T. A. 2010. Mechanisms Determining the Morphology of the Peripheral ER. *Cell,* 143**,** 774-788.

Singaraja, R. R., Huang, K., Sanders, S. S., Milnerwood, A. J., Hines, R., Lerch, J. P., Franciosi, S., Drisdel, R. C., Vaid, K., Young, F. B., Doty, C., Wan, J., Bissada, N., Henkelman, R. M., Green, W. N., Davis, N. G., Raymond, L. A. & Hayden, M. R. 2011. Altered palmitoylation and neuropathological deficits in mice lacking HIP14. *Hum Mol Genet,* 20**,** 3899-909.

Skytte Rasmussen, M., Mouilleron, S., Kumar Shrestha, B., Wirth, M., Lee, R., Bowitz Larsen, K., Abudu Princely, Y., O'reilly, N., Sjottem, E., Tooze, S. A., Lamark, T. & Johansen, T. 2017. ATG4B contains a C-terminal LIR motif important for binding and efficient cleavage of mammalian orthologs of yeast Atg8. *Autophagy,* 13**,** 834-853.

Smith, M. D., Harley, M. E., Kemp, A. J., Wills, J., Lee, M., Arends, M., Von Kriegsheim, A., Behrends, C. & Wilkinson, S. 2018. CCPG1 Is a Non-canonical Autophagy Cargo Receptor Essential for ER-Phagy and Pancreatic ER Proteostasis. *Dev Cell,* 44**,** 217-232.e11.

Sonenberg, N. & Hinnebusch, A. G. 2009. Regulation of Translation Initiation in Eukaryotes: Mechanisms and Biological Targets. *Cell,* 136**,** 731-745.

Stadler, C., Rexhepaj, E., Singan, V. R., Murphy, R. F., Pepperkok, R., Uhlén, M., Simpson, J. C. & Lundberg, E. 2013. Immunofluorescence and fluorescent-protein tagging show high correlation for protein localization in mammalian cells. *Nature Methods,* 10**,** 315.

Sternberg, S. H. & Doudna, J. A. 2015. Expanding the Biologist's Toolkit with CRISPR-Cas9. *Mol Cell,* 58**,** 568-74.

Sternsdorf, T., Jensen, K., Züchner, D. & Will, H. 1997. Cellular Localization, Expression, and Structure of the Nuclear Dot Protein 52. *The Journal of Cell Biology,* 138**,** 435.

Stolz, A., Ernst, A. & Dikic, I. 2014. Cargo recognition and trafficking in selective autophagy. *Nat Cell Biol,* 16**,** 495-501.

Sun, Z. & Brodsky, J. L. 2019. Protein quality control in the secretory pathway. *The Journal of Cell Biology***,** jcb.201906047.

Sutton, L. M., Sanders, S. S., Butland, S. L., Singaraja, R. R., Franciosi, S., Southwell, A. L., Doty, C. N., Schmidt, M. E., Mui, K. K., Kovalik, V., Young, F. B., Zhang, W. & Hayden, M. R. 2013. Hip14l-deficient mice develop neuropathological and behavioural features of Huntington disease. *Hum Mol Genet,* 22**,** 452-65.

Takahashi, K., Inuzuka, M. & Ingi, T. 2004. Cellular signaling mediated by calphoglin-induced activation of IPP and PGM. *Biochemical and Biophysical Research Communications,* 325**,** 203-214.

Takahashi, Y., Meyerkord, C. L., Hori, T., Runkle, K., Fox, T. E., Kester, M., Loughran, T. P. & Wang, H.-G. 2011. Bif-1 regulates Atg9 trafficking by mediating the fission of Golgi membranes during autophagy. *Autophagy,* 7**,** 61-73.

Tang, C., Iwahara, J. & Clore, G. M. 2006. Visualization of transient encounter complexes in protein–protein association. *Nature,* 444**,** 383-386.

Tang, Z., Takahashi, Y., He, H., Hattori, T., Chen, C., Liang, X., Chen, H., Young, M. M. & Wang, H.-G. 2019a. TOM40 Targets Atg2 to Mitochondria-Associated ER Membranes for Phagophore Expansion. *Cell Reports,* 28**,** 1744-1757.e5.

Tang, Z., Takahashi, Y. & Wang, H.-G. 2019b. ATG2 regulation of phagophore expansion at mitochondria-associated ER membranes. *Autophagy,* 15**,** 2165-2166.

Taniguchi, M., Nadanaka, S., Tanakura, S., Sawaguchi, S., Midori, S., Kawai, Y., Yamaguchi, S., Shimada, Y., Nakamura, Y., Matsumura, Y., Fujita, N., Araki, N., Yamamoto, M., Oku, M., Wakabayashi, S., Kitagawa, H. & Yoshida, H. 2015. TFE3 Is a bHLH-ZIP-type Transcription Factor that Regulates the Mammalian Golgi Stress Response. *Cell Structure and Function,* 40**,** 13-30.

Taniguchi, M. & Yoshida, H. 2017. TFE3, HSP47, and CREB3 Pathways of the Mammalian Golgi Stress Response. *Cell Structure and Function,* 42**,** 27-36.

Tao, Y.-X. & Conn, P. M. 2018. Pharmacoperones as Novel Therapeutics for Diverse Protein Conformational Diseases. *Physiological Reviews,* 98**,** 697-725.

Tate, E. W., Kalesh, K. A., Lanyon-Hogg, T., Storck, E. M. & Thinon, E. 2015. Global profiling of protein lipidation using chemical proteomic technologies. *Current Opinion in Chemical Biology,* 24**,** 48-57.

Tekirdag, K. & Cuervo, A. M. 2018. Chaperone-mediated autophagy and endosomal microautophagy: Jointed by a chaperone. *Journal of Biological Chemistry,* 293**,** 5414-5424.

Teske, B. F., Wek, S. A., Bunpo, P., Cundiff, J. K., Mcclintick, J. N., Anthony, T. G. & Wek, R. C. 2011. The eIF2 kinase PERK and the integrated stress response facilitate activation of ATF6 during endoplasmic reticulum stress. *Mol Biol Cell,* 22**,** 4390-405.

Thuerauf, D. J., Marcinko, M., Belmont, P. J. & Glembotski, C. C. 2007. Effects of the isoform-specific characteristics of ATF6 alpha and ATF6 beta on endoplasmic reticulum stress response gene expression and cell viability. *J Biol Chem,* 282**,** 22865-78.

Thuerauf, D. J., Morrison, L. & Glembotski, C. C. 2004. Opposing roles for ATF6alpha and ATF6beta in endoplasmic reticulum stress response gene induction. *J Biol Chem,* 279**,** 21078-84.

Thuerauf, D. J., Morrison, L. E., Hoover, H. & Glembotski, C. C. 2002. Coordination of ATF6-mediated transcription and ATF6 degradation by a domain that is shared with the viral transcription factor, VP16. *J Biol Chem,* 277**,** 20734-9.

Thurston, T. L. M., Ryzhakov, G., Bloor, S., Von Muhlinen, N. & Randow, F. 2009. The TBK1 adaptor and autophagy receptor NDP52 restricts the proliferation of ubiquitin-coated bacteria. *Nature Immunology,* 10**,** 1215.

Thurston, T. L. M., Wandel, M. P., Von Muhlinen, N., Foeglein, Á. & Randow, F. 2012. Galectin 8 targets damaged vesicles for autophagy to defend cells against bacterial invasion. *Nature,* 482**,** 414.

Tirasophon, W., Lee, K., Callaghan, B., Welihinda, A. & Kaufman, R. J. 2000. The endoribonuclease activity of mammalian IRE1 autoregulates its mRNA and is required for the unfolded protein response. *Genes Dev,* 14**,** 2725-36.

Tirasophon, W., Welihinda, A. A. & Kaufman, R. J. 1998. A stress response pathway from the endoplasmic reticulum to the nucleus requires a novel bifunctional protein kinase/endoribonuclease (Ire1p) in mammalian cells. *Genes Dev,* 12**,** 1812-24.

Towbin, H., Staehelin, T. & Gordon, J. 1979. Electrophoretic transfer of proteins from polyacrylamide gels to nitrocellulose sheets: procedure and some applications. *Proc Natl Acad Sci U S A,* 76**,** 4350-4.

Tumbarello, D. A., Manna, P. T., Allen, M., Bycroft, M., Arden, S. D., Kendrick-Jones, J. & Buss, F. 2015. The Autophagy Receptor TAX1BP1 and the Molecular Motor Myosin VI Are Required for Clearance of Salmonella Typhimurium by Autophagy. *PLoS Pathog,* 11**,** e1005174.

Tumbarello, D. A., Waxse, B. J., Arden, S. D., Bright, N. A., Kendrick-Jones, J. & Buss, F. 2012. Autophagy receptors link myosin VI to autophagosomes to mediate Tom1-dependent autophagosome maturation and fusion with the lysosome. *Nature Cell Biology,* 14**,** 1024.

Turco, E., Fracchiolla, D. & Martens, S. 2019a. Recruitment and Activation of the ULK1/Atg1 Kinase Complex in Selective Autophagy. *Journal of Molecular Biology*.

Turco, E., Witt, M., Abert, C., Bock-Bierbaum, T., Su, M.-Y., Trapannone, R., Sztacho, M., Danieli, A., Shi, X., Zaffagnini, G., Gamper, A., Schuschnig, M., Fracchiolla, D., Bernklau, D., Romanov, J., Hartl, M., Hurley, J. H., Daumke, O. & Martens, S. 2019b. FIP200 Claw Domain Binding to p62 Promotes Autophagosome Formation at Ubiquitin Condensates. *Molecular Cell,* 74**,** 330-346.e11.

Tuttle, D. L. & Dunn, W. A., Jr. 1995. Divergent modes of autophagy in the methylotrophic yeast Pichia pastoris. *J Cell Sci,* 108 (Pt 1)**,** 25-35.

Uttenweiler, A., Schwarz, H., Neumann, H. & Mayer, A. 2007. The Vacuolar Transporter Chaperone (VTC) Complex Is Required for Microautophagy. *Molecular Biology of the Cell,* 18**,** 166-175.

Uytterhoeven, V., Lauwers, E., Maes, I., Miskiewicz, K., Melo, M. N., Swerts, J., Kuenen, S., Wittocx, R., Corthout, N., Marrink, S. J., Munck, S. & Verstreken, P. 2015. Hsc70-4 Deforms Membranes to Promote Synaptic Protein Turnover by Endosomal Microautophagy. *Neuron,* 88**,** 735-48.

Valverde, D. P., Yu, S., Boggavarapu, V., Kumar, N., Lees, J. A., Walz, T., Reinisch, K. M. & Melia, T. J. 2019. ATG2 transports lipids to promote autophagosome biogenesis. *The Journal of Cell Biology,* 218**,** 1787.

Van Anken, E. & Braakman, I. 2005. Versatility of the endoplasmic reticulum protein folding factory. *Crit Rev Biochem Mol Biol,* 40**,** 191-228.

Vargas, J. N. S., Wang, C., Bunker, E., Hao, L., Maric, D., Schiavo, G., Randow, F. & Youle, R. J. 2019. Spatiotemporal Control of ULK1 Activation by NDP52 and TBK1 during Selective Autophagy. *Molecular Cell,* 74**,** 347-362.e6.

Vasco Ferreira, J., Rosa Soares, A., Silva Ramalho, J., Pereira, P. & Girao, H. 2015. K63 linked ubiquitin chain formation is a signal for HIF1A degradation by Chaperone-Mediated Autophagy. *Scientific Reports,* 5**,** 10210.

Venditti, R., Rega, L. R., Masone, M. C., Santoro, M., Polishchuk, E., Sarnataro, D., Paladino, S., D'auria, S., Varriale, A., Olkkonen, V. M., Di Tullio, G., Polishchuk, R. & De Matteis, M. A. 2019. Molecular determinants of ER-Golgi contacts identified through a new FRET-FLIM system. *J Cell Biol,* 218**,** 1055-1065.

Voeltz, G. K., Prinz, W. A., Shibata, Y., Rist, J. M. & Rapoport, T. A. 2006. A Class of Membrane Proteins Shaping the Tubular Endoplasmic Reticulum. *Cell,* 124**,** 573-586.

Voeltz, G. K., Rolls, M. M. & Rapoport, T. A. 2002. Structural organization of the endoplasmic reticulum. *EMBO reports,* 3**,** 944-950.

Von Muhlinen, N., Akutsu, M., Ravenhill, B. J., Foeglein, Á., Bloor, S., Rutherford, T. J., Freund, S. M. V., Komander, D. & Randow, F. 2013. An essential role for the ATG8 ortholog LC3C in antibacterial autophagy. *Autophagy,* 9**,** 784-786.

Von muhlinen, N., Akutsu, M., Ravenhill, Benjamin j., Foeglein, Á., Bloor, S., Rutherford, Trevor j., Freund, Stefan m. V., Komander, D. & Randow, F. 2012. LC3C, Bound Selectively by a Noncanonical LIR Motif in NDP52, Is Required for Antibacterial Autophagy. *Molecular Cell,* 48**,** 329-342.

Walter, P. & Ron, D. 2011. The Unfolded Protein Response: From Stress Pathway to Homeostatic Regulation. *Science,* 334**,** 1081.

Wang, X., Li, S., Wang, H., Shui, W. & Hu, J. 2017. Quantitative proteomics reveal proteins enriched in tubular endoplasmic reticulum of Saccharomyces cerevisiae. *eLife,* 6**,** e23816.

Wang, Y. & Seemann, J. 2011. Golgi Biogenesis. *Cold Spring Harbor Perspectives in Biology,* 3.

Webster, C. P., Smith, E. F., Bauer, C. S., Moller, A., Hautbergue, G. M., Ferraiuolo, L., Myszczynska, M. A., Higginbottom, A., Walsh, M. J., Whitworth, A. J., Kaspar, B. K., Meyer, K., Shaw, P. J., Grierson, A. J. & De Vos, K. J. 2016. The C9orf72 protein interacts with Rab1a and the ULK1 complex to regulate initiation of autophagy. *Embo j,* 35**,** 1656-76.

Weidberg, H., Shvets, E. & Elazar, Z. 2011. Biogenesis and cargo selectivity of autophagosomes. *Annu Rev Biochem,* 80**,** 125-56.

Wek, R. C. & Cavener, D. R. 2007. Translational control and the unfolded protein response. *Antioxid Redox Signal,* 9**,** 2357-71.

Welsch, S., Miller, S., Romero-Brey, I., Merz, A., Bleck, C. K., Walther, P., Fuller, S. D., Antony, C., Krijnse-Locker, J. & Bartenschlager, R. 2009. Composition and three-dimensional architecture of the dengue virus replication and assembly sites. *Cell Host Microbe,* 5**,** 365-75.

Whang, M. I., Tavares, R. M., Benjamin, D. I., Kattah, M. G., Advincula, R., Nomura, D. K., Debnath, J., Malynn, B. A. & Ma, A. 2017. The Ubiquitin Binding Protein TAX1BP1 Mediates Autophagosome Induction and the Metabolic Transition of Activated T Cells. *Immunity,* 46**,** 405-420.

Wiemann, S., Arlt, D., Huber, W., Wellenreuther, R., Schleeger, S., Mehrle, A., Bechtel, S., Sauermann, M., Korf, U., Pepperkok, R., Sultmann, H. & Poustka, A. 2004. From ORFeome to biology: a functional genomics pipeline. *Genome Res,* 14**,** 2136-44.

Wilkinson, S. 2019a. Emerging Principles of Selective ER Autophagy. *Journal of Molecular Biology*.

Wilkinson, S. 2019b. ER-phagy: shaping up and de-stressing the endoplasmic reticulum. *FEBS J,* 286**,** 2645-2663.

Wilkinson, S. 2019c. ER-phagy: shaping up and destressing the endoplasmic reticulum. *The FEBS Journal,* 286**,** 2645-2663.

Wilson, B. S., Nuoffer, C., Meinkoth, J. L., Mccaffery, M., Feramisco, J. R., Balch, W. E. & Farquhar, M. G. 1994. A Rab1 mutant affecting guanine nucleotide exchange promotes disassembly of the Golgi apparatus. *The Journal of Cell Biology,* 125**,** 557.

Wirth, M., Zhang, W., Razi, M., Nyoni, L., Joshi, D., O'reilly, N., Johansen, T., Tooze, S. A. & Mouilleron, S. 2019. Molecular determinants regulating selective binding of autophagy adapters and receptors to ATG8 proteins. *Nat Commun,* 10**,** 2055.

Wissmueller, S., Font, J., Liew, C. W., Cram, E., Schroeder, T., Turner, J., Crossley, M., Mackay, J. P. & Matthews, J. M. 2011. Protein-protein interactions: analysis of a false positive GST pulldown result. *Proteins,* 79**,** 2365-71.

Wright, A. V., Nunez, J. K. & Doudna, J. A. 2016. Biology and Applications of CRISPR Systems: Harnessing Nature's Toolbox for Genome Engineering. *Cell,* 164**,** 29-44.

Wu, M. J., Ke, P. Y., Hsu, J. T., Yeh, C. T. & Horng, J. T. 2014. Reticulon 3 interacts with NS4B of the hepatitis C virus and negatively regulates viral replication by disrupting NS4B self-interaction. *Cell Microbiol,* 16**,** 1603-18.

Yamaguchi, Y., Larkin, D., Lara-Lemus, R., Ramos-Castaneda, J., Liu, M. & Arvan, P. 2008. Endoplasmic reticulum (ER) chaperone regulation and survival of cells compensating for deficiency in the ER stress response kinase, PERK. *J Biol Chem,* 283**,** 17020-9.

Yamamoto, K., Sato, T., Matsui, T., Sato, M., Okada, T., Yoshida, H., Harada, A. & Mori, K. 2007. Transcriptional induction of mammalian ER quality control proteins is mediated by single or combined action of ATF6alpha and XBP1. *Dev Cell,* 13**,** 365-76.

Yang, C. K., Kim, J. H. & Stallcup, M. R. 2006. Role of the N-terminal activation domain of the coiled-coil coactivator in mediating transcriptional activation by beta-catenin. *Mol Endocrinol,* 20**,** 3251-62.

Yang, G. & Cynader, M. S. 2011. Palmitoyl Acyltransferase zD17 Mediates Neuronal Responses in Acute Ischemic Brain Injury by Regulating JNK Activation in a Signaling Module. *The Journal of Neuroscience,* 31**,** 11980.

Yang, G., Zhou, X., Zhu, J., Liu, R., Zhang, S., Coquinco, A., Chen, Y., Wen, Y., Kojic, L., Jia, W. & Cynader, M. S. 2013. JNK3 couples the neuronal stress response to inhibition of secretory trafficking. *Sci Signal,* 6**,** ra57.

Yoshida, H. 2007. ER stress and diseases. *The FEBS Journal,* 274**,** 630-658.

Yoshida, H., Matsui, T., Yamamoto, A., Okada, T. & Mori, K. 2001. XBP1 mRNA is induced by ATF6 and spliced by IRE1 in response to ER stress to produce a highly active transcription factor. *Cell,* 107**,** 881-91.

Yoshida, H., Oku, M., Suzuki, M. & Mori, K. 2006. pXBP1(U) encoded in XBP1 pre-mRNA negatively regulates unfolded protein response activator pXBP1(S) in mammalian ER stress response. *J Cell Biol,* 172**,** 565-75.

Yoshida, H., Uemura, A. & Mori, K. 2009. pXBP1(U), a negative regulator of the unfolded protein response activator pXBP1(S), targets ATF6 but not ATF4 in proteasome-mediated degradation. *Cell Struct Funct,* 34**,** 1-10.

Yu, L., Chen, Y. & Tooze, S. A. 2018. Autophagy pathway: Cellular and molecular mechanisms. *Autophagy,* 14**,** 207-215.

Yuan, W., Tuttle, D. L., Shi, Y. J., Ralph, G. S. & Dunn, W. A. 1997. Glucose-induced microautophagy in Pichia pastoris requires the alpha-subunit of phosphofructokinase. *Journal of Cell Science,* 110**,** 1935.

Zaffagnini, G. & Martens, S. 2016. Mechanisms of Selective Autophagy. *Journal of Molecular Biology,* 428**,** 1714-1724.

Zhang, H. & Hu, J. 2016. Shaping the Endoplasmic Reticulum into a Social Network. *Trends in Cell Biology,* 26**,** 934-943.

Zhao, Y. G., Liu, N., Miao, G., Chen, Y., Zhao, H. & Zhang, H. 2018. The ER Contact Proteins VAPA/B Interact with Multiple Autophagy Proteins to Modulate Autophagosome Biogenesis. *Current Biology,* 28**,** 1234-1245.e4.

Zhao, Y. G. & Zhang, H. 2019. Autophagosome maturation: An epic journey from the ER to lysosomes. *The Journal of Cell Biology,* 218**,** 757.

CALCOCO1 acts with VAMP-Associated Proteins to mediate ER-phagy

Thaddaeus Mutugi Nthiga, Birendra Kumar Shrestha, Eva Sjøttem, Jack-Ansgar Bruun, Kenneth Bowitz Larsen, Trond Lamark* and Terje Johansen*

Molecular Cancer Research Group, Department of Medical Biology, University of Tromsø – The Arctic University of Norway, 9037 Tromsø, Norway.

*Corresponding authors: Tel: +47 77644720; Email: trond.lamark@uit.no and Tel: +47 77644720; Email: terje.johansen@uit.no

Running Title: CALCOCO1 is a soluble ER-phagy receptor

Keywords: Autophagy, CALCOCO1, ER-phagy, VAPA,VAPB, Golgi, TAX1BP1, FFAT

Abstract

The endoplasmic reticulum plays important roles in protein synthesis, folding and calcium storage. The volume of the ER and expression of its resident proteins are increased in response to physiological conditions such as nutrient stress. ER-phagy, a selective form of autophagy, is involved in the degradation of the excess components of the ER to restore homeostasis. Six ER resident proteins have been identified as ER-phagy receptors so far. In this study, we have identified CALCOCO1 as an ER-phagy receptor for the degradation of the tubular ER in response to proteotoxic and nutrient stress. CALCOCO1 is a homomeric protein that binds directly to ATG8 proteins via LIR and UDS interacting region (UIR) motifs acting co-dependently. CALCOCO1-mediated ER-phagy requires interaction with VAMP-associated proteins VAPA and VAPB on the ER membranes via a conserved FFAT-like motif. Depletion of CALCOCO1 causes expansion of the ER and inefficient basal autophagy flux. Unlike the already identified ER-phagy receptors, CALCOCO1 is peripherally associated with the ER. Therefore, we define CALCOCO1 as a soluble ER-phagy receptor.

Introduction

Organelles are intracellular membrane-confined structures that carry out specialized functions important for cell function and survival. Eukaryotic cells have different organelles such as the endoplasmic reticulum (ER), Golgi apparatus, mitochondria, lysosomes and peroxisomes. The amount and vitality of each organelle is regulated depending on the energetic and functional needs of cells (Anding and Baehrecke, 2017). Surplus and damaged organelles are cleared through macroautophagy (henceforth autophagy)(Anding and Baehrecke, 2017, Okamoto, 2014), an evolutionary conserved process that delivers cytoplasmic materials for degradation in the lysosome (Mizushima and Komatsu, 2011, Ohsumi, 2014). Autophagy involves sequestration of cytoplasmic contents into double-membraned vesicles called autophagosomes, which then fuse with lysosomes to degrade their contents. At basal level, autophagy occurs in cells to maintain homeostasis by facilitating constitutive turnover of cytoplasmic contents. Autophagy also acts selectively in the degradation of excess components or toxic materials in the cell such as surplus or damaged organelles, protein aggregates and invading pathogens (Gatica et al., 2018, Johansen and Lamark, 2011, Johansen and Lamark, 2019, Kirkin, 2019, Stolz et al., 2014). Autophagy is activated during stresses, such as starvation, to degrade cellular macromolecules in order to recycle nutrients and generate energy (Ohsumi, 2014, Schroder, 2008).

Autophagosome formation is mediated by evolutionary conserved core autophagy (ATG) proteins, which assemble into temporal hierarchical complexes to initiate the formation and expansion of the phagophores and their closure around the cargo to form autophagosomes. The co-ordinated actions of the first two complexes, ULK complex comprising FIP200, ATG13, ATG101 and ULK1/2, and PI3KC3 complex I comprising VPS34, BECN1, VPS15 and ATG14L, at the phagophore formation site, generate phosphatidylinositol-3-phopshate (PI3P). This recruits the PI3P-binding ATG2-WIPI complex, and the two ubiquitin like conjugation systems mediating the formation of the ATG5-ATG12:ATG16L complex for the lipidation of ATG8 family proteins to the growing phagophore. The only integral membrane protein of the conserved core autophagy components, ATG9, is involved in the trafficking of vesicles adding some unknown components to the growing pahogohore in a kiss and run fashion (Bento et al., 2016, Mizushima et al., 2011).

The selectivity in autophagy is mediated by selective autophagy receptors (SARs), which link the cargo material to the phagophore membranes (Gatica et al., 2018, Johansen and

Lamark, 2011, Johansen and Lamark, 2019, Kirkin, 2019, Stolz et al., 2014). The linkage involves SAR binding to the cargo on one hand and to ATG8 family proteins on the phagophore membrane on the other (Birgisdottir et al., 2013, Johansen and Lamark, 2019, Pankiv et al., 2007, Rogov et al., 2014). The interaction with ATG8 family proteins is mediated by a LIR (LC3 interacting region) motif, which has a core sequence of [W/F/Y]xx[L/V/I], but also contains negatively charged residues inside or adjacent to the core motif. This motif interacts with a LIR docking site (LDS) in the ATG8 family protein, consisting of two hydrophobic pockets mediating the interaction with the core motif and adjacent positively charged side chains forming electrostatic interactions (Johansen and Lamark, 2019, Wirth et al., 2019). Recently, it has emerged that ATG8 family proteins may also recognize ubiquitin-interacting motif (UIM)-like sequences present on some receptors, like RPN10, to recruit cargo-receptor complexes to the phagophore membranes (Marshall et al., 2019). The binding site for UIM-like motifs is called UIM-docking site (UDS) and is on the opposite side of the ATG8 molecule relative to the LDS. In mammals, there are 6 different ATG8 family proteins, i. e. the MAP1LC3 (microtubule associated protein 1 light chain 3) subfamily consisting of LC3A (two isoforms), LC3B and LC3C, and the GABARAP (GABA type A receptor-associated protein) subfamily consisting of GABARAP, GABARAPL1 and GABARAPL2 . The lipidated ATG8 proteins act as adaptors for the recruitment of LDS- or UDS interacting proteins to the phagophore. One essential function of ATG8 proteins in selective autophagy is to act as adaptors for the attachment of SARs and cargos to the inner surface of phagophore. However, ATG8 family proteins are also essential for autophagosome formation and maturation, mediated, at least in part, by recruiting core autophagy proteins and proteins involved in the transport or fusion of autophagosomes with lysosomes (Johansen and Lamark, 2019, Kriegenburg et al., 2018). Expanding phagophores and autophagosomes therefore are congregates of autophagy regulatory proteins, cargo materials and receptors, all associating directly or indirectly.

Clearance of surplus or damaged organelles, such as endoplasmic reticulum (ER), is an important function of selective autophagy (Wilkinson, 2019b). Mammalian ER is a continuous membrane bound organelle consisting of the nuclear envelope (NE) and a cytoplasmic peripheral ER made up of sheets and reticulated tubular network. The ER plays important roles in processes such as protein synthesis and folding, mitochondrial division, calcium storage and signaling, lipid synthesis and transfer and detoxification (Chen et al., 2013, Nixon-Abell et al., 2016, Schwarz and Blower, 2016). In response to physiological or pathological conditions such

as nutrient deprivation, accumulation of unfolded proteins or exposure to chemicals, the ER engages the unfolded protein response pathways (UPR) to restore homeostasis.

The UPR is characterized by signalling events from ER-integral membrane sensor proteins: protein kinase RNA-like ER kinase (PERK), activacting transcription factor 6 (ATF6), and inositor-requiring enzyme 1α (IRE1α), which cumulatively trigger inhibition of global protein translation while transcriptionally upregulating ER chaperones, ER-associated degradation (ERAD) proteins and apoptotic mediators, causing the ER to undergo spatiotemporal changes in morphology, molecular composition and functional specification. More particularly, UPR increases the ER volume and the expression of ER-resident proteins to buffer ER functions. At the same time, there is a continuous remodelling and turnover of the ER to restore homeostasis. Selective autophagic degradation of ER fragments and components, called ER-phagy, contributes to this remodelling(Bernales et al., 2007, Fregno and Molinari, 2018, Wilkinson, 2019b). Autophagy-deficient cell lines contain expanded ER while inhibition of general autophagy by depleting ATG5 or ATG7 has been shown to cause ER stress and dilation, suggesting that ER-phagy is a critical process for ER homeostasis (Antonucci et al., 2015, Jia et al., 2011).

ER-phagy in yeast is mediated by two receptors, Atg39 and Atg40, which play critical roles in sequestering ER fragments into autophagosomes (Mochida et al., 2015). In mammals, six ER-phagy receptors, targeting different ER sub-domains for degradation, have so far been identified: FAM134B, RTN3L, SEC62, CCPG1, ATL3, and TEX264 (An et al., 2019, Chen et al., 2019, Chino et al., 2019, Fumagalli et al., 2016, Grumati et al., 2017a, Khaminets et al., 2015, Smith et al., 2018). A recent study also found that COPII subunit, SEC24C, was required for starvation-induced ER-phagy in concert with FAM134B and RTN3 ER-phagy receptors (Cui et al., 2019). FAM134B is a reticulon homology domain-containing protein and it has been shown to mediate basal and starvation-induced degradation of ER sheets through interaction with atlastin2 (ATL2) (Khaminets et al., 2015, Liang et al., 2018). FAM134B also interacts with calnexin to mediate degradation of misfolded procollagen (PC) (Forrester et al., 2019). RTN3L mediates starvation-induced degradation of tubular ER and also contain a reticulon homology domain which anchors it to the ER tubules (Grumati et al., 2017b).

ATL3 is a GABARAP-interacting ER-phagy receptor for the degradation of tubular ER while SEC62, a component of the ER translocon that promotes co-translational of proteins into ER, has been shown to function as ER-phagy receptor during recovery from ER stress (Chen et

al., 2019, Fumagalli et al., 2016). CCPG1 is an ER transmembrane protein that mediates ER-phagy of the tubular ER during starvation and ER stress by interacting with GABARAP and FIP200 (Smith et al., 2018). TEX264 was recently identified as single pass transmembrane ER-phagy receptor responsible for the turnover of a large number of ER proteins during nutrient starvation (An et al., 2019, Chino et al., 2019). Very recently, p62 and the ER transmembrane E3 ligase TRIM13 was implicated in ER-phagy induced by proteotoxic stress via the N-degron pathway (Ji et al., 2019). This ER-phagy pathway is important in ER protein quality control and is activated by the binding of p62 to N-terminally arginylated proteins. Binding of p62 to TRIM13 then activates the E3 ligase and this creates a platform for ER-phagy induction. The involvement of p62 in this autophagy pathway shows that resident ER proteins and soluble SARs may co-operate in ER-phagy processes. Despite the growing number of identified ER-phagy receptors, it is not known how and whether the receptors co-operate to promote degradation of the ER and how such co-operation could be regulated. In addition, loss of the known receptors does not block ER-phagy completely and the effects of their loss appears to be tissue-restricted (Wilkinson, 2019b), suggesting that the loss is compensated by yet unidentified receptors.

CALCOCO1 is an evolutionary conserved protein and a paralog to TAX1BP1 and NDP52, two well-known selective autophagy receptor proteins. The three proteins form a small protein family with substantial similarity and identity with a similar domain structure composed of an N-terminal SKICH domain, middle coil-coil regions (CC) and varying carboxy terminal (CT) domains that contain one or two zinc finger domains. In addition, they contain an atypical LIR (CLIR) motif (LVV) in the linker region between the SKICH domain and the coiled-coil domain (Tumbarello et al., 2015, von Muhlinen et al., 2012) (**Fig 1A**). Despite this similarity, no role for CALCOCO1 in autophagy has been defined so far. However, in a quantitative proteomics study aimed at identifying novel and known autophagosome-enriched proteins in human cells, CALCOCO1 was found to be enriched in autophagosomes from pancreatic cancer cell lines (Mancias et al., 2014). CALCOCO1 was also one of the top hits in another quantitative proteomics study of proteins that were stabilized in ATG16L1 KO murine bone marrow-derived macrophages relative to WT controls (Samie et al., 2018). Here, we show that CALCOCO1 is continuously degraded by autophagy. Detailed studies revealed that CALCOCO1 is homomeric and has both LIR and UIR motifs for co-dependent binding to GABARAP subfamily proteins. CALCOCO1 acts as a soluble selective autophagy receptor for ER-phagy. It accomplishes this by interacting with ER tethering proteins VAPA and VAPB via a FFAT motif.

Results

CALCOCO1 is homomeric

TAX1BP1 and NDP52 self-associate through their coiled-coil domains (Ling and Goeddel, 2000, Sternsdorf et al., 1997), and heterodimerizes with each other (Morriswood et al., 2007). To explore whether CALCOCO1 is homomeric, full length EGFP-CALCOCO1 and Myc-CALCOCO1 were co-expressed in HEK293 cells and EGFP-CALCOCO1 was pulled down from cell extracts using GFP-TRAP. An efficient co-precipitation of Myc-CALCOCO1 indicated that CALCOCO1 is homomeric (**Fig 1B**). To clarify which domain in CALCOCO1 is mediating the self-association, Myc-tagged deletion mutants of CALCOCO1 were tested in the same immunoprecipitation experiment for interaction with full length GFP-CALCOCO1. Only the deletion mutant containing the CC domain (145-513) was immunoprecipitated by full-length EGFP-CALCOCO1, implying that the observed self- association is mediated by the CC domain (**Fig 1B**). Supporting such a conclusion, a deletion construct lacking the CC domain (Δ145-513) did not interact with full-length CALCOCO1 (**Fig 1B**). Further, we tested whether the self-oligomerization of CALCOCO1 occurred by direct interaction. The same combinations of full length GFP-CALCOCO1 and Myc-tagged deletion mutants were now co-translated *in vitro* in the presence of ^{35}S-methionine. Immunoprecipitations were then performed followed by autoradiography analysis. As in the HEK293 cell extracts, the only deletion construct that co-precipitated with GFP-CALCOCO1 was Myc-CALCOCO1(145-513) encompassing the CC domain (**Fig EV1A**). The CC domain of CALCOCO1 is separated into three coiled-coil regions (CC1-3) (**Fig 1A**). To determine which of the CCs contributes to the homomerization, Myc-CALCOCO1 constructs containing a specific deletion of each of the coiled-coil regions were also tested. A specific deletion of CC3 (Δ413-513) prevented the interaction and clearly had a much more pronounced effect than a deletion of any of the other internal coiled-coil regions (**Fig EV1A**).

Next, we tested whether CALCOCO1 heterodimerizes with TAX1BP1 and NDP52. GFP-CALCOCO1 was *in vitro* co-translated with either Myc-CALCOCO1, Myc-NDP52 or Myc-TAX1BP1 followed by immunoprecipitation using GFP-Trap. Autoradiography analysis showed that GFP-CALCOCO1 co-precipitated with Myc-CALCOCO1, but neither with Myc-TAX1BP1 nor Myc-NDP52, indicating that CALCOCO1 does not heterodimerize with these paralogs **(Fig EV1B**).

An important difference between CALCOCO1 and its paralogs is the presence of ubiquitin-binding zinc fingers in NDP52 and TAX1BP1. However, although CALCOCO1 contains a C-terminal zinc finger domain too, it does not bind to ubiquitin (Thurston et al., 2009). The C-terminus of NDP52 also interacts with galectins to mediate xenophagy (Thurston et al., 2012). To determine whether CALCOCO1 interacts with galectins, Myc-CALCOCO1 was *in vitro* translated and tested for interaction with GST-tagged galectin-3 and galectin-8 in *in vitro* pulldowns assay, whereupon no interaction was found. In contrast, galectin-3 and galectin-8 interacted with both TAX1BP1 and NDP52 (**Fig EV1C**).

CALCOCO1 is degraded by macro-autophagy

To investigate the possible role of CALCOCO1 in autophagy, we first tested whether CALCOCO1 is degraded in the lysosome or in the proteasome by monitoring levels in the presence of either the lysosomal and autophagy inhibitor bafilomycin A1 (Baf A1), or the proteasome inhibitor, MG132. In normally growing HeLa (**Fig 1C**) and MEFs (**Fig 1D**) wild type cells, treatment with Baf A1 resulted in an accumulation of CALCOCO1, similar to the accumulation observed for autophagy receptor p62, suggesting basal turnover of CALCOCO1 by autophagy. Upon induction of autophagy by nutrient starvation, the amount of CALCOCO1 in the starved cells reduced significantly after six hours. The reduction was blocked by treating the cells with Baf A1 during the starvation period (**Fig 1C and D**), suggesting that CALCOCO1 is an autophagy substrate during starvation. The lysosomal degradation of endogenous CALCOCO1 was confirmed by western blots of extracts from human BJ-1 diploid fibroblasts treated for different times with Baf A1 or MG132 (**Fig EV2A**). To clarify whether macro-autophagy was involved in the degradation, we investigated the turnover of CALCOCO1 in autophagy-deficient cells. In autophagy-deficient ATG8 knock out (KO) HeLa cells (**Fig 1C**), ULK1 KO MEF cells (**Fig EV2B**), and Atg5 KO MEF cells (**Fig 1D**), both basal and starvation-induced degradation of CALCOCO1 were impaired, suggesting that the degradation of CALCOCO1 is dependent on macro-autophagy.

Next, we tried to look at the intracellular localization of endogenous CALCOCO1, but the endogenous protein was poorly detected by immunostaining. Therefore, we stably expressed EGFP-CALCOCO1 from a tetracycline-inducible promoter in CALCOCO1 KO FlpIn T-REx HeLa cells (**Fig EV3**). Imaging of these cells revealed that a large proportion of the stably expressed EGFP-CALCOCO1 formed a perinuclear pattern characteristic of Golgi

and endoplasmic reticulum (ER) localization. Co-imaging with the cis-Golgi marker protein GM130 displayed extensive co-localization, strongly indicating that a significant fraction of CALCOCO1 is localized in cis-Golgi structures (**Fig 1E**). We also observed extensive co-localization of EGFP-CALCOCO1 with endogenous p62 and LC3 in cytoplasmic puncta (**Fig 1F, G and H**). Addition of Baf A1 strongly increased the number of puncta with co-localization, suggesting that CALCOCO1 is degraded by autophagy together with p62 and LC3 (Bjørkøy et al., 2005). LAMP1 staining of cells treated with Baf A1 demonstrated localization of EGFP-CALCOCO1 dots inside LAMP1-labelled structures (**Fig 1I**), further supporting that CALCOCO1 is degraded by autophagy. In response to starvation, the localization pattern of EGFP-CALCOCO1 became more punctated and dispersed (**EV2C and D**). Similarly, immunofluorescence analysis of the cells revealed a strong co-localization of EGFP-CALCOCO1 with endogenous p62 and LC3 both in full medium and in autophagic vesicles induced with starvation (**Fig EV2E**). Under starvation conditions, EGFP-CALCOCO1 also co-localized with GABARAP in puncta (**Fig EV2E**).

CALCOCO1 binds directly to ATG8 family proteins with preference for the GABARAP subfamily

In *in vitro* GST pull-down binding assays CALCOCO1 interacted with several of the human ATG8 family proteins (**Fig 2A**). The strongest interaction was seen with GST-tagged GABARAP, but a strong interaction was also seen with GABARAPL1 and GABARAPL2 and a weaker interaction with LC3B and LC3C. We also performed GST pulldown assays using HeLa cell extracts from cells transfected with Myc-CALCOCO1. This assay similarly revealed a binding preference for the GABARAP subfamily (**Fig 2B**).

Previous studies have reported that an atypical LIR core motif (LVV), engaging only one of the hydrophobic pockets used by canonical LIRs, mediate the interactions of TAX1BP1 and NDP52 with ATG8 family protein family (von Muhlinen et al., 2012, Whang et al., 2017). To define the role of this LIR motif in CALCOCO1, we mutated the core motif (LVV to AAA) resulting in a substantially reduced interaction with GABARAPL2. However, the interactions with the other ATG8s were only partially reduced (**Fig 2C and D**), suggesting the existence of an additional binding motif. Hence, we generated deletion mutants lacking or containing SKICH+LIR (1-144), CC (145-513) and CT (514-691), and some of the constructs also carrying the LVV to AAA LIR mutation (mLIR) (**Fig 2C)**. A simultaneous mutation of LIR and deletion

of CT (mLIR ΔCT) completely abrogated the interaction with all the tested ATG8 family proteins (**Fig 2D**). Thus, our data support an important role for the LIR motif, but the interaction also depends on an additional ATG8 family interaction motif in the C-terminal region of CALCOCO1. We also noted that CALCOCO1 ΔCC containing both binding motifs interacted strongly with ATG8 proteins, while constructs containing only one of the binding motifs appeared to depend on the CC domain for efficient interaction (**Fig 2D**).

To identify the C-terminal motif, we deleted 11, 21, 31, 41, 51, or 61 residues from the C-terminal end of CALCOCO1 ΔLIR (Δ126-144), and tested the interaction with GABARAP subfamily proteins (**Fig 2E and EV4A**). While a deletion of 41 amino acids (Δ651-691), had no apparent effect on the interaction, a deletion of the C-terminal 51 amino acids (Δ641-691) abolished the interaction (**Fig 2E**). A deletion of the C-terminal 68 amino acids (Δ623-691) similarly abolished the interaction (**Fig 2F**). We also compared the effect of deleting residues 651-679 or 654-679, and found that the extended deletion of residues 651-653 had a small but detectable effect on the interaction (**Fig EV4B**). We therefore consider these residues to form part of the ATG8 interacting motif. However, the zinc finger domain (residues 655-679) does not seem to be important for the interaction. To identify the N-terminal extension of the interaction, we made several internal deletions within the predicted ATG8 interacting region of CALCOCO1, and two of these (Δ615-634 and Δ619-646) strongly reduced the interaction (**Figure 2G and H**). Thus, we propose that the ATG8 interaction is mediated by the region encompassing amino acids 615-653 (**Fig 2C**).

CALCOCO1 binds both to LDS and UDS of ATG8 family proteins

Recently, a novel docking site on ATG8 family proteins binding to ubiquitin interacting motif (UIM)-like sequences was reported (Marshall et al., 2019). This UIM-docking site (UDS) is located on the opposite side of the ATG8 proteins relative to the LDS. This makes it possible for ATG8 proteins to simultaneously recruit both LIR and UIM-containing proteins (Marshall et al., 2019). To test if CALCOCO1 interacts with the two sites, we made GST-tagged GABARAP subfamily constructs with LDS (mLDS) or UDS (mUDS) point mutations and tested their binding to *in vitro* translated CALCOCO1. All the tested UDS and LDS+UDS mutants completely lostthe interaction with full-length CALCOCO1 (**Fig 3A**). These results suggest that GABARAP subfamily proteins require UDS contacts to stabilize their interactions

with CALCOCO1, suggesting that the C-terminal motif interacts with the UDS. The mutation of LDS in GABARAP and GABARAPL1 strongly inhibited the interaction with CALCOCO1 (**Fig 3A**), but a similar LDS mutation in GABARAPL2 had no effect on the interaction (**Fig 3A**).

The tolerance of the GABARAPL2-CALCOCO1 interaction towards a loss of the LDS was unexpected, since this interaction was strongly affected by a LIR mutation (**Fig 2D**). To specifically look at the LIR-LDS interaction, we performed GST pulldown assays with LDS mutated ATG8 family proteins and CALCOCO1 ΔCT (**Fig 3B**). As expected, since binding to the ΔCT construct depends on the LIR-LDS interaction, binding of all ATG8s, including GABARAPL2, was strongly impaired by an LDS mutation (**Fig 3B**). Similarly, we tested CALCOCO1 constructs lacking the LIR motif, i. e. mLIR or ΔSKICH. It appeared that the LDS mutation in GABARAPL2 had a strong and positive effect on its interaction with LIR deleted CALCOCO1 constructs (**Fig 3B**). This probably explains why the LDS mutation in GABARAPL2 did not inhibit the full-length CALCOCO1 interaction, but it also seems to indicate that a mutation of LDS in GABARAPL2 has an unexpected positive effect on the UDS interaction.

Because of the possibility that mutations in the LDS or UDS site of ATG8 family could interfere with binding of proteins to the UDS or LDS site respectively, we tested the binding of the LDS and UDS mutants to p62/SQSTM1, a protein known to bind ATG8 family proteins via LIR-LDS contact only (Pankiv et al., 2007). As expected, the LDS mutants lost interactions with p62 but UDS mutants had no effect on the binding (**Fig 3C**), suggesting that mutation of UDS sites did not interfere with interactions at the LDS sites.

TAX1BP1, but not NDP52, binds to GABARAP via a region interacting with the UDS

NDP52 is reported to bind preferentially to LC3C via its LIR motif while TAX1BP1 interacts with LC3C, GABARAP and GABARAPL1 (von Muhlinen et al., 2012, Whang et al., 2017). In in vitro GST pulldown assays, we confirmed that NDP52 binds preferentially to LC3C as reported (von Muhlinen et al., 2012), but also observed a potent interaction with GABARAP (**Fig EV4C**). TAX1BP1 interacted most strongly with LC3C and GABARAP (**Fig EV4D**). Mutation of the LIR motif (LVV to AAA) in NDP52 abolished the interaction with both LC3C and GABARAP (**Fig EV4C**). Similar to CALCOCO1, mutation of the LIR (mLIR) sequence

in TAX1BP1 only reduced the interaction with GABARAP but did not eliminate binding (**Fig 3D**). Given that CALCOCO1 and TAX1BP1 are paralogous proteins, we reasoned that TAX1BP1 could also have UIM-like motif in the C-terminal half that binds to the UDS site of GABARAP. We therefore tested the binding of GABARAP LDS, UDS and LDS+UDS mutants to TAX1BP1. Both GABARAP UDS and GABARAP LDS+UDS mutants completely abolished the interaction with TAX1BP1 (**Fig 3D**), suggesting involvement of UIM-UDS interface in the binding of TAX1BP1 to GABARAP, additively to the LIR-LDS interface.

To identify the UIM motif in TAX1BP1, we made a series of deletions in the C-terminal half of TAX1BP1 mLIR and examined their binding to WT, LDS and UDS mutants of GABARAP. TAX1BP1 mLIR bearing a deletion of amino acids 701-789 abolished interaction with both the WT and mLDS versions of GABARAP (**Fig 3D**), suggesting amino acids 701-789 contain the region for UDS contact during TAX1BP1 interaction with GABARAP. A strong inhibition was also caused by a deletion of residues 725-789 (**Fig EV4D and E**). These results indicate that TAX1BP1, like CALCOCO1, bears both LIR and UIM-like motifs that interact with ATG8 family proteins co-dependently. However, inspection of the sequences of the regions of CALCOCO1 (amino acids 615-653) and TAX1BP1 (aminio acids 725-786) required for binding to UDS reveal no homology and there is also no homology to the UIM sequences reported to bind to ATG8s by Marshall et al. (Marshall et al., 2019). Therefore, we suggest to call these regions UDS interacting regions (UIR).

Degradation of CALCOCO1 is dependent on binding to ATG8 family proteins

To test whether the degradation of CALCOCO1 is dependent on its binding to ATG8 family proteins, we stably expressed EGFP-CALCOCO1 mLIR+Δ623-691 in FlpIn T-REx CALCOCO1 KO HeLa cells. In these cells, reconstituted EGFP-CALCOCO1 strongly accumulated in response to the treatment with Baf A1 (**Fig 3E**), indicating efficient degradation of the wild type protein by autophagy. However, the amount of the reconstituted EGFP-CALCOCO1 mLIR+Δ623-691 was neither affected by addition of bafilomycin A1 nor by starvation (**Fig 3E**). This strongly suggests that the degradation of CALCOCO1 is dependent on binding to ATG8 family proteins via LIR and UIR binding motifs. HeLa CALCOCO1 KO cells reconstituted with EGFP-CALCOCO1 mLIR+Δ623-691 also revealed a complete loss of co-localization with p62/LC3 positive puncta in cells treated with Baf A1 (**Fig 3F**). Furthermore, the mutant construct did not respond to starvation, and the starvation induced

redistribution into puncta seen for WT CALCOCO1 was not seen with the mutant (**Fig EV5A and B**).

CALCOCO1 promotes autophagic flux

In response to starvation, EGFP-CALCOCO1 redistributed into a more peripheral localization pattern. Its Golgi localization became more dispersed and the number of cytoplasmic puncta increased. Co-staining of the HBSS-treated cells with WIPI2 and ATG13 antibodies demonstrated co-localization of EGFP-CALCOCO1, WIPI2 and ATG13 in the cytoplasmic puncta (**Fig 4A**), suggesting that CALCOCO1 is recruited to early autophagic structures formed in response to starvation.

Because of its degradation by autophagy we speculated that CALCOCO1, like its paralogues NDP52 and TAX1BP1, could be playing a role in autophagy. Hence, we generated CALCOCO1 knockout (KO) HeLa and HEK293 cells by CRISPR/Cas9 (**Fig EV3**), and investigated how the absence of CALCOCO1 affected the autophagy process. Lipidated LC3B (LC3B-II) and GABARAP are components of mature autophagosomes and are degraded together with the cargo and therefore their abundance can be used to measure autophagy flux. Compared to the wild type cells, CALCOCO1 KO HeLa and HEK 293 cells retained higher amount of LC3B-II and GABARAP-II under basal conditions (**Fig 4B and C**). Treatment of the cells with Baf A1 led to an accumulation of comparatively equal amounts in both wild type and KO cells (**Fig 4B and C**), suggesting that the increased amount of LC3B-II and GABARAP-II in the KO cells was caused by a less efficient autophagy process.

Completion of the autophagy process can be measured by monitoring the abundance of substrates such as selective autophagy receptors (SARs). To further test whether the absence of CALCOCO1 impaired degradation by autophagy, we monitored the turnover of some of the known SARs. Compared to the wild type cells, the basal levels of p62, NBR1 and NDP52 were higher in the CALCOCO1 KO HeLa and HEK293 cells (**Fig 4B and C**). The levels of the receptors were comparatively equal when the cells were treated with Baf A1 (**Fig 4B and C**), suggesting that the increased basal amounts of the receptors in the absence of CALCOCO1 was caused by impaired degradation. To clarify whether absence of CALCOCO1 was causing the impairment, we reconstituted KO HeLa cells with inducible EGFP-CALCOCO1 and monitored the effect on degradation. Induced expression of EGFP-CALCOCO1 rescued the turnover of

LC3B-II, GABARAP-II, p62, NBR1 and NDP52 as in wild type cells (**Fig 4D and E**). Taken together, these results suggest that CALCOCO1 promotes basal autophagy flux.

CALCOCO1 interacts with VAP-A/B via a FFAT motif

The ER and Golgi localization of CALCOCO1 raised the possibility that it interacts with ER and Golgi associated proteins. Hence, we performed IP experiments using EGFP-CALCOCO1 expressed stably in HEK293 cells as bait and identified the bound proteins by mass spectrometry. After stringent filtering against GFP control, about 30% of the identified proteins were either ER- or Golgi associated (**Fig 5A**). Among the proteins in the CALCOCO1 interactome was the ER tethering protein VAPA.

VAPA and VAPB are integral ER membrane proteins involved mainly in forming contacts between the ER and other membranes via interaction with proteins bearing the VAP-interacting motif called FFAT (two phenylalanines (FF) in an acidic tract (AT) using their N-terminal major sperm domain (MSP) (Murphy and Levine, 2016). The interaction is initiated by the acidic tract binding to the electro-positive surface of MSP domain and then cemented by specific interactions with the core FFAT motif. Given the perinuclear localization of CALCOCO1, VAP proteins were prime candidates for recruiting CALCOCO1 to the ER and therefore we focused on them in our study. To validate the interactome and test whether CALCOCO1 and VAP proteins interacted, we co-expressed EGFP-CALCOCO1 with either Myc-VAPA or Myc-VAPB in HEK293 cells and investigated their interaction by immunoprecipitation. Both Myc-VAPA and Myc-VAPB were co-precipitated by EGFP-CALCOCO1, suggesting interaction of CALCOCO1 with VAPA/VAPB in cells **(Fig 5B**).

The critical residues in the MSP domain involved in the binding to FFAT motifs are K94/M96 and K87/M89 for VAPA and VAPB, respectively. The interaction can be blocked by double charge substitutions; K94D/M96D and K87D/M89D (KD/MD mutants) (Murphy and Levine, 2016). To determine whether the interaction of CALCOCO1 with VAPA and VAPB was via the FFAT motif, we made KD/MD mutants of VAPA and VAPB and tested their binding to CALCOCO1 in *in vitro* GST pulldown assays. Wild type GST-tagged VAPA and VAPB interacted with in vitro-translated Myc-CALCOCO1, suggesting direct interaction between CALCOCO1 with VAP proteins. The interaction was stronger with VAPA than with

VAPB. KD/MD mutants of VAPA and VAPB abolished the interactions (**Fig 5C**), suggesting existence of a FFAT or FFAT-like motif in CALCOCO1.

To test whether CALCOCO1 actually has a FFAT motif, we made deletion mutants lacking either the SKICH domain (Δ1-144), coil-coil domain (Δ145-513) or C-terminal region (Δ514-691) and investigated which region of CALCOCO1 was binding to VAP proteins. Only deletion of the C-terminal region (Δ514-691) abolished the interaction of CALCOCO1 with VAPA and VAPB (**Fig 5D**), suggesting involvement of the C-terminal region in the interaction. Analysis of the CALCOCO1 primary structure in this region identified the sequence 680-FFFSTQD-686 as a potential FFAT-like motif. To test if this motif is responsible for the interaction, we made further mutations in CALCOCO1 ΔSKICH + ΔLIR, a construct strongly interacting with the VAPs (**Fig 5D**). Mutations of the first three residues of the predicted core FFAT-like motif (FFF/AAA) (Murphy and Levine, 2016) abolished most of the interaction with VAPs (**Fig 5D**). A simultaneous deletion of the core FFAT-like motif and the flanking upstream acidic tract region (Δ671-691) completely abolished the interactions (**Figure 5D**), suggesting that the FFAT-like motif was specifically mediating the interactions. Co-expression of EGFP-CALCOCO1 with either Myc-VAPA or Myc-VAPB showed perinuclear co-localization (**Fig 5E**), suggesting association of CALCOCO1 and VAPs in cells. Taken together, these results show that CALCOCO1 binds directly to ER integral membrane tethering proteins VAPA and VAPB via a FFAT-like motif.

VAP proteins promote autophagy and starvation-induced degradation of tubular ER

Two recent studies showed that VAP proteins promote autophagy flux by positively augmenting the endosomal pathway and autophagosome biogenesis (Mao et al., 2019, Zhao et al., 2018). Despite their localization in the ER membrane, the role of VAP proteins in ER-phagy has not been clarified. ER-phagy degrades specific sub-domains of ER in response to physiological or pathological conditions such as proteotoxic stress and nutrient starvation. Given our discovery of the interaction of VAP proteins with CALCOCO1 and its degradation by autophagy, we asked whether VAPs are degraded by autophagy and what could be their effect on ER-phagy. Consequently, we investigated how inhibition of autophagy influences turnover of ER proteins, including VAP proteins, in cultured mammalian cells. In autophagy-deficient Atg5 knockout (KO) MEF cells, starvation and proteotoxic stress-induced degradation of ER proteins VAPA, VAPB and FAM134B was impaired compared to wild type cells (**Fig**

6A). This suggests involvement of autophagy in starvation and stress-induced degradation of the ER proteome consistent with recent reports (Grumati et al., 2017a, Smith et al., 2018). Treatment of the wild type cells with Baf A1 caused accumulation of VAPA, VAPB and FAM134B (**Fig 6A**), suggesting involvement of autophagy also in their basal turnover in cells. Hence, we investigated how absence of VAP proteins influenced autophagy. Depletion of both VAPA and VAPB with siRNAs in HeLa cells caused increased levels of LC3B, GABARAP and CALCOCO1 compared to cells transfected with control siRNA (**Fig 6B** and **C**). Treatment of the cells with Baf A1 caused comparable accumulation of the proteins in both VAPA/B depleted and control cells (**Fig 6C**), suggesting that the observed increased levels in VAPA/B-depleted cells was due to impaired lysosomal degradation, thus confirming recent reports (Mao et al., 2019, Zhao et al., 2018) that VAPs promote autophagy flux.

The degradation of VAP proteins by autophagy and their integral ER membrane localization suggested they could play a role in ER-phagy. To clarify the role of VAP proteins in ER-phagy, we made HeLa cells expressing EGFP-VAPA under the control of tetracycline-inducible promoter and monitored turnover of endogenous ER proteins. Induced expression of VAPA promoted starvation-induced decrease in the levels of endogenous CALCOCO1 and tubular ER proteins VAPB and RTN3 (**Fig 6D**), suggesting involvement of VAPA in the degradation of CALCOCO1 and tubular ER. In basal conditions, VAPA expression promoted degradation of CALCOCO1, VAPB, RTN3, p62 and GABARAP. Given depletion of VAPs led to defective degradation (**Fig 6C**), these results reciprocally suggest that VAPs promote autophagy flux.

To clarify whether CALCOCO1 and VAPA/B–positive ER fragments traffic together to the autophagosomes, we assessed their co-localization with LC3B under starvation conditions in the presence of Baf A1. Co-expressed EGFP-CALCOCO1 and either Myc-VAPA or Myc-VAPB formed perinuclear and cytoplasmic puncta that co-localized with endogenous puncta of LC3B (**Fig 6E**), suggesting that CALCOCO1 and VAPs-positive fragments traffic together in the autophagosomes.

CALCOCO1 is a soluble ER-phagy receptor

Given that CALCOCO1 interacts directly with transmembrane ER tethering proteins VAPA and VAPB, we surmised that CALCOCO1 could mediate ER-phagy in response to proteotoxic stress and nutrient starvation. CALCOCO1 fits the criteria for a ER-phagy receptor (Wilkinson, 2019b). Firstly, the interaction with VAP proteins gives it specificity for tubular ER membranes. Secondly, the strong interaction with ATG8 family proteins suggests that CALCOCO1 could not only form the platform for the recognition of the ER membranes by phagophores, but could also promote feedforward recruitment of autophagy machinery required for autophagosome biogenesis and clustering-mediated ER fragmentation. To clarify the role of CALCOCO1 in ER turnover, we investigated how lack of CALCOCO1 influenced ER-phagy using CALCOCO1 KO HeLa cells. When compared to the wild type cells, the absence of CALCOCO1 inhibited starvation-induced turnover of ER tubular proteins, but not ER sheet markers and other autophagy receptors. More specifically, CALCOCO1 KO impaired starvation-induced degradation of tubular ER proteins VAPA and VAPB but not ER sheets marker FAM134B or autophagy receptor p62 (**Fig 7A**).

To check whether re-introduction of CALCOCO1 could rescue the turnover of tubular ER, we reconstituted the CALCOCO1 KO cells with tetracycline-inducible EGFP-CALCOCO1. Compared to the non-induced cells, induced expression of EGFP-CALCOCO1 restored starvation and proteotoxic stress-induced degradation of tubular ER proteins RTN3, VAPA and VAPB (**Fig 7B**).

In response to physiological conditions such as nutrients deprivation, the ER increases in size through increased synthesis of ER resident proteins to augment its functions (Bernales et al., 2006, Wilkinson, 2019b). During recovery, ER-phagy is involved in remodelling the ER back to physiological size by sequestering ER sub-domains and excess membrane proteins for degradation in the lysosome. Because CALCOCO1 could mediate selective degradation of tubular ER, it was postulated that it could be involved in ER-phagy-mediated remodelling of ER in response to physiological conditions. We used immunofluorescence analysis of endogenous RTN3 to monitor the effect of CALCOCO1 on ER morphology and distribution during normal and starvation conditions. Induced expression of EGFP-CALCOCO1 for 24 hours at basal conditions in HeLa cells showed reduced ER to cytoplasm ratio when compared to the non-induced cells (**Fig 7C**), suggesting that CALCOCO1 promoted reduction of peripheral ER. The ER-to-cytoplasm ratio when the cells were stimulated by nutrients

starvation for 6 hours was higher in the non-induced cells than in the CALCOCO1-expressing cells. The ratios increased slightly when cells were treated with Baf A1, suggesting that CALCOCO1 was involved in the degradation of the peripheral ER, similarly as observed with the knockouts of other ER-phagy receptors FAM134B, CCPG1 and TEX164 (Chino et al., 2019, Khaminets et al., 2015, Smith et al., 2018). Immunoblotting analysis of the same cells revealed that the non-induced cells retained greater amounts of tubular ER proteins RTN3, VAPA, and VAPB at all the time points tested but not the ER sheet protein marker FAM134B (**Fig 7D**). We interpreted these results to mean that CALCOCO1 facilitates selective degradation of the tubular ER.

To define whether VAPs are required for CALCOCO1-mediated tubular ER degradation, we investigated how depletion of VAPs in the reconstituted cells influences ER-phagy and autophagy. Double depletion of VAPA and VAPB with siRNA impaired starvation-induced turnover of RTN3 as well as autophagy marker GABARAP in the induced cells (**Fig 7E**). We interpret this to mean that CALCOCO1 interacts with VAP proteins at the ER membrane to facilitate degradation of tubular ER.

Interaction with ATG8s is required for CALCOCO1-mediated ER-phagy

To clarify whether the turnover was mediated by macro-autophagy, we investigated how inhibition of autophagy in the reconstituted cells affected ER-phagy. The cells were treated with SAR405, an inhibitor of PIK3C3, the catalytic subunit of the PI3K class III complex (Ronan et al., 2014). PI3KC3 is critical for generation of PI3P required for autophagosome biogenesis. SAR405 treatment impaired CALCOCO1-mediated starvation-induced degradation of RTN3, VAPA and VAPB (**Fig 8A**), suggesting dependency of the CALCOCO1-mediated degradation of the ER tubular proteins on macro-autophagy.

Selective degradation by autophagy involves a receptor bridging the cargo to the autophagosome via interaction with ATG8 family proteins (Johansen and Lamark, 2019, Rogov et al., 2014, Stolz et al., 2014). To clarify whether ATG8 family interaction is required for CALCOCO1-mediated degradation of tubular ER, the CALCOCO1 KO cells were reconstituted with EGFP-CALCOCO1 mLIR+Δ623-691, a deletion mutant incapable of ATG8 family interaction and VAP interaction. Compared to the wild type EGFP-CALCOCO1 reconstituted cells (**Fig 7B**), reconstitution of the CALCOCO1 KO cells with EGFP-

CALCOCO1 mLIR+Δ623-691 impaired the starvation-induced degradation of RTN3 and VAPA, but not autophagy receptor p62 (**Fig 8B**). We interpreted this to mean that CALCOCO1 is a specific autophagy receptor for the degradation of ER tubules.

Autophagosomes deliver their cargo to lysosomes for degradation. We used immunofluorescence to assess delivery of CALCOCO1 and VAPA-positive autophagosomes to the lysosomes for degradation in HeLa cells. To adequately capture autophagosome-lysosome co-localization, cells were treated with Baf A1. In both basal and starved conditions, co-expressed mCherry-CALCOCO1 and Myc-VAPA formed cytoplasmic puncta that co-localized with EGFP-LAMP1, a lysosomal membrane marker (**Fig 8C**), suggesting delivery of CALCOCO1-bound VAPA-positive fragments to the lysosomes. A model of how we envision CALCOCO1 may be acting as a soluble ER-phagy receptor via binding to ATG8s and VAPA/B is shown in **Fig 8D**.

Discussion

ER-phagy remodels ER by sequestering specific subdomains for degradation in the lysosomes(Dikic, 2018, Wilkinson, 2019b). Recent studies have identified six mammalian ER resident membrane proteins as ER-phagy receptors that recruit autophagy machinery to initiate autophagosome formation around the portions of the ER to be degraded (An et al., 2019, Chen et al., 2019, Chino et al., 2019, Fumagalli et al., 2016, Grumati et al., 2017b, Khaminets et al., 2015, Smith et al., 2018). In addition, p62 acts as a soluble receptor by binding to TRIM13 anchored in the ER membrane to mediate ER-phagy via the N-degron pathway (Ji et al., 2019). In this study, we have identified CALCOCO1 as a specific soluble ER-phagy receptor for the degradation of tubular ER in response to starvation and proteotoxic stress. The ER subdomains are characterized by the presence of key proteins performing different functions. FAM134B, a known ER-phagy receptor, is localized in the ER sheets while RTN family proteins and VAPA/B preferentially localize to the ER tubules (Grumati et al., 2017b, Khaminets et al., 2015, Wang et al., 2017). We have shown that CALCOCO1 regulates the turnover of RTN3, VAPA and VAPB but not ER sheet protein FAM134B.

CALCOCO1 is unique relative to already identified receptors for having both a LIR motif and a second ATG8 family interaction motif that binds to the UDS. We named the second interacting motif UIR, since there was no UIM-like motif within the interacting region (residues

615-653) of CALCOCO1 or TAX1BP1. Also, ATG4B similarly interacts both with the LDS and the UDS (Satoo et al., 2009, Skytte Rasmussen et al., 2017), but no UIM-like motif can be identified in the region of ATG4B interacting with the UDS. Our results suggest that simultaneous interaction of the two motifs with ATG8 family proteins is required for strong and stable binding. The preferred interaction partner of CALCOCO1 is either GABARAP, GABARAPL1 or GABARAPL2. The ability to iteract with ATG8 family proteins was required for its own degradation by autophagy and for CALCOCO1-mediated degradation of the ER, suggesting, in our opinion, that CALCOCO1 is an ER-phagy receptor. Consistently, CALCOCO1-mediated ER degradation was lost when autophagy was impaired by the inhibition of the PI3KC3 complex. In contrast to other ER-phagy receptors in which depletion does not affect basal autophagy flux (Wilkinson, 2019a), loss of CALCOCO1 impaired the degradation of both ATG8 family and p62 in full medium, implying that CALCOCO1 promotes basal autophagy flux.

CALCOCO1 is not an ER transmembrane protein, setting it apart from most of the already identified ER-phagy receptors. Instead, our data show that CALCOCO1 is targeted to the ER by interacting with ER transmembrane proteins VAPA and/or VAPB via a C-terminal FFAT-like motif. Therefore, we suggest to classify CALCOCO1 as a soluble ER-phagy receptor, perhaps akin to p62 acting with TRIM13 (Ji et al., 2019), to distinguish it from other ER-resident ER-phagy receptors. Loss of VAP proteins impaired CALCOCO1-mediated degradation of tubular ER, implying that the CALCOCO1-VAP interaction is required for CALCOCO1-mediated ER-phagy. Conversely, overexpression of VAPA promoted degradation of CALCOCO1 and the short isoform of RTN3, a tubular ER remodelling protein. These results suggest a model where CALCOCO1 bound to VAPs recruit autophagy machinery via ATG8 family to specific ER sub-domains to initiate autophagosome biogenesis and capture of the degradable cargo (**Fig 8D**). Emerging evidence suggest that the ER membrane fragmentation required for ER-phagy depend on ATG8 family-mediated clustering (Wilkinson, 2019a). We therefore postulate that CALCOCO1-VAP coupling mediates recognition of specific tubular ER regions by autophagy machinery via ATG8 family proteins. This in turn initiates autophagosome biogenesis in the vicinity of those regions for engulfment and degradation, consistent with the emerging notion from recent studies that receptors act upstream of the autophagy machinery (Turco et al., 2019). The co-localization of early phagophore markers WIPI2 and ATG13 with CALCOCO1 puncta in this study and with VAPA/B in a previous study (Zhao et al., 2018), supports this proposition.

Overexpression of VAPA/B causes ER punctation and previous studies have determined that FFAT-VAP interaction may regulate ER morphology (Kaiser et al., 2005). Moreover, we have shown in this study that nutrient starvation upregulated ER tubular proteins RTN3, VAPA and VAPB. We envisage that the targeted regions of the ER are VAP-rich tubular extrusions generated by the remodelling activities of the ER in response to fluctuating conditions. The extrusions could be generated by the action of VAPs or by ER membrane reshaping proteins. In support of this proposistion, a recent study determined that VAPA and VAPB are present in interactomes of ER membrane reshaping proteins (Grumati et al., 2017b).

Protein-protein interactions and self-interaction of receptors play critical roles in driving morphological rearrangements of the ER required for packaging into autophagosomes (Wilkinson, 2019a). Consistent with this notion, VAP interacts with itself via its coiled-coil domain to form homodimers and with other ER proteins via either the coiled-coil domain or the transmembrane domain to form oligomeric chains. In addition, dimerization occurs between two FFAT motifs already bound to the VAP (Kaiser et al., 2005, Kim et al., 2010). Because CALCOCO1 is dimeric, it could use its bivalent interaction with VAP dimers or oligomeric chains to target the ER membrane more tightly and recruit increased amounts of autophagy machinery proteins, resulting in increased ER morphological changes and fragmentation.

The C-terminal regions of both TAX1BP1 and NDP52 contain two zinc finger domains, which mediate autophagy-critical interactions with ubiquitin, myosin VI, and galectins (Thurston et al., 2009, Tumbarello et al., 2012, von Muhlinen et al., 2012). In contrast, the C-terminal region of CALCOCO1, including its zinc finger domain, has not been well characterized and CALCOCO1 binds neither ubiquitin nor galectins. In this study, we have shown that the C-terminal region of CALCOCO1 contains a UIR motif that interacts with ATG8 family proteins and a FFAT-like motif that interacts with VAPA and VAPB. The FFAT (two phenylalanines in an acidic tract) motif targets proteins to the cytoplasmic face of the endoplasmic reticulum by binding to the VAP protein family. The consensus amino acid sequence of the core FFAT motif is EFFDAxE with an upstream acidic tract region (Loewen et al., 2003). The FFAT motif interaction with VAP involves both the acidic tract and the core FFAT motif (Furuita et al., 2010). The upstream acidic tract of the identified FFAT-like motif in CALCOCO1 (680-FFFSTQD-686) overlaps with the putative zinc finger domain. The core motif differs from the canonical FFAT motif at positions 1, 3, 4 and 7, consistent with other FFAT-like motifs (Mikitova and Levine, 2012). Analysis of CALCOCO1 showed that the motif is evolutionary conserved across species, implying the importance of the motif to its function.

Besides their role in targeting peripheral proteins to the ER, FFAT-VAP interactions have been associated with cytoskeletal organization, membrane trafficking, calcium signalling, ER-associated degradation (ERAD), and autophagosome biogenesis (Murphy and Levine, 2016, Zhao et al., 2018). We show in this study that FFAT-mediated interaction of CALCOCO1 with VAP targets tubular ER for degradation by autophagy. An important question is how CALCOCO1-mediated ER-phagy is regulated considering there are many FFAT-containing proteins conceivably competing for VAP interaction (Murphy and Levine, 2016). It is also plausible that CALCOCO1-VAP coupling could play other roles than ER-phagy. For instance, because VAP is part of different bridges between the ER and other organelles and CALCOCO1 is localized in the Golgi, CALCOCO1 could constitute part of ER-Golgi contact sites.

Materials and Methods

Antibodies: Mouse monoclonal anti-CALCOCO1 (A-10) (Santa Cruz Biotech Cat#sc-515670), rabbit polyclonal anti-CALCOCO1 (Sigma-Aldrich Cat#HPA038314), mouse polyclonal anti-CALCOCO1 (Abcam Cat# ab167237), rabbit polyclonal anti-VAPA (Proteintech Cat#15275-1-AP), rabbit polyclonal anti-VAPB (clone 4F6A6)(Proteintech Cat#66191-1-IG), rabbit polyclonal anti-GFP (Abcam Cat #ab290), mouse monoclonal anti-p62 (BD Biosciences Cat #610833), guinea pig polyclonal anti-p62 (Progen Cat #GP62-C), rabbit polyclonal anti-CALCOCO2 (Sigma-Aldrich Cat #HPA023195), rabbit anti-CALCOCO2 (Abcam Cat #ab68588), rabbit monoclonal anti-ATG7 (Cell Signaling Cat #D12B11), rabbit polyclonal anti-LC3B (Novus Bio Cat #NB100-2220), rabbit polyclonal anti-LC3B (Sigma-Aldrich Cat # L7543), mouse monoclonal anti-GABARAP(MBL Cat # M135-3), mouse monoclonal anti-Myc tag (9B11) cell signalling #2276), mouse monoclonal anti-RTN3 (F-6) (Santa Cruz Biotechnology Cat #sc-374599), rabbit polyclonal FAM134B (Proteintech Cat #21537-1-AP), mouse polyclonal anti-NBR1 (Santa cruz biotechnology #sc-130380), rabbit polyclonal anti-GAPDH (Sigma-Aldrich Cat#G9545), rabbit polyclonal anti-Actin (Sigma-Aldrich Cat #A2066), HRP-conjugated goat polyclonal anti-rabbit (BD Biosciences Cat #554021), HRP-conjugated goat polyclonal anti-mouse (BD Biosciences Cat #554002)

Reagents/Chemicals: Bafilomycin A1 (Santa Cruz Biotech sc-201550), MG132 (Sigma-Aldrich #C2211), [35S] methionine (PerkinElmer NEG709A500UC), T7 coupled reticulocyte lysate system (Promega #14610), Ponceau S (sigma #P3504), Dulbeco's modified

Eagle's medium (DMEM) (Sigma-Aldrich #D6046), HBSS (Sigma-Aldrich #H9269), Hygromycin (Thermofisher #10687-010), Tetracycline (Sigma-Aldrich #87128), Doxycycline (Sigma-Aldrich #D9891), Pen/Strep (Sigma-Aldrich #P4333), Metafectene Pro (Biontex #T040), Fetal bovine serum (FBS) (Biochrom #S0615), Lipofectamine RNAiMAX (Thermofisher #13778), Complete EDTA-free Protease inhibitor (Roche #11836170001), Chemiluminescent HRP substrate (Sigma-Aldrich), GFP-TRAP (Chromotek #GA-20), Glutathione sepharose beads (GE Healthcare #17-5132-01). The following siRNA oligonucleotides were used: CALCOCO1; 5'-GAAGCUGAGUGCAGAGAUA-3' (Sigma), VAPA; 5'-CCUGAGAGAUGAAGGUUUA-3' (Sigma), VAPB; 5'-GGAAGACAGUGCAGAGCAA-3'(Sigma), Smartpool siGENOME VAPA siRNA (Dharmacon, M-021382-01-0005) and Smartpool siGENOME VAPB siRNA (Dharmacon, M-017795-00-0005).

Plasmid constructs

All the plasmid constructs used in this study are listed in Appendix Table S1. The constructs were made using conventional cloning techniques and the Gateway recombination system (Invitrogen). Mutagenesis was performed using the QuickChange site-directed mutagenesis kit (Stratagene). Oligonucleotides for mutagenesis and sequencing were from Invitrogen. All constructs were verified by sequencing (BigDye, Applied Biosystems). pDONR201-CALCOCO1 was obtained from Harvard plasmid collection (HSCD00081507), pEGFPC1-hVAPA and pEGFPC1-hVAPB were obtained from Addgene (#104447 and #104448, respectively.).

Mammalian cell culture and cell treatments

We used human HeLa cells (ATCC CCL-2), MEFs and Atg5 KO MEFs (Kuma et al., 2004), and HeLa KO for all six ATG8 family genes (Abudu et al., in preparation). All cells were cultured in DMEM (Sigma-Aldrich, D6046) supplemented with 10% fetal bovine serum (Biochrom, S 0615) and 1% streptomycin-penicillin (Sigma-Aldrich, P4333) and kept in a humidified incubator at 37^0C and 5% CO_2. Starvation experiments were conducted by incubating cells in Hanks' Balanced Salt solution (Sigma-Aldrich, H9269). Cells were treated with 1 µg/ml of tetracycline (Sigma-Aldrich), 200 ng/ml bafilomycin A1 (Santa Cruz

Biotechnology, sc-201550), 25 µM MG132, for the indicated time periods. DNA transfection were done with metafectene Pro(Biontex #T040) according to manufacturers protocol. SiRNA transfections were done with RNAiMAX according to manufacturer's protocol

Generation and propagation of inducible stable cell lines

Flp-In Trex HeLa cells and Flp-In Trex HEK293 cells were used to create inducible stable cell lines and to produce CALCOCO1 knockout cells. Tagged constructs were cloned into pcDNA5/FRT/TO vector using the Gateway technology and then co-transfected with recombinase pOG44 into the Flp-In Trex cells. After 48 hours, colonies of cells with the gene of interest integrated into the FRT site were selected with 200 µg/ml of hygromycin (Calbiochem, 400051) and 7.5 µg/ml blasticidin. Polyclonal hygromycin-resistant cells were then expanded in the selection media and later tested for expression by immunoblotting and immunofluorescence. The expression of the gene was induced with 1µg/ml tetracycline for 24 hours..EGFP-p62 MEF cells were generated by lentiviral delivery of EGFP-p62 coding sequence in pCDNA5/LTR vector into MEF knockout cells followed by selection for stable integration with blasticidin. Viruses for infection were produced in Platinum E cells. Induction was performed with 1 µg/ml doxycycline.

Generation of knockout cell lines using CRISPR-Cas9

Specific RNA-guides were designed using the CHOPCHOP web tool (found at https://chopchop.cbu.uib.no) (Labun et al., 2019). The sequences of the sgRNA used are 5' CACCGGAAGAATCACCACTAAGCC 3', 5'- CACCGAGAAAGTTGACTCCACCAC-3'and 5'- CACCGTTCCGATATGTGAACCGCC-3' (see Fig EV3). The sense and antisense oligonucleotides were annealed and phosphorylated and then ligated into a BbsI linearized pSpCas9(BB)-2A-Puro (PX459) vector (Addgene #62988). To generate CALCOCO1 knockout Flp-In T-Rex HeLa cells were transfected with the PX459 vector containing sgRNA targeting exon 2 while to generate CALCOCO1 knockout Flp-In T-Rex HEK293 cells, cells were transfected with PX459 vector containing sgRNA targeting exon2 and 4 using Metafectene Pro (Biontex #T040). 24 hours post transfection, the cells were selected by treatment with puromycin at 1 µg/mL for 72 hours. Puromycin-resistant cells were then singly sorted into 96-well plates. The clones were then expanded and screened by immunoblotting. Once knockout were confirmed by immunoblotting, genomic DNA were extracted and the area of interest

amplified by PCR. The amplified region was ligated into the PGEM vector (Promega #A3600) and sequenced to identify the indels.

Western blotting

Cells were directly lysed in 2x Laemli buffer (50 mM Tris pH 7.4, 2% SDS, 10% Glycerol, 200 mM dithiothreitol (DTT, Sigma, #D0632) and heated for 10 min. Protein concentrations were measured by Pierce BCA Protein Assay Kit (Thermofischer Scientific, #23227) and 30-40 µg protein of the sample were resolved by SDS-PAGE and transferred to nitrocellulose membrane. Membranes were blocked in PBS or TBS containing 0.1% Tween and 5% low fat milk and then incubated overnight at 4°C with the indicated primary antibodies in the blocking solution. Immuno-blot bands were quantified using ImageJ program.

Immunoprecipitation

Lysates from cells stably or transiently expressing EGFP or Myc-tagged proteins were immunoprecipitated by GFP/Myc-TRAP (Chromotek, # gta-20) or GST fusion immobilised on GST beads. Briefly, cells were lysed in modified RIPA buffer (50 mM Tris-Cl pH 7.4, 120 mM NaCl, 1 mM EDTA pH 8.0, 1% NP-40, 0,25% Triton X-100) supplemented with cOmplete Mini EDTA-free protease inhibitor cocktail tablets (Roche AppliedScience, #11836170001) on ice for 30 min and then pelleted by centrifugation at 10.000 x g for 10 min. Supernatants were incubated with either GFP-TRAP, Myc-TRAP or GST-fusion protein loaded beads for 1 h or overnight at 4 ^{0}C and then washed five times with RIPA buffer. Proteins were then eluted by boiling in 2X SDS sample buffer, resolved in SDS-PAGE and immunoblotting. GFP-tagged proteins were also immunoprecipitated using the µMACS GFP Isolation Kit (Miltenyi Biotec) according to the instruction manual

Mass spectrometry

Gel pieces were subjected to in gel reduction, alkylation, and tryptic digestion using 6 ng/µl trypsin (V511A, Promega, Wisconsin, USA) . OMIX C18 tips (Varian, Inc., Palo Alto, CA, USA) was used for sample cleanup and concentration. Peptide mixtures containing 0.1% formic

acid were loaded onto a Thermo Fisher Scientific EASY-nLC1000 system and EASY-Spray column (C18, 2µm, 100 Å, 50µm, 50 cm). Peptides were fractionated using a 2-100% acetonitrile gradient in 0.1 % formic acid over 50 min at a flow rate of 200 nl/min. The separated peptides was analysed using a Thermo Scientific Q-Exactive mass spectrometer. Data was collected in data dependent mode using a Top10 method. The raw data were processes using the MaxQuant software v1.6.0.16 using label-free quantification (LFQ) method. MS/MS data was searched against a Uniprot human database. A FDR ratio of 0.01 were needed to give a protein identification. Perseus v1.6.0.7 was used for statistical analysis

GST-pulldown assays

GST-fusion proteins (LC3s, GABARAPs, CALCOCO1, VAPs) were expressed in Escherichia coli SoluBL21 (DE3) (Genlantis, # C700200) in LB medium. Protein expression were induced by addition of 0.5 mM IPTG and cells were incubated with shaking at 37°C for 4 hours. Harvested cells were sonicated in the lysis buffer (20 mM Tris-HCl pH 7.5, 10 mM EDTA, 5 mM EGTA, 150 mM NaCl) and the GST-fused proteins then immobilized on Glutathione Sepharose 4 Fast Flow beads (GE Healthcare, #17-5132-01) by incubating in a rotator at 4^0C for one hour. Fusion protein-bound beads were then used directly in GST pull down assays with in vitro-translated proteins. In-vitro translation was done in the presence of radioactive ^{35}S-methionine using the TNT T7 Reticulocyte Lysate System (Promega, #l4610). 12 µL of the in-vitro translated protein were then pre-cleared by incubation with 10 µL of empty Glutathione sepharose beads in 100 µL of NETN buffer (50 mM Tris pH 8.0, 150 mM NaCl, 1 mM EDTA, 0.5% NP-40) supplemented with cOmplete Mini EDTA-free protease inhibitor for 30 min at 4 ^{0}C to remove non-specific binding. The precleared lysates were then incubated with the GST-fusion protein loaded beads for 1 hour at 4 ^{0}C. The beads were then washed five times with NETN buffer followed by resuspension in sample loading buffer (100 mM Tris pH 7.4, 4% SDS, 20% Glycerol, 0.2% Bromophenol blue and 200 mM dithiothreitol DTT (Sigma, # D0632) and boiled for 10 minutes and then resolution in SDS-PAGE. Gels were stained with Coomassie Brilliant Blue R-250 Dye (ThermoFisher Scientific, #20278) for 30 min to visualize the fusion proteins, washed and then vacuum-dried (in Saskia HochVakuum combined with BIO-RAD Gel dryer model 583, #1651746) for 30 min. Radioactive signals were analysed by Fujifilm bioimaging analyzer BAS-5000 (Fujifilm).

Immunofluorescence

Cells were plated on glass coverslips (VWR, #631-0150) or in Lab-Tek chambered coverglass (Thermo Scientific, #155411) and fixed in 4% (wt/vol) formaldehyde for 10 min at room temperature and then permeabilized with 0.1% Triton X-100 in PBS at room temperature for 5 min and blocked in PBS containing 3% goat serum for 1 hr at room temperature. Cells were then incubated overnight at 4° C with primary antibody diluted in PBS containing 2% goat serum. After five washes in PBS, they were incubated with AlexaFluor secondary antibodies in PBS containing 2% goat serum for 1 hr at room temperature followed by five washes in PBS. Nuclei were stained with 1 μg/ml DAPI in PBS for 10 min, followed by one final wash in PBS. Coverslips were mounted in 10 μl of Mowiol and placed on a glass microscope slide.

Light Microscopy

Cells were imaged on an Observer Z.1 inverted microscope, equipped either with an LSM880 scanner for confocal microscopy or an Axiocam 506 monochromatic camera for widefield microscopy followed by deconvolution (both systems Carl Zeiss Microscopy). Images were collected in ZEN software using a 63X NA1.4 oil immersion lens for coverslips, or a 40X NA1.2 water immersion lens for chambered coverglass. Optimal excitation and emission settings were determined using the Smart Setup function. Selected regions of interest in confocal images were further imaged with Airyscan super-resolution using optimal pixel size and z spacing as suggested by ZEN, and processed with a strength setting of 6.0. For deconvolution microscopy, z-stacks were obtained with 0.1 μm step size and without camera binning, resulting in a lateral pixel spacing of 114 nm. Images were deconvolved in Huygens (Scientific Volume Imaging) ver. 19.04 using the Classic Maximum Likelihood Estimation (CMLE) algorithm with built-in theoretical point spread functions for each fluorophore. All fluorescence channels were recorded at non-saturating levels and settings were kept identical between all samples used for comparisons or quantifications. For quantitative microscopy, images were acquired on a CellDiscoverer 7 widefield system running ZEN ver. 3.0 (Carl Zeiss Microscopy) using a 50X NA1.2 water immersion lens with a 2X optovar, and an ORCA-Flash 4.0 V3 sCMOS camera (Hamamatsu), resulting in images with lateral pixel spacing of 65 nm. For each treatment, 50–60 z-stacks ($z = 5$, $\Delta Z = 0.31$ μm) were recorded at randomly positioned xy coordinates. All camera and illumination settings were kept at identical (non-saturating) levels throughout the experiment.

Image Analysis

The abundance of ER was quantified from widefield fluorescence images of endogenous RTN3, acquired in random fashion using the Tiles & Positions module of ZEN. For each condition analysed, 25 regions of interest (typically containing 1,200 – 1,800 cells in total) were randomly distributed across each well. Cells were autofocussed in the DAPI channel and images acquired with identical illumination and camera settings between wells. Images were analysed in Volocity (PerkinElmer) ver. 6.3 using a custom-made measurement protocol to segment images into populations of objects representing nuclei, total cell area, and ER. To quantify changes in ER abundance, the ratio *(ER area / total cell area)* was calculated for all images, and the average ratio reported for each treatment group.

EGFP-CALCOCO1, p62, and LC3B puncta were quantified per image for >250 cells using a custom-made macro in Fiji (Schindelin et al., 2012). Briefly, EGFP-CALCOCO1 positive cell outlines were detected by automatically thresholding the EGFP channel and used to create a binary mask. Within this mask, puncta were detected and counted using Find Maxima in each channel. Counts were then divided by total EGFP-CALCOCO1 cell area to normalize for cell number and cell size. Finally, normalized counts were averaged for each treatment and normalized to the MEM control.

To determine p62 and LC3B colocalization in EGFP-CALCOCO1 puncta, object colocalization was quantified using Volocity ver. 6.3 (PerkinElmer). To this end, >100 typical EGFP-CALCOCO1 puncta (in 25–100 cells, depending on the density of puncta in each treatment) were individually identified and selected using the Stamp tool, creating circular ROIs matching puncta size. Fluorescence intensity values in the p62 and LC3B channels were then measured for each ROI. ROIs were scored as p62 positive, LC3B positive, and p62/LC3B positive if the relevant channel value was two times greater than the average cytoplasmic (non-puncta) intensity in each channel.

Acknowledgements

The technical assistance of Gry Evjen is greatly appreciated. We thank the Bioimaging core facility (KAM) at the Institute of Medical Biology (UiT – The Arctic University of Norway) for the use of instrumentation and expert assistance. This work was funded by grants from the FRIBIOMED (grant number 214448) and the TOPPFORSK (grant number 249884) programmes of the Research Council of Norway to T.J.

Author contributions

TMN designed the experiments, performed most of the experiments and interpreted the results. BKS, ES and KBL performed imaging experiments and analyzed data. J-AB performed mass spectrometry analyses. TJ, TL and TMN conceived the project and analyzed data. TMN, TL and TJ wrote the manuscript.

Conflict of interest

The authors declare that they have no conflict of interest.

References

An, H., Ordureau, A., Paulo, J. A., Shoemaker, C. J., Denic, V. & Harper, J. W. 2019. TEX264 Is an Endoplasmic Reticulum-Resident ATG8-Interacting Protein Critical for ER Remodeling during Nutrient Stress. *Mol Cell,* 74**,** 891-908.

Anding, A. L. & Baehrecke, E. H. 2017. Cleaning House: Selective Autophagy of Organelles. *Developmental Cell,* 41**,** 10-22.

Antonucci, L., Fagman, J. B., Kim, J. Y., Todoric, J., Gukovsky, I., Mackey, M., Ellisman, M. H. & Karin, M. 2015. Basal autophagy maintains pancreatic acinar cell homeostasis and protein synthesis and prevents ER stress. *Proceedings of the National Academy of Sciences,* 112**,** E6166-74.

Bento, C. F., Renna, M., Ghislat, G., Puri, C., Ashkenazi, A., Vicinanza, M., Menzies, F. M. & Rubinsztein, D. C. 2016. Mammalian Autophagy: How Does It Work? *Annual Review of Biochemistry,* 85**,** 685-713.

Bernales, S., Mcdonald, K. L. & Walter, P. 2006. Autophagy Counterbalances Endoplasmic Reticulum Expansion during the Unfolded Protein Response. *PLOS Biology,* 4**,** e423.

Bernales, S., Schuck, S. & Walter, P. 2007. ER-Phagy: Selective Autophagy of the Endoplasmic Reticulum. *Autophagy,* 3**,** 285-287.

Birgisdottir, A. B., Lamark, T. & Johansen, T. 2013. The LIR motif - crucial for selective autophagy. *J Cell Sci,* 126**,** 3237-47.

Bjørkøy, G., Lamark, T., Brech, A., Outzen, H., Perander, M., Øvervatn, A., Stenmark, H. & Johansen, T. 2005. p62/SQSTM1 forms protein aggregates degraded by autophagy and has a protective effect on huntingtin-induced cell death. *The Journal of Cell Biology,* 171**,** 603.

Chen, Q., Xiao, Y., Chai, P., Zheng, P., Teng, J. & Chen, J. 2019. ATL3 Is a Tubular ER-Phagy Receptor for GABARAP-Mediated Selective Autophagy. *Current Biology,* 29**,** 846-855.e6.

Chen, S., Novick, P. & Ferro-Novick, S. 2013. ER structure and function. *Current Opinion in Cell Biology,* 25**,** 428-433.

Chino, H., Hatta, T., Natsume, T. & Mizushima, N. 2019. Intrinsically Disordered Protein TEX264 Mediates ER-phagy. *Molecular Cell,* 74**,** 909-921.e6.

Cui, Y., Parashar, S., Zahoor, M., Needham, P. G., Mari, M., Zhu, M., Chen, S., Ho, H.-C., Reggiori, F., Farhan, H., Brodsky, J. L. & Ferro-Novick, S. 2019. A COPII subunit acts with an autophagy receptor to target endoplasmic reticulum for degradation. *Science,* 365**,** 53.

Dikic, I. 2018. Open questions: why should we care about ER-phagy and ER remodelling? *BMC Biol,* 16**,** 131.

Forrester, A., De Leonibus, C., Grumati, P., Fasana, E., Piemontese, M., Staiano, L., Fregno, I., Raimondi, A., Marazza, A., Bruno, G., Iavazzo, M., Intartaglia, D., Seczynska, M., Van Anken, E., Conte, I., De Matteis, M. A., Dikic, I., Molinari, M. & Settembre, C. 2019. A selective ER-phagy exerts procollagen quality control via a Calnexin-FAM134B complex. *EMBO J,* 38**,** e99847.

Fregno, I. & Molinari, M. 2018. Endoplasmic reticulum turnover: ER-phagy and other flavors in selective and non-selective ER clearance. *F1000Res,* 7**,** 454.

Fumagalli, F., Noack, J., Bergmann, Timothy j., Cebollero, E., Pisoni, Giorgia b., Fasana, E., Fregno, I., Galli, C., Loi, M., Soldà, T., D'antuono, R., Raimondi, A., Jung, M., Melnyk, A., Schorr, S., Schreiber, A., Simonelli, L., Varani, L., Wilson-Zbinden, C., Zerbe, O., Hofmann, K., Peter, M., Quadroni, M., Zimmermann, R. & Molinari, M. 2016. Translocon component Sec62 acts in endoplasmic reticulum turnover during stress recovery. *Nature Cell Biology,* 18**,** 1173.

Furuita, K., Jee, J., Fukada, H., Mishima, M. & Kojima, C. 2010. Electrostatic Interaction between Oxysterol-binding Protein and VAMP-associated Protein A Revealed by NMR and Mutagenesis Studies. *Journal of Biological Chemistry,* 285**,** 12961-12970.

Gatica, D., Lahiri, V. & Klionsky, D. J. 2018. Cargo recognition and degradation by selective autophagy. *Nat Cell Biol,* 20**,** 233-242.

Grumati, P., Morozzi, G., Holper, S., Mari, M., Harwardt, M. I., Yan, R., Muller, S., Reggiori, F., Heilemann, M. & Dikic, I. 2017a. Full length RTN3 regulates turnover of tubular endoplasmic reticulum via selective autophagy. *eLife,* 6**,** e25555.

Grumati, P., Morozzi, G., Hölper, S., Mari, M., Harwardt, M.-L. I. E., Yan, R., Müller, S., Reggiori, F., Heilemann, M. & Dikic, I. 2017b. Full length RTN3 regulates turnover of tubular endoplasmic reticulum via selective autophagy. *eLife,* 6**,** e25555.

Ji, C. H., Kim, H. Y., Heo, A. J., Lee, S. H., Lee, M. J., Kim, S. B., Srinivasrao, G., Mun, S. R., Cha-Molstad, H., Ciechanover, A., Choi, C. Y., Lee, H. G., Kim, B. Y. & Kwon, Y. T. 2019. The N-Degron Pathway Mediates ER-phagy. *Mol Cell,* 75**,** 1058-1072 e9.

Jia, W., Pua, H. H., Li, Q.-J. & He, Y.-W. 2011. Autophagy Regulates Endoplasmic Reticulum Homeostasis and Calcium Mobilization in T Lymphocytes. *The Journal of Immunology,* 186**,** 1564.

Johansen, T. & Lamark, T. 2011. Selective autophagy mediated by autophagic adapter proteins. *Autophagy,* 7**,** 279-296.

Johansen, T. & Lamark, T. 2019. Selective Autophagy: ATG8 Family Proteins, LIR Motifs and Cargo Receptors. *Journal of Molecular Biology*.

Kaiser, S. E., Brickner, J. H., Reilein, A. R., Fenn, T. D., Walter, P. & Brunger, A. T. 2005. Structural Basis of FFAT Motif-Mediated ER Targeting. *Structure,* 13**,** 1035-1045.

Khaminets, A., Heinrich, T., Mari, M., Grumati, P., Huebner, A. K., Akutsu, M., Liebmann, L., Stolz, A., Nietzsche, S., Koch, N., Mauthe, M., Katona, I., Qualmann, B., Weis, J., Reggiori, F., Kurth, I., Hubner, C. A. & Dikic, I. 2015. Regulation of endoplasmic reticulum turnover by selective autophagy. *Nature,* 522**,** 354-8.

Kim, S., Leal, S. S., Ben Halevy, D., Gomes, C. M. & Lev, S. 2010. Structural Requirements for VAP-B Oligomerization and Their Implication in Amyotrophic Lateral Sclerosis-associated VAP-B(P56S) Neurotoxicity. *Journal of Biological Chemistry,* 285**,** 13839-13849.

Kirkin, V. 2019. History of the Selective Autophagy Research: How Did It Begin and Where Does It Stand Today? *Journal of Molecular Biology*.

Kriegenburg, F., Ungermann, C. & Reggiori, F. 2018. Coordination of Autophagosome-Lysosome Fusion by Atg8 Family Members. *Curr Biol,* 28**,** R512-R518.

Kuma, A., Hatano, M., Matsui, M., Yamamoto, A., Nakaya, H., Yoshimori, T., Ohsumi, Y., Tokuhisa, T. & Mizushima, N. 2004. The role of autophagy during the early neonatal starvation period. *Nature,* 432**,** 1032-6.

Labun, K., Montague, T. G., Krause, M., Torres cleuren, Y. N., Tjeldnes, H. & Valen, E. 2019. CHOPCHOP v3: expanding the CRISPR web toolbox beyond genome editing. *Nucleic Acids Research,* 47**,** W171-W174.

Liang, J. R., Lingeman, E., Ahmed, S. & Corn, J. E. 2018. Atlastins remodel the endoplasmic reticulum for selective autophagy. *The Journal of Cell Biology,* 217**,** 3354.

Ling, L. & Goeddel, D. V. 2000. T6BP, a TRAF6-interacting protein involved in IL-1 signaling. *Proc Natl Acad Sci U S A,* 97**,** 9567-72.

Loewen, C. J. R., Roy, A. & Levine, T. P. 2003. A conserved ER targeting motif in three families of lipid binding proteins and in Opi1p binds VAP. *EMBO J,* 22**,** 2025-2035.

Mancias, J. D., Wang, X., Gygi, S. P., Harper, J. W. & Kimmelman, A. C. 2014. Quantitative proteomics identifies NCOA4 as the cargo receptor mediating ferritinophagy. *Nature,* 509**,** 105.

Mao, D., Lin, G., Tepe, B., Zuo, Z., Tan, K. L., Senturk, M., Zhang, S., Arenkiel, B. R., Sardiello, M. & Bellen, H. J. 2019. VAMP associated proteins are required for autophagic and lysosomal degradation by promoting a PtdIns4P-mediated endosomal pathway. *Autophagy,* 15**,** 1214-1233.

Marshall, R. S., Hua, Z., Mali, S., Mcloughlin, F. & Vierstra, R. D. 2019. ATG8-Binding UIM Proteins Define a New Class of Autophagy Adaptors and Receptors. *Cell,* 177**,** 766-781.e24.

Mikitova, V. & Levine, T. P. 2012. Analysis of the Key Elements of FFAT-Like Motifs Identifies New Proteins That Potentially Bind VAP on the ER, Including Two AKAPs and FAPP2. *PLOS ONE,* 7**,** e30455.

Mizushima, N. & Komatsu, M. 2011. Autophagy: renovation of cells and tissues. *Cell,* 147**,** 728-41.

Mizushima, N., Yoshimori, T. & Ohsumi, Y. 2011. The role of Atg proteins in autophagosome formation. *Annu Rev Cell Dev Biol,* 27**,** 107-32.

Mochida, K., Oikawa, Y., Kimura, Y., Kirisako, H., Hirano, H., Ohsumi, Y. & Nakatogawa, H. 2015. Receptor-mediated selective autophagy degrades the endoplasmic reticulum and the nucleus. *Nature,* 522**,** 359.

Morriswood, B., Ryzhakov, G., Puri, C., Arden, S. D., Roberts, R., Dendrou, C., Kendrick-Jones, J. & Buss, F. 2007. T6BP and NDP52 are myosin VI binding partners with potential roles in cytokine signalling and cell adhesion. *Journal of Cell Science,* 120**,** 2574.

Murphy, S. E. & Levine, T. P. 2016. VAP, a Versatile Access Point for the Endoplasmic Reticulum: Review and analysis of FFAT-like motifs in the VAPome. *Biochimica et Biophysica Acta (BBA) - Molecular and Cell Biology of Lipids,* 1861**,** 952-961.

Nixon-Abell, J., Obara, C. J., Weigel, A. V., Li, D., Legant, W. R., Xu, C. S., Pasolli, H. A., Harvey, K., Hess, H. F., Betzig, E., Blackstone, C. & Lippincott-Schwartz, J. 2016. Increased spatiotemporal resolution reveals highly dynamic dense tubular matrices in the peripheral ER. *Science,* 354**,** aaf3928.

Ohsumi, Y. 2014. Historical landmarks of autophagy research. *Cell Res,* 24**,** 9-23.

Okamoto, K. 2014. Organellophagy: eliminating cellular building blocks via selective autophagy. *J Cell Biol,* 205**,** 435-45.

Pankiv, S., Clausen, T. H., Lamark, T., Brech, A., Bruun, J.-A., Outzen, H., Øvervatn, A., Bjørkøy, G. & Johansen, T. 2007. p62/SQSTM1 Binds Directly to Atg8/LC3 to Facilitate Degradation of Ubiquitinated Protein Aggregates by Autophagy. *Journal of Biological Chemistry,* 282**,** 24131-24145.

Rogov, V., Dötsch, V., Johansen, T. & Kirkin, V. 2014. Interactions between Autophagy Receptors and Ubiquitin-like Proteins Form the Molecular Basis for Selective Autophagy. *Molecular Cell,* 53**,** 167-178.

Ronan, B., Flamand, O., Vescovi, L., Dureuil, C., Durand, L., Fassy, F., Bachelot, M. F., Lamberton, A., Mathieu, M., Bertrand, T., Marquette, J. P., El-Ahmad, Y., Filoche-Romme, B., Schio, L., Garcia-Echeverria, C., Goulaouic, H. & Pasquier, B. 2014. A highly potent and selective Vps34 inhibitor alters vesicle trafficking and autophagy. *Nat Chem Biol,* 10**,** 1013-9.

Samie, M., Lim, J., Verschueren, E., Baughman, J. M., Peng, I., Wong, A., Kwon, Y., Senbabaoglu, Y., Hackney, J. A., Keir, M., Mckenzie, B., Kirkpatrick, D. S., Van Lookeren Campagne, M. & Murthy, A. 2018. Selective autophagy of the adaptor TRIF regulates innate inflammatory signaling. *Nature Immunology,* 19**,** 246-254.

Satoo, K., Noda, N. N., Kumeta, H., Fujioka, Y., Mizushima, N., Ohsumi, Y. & Inagaki, F. 2009. The structure of Atg4B-LC3 complex reveals the mechanism of LC3 processing and delipidation during autophagy. *EMBO J,* 28**,** 1341-50.

Schindelin, J., Arganda-Carreras, I., Frise, E., Kaynig, V., Longair, M., Pietzsch, T., Preibisch, S., Rueden, C., Saalfeld, S., Schmid, B., Tinevez, J. Y., White, D. J., Hartenstein, V., Eliceiri, K., Tomancak, P. & Cardona, A. 2012. Fiji: an open-source platform for biological-image analysis. *Nat Methods,* 9**,** 676-82.

Schroder, M. 2008. Endoplasmic reticulum stress responses. *Cell Mol Life Sci,* 65**,** 862-94.

Schwarz, D. S. & Blower, M. D. 2016. The endoplasmic reticulum: structure, function and response to cellular signaling. *Cell Mol Life Sci,* 73**,** 79-94.

Skytte Rasmussen, M., Mouilleron, S., Kumar Shrestha, B., Wirth, M., Lee, R., Bowitz Larsen, K., Abudu Princely, Y., O'reilly, N., Sjottem, E., Tooze, S. A., Lamark, T. & Johansen, T. 2017. ATG4B contains a C-terminal LIR motif important for binding and efficient cleavage of mammalian orthologs of yeast Atg8. *Autophagy,* 13**,** 834-853.

Smith, M. D., Harley, M. E., Kemp, A. J., Wills, J., Lee, M., Arends, M., Von Kriegsheim, A., Behrends, C. & Wilkinson, S. 2018. CCPG1 Is a Non-canonical Autophagy Cargo Receptor Essential for ER-Phagy and Pancreatic ER Proteostasis. *Dev Cell,* 44**,** 217-232.e11.

Sternsdorf, T., Jensen, K., Züchner, D. & Will, H. 1997. Cellular Localization, Expression, and Structure of the Nuclear Dot Protein 52. *The Journal of Cell Biology,* 138**,** 435.

Stolz, A., Ernst, A. & Dikic, I. 2014. Cargo recognition and trafficking in selective autophagy. *Nat Cell Biol,* 16**,** 495-501.

Thurston, T. L. M., Ryzhakov, G., Bloor, S., Von Muhlinen, N. & Randow, F. 2009. The TBK1 adaptor and autophagy receptor NDP52 restricts the proliferation of ubiquitin-coated bacteria. *Nature Immunology,* 10**,** 1215.

Thurston, T. L. M., Wandel, M. P., Von Muhlinen, N., Foeglein, Á. & Randow, F. 2012. Galectin 8 targets damaged vesicles for autophagy to defend cells against bacterial invasion. *Nature,* 482**,** 414.

Tumbarello, D. A., Manna, P. T., Allen, M., Bycroft, M., Arden, S. D., Kendrick-Jones, J. & Buss, F. 2015. The Autophagy Receptor TAX1BP1 and the Molecular Motor Myosin VI Are Required for Clearance of Salmonella Typhimurium by Autophagy. *PLoS Pathog,* 11**,** e1005174.

Tumbarello, D. A., Waxse, B. J., Arden, S. D., Bright, N. A., Kendrick-Jones, J. & Buss, F. 2012. Autophagy receptors link myosin VI to autophagosomes to mediate Tom1-dependent autophagosome maturation and fusion with the lysosome. *Nature Cell Biology,* 14**,** 1024.

Turco, E., Fracchiolla, D. & Martens, S. 2019. Recruitment and Activation of the ULK1/Atg1 Kinase Complex in Selective Autophagy. *Journal of Molecular Biology*.

Von muhlinen, N., Akutsu, M., Ravenhill, Benjamin j., Foeglein, Á., Bloor, S., Rutherford, Trevor j., Freund, Stefan m. V., Komander, D. & Randow, F. 2012. LC3C, Bound Selectively by a Noncanonical LIR Motif in NDP52, Is Required for Antibacterial Autophagy. *Molecular Cell,* 48**,** 329-342.

Wang, X., Li, S., Wang, H., Shui, W. & Hu, J. 2017. Quantitative proteomics reveal proteins enriched in tubular endoplasmic reticulum of Saccharomyces cerevisiae. *eLife,* 6**,** e23816.

Whang, M. I., Tavares, R. M., Benjamin, D. I., Kattah, M. G., Advincula, R., Nomura, D. K., Debnath, J., Malynn, B. A. & Ma, A. 2017. The Ubiquitin Binding Protein TAX1BP1 Mediates Autophagosome Induction and the Metabolic Transition of Activated T Cells. *Immunity,* 46**,** 405-420.

Wilkinson, S. 2019a. Emerging Principles of Selective ER Autophagy. *Journal of Molecular Biology*.

Wilkinson, S. 2019b. ER-phagy: shaping up and de-stressing the endoplasmic reticulum. *FEBS J,* 286**,** 2645-2663.

Wirth, M., Zhang, W., Razi, M., Nyoni, L., Joshi, D., O'reilly, N., Johansen, T., Tooze, S. A. & Mouilleron, S. 2019. Molecular determinants regulating selective binding of autophagy adapters and receptors to ATG8 proteins. *Nat Commun,* 10**,** 2055.

Zhao, Y. G., Liu, N., Miao, G., Chen, Y., Zhao, H. & Zhang, H. 2018. The ER Contact Proteins VAPA/B Interact with Multiple Autophagy Proteins to Modulate Autophagosome Biogenesis. *Current Biology,* 28**,** 1234-1245.e4.

FIGURE LEGENDS

Figure 1. CALCOCO1 is degraded by macro-autophagy.

A Domain architecture of CALCOCO paralogs showing the SKICH domain, a conserved LIR motif (LVV), coiled-coli regions (CC) and zinc finger domains (ZF).

B Co-immunoprecipitation (co-IP) of Myc-CALCOCO1 with EGFP-CALCOCO1, following transient co-transfection of EGFP-CALCOCO1 and indicated Myc-CALCOCO1 constructs in HEK293 cells.

C, D Immunoblot analysis of indicated cell lines, starved for 6 hours (HBSS) as indicated, and treated with 25 μM MG132 or 200 ng/ml of bafilomycin A1 (Baf A1) for the indicated times. The numbers below the blots represent relative intensity of the bands normalized against actin loading control from an experiment representative of more than three independent experiments.

E A representative micrograph using widefield and deconvolution microscopy of HeLa CALCOCO1 KO cells stably expressing EGFP-CALCOCO1 and immunostained for endogenous GM130. Scale bars are 5 μm and 2 μm (zoomed inset).

F Same cells as in E were left untreated or treated with Baf A1 for 6 hours, and then immunostained for endogenous p62 and LC3B. Scale bars are 5 μm for the confocal microscopy images and 2 μm for the airyscans.

G Fold increase in CALCOCO1 puncta in response to starvation for 6 hours (HBSS) and/or treatment with Baf A1 for 6 hours.

H Percentage of co-localization of CALCOCO1 puncta with p62 and/or LC3B in cells treated as indicated.

I Same cells as in E were treated with Baf A1 for 6 hours before immunostaining with anti-LAMP1 antibody. Scale bars are 5 μm for the confocal microscopy images and 2 μm for the airyscans.

Figure 2. CALCOCO1 binds directly to ATG8 family proteins with preference for the GABARAP subfamily.

A GST pulldown binding assay of *in vitro* transcribed/translated ^{35}S-Myc-CALCOCO1 with recombinant GST-tagged ATG8 family proteins. GST and GST fusion proteins were visualized by coomassie brilliant blue staining (bottom panel), and the co-precipitated Myc-CALCOCO1 was detected by autoradiography (upper panel). The numbers represent % binding in an experiment representative of more than three independent experiments.

B GST pulldown assay of transiently transfected Myc-CALCOCO1 from HEK293 cell extracts with recombinant GST-tagged ATG8 family proteins. GST and GST fusions were visualized by Ponceau S staining (bottom panel), and co-precipitated Myc-CALCOCO1 detected by immunobloting with anti-Myc antibody (upper panel).

C CALCOCO1 deletion constructs used to map the ATG8 interactions. The red X indicate a point mutation or deletion of the LIR motif. Constructs with no or very weak interaction are indicated in orange.

D-H GST pulldown assays of indicated *in vitro* transcribed/translated ^{35}S-Myc-CALCOCO1 constructs with indicated recombinant GST-tagged ATG8 family proteins. Precipitated GST and GST fusions and co-precipitated Myc-CALCOCO1 constructs were analyzed as in A.

Figure 3. CALCOCO1 binds both to LDS and UDS of ATG8 family proteins.

A, B GST pulldowns testing binding of indicated in vitro transcribed/translated ^{35}S-Myc-CALCOCO1 constructs with indicated recombinant GST-tagged ATG8 family proteins (left). Cartoon of CALCOCO1 with domain organization indicated and the location of LIR and UIR motifs. The presence of two well separated binding surfaces on ATG8 proteins binding to LIR (LDS) and UIR (UDS) is indicated (right).

C GST pulldown assays of *in vitro* transcribed/translated ^{35}S-Myc-CALCOCO1 and ^{35}S-Myc-p62 with recombinant GST-GABARAPL2 (WT and indicated mutants).

D GST pulldown assays of *in vitro* transcribed/translated ^{35}S-Myc-TAX1BP1 (WT and indicated mutants) with recombinant GST-GABARAP (WT and indicated mutants).

E Immunoblot analysis of HeLa CALCOCO1 KO cell lines stably transfected with WT EGFP-CALCOCO1 or EGFP-CALCOCO1 mLIR+Δ623-691. Cells were induced with tetracycline for 24 hours and then starved or treated with MG132 or Baf A1 as indicated.

F HeLa CALCOCO1 KO cells stably expressing EGFP-CALCOCO1 or EGFP-CALCOCO1 mLIR+Δ623-691 grown in full medium and treated with Baf A1 as indicated were immunostained for endogenous p62 and LC3B. Scale bars, 5 μm.

Figure 4. CALCOCO1 promotes autophagic flux.

A HeLa CALCOCO1 KO cells stably expressing EGFP-CALCOCO1 were starved for 4 hours and then immunostained with anti-ATG13 and anti-WIPI2 antibodies. Scale bars are 5 μm for the confocal microscopy images and 2 μm for the airyscans.

B, C Immunoblot analysis of indicated WT or CALCOCO1 KO cell lines treated as indicated with Baf A1. The numbers below the blots represent relative intensity of the bands normalized against GAPDH loading control from an experiment representative of more than three independent experiments.

D, E Immunoblot analysis of HeLa CALCOCO1 KO cell lines stably expressing EGFP-CALCOCO1 and treated with Baf A1 as indicated. The numbers below the blots represent relative intensity of the bands normalized against actin loading control from an experiment representative of five independent experiments. For the bar graphs in E, n=5.

Figure 5. CALCOCO1 interacts with VAPA/B via a C-terminal FFAT motif.

A Stably expressed EGFP or EGFP-CALCOCO1 in HEK293 cells were immunoprecipitated from the cell lysates followed by mass spectrometry identification of interacting proteins. Only some of the identified proteins are shown.

B Co- IP of Myc-VAPA or Myc-VAPB with EGFP-CALCOCO1 from transiently transfected HEK293 cells.

C, D GST pulldown assays of *in vitro* transcribed/translated ^{35}S-Myc-CALCOCO1 constructs with indicated recombinant GST-VAPA or GST-VAPB constructs.

E HeLa cells transiently co-transfected with EGFP-CALCOCO1 and Myc-VAPA or –VAPB were immunostained with anti-Myc antibody. Scale bars, 5 μm.

Figure 6. VAP proteins promote autophagy and starvation-induced degradation of tubular ER.

A Immunoblot analysis of indicated cell lines, starved for 6 hours (HBSS) as indicated, and treated with MG132 or Baf A1 as indicated. The relative intensities of the bands normalized against GAPDH loading control indicated are representative of more than three independent experiments.

B Immunoblot analysis of HeLa cells transfected with the indicated siRNAs.

C Immunoblot analysis of HeLa cells transfected with the indicated siRNAs and treated with Baf A1 as indicated.

D Immunoblot analysis of induced or uninduced HeLa cells stably expressing with EGFP-VAPA. Expression of EGFP-VAPA was induced with tetracycline and the cells were then starved or treated with Baf A1 as indicated. The relative intensities of the bands normalized against GAPDH loading control indicated are representative of more than three independent experiments.

E HeLa KO CALCOCO1 cells were transiently co-transfected with EGFP-CALCOCO1 and Myc-VAPA or Myc-VAPB, and then immunostained with anti-Myc and anti-LC3B antibodies. Arrows indicate dots of co-localization of all three proteins. Scale bars, 5 μm for large merged images and 1 μm for zoomed images.

Figure 7. CALCOCO1 is a soluble ER-phagy receptor.

A Immunoblot analysis of HeLa WT and HeLa CALCOCO1 KO cells. The cells were starved for 6 hours (HBSS) as indicated and treated with Baf A1 as indicated. The relative intensities of the bands normalized against GAPDH loading control indicated are representative of more than three independent experiments.

B Immunoblot analysis of HeLa CALCOCO1 KO cell lines reconstituted with GFP-CALCOCO1. Expression of EGFP-CALCOCO1 was induced or not with tetracycline and the cells were treated with MG132 or Baf A1 as indicated. The relative intensities of the bands normalized against GAPDH loading control indicated are representative of more than three independent experiments.

C HeLa CALCOCO1 KO cell lines reconstituted with EGFP-CALCOCO1 were added tetracycline or not to induce expression of EGFP-CALCOCO1. Abundance of ER was quantified from widefield fluorescence images of endogenous RTN3 staining (see Materials and methods). Data are presented as mean ± sd. Statistical comparison was analyzed by one-way ANOVA and significance displayed as ***$p < 0.001$, **$p < 0.005$, *$p < 0.01$; ns is not significant.

D Immunoblot analysis of cells analyzed in C.

E Immunoblot analysis of HeLa CALCOCO1 KO cells stably expressing EGFP-CALCOCO1 in fed or starved conditions and transfected with the indicated VAPA/B siRNAs.

Figure 8. Interaction with ATG8 proteins is required for CALCOCO1-mediated ER-phagy.

A Immunoblot analysis of HeLa CALCOCO1 KO cells stably expressing EGFP-CALCOCO1 in fed or starved conditions and treated as indicated with Baf A1 or PI3KC3 inhibitor SAR405.

B Immunoblot analysis of HeLa CALCOCO1 KO cells stably expressing EGFP-CALCOCO1 mLIR+ΔUIM for 24 hours and then treated as indicated in the figure.

C Representative confocal images of HeLa CALCOCO1 KO cells transiently co-transfected with mCherry-CALCOCO1, Myc-VAPA and EGFP-LAMP1, and then treated as indicated before immunostaining with anti-Myc anti-body. Arrows indicate

co-localization. Scale bars, 5 μm for large merged images and 1 μm for zoomed images.

D Model of ER-phagy mediated by CALCOCO1 dimers illustrating the dual LIR-LDS and UIR-UDS interaction with lipidated GABARAP subfamily proteins on the phagophore, and the FFAT-like motif mediated interaction with MSP domains of VAP proteins on tubular ER.

Figure EV1. CALCOCO1 homomerizes via coiled-coil domains, but does not heterodimerize with TAX1BP1 or NDP52.

A Co-IP of Myc-CALCOCO1 with EGFP-CALCOCO1. ^{35}S-GFP-CALCOCO1 (upper panels) or ^{35}S-GFP (lower panels) were *in vitro* co-transcribed/translated with indicated ^{35}S-Myc-CALCOCO1 constructs. GFP-CALCOCO1 or GFP, respectively, were immunoprecipitated with GFP-TRAP and the immunoprecipitates then resolved by SDS-PAGE. The resolved immunoprecipitates were detected by autoradiography.

B GFP-CALCOCO1 or GFP were *in vitro* co-transcribed/translated with Myc-CALCOCO1, Myc-NDP52 or Myc-TAX1BP1 and then immunoprecipitated with GFP-TRAP. The analysis of the immunoprecipitates was done as in A. GFP construct are indicated with a circle and Myc-constructs with a star.

C GST pulldown analyses of binding of *in vitro* transcribed/translated ^{35}S-Myc-CALCOCO1 with recombinant GST-tagged Galectin-3 and-8. *In vitro* transcribed/translated Myc-NDP52 and Myc-TAX1BP1 were included as positive controls.

Figure EV2. CALCOCO1 co-localizes with p62 and LC3B positive dots and is degraded by autophagy.

A, B Immunoblot analysis of indicated cell lines, starved for 6 hours (HBSS) as indicated, and treated with MG132 or Baf A1 as indicated.

C Extension of Fig 1F. HeLa CALCOCO1 KO cells stably transfected with EGFP-CALCOCO1 were induced with tetracycline for 24 hours and then starved (HBSS) with or without Baf A1 treatment as indicated, before immunostaining for endogenous p62 and LC3B. Scale bars, 5 μm for confocal microscopy images, 2 μm for airyscans.

D Similar to Fig 1G, but extended to show fold increase in p62 puncta and LC3B puncta.

E HeLa cells stably transfected with EGFP-CALCOCO1 were added tetracycline for 24 hours to induce expression of GFP-CALCOCO1. Cells were then starved or not and immunostained with anti-p62, anti-LC3 and anti-GABARAP antibodies as indicated. Co-localization in dots is indicated by circles, and supported using line plots. Scale bars, 10 μm.

Figure EV3.Generation of CRISPR/CAS9-mediated HeLa and HEK293 FlpIn CALCOCO1 KO cells,

A Hela FlpIn CALCOCO1 KO cells generated with indicated gRNA for genomic editing of targeted exons 2. Shown are the genomic sequences of four mutated alleles in CALCOCO1 KO clone 38.

B HEK293 FlpIn CALCOCO1 KO cells generated targeting exon 2 and exon 4 with two different gRNAs. CALCOCO1 KO cells verified with both western blot and genomic sequencing of regions encompassing exon 2 and exon 4.

Figure EV4. The C-terminal parts of CALCOCO1 and TAX1BP1 contribute to their interaction with ATG8 family proteins.

A, B GST pulldowns of binding of indicated *in vitro* transcribed/translated ^{35}S-Myc-CALCOCO1 constructs with recombinant GST-tagged ATG8 family proteins.

A GST pulldowns analyses of binding of *in vitro* transcribed/translated WT or LIR-mutated (LVV/AAA) ^{35}S-Myc-NDP52 with recombinant GST-tagged ATG8 family proteins.

D, E GST pulldowns analyses of binding of indicated *in vitro* transcribed/translated ^{35}S-Myc- TAX1BP1 constructs with indicated recombinant GST-tagged ATG8 family proteins.

Figure EV5. Co-localization of CALCOCO1 with p62 and LC3B depends on the LIR and UIR motifs.

A, B HeLa CALCOCO1 KO cells reconstituted with EGFP-CALCOCO1 (A) or EGFP-CALCOCO1 mLIR+ΔUIR (B) were starved with or without Baf A1 treatment as indicated, and then immunostained for endogenous p62 and LC3B. Scale bars, 5 μm.

FIGURE 1

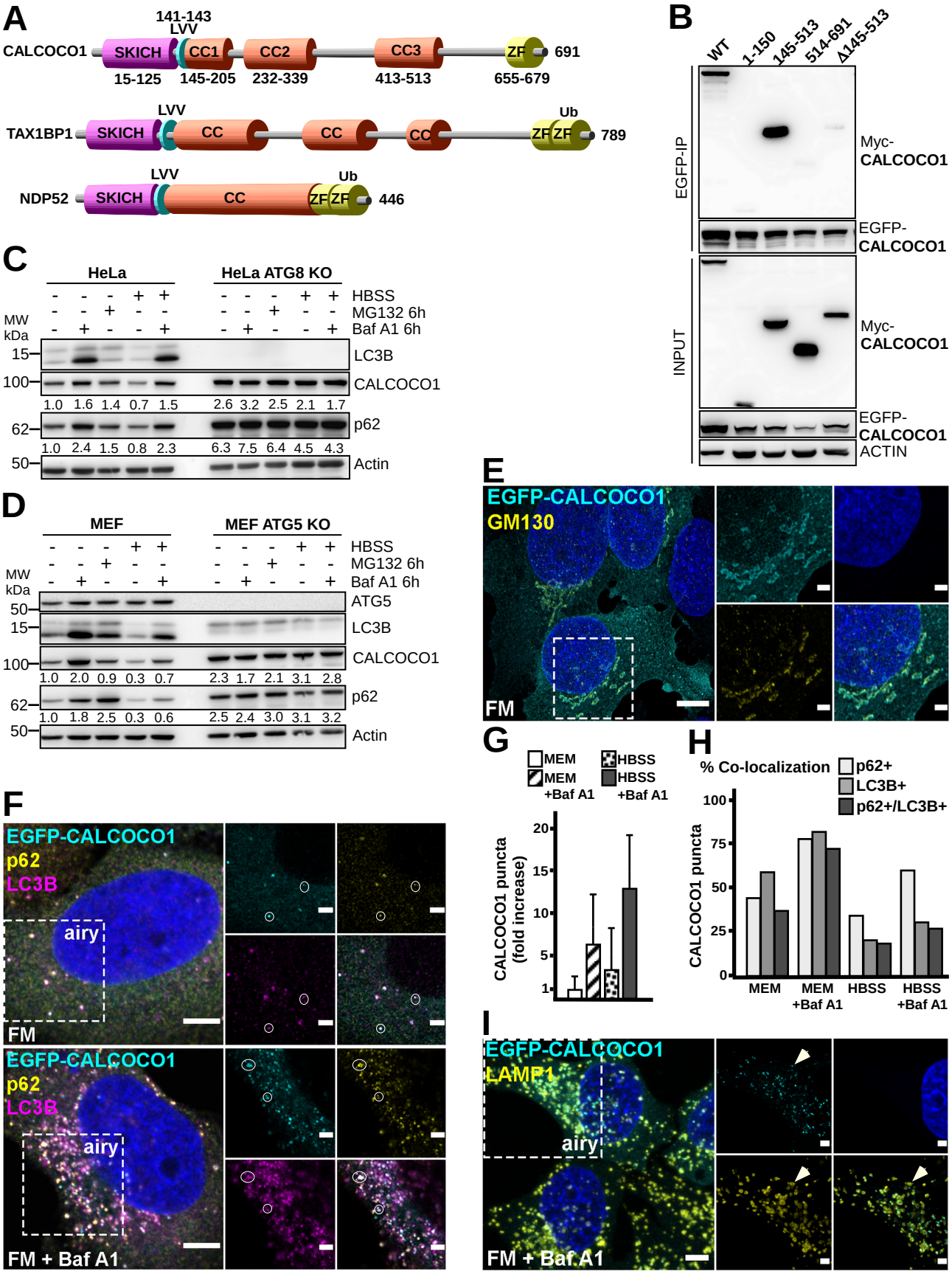
A
CALCOCO1
SKICH
CC1
CC2
CC3
ZF
691
141-143 LVV
15-125
145-205
232-339
413-513
655-679
TAX1BP1
LVV
CC
Ub
ZF ZF
789
NDP52
446
B
WT
1-150
145-513
514-691
Δ145-513
EGFP-IP
INPUT
Myc-CALCOCO1
EGFP-CALCOCO1
ACTIN
C
HeLa
HeLa ATG8 KO
HBSS
MG132 6h
Baf A1 6h
MW kDa
LC3B
CALCOCO1
p62
Actin
D
MEF
MEF ATG5 KO
ATG5
E
EGFP-CALCOCO1
GM130
FM
F
p62
LC3B
airy
FM + Baf A1
G
MEM
HBSS
+Baf A1
CALCOCO1 puncta (fold increase)
H
% Co-localization
p62+
LC3B+
p62+/LC3B+
CALCOCO1 puncta
I
LAMP1

FIGURE 2

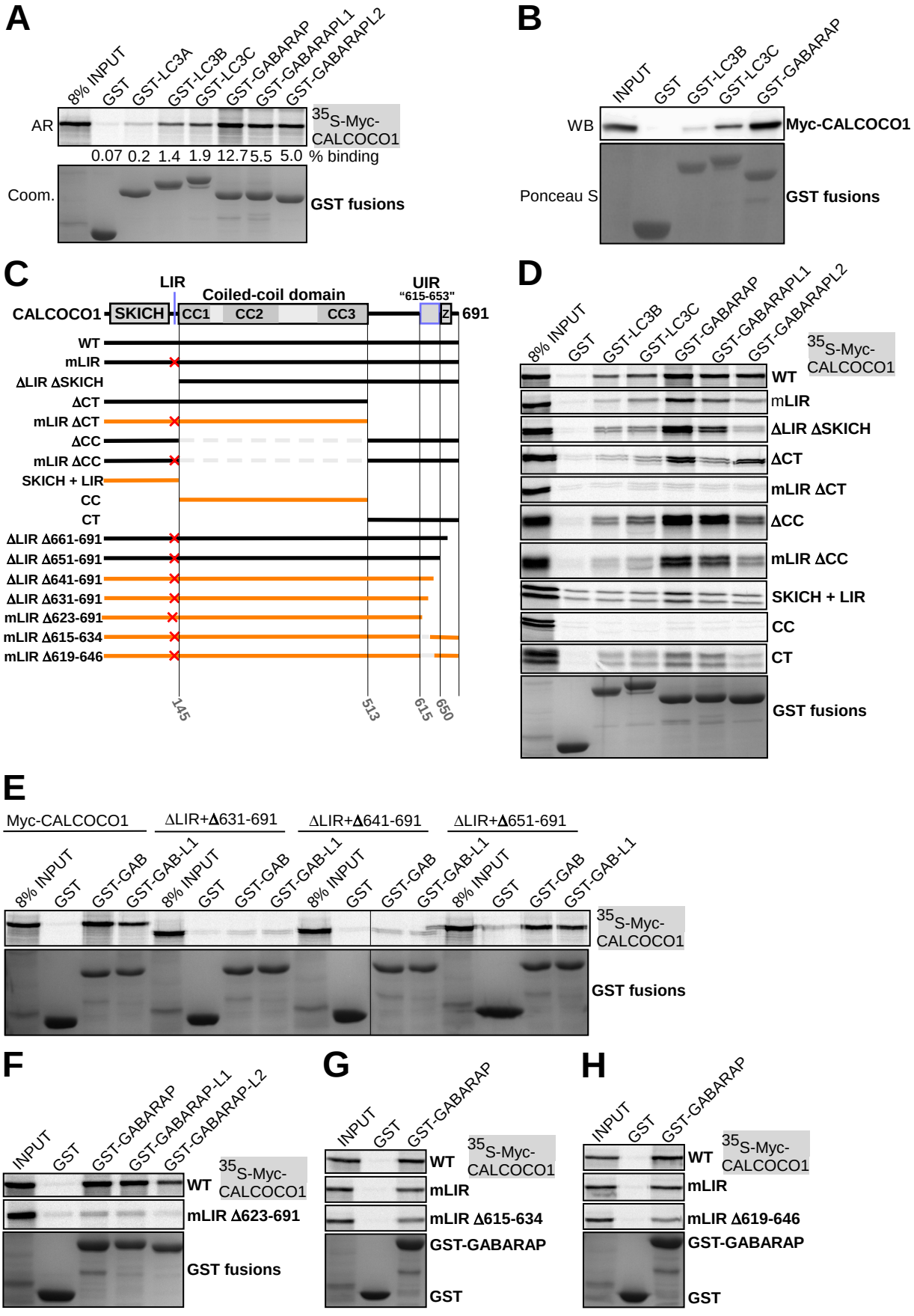
A
8% INPUT
GST
GST-LC3A
GST-LC3B
GST-LC3C
GST-GABARAP
GST-GABARAPL1
GST-GABARAPL2
AR
35S-Myc-CALCOCO1
0.07 0.2 1.4 1.9 12.7 5.5 5.0 % binding
Coom.
GST fusions
B
INPUT
GST
GST-LC3B
GST-LC3C
GST-GABARAP
WB
Myc-CALCOCO1
Ponceau S
GST fusions
C
LIR
Coiled-coil domain
UIR
"615-653"
CALCOCO1
SKICH
CC1
CC2
CC3
Z
691
WT
mLIR
ΔLIR ΔSKICH
ΔCT
mLIR ΔCT
ΔCC
mLIR ΔCC
SKICH + LIR
CC
CT
ΔLIR Δ661-691
ΔLIR Δ651-691
ΔLIR Δ641-691
ΔLIR Δ631-691
mLIR Δ623-691
mLIR Δ615-634
mLIR Δ619-646
145
513
615
650
D
8% INPUT
GST
GST-LC3B
GST-LC3C
GST-GABARAP
GST-GABARAPL1
GST-GABARAPL2
35S-Myc-CALCOCO1
WT
mLIR
ΔLIR ΔSKICH
ΔCT
mLIR ΔCT
ΔCC
mLIR ΔCC
SKICH + LIR
CC
CT
GST fusions
E
Myc-CALCOCO1
ΔLIR+Δ631-691
ΔLIR+Δ641-691
ΔLIR+Δ651-691
8% INPUT
GST
GST-GAB
GST-GAB-L1
35S-Myc-CALCOCO1
GST fusions
F
INPUT
GST
GST-GABARAP
GST-GABARAP-L1
GST-GABARAP-L2
35S-Myc-CALCOCO1
WT
mLIR Δ623-691
GST fusions
G
INPUT
GST
GST-GABARAP
35S-Myc-CALCOCO1
WT
mLIR
mLIR Δ615-634
GST-GABARAP
GST
H
INPUT
GST
GST-GABARAP
35S-Myc-CALCOCO1
WT
mLIR
mLIR Δ619-646
GST-GABARAP
GST

FIGURE 3

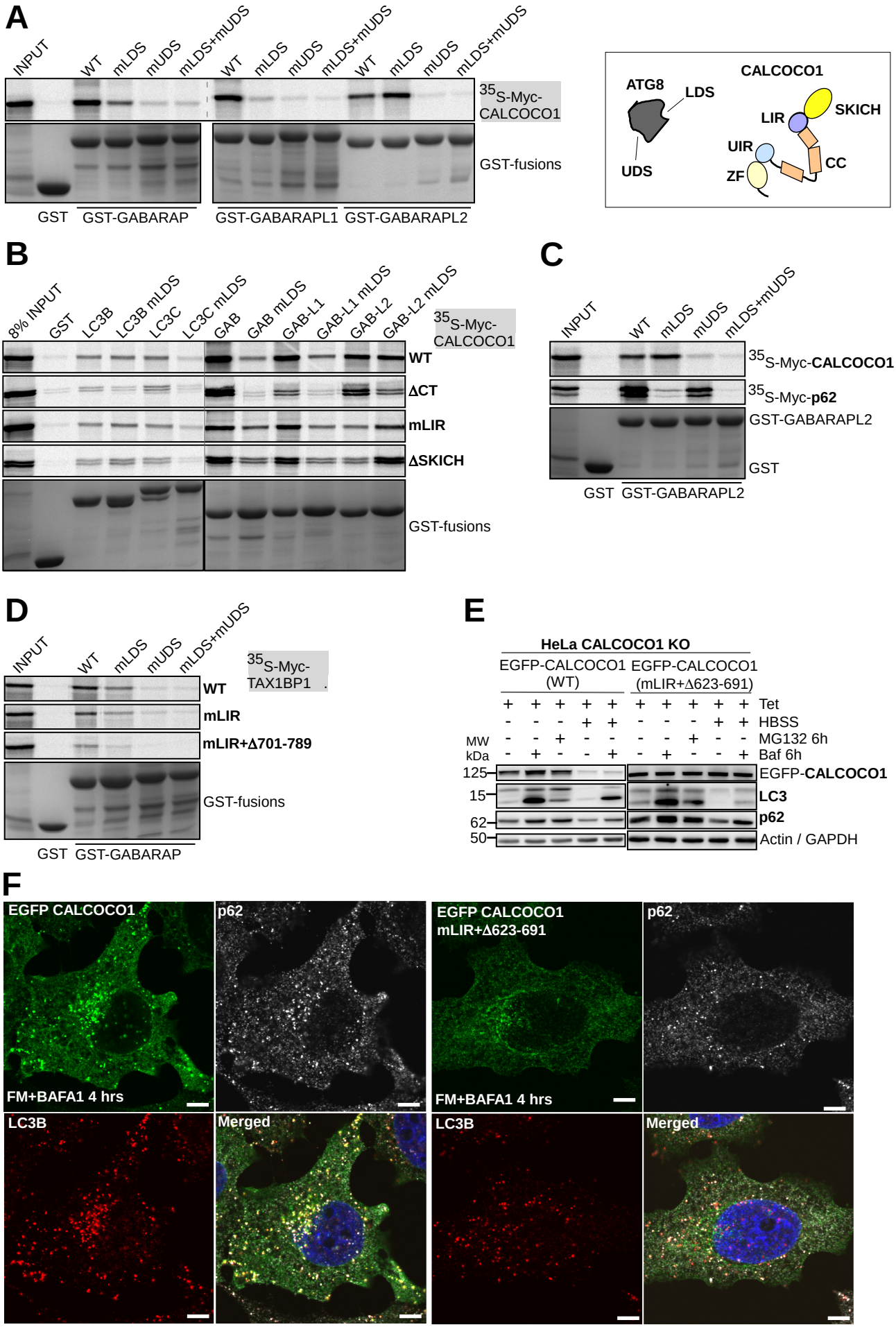
A
INPUT
WT
mLDS
mUDS
mLDS+mUDS
35S-Myc-CALCOCO1
GST-fusions
GST
GST-GABARAP
GST-GABARAPL1
GST-GABARAPL2
ATG8
LDS
UDS
CALCOCO1
LIR
SKICH
UIR
CC
ZF
B
8% INPUT
GST
LC3B
LC3B mLDS
LC3C
LC3C mLDS
GAB
GAB mLDS
GAB-L1
GAB-L1 mLDS
GAB-L2
GAB-L2 mLDS
35S-Myc-CALCOCO1
WT
ΔCT
mLIR
ΔSKICH
GST-fusions
C
INPUT
WT
mLDS
mUDS
mLDS+mUDS
35S-Myc-CALCOCO1
35S-Myc-p62
GST-GABARAPL2
GST
GST
GST-GABARAPL2
D
INPUT
WT
mLDS
mUDS
mLDS+mUDS
35S-Myc-TAX1BP1
WT
mLIR
mLIR+Δ701-789
GST-fusions
GST
GST-GABARAP
E
HeLa CALCOCO1 KO
EGFP-CALCOCO1 (WT)
EGFP-CALCOCO1 (mLIR+Δ623-691)
Tet
HBSS
MG132 6h
Baf 6h
MW kDa
125
15
62
50
EGFP-CALCOCO1
LC3
p62
Actin / GAPDH
F
EGFP CALCOCO1
FM+BAFA1 4 hrs
p62
LC3B
Merged
EGFP CALCOCO1 mLIR+Δ623-691
FM+BAFA1 4 hrs
p62
LC3B
Merged

FIGURE 4

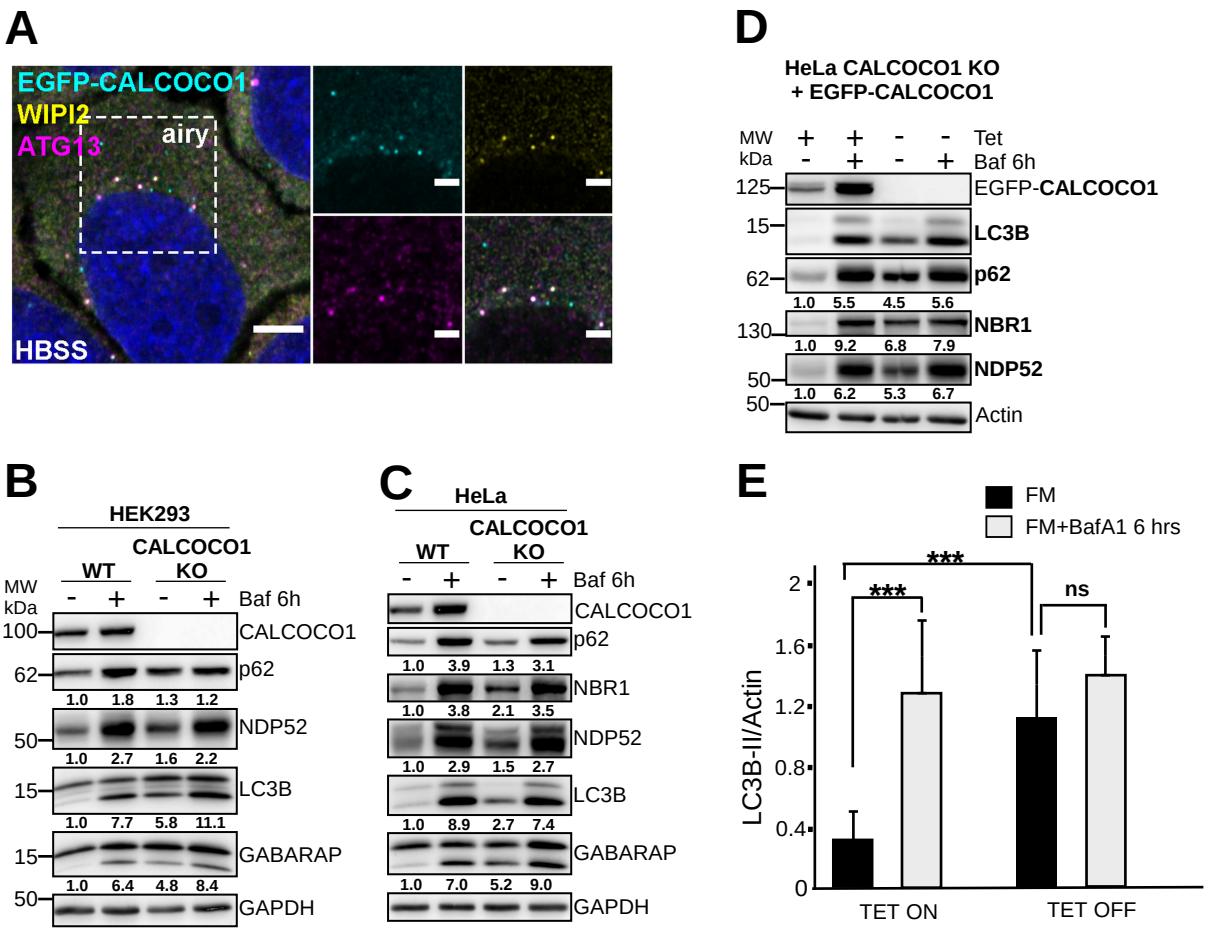
A
EGFP-CALCOCO1
WIPI2
ATG13
airy
HBSS
D
HeLa CALCOCO1 KO
+ EGFP-CALCOCO1
MW
kDa
Tet
Baf 6h
EGFP-CALCOCO1
LC3B
p62
NBR1
NDP52
Actin
B
HEK293
CALCOCO1
WT
KO
Baf 6h
CALCOCO1
p62
NDP52
LC3B
GABARAP
GAPDH
C
HeLa
CALCOCO1
WT
KO
Baf 6h
CALCOCO1
p62
NBR1
NDP52
LC3B
GABARAP
GAPDH
E
FM
FM+BafA1 6 hrs
LC3B-II/Actin
***
***
ns
TET ON
TET OFF

FIGURE 5

A

Protein name	# of peptides	Av. coverage (%)
CALCOCO1	53	70
Clathrin heavy chain	93	66
HSPD1	39	73
ATAD3B	35	66
AP-2 complex subunit β	50	64
AP-2 complex subunit α–1	45	57
ATAD3A	28	52
AP-2 complex subunit α–2	35	53
MTPAP	22	46
Tubulin β-4a	19	62
AP-2 complex subunit μ	21	53
AP-1 complex subunit β–1	24	26
PIK3C2	29	20
MICOS complex subunit MIC60	33	56
MICOS complex subunit MIC60	28	50
Clathrin interactor 1	17	31
VAPA	2	10

B

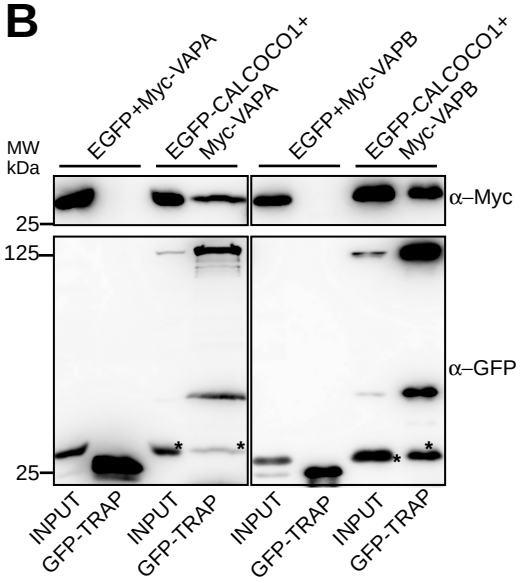

C

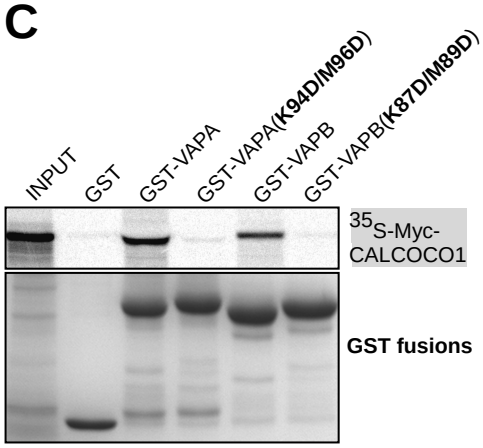

D

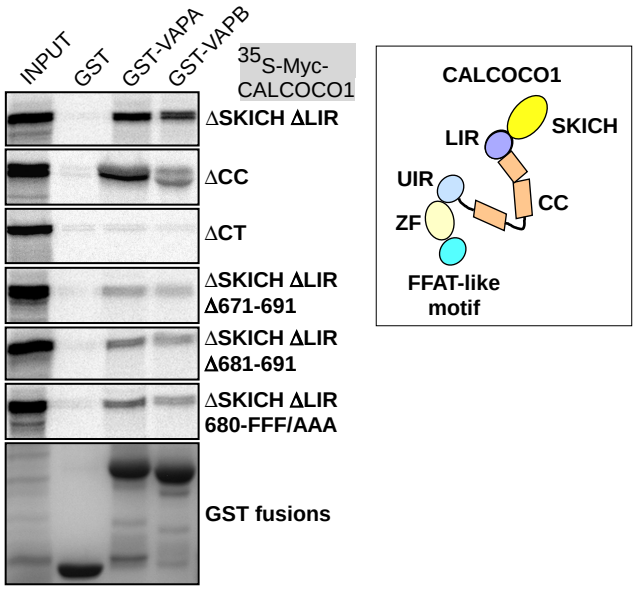

E

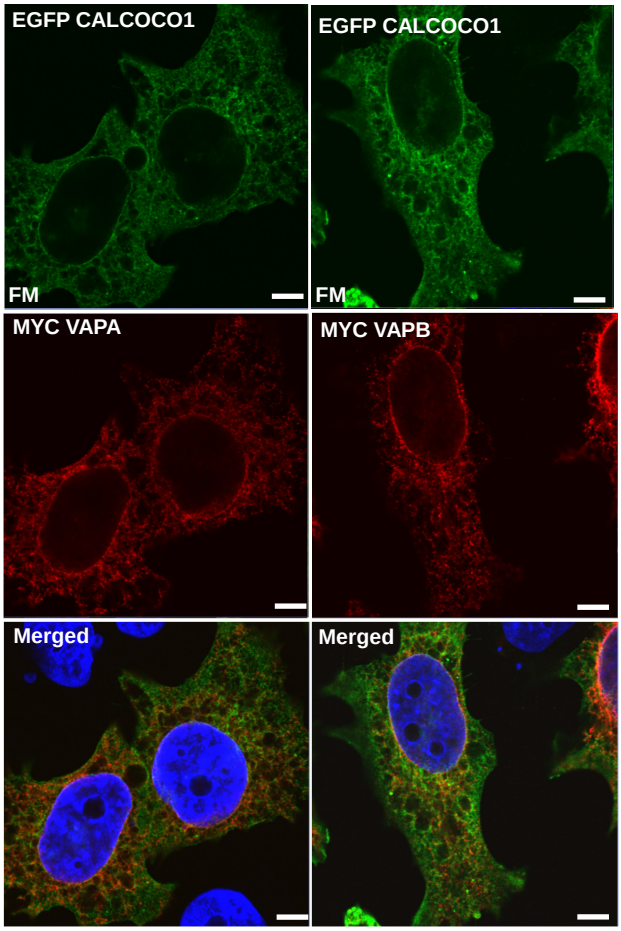

FIGURE 6

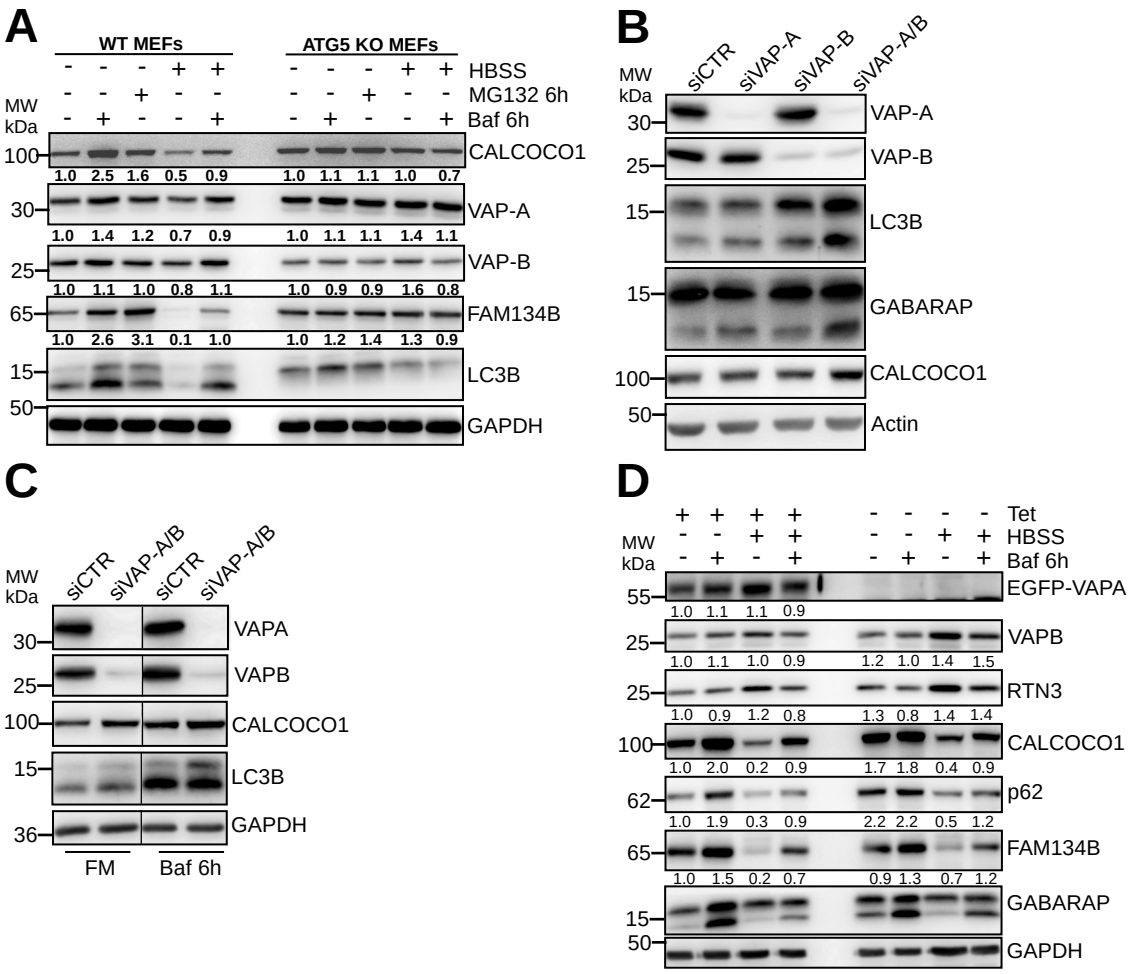
A
WT MEFs
ATG5 KO MEFs
HBSS
MG132 6h
Baf 6h
MW kDa
100
CALCOCO1
1.0 2.5 1.6 0.5 0.9 1.0 1.1 1.1 1.0 0.7
30
VAP-A
1.0 1.4 1.2 0.7 0.9 1.0 1.1 1.1 1.4 1.1
25
VAP-B
1.0 1.1 1.0 0.8 1.1 1.0 0.9 0.9 1.6 0.8
65
FAM134B
1.0 2.6 3.1 0.1 1.0 1.0 1.2 1.4 1.3 0.9
15
LC3B
50
GAPDH
B
siCTR
siVAP-A
siVAP-B
siVAP-A/B
MW kDa
30
VAP-A
25
VAP-B
15
LC3B
15
GABARAP
100
CALCOCO1
50
Actin
C
siCTR
siVAP-A/B
siCTR
siVAP-A/B
MW kDa
30
VAPA
25
VAPB
100
CALCOCO1
15
LC3B
36
GAPDH
FM
Baf 6h
D
Tet
HBSS
Baf 6h
MW kDa
55
EGFP-VAPA
1.0 1.1 1.1 0.9
25
VAPB
1.0 1.1 1.0 0.9 1.2 1.0 1.4 1.5
25
RTN3
1.0 0.9 1.2 0.8 1.3 0.8 1.4 1.4
100
CALCOCO1
1.0 2.0 0.2 0.9 1.7 1.8 0.4 0.9
62
p62
1.0 1.9 0.3 0.9 2.2 2.2 0.5 1.2
65
FAM134B
1.0 1.5 0.2 0.7 0.9 1.3 0.7 1.2
15
GABARAP
50
GAPDH

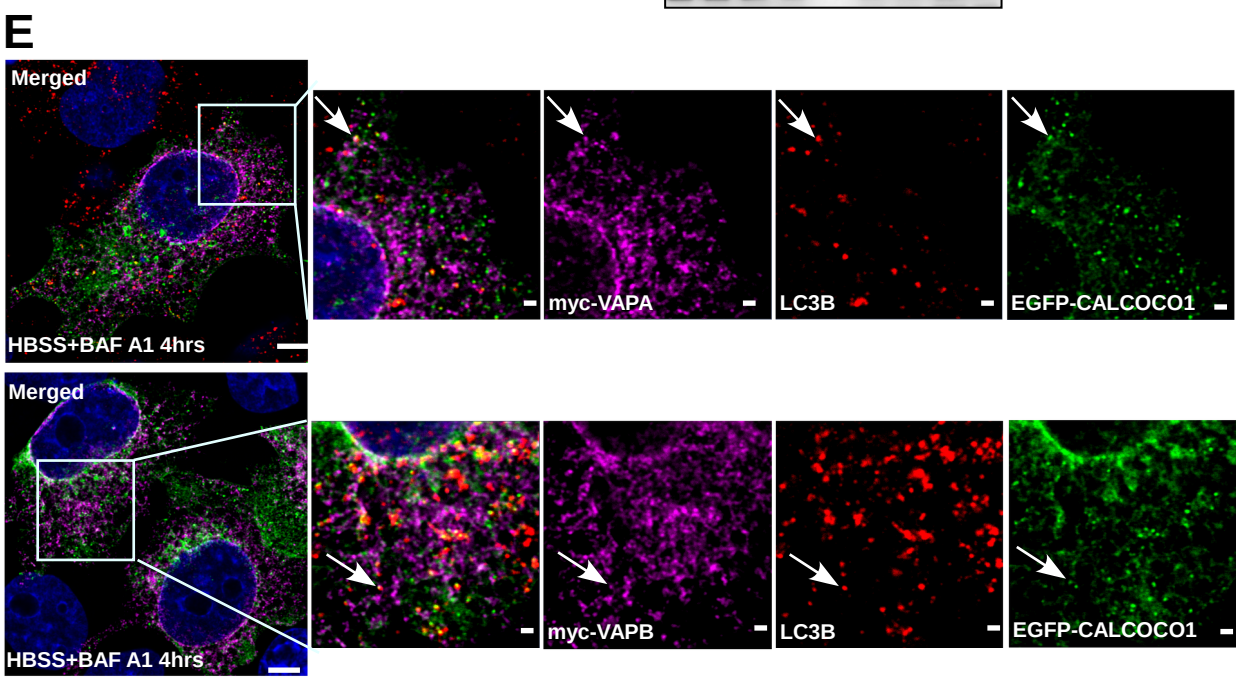
E
Merged
HBSS+BAF A1 4hrs
myc-VAPA
LC3B
EGFP-CALCOCO1
Merged
HBSS+BAF A1 4hrs
myc-VAPB
LC3B
EGFP-CALCOCO1

FIGURE 7

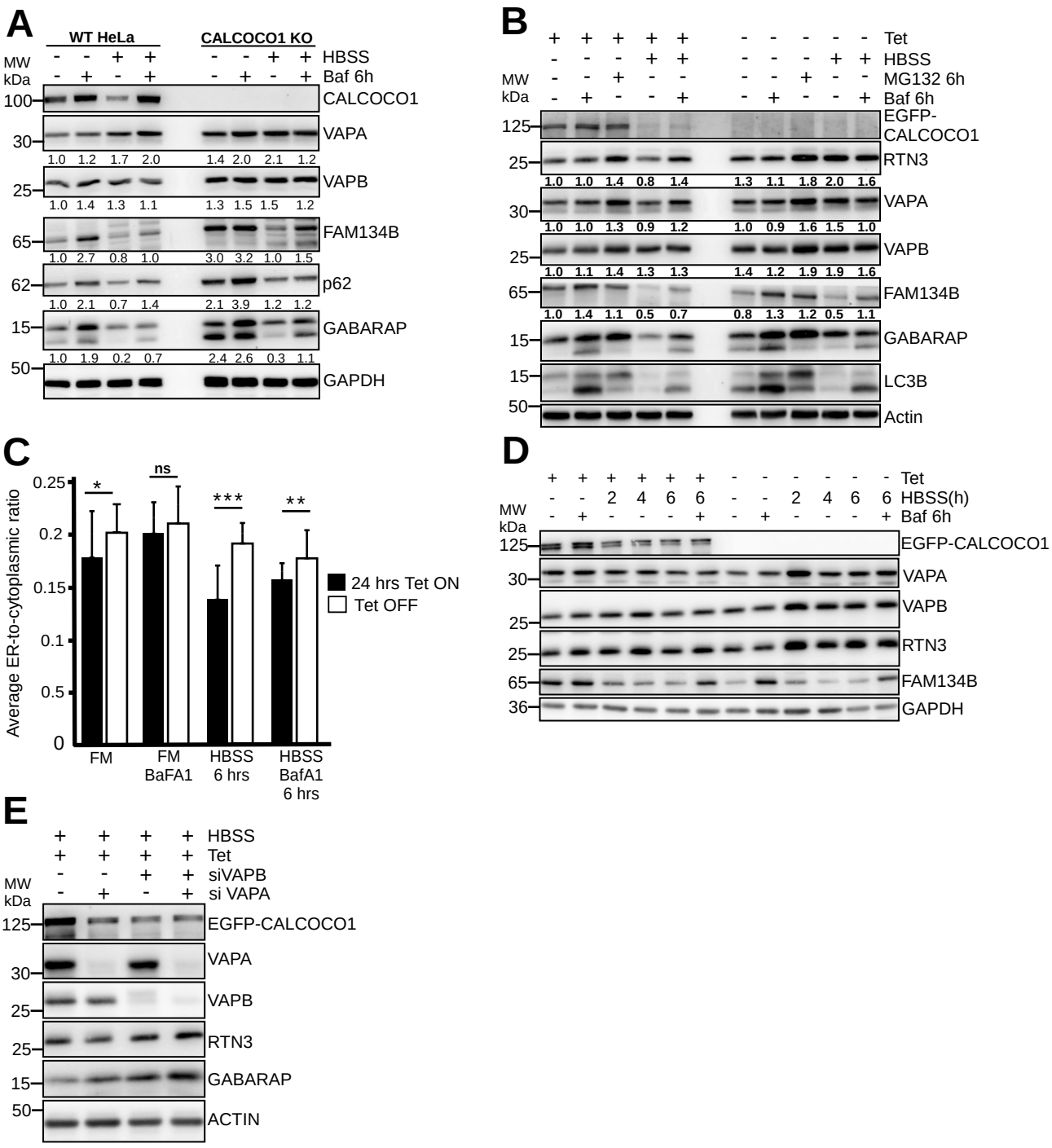
A
WT HeLa
CALCOCO1 KO
MW
kDa
HBSS
Baf 6h
CALCOCO1
VAPA
VAPB
FAM134B
p62
GABARAP
GAPDH
B
Tet
HBSS
MG132 6h
Baf 6h
EGFP-CALCOCO1
RTN3
VAPA
VAPB
FAM134B
GABARAP
LC3B
Actin
C
Average ER-to-cytoplasmic ratio
ns
24 hrs Tet ON
Tet OFF
FM
FM BaFA1
HBSS 6 hrs
HBSS BafA1 6 hrs
D
Tet
HBSS(h)
Baf 6h
EGFP-CALCOCO1
VAPA
VAPB
RTN3
FAM134B
GAPDH
E
HBSS
Tet
siVAPB
si VAPA
EGFP-CALCOCO1
VAPA
VAPB
RTN3
GABARAP
ACTIN

FIGURE 8

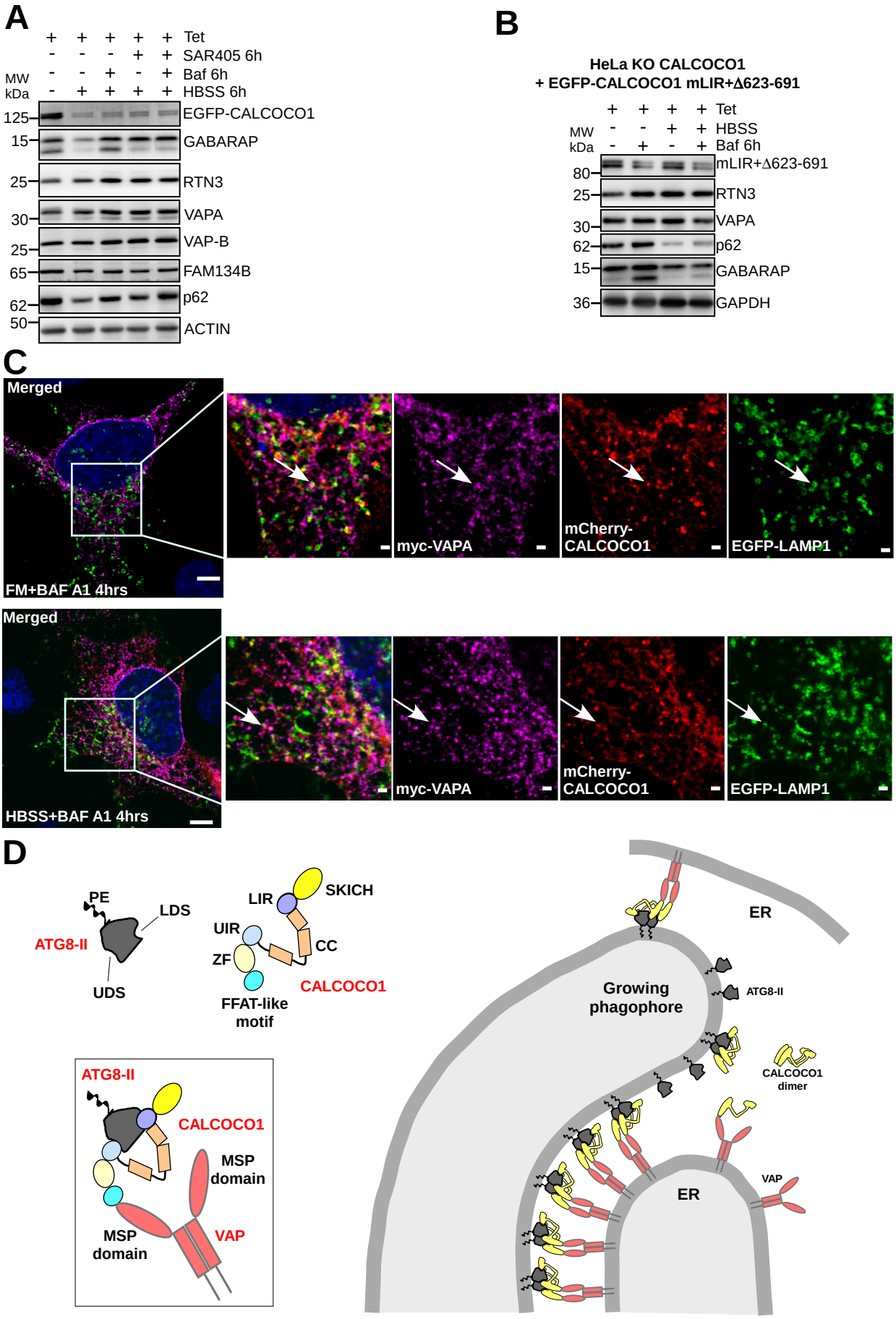
A
Tet
SAR405 6h
Baf 6h
HBSS 6h
MW kDa
125
EGFP-CALCOCO1
15
GABARAP
25
RTN3
30
VAPA
25
VAP-B
65
FAM134B
62
p62
50
ACTIN
B
HeLa KO CALCOCO1
+ EGFP-CALCOCO1 mLIR+Δ623-691
Tet
HBSS
Baf 6h
MW kDa
80
mLIR+Δ623-691
25
RTN3
30
VAPA
62
p62
15
GABARAP
36
GAPDH
C
Merged
FM+BAF A1 4hrs
myc-VAPA
mCherry-CALCOCO1
EGFP-LAMP1
Merged
HBSS+BAF A1 4hrs
myc-VAPA
mCherry-CALCOCO1
EGFP-LAMP1
D
PE
LDS
ATG8-II
UDS
LIR
SKICH
UIR
CC
ZF
CALCOCO1
FFAT-like motif
ATG8-II
CALCOCO1
MSP domain
MSP domain
VAP
ER
Growing phagophore
ATG8-II
CALCOCO1 dimer
VAP
ER

FIGURE EV1

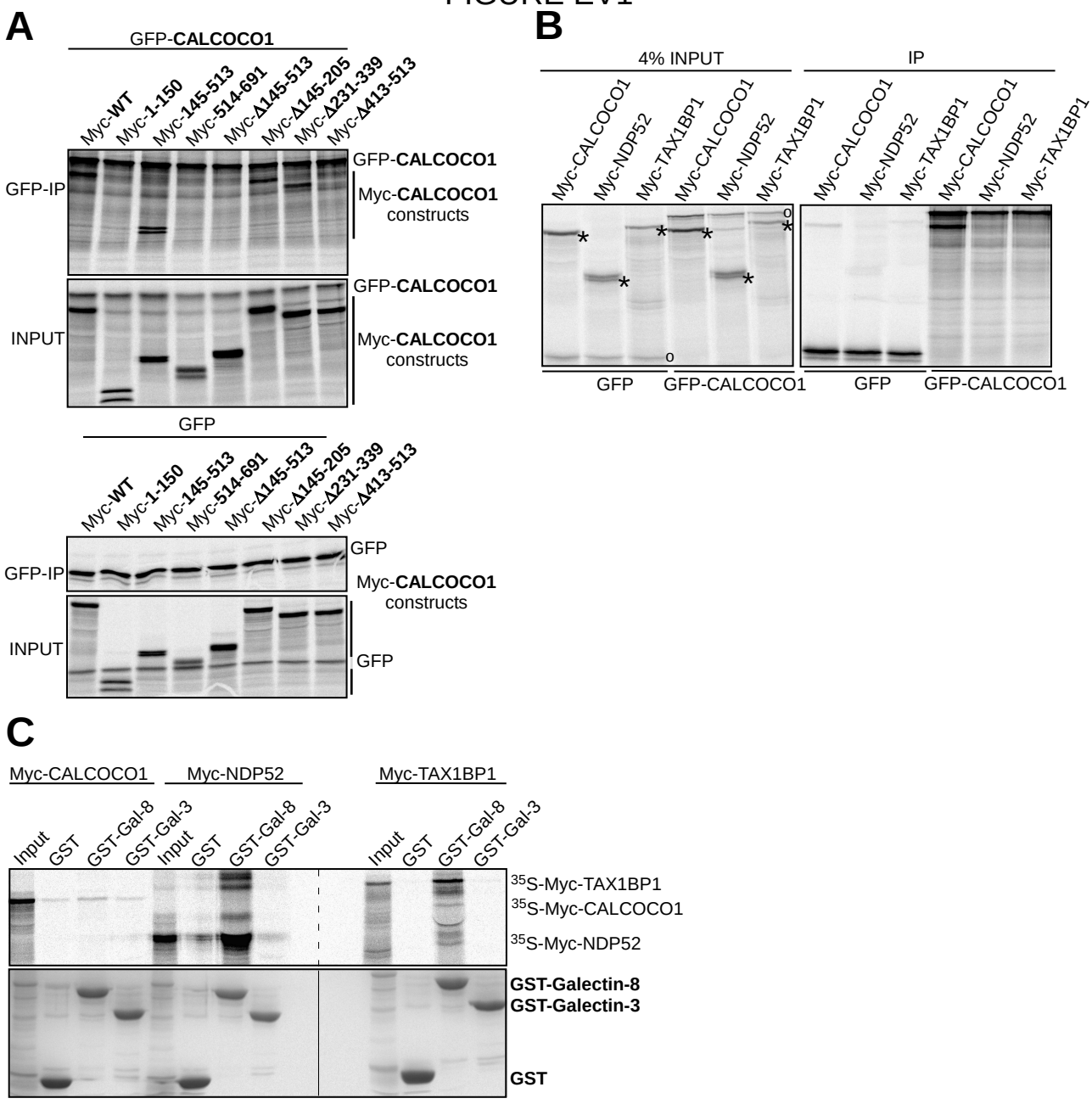
A
GFP-CALCOCO1
Myc-WT
Myc-1-150
Myc-145-513
Myc-514-691
Myc-Δ145-513
Myc-Δ145-205
Myc-Δ231-339
Myc-Δ413-513
GFP-IP
INPUT
GFP-CALCOCO1
Myc-CALCOCO1 constructs
GFP
GFP
B
4% INPUT
IP
Myc-CALCOCO1
Myc-NDP52
Myc-TAX1BP1
GFP
GFP-CALCOCO1
C
Myc-CALCOCO1
Myc-NDP52
Myc-TAX1BP1
Input
GST
GST-Gal-8
GST-Gal-3
35S-Myc-TAX1BP1
35S-Myc-CALCOCO1
35S-Myc-NDP52
GST-Galectin-8
GST-Galectin-3
GST

FIGURE EV2

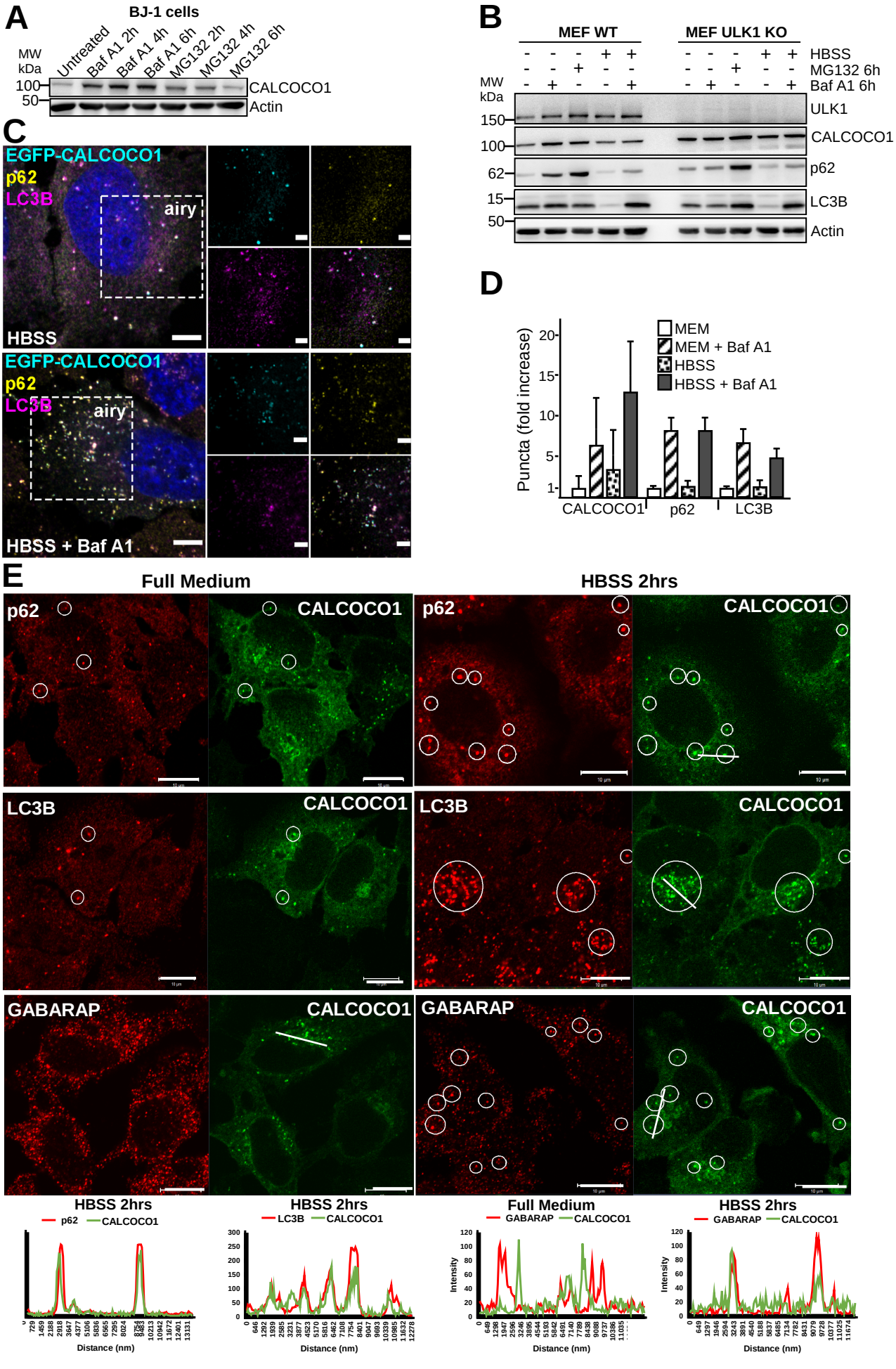
A
BJ-1 cells
MW kDa
Untreated
Baf A1 2h
Baf A1 4h
Baf A1 6h
MG132 2h
MG132 4h
MG132 6h
100
50
CALCOCO1
Actin
B
MEF WT
MEF ULK1 KO
HBSS
MG132 6h
Baf A1 6h
MW kDa
150
100
62
15
50
ULK1
CALCOCO1
p62
LC3B
Actin
C
EGFP-CALCOCO1
p62
LC3B
airy
HBSS
HBSS + Baf A1
D
Puncta (fold increase)
20
15
10
5
1
MEM
MEM + Baf A1
HBSS
HBSS + Baf A1
CALCOCO1
p62
LC3B
E
Full Medium
HBSS 2hrs
p62
CALCOCO1
LC3B
GABARAP
HBSS 2hrs
p62 CALCOCO1
HBSS 2hrs
LC3B CALCOCO1
Full Medium
GABARAP CALCOCO1
HBSS 2hrs
GABARAP CALCOCO1
Intensity
Distance (nm)

FIGURE EV3

A

CRISPR/CAS9 CALCOCO1 KO in HeLa FlpIn cells

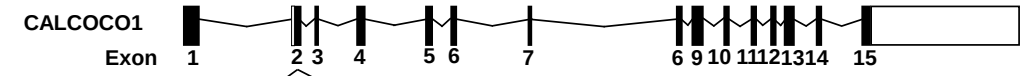

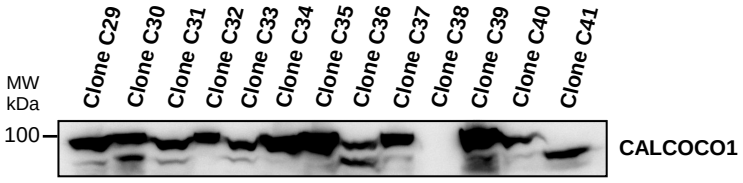


```
CALCOCO1 WT  AGGCCAGGATGGAAGAATCACCACTAA-GCCGGGCACCATCCCG 43
CALCOCO1 C38 AGGCCAGGATGGAAGAATCACCACTAAGCCGGGCACCATCCCG 44
CALCOCO1 C38 AGGCCAGGATGGAAGAATCACCACTCAAGTCAGAGGTGGCGAAA
             CCCGACAGGACTATAAAGATACCAGGCGTTTCCCCCTGGAAGCT
             CCCTCGTGCGCTCTCCTGTTCCGACCCTGCCGCTTACCGGATAC
             CTGTCCGCCTTTCTCCCTTCGGGAAGCGTGGCGCTTTCTCATAG
             CTCACGCTGTAGGTATCTCAGTTCGGTGTAGGTCGTTCGCTCCA
             AGCCGGGCACCATCCCG                          237
CALCOCO1 C38 AGGCCAGGATGGAAGAATCACCACTGCGCCCAATACGCAAACCG
             CCTCTCCCCGCGCGTTGGCCGATTCATTAATGCAGCTGGCACGA
             CAGGTTTCCCGACTGGAAAGCGGGCAGTGAGCGCAACGCAATTA
             ATGTGAGTTAGCTCACTCATTAGGCACCCCAGGCTTTACACTTT
             ATGCTTCCGGCTCGTATGTTGTGTGGAATTGTGAGCGGATAACA
             ATTTCACACAGGAAACAGCTATGACCATGATTACGCCGGGCACC
             ATCCCG                                     270
CALCOCO1 C38 AGGCCAGGATGGAAGAATCACCACTATACGCAAACCGCCTCTCC
             CCGCGCGTTGGCCGATTCATTAATGCAGCTGGCACGACAGGTTT
             CCCGACTGGAAAGCGGGCAGTGAGCGCAACGCAATTAATGTGAG
             TTAGCTCACTCATTAGGCACCCCAGGCTTTACACTTTATGCTTC
             CGGCTCGTATGTTGTGTGGAATTGTGAGCGGATAACAATTTCAC
             ACAGGAAACAGCTATGACCATGATTACGCCAAGCTATTTAGGTG
             ACACTATAGAATACTCAAGCTATGCATCCAACGCGTTGGGAGCT
             CTCCCATATGGTCGACCTGCAGGCGGCCGCGAATTCACTAGTGA
             TTCTCACAGCCCATAAACCTAAGCCGGGCACCATCCCG     390
```

B

CRISPR/CAS9 CALCOCO1 KO in HEK293 FlpIn cells

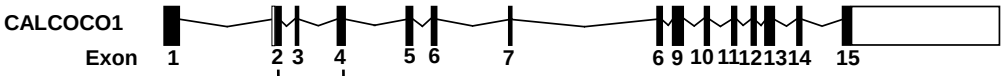

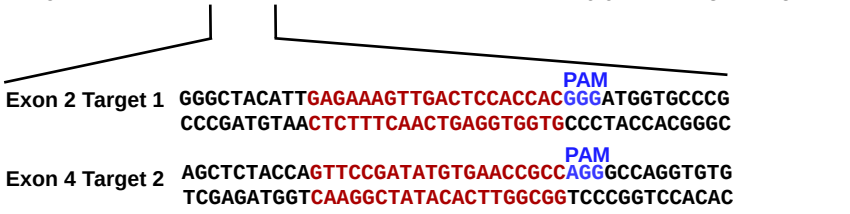

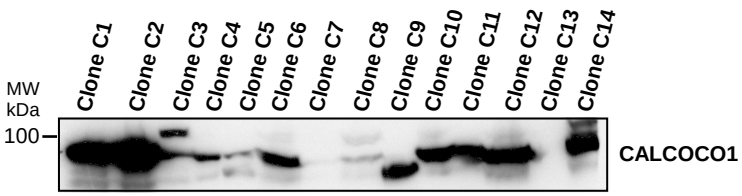

FIGURE EV4

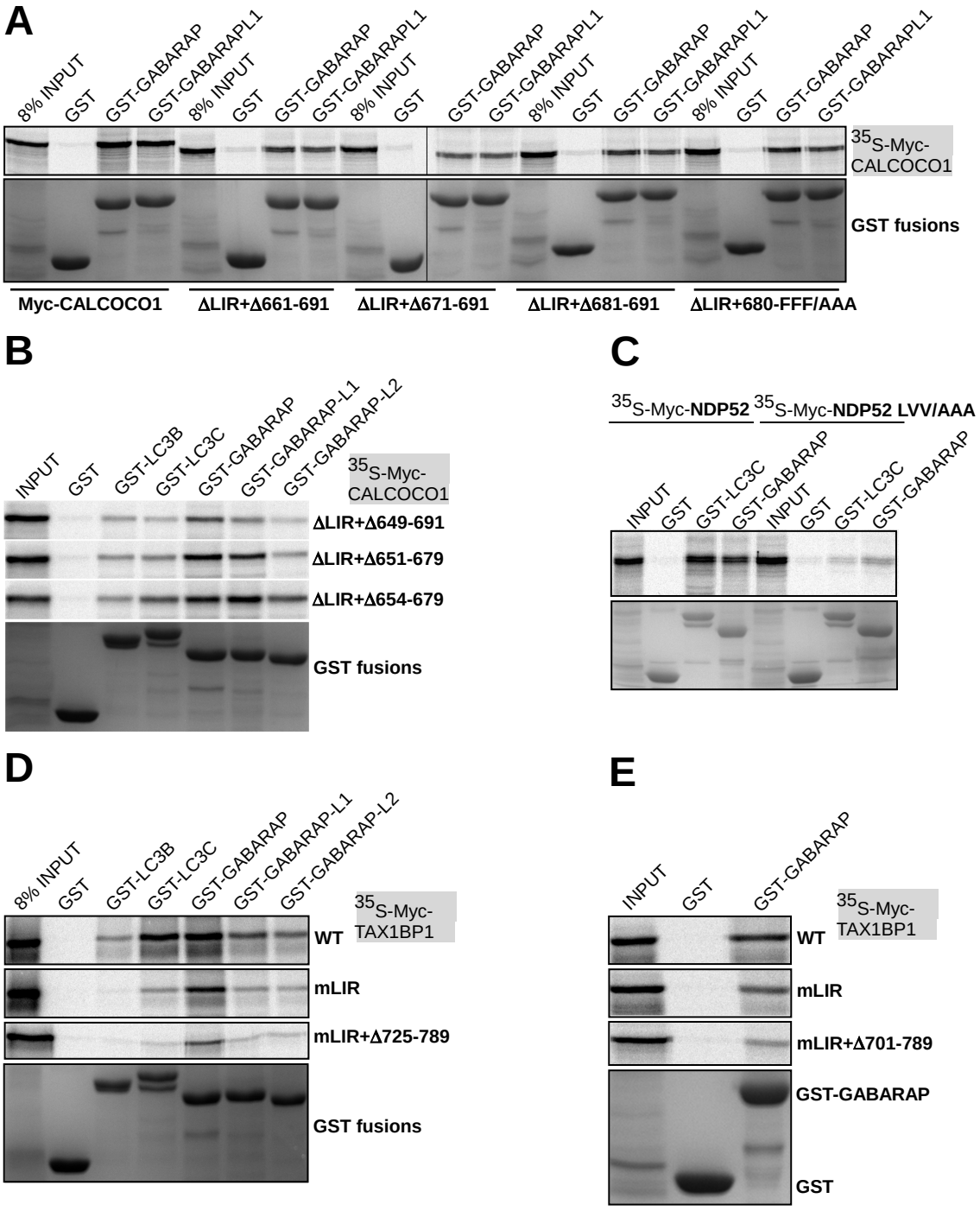
A
8% INPUT
GST
GST-GABARAP
GST-GABARAPL1
35S-Myc-CALCOCO1
GST fusions
Myc-CALCOCO1
ΔLIR+Δ661-691
ΔLIR+Δ671-691
ΔLIR+Δ681-691
ΔLIR+680-FFF/AAA
B
INPUT
GST-LC3B
GST-LC3C
GST-GABARAP
GST-GABARAP-L1
GST-GABARAP-L2
35S-Myc-CALCOCO1
ΔLIR+Δ649-691
ΔLIR+Δ651-679
ΔLIR+Δ654-679
GST fusions
C
35S-Myc-NDP52
35S-Myc-NDP52 LVV/AAA
INPUT
GST
GST-LC3C
GST-GABARAP
D
8% INPUT
GST-LC3B
GST-LC3C
GST-GABARAP
GST-GABARAP-L1
GST-GABARAP-L2
35S-Myc-TAX1BP1
WT
mLIR
mLIR+Δ725-789
GST fusions
E
INPUT
GST
GST-GABARAP
35S-Myc-TAX1BP1
WT
mLIR
mLIR+Δ701-789
GST-GABARAP
GST

FIGURE EV5

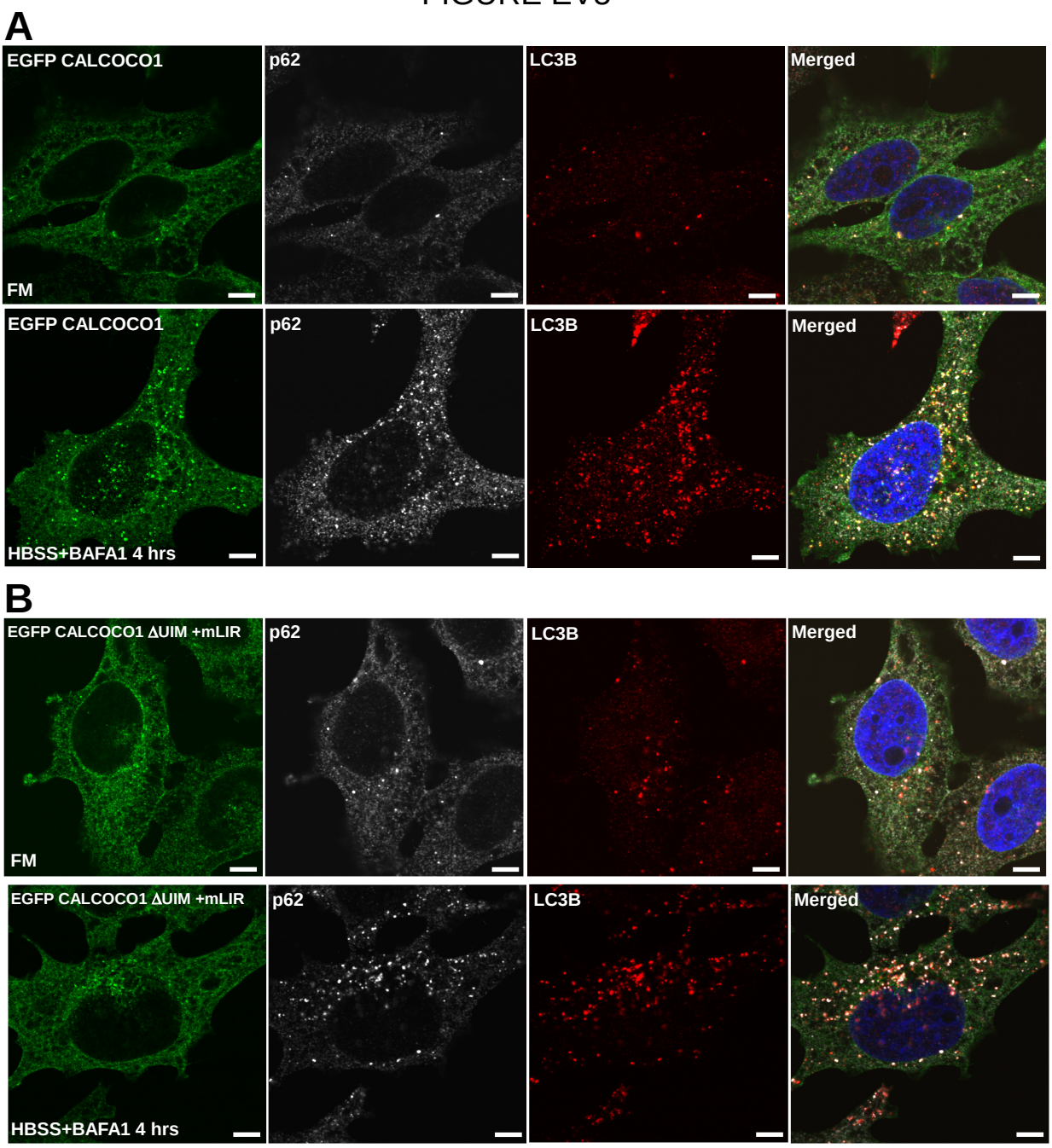
A
EGFP CALCOCO1
p62
LC3B
Merged
FM
EGFP CALCOCO1
p62
LC3B
Merged
HBSS+BAFA1 4 hrs
B
EGFP CALCOCO1 ΔUIM +mLIR
p62
LC3B
Merged
FM
EGFP CALCOCO1 ΔUIM +mLIR
p62
LC3B
Merged
HBSS+BAFA1 4 hrs

Appendix Table S1. **Plasmids used in this study**

pDONOR221-CALCOCO1	This study
pDONOR221-CALCOCO1 141-LVV/141-AAA	This study
pDONOR221-CALCOCO1 (1-150)	This study
pDONOR221-CALCOCO1(145-513)	This study
pDONOR221-CALCOCO1(514-691)	This study
pDONOR221-CALCOCO1ΔSKICH	This study
pDONOR221-CALCOCO1ΔCC	This study
pDONOR221-CALCOCO1Δ514-691	This study
pDONOR221-CALCOCO1ΔLIRΔ514-691	This study
pDONOR221-CALCOCO1ΔLIRΔ623-691	This study
pDONOR221-CALCOCO1Δ145-205	This study
pDONOR221-CALCOCO1Δ231-339	This study
pDONOR221-CALCOCO1Δ413-513	This study
pDONOR221-CALCOCO1(145-670)	This study
pDONOR221-CALCOCO1(145-680)	This study
pDONOR221-CALCOCO1(680-FFF/AAA)	This study
pDest-MYC-CALCOCO1	This study
pDest-MYC-CALCOCO1ΔLIR	This study
pDest-MYC-CALCOCO1 (1-150)	This study
pDest-MYC-CALCOCO1-(145-513)	This study
pDest-MYC-CALCOCO1(514-691)	This study

pDest-MYC-CALCOCO1ΔSKICHΔLIR	This study
pDest-MYC-CALCOCO1ΔCC	This study
pDest-MYC-CALCOCO1Δ514-691	This study
pDest-MYC-CALCOCO1ΔLIRΔ623-691	This study
pDest-MYC-CALCOCO1Δ145-205	This study
pDest-MYC-CALCOCO1Δ231-339	This study
pDest-MYC-CALCOCO1Δ413-513	This study
pDest-MYC-CALCOCO1(145-670)	This study
pDest-MYC-CALCOCO1(145-680)	This study
pDest-MYC-CALCOCO1Δ(680-FFF/AAA)	This study
PDest53-CALCOCO1	This study
pcDNA-Dest53 (GFP fusion)	Invitrogen
pDest-EGFP-C1	Lamark et al., 2003
pDest-EGFP-CALCOCO1	This study
pDest-FlpIn-EGFP-CALCOCO1	This study
pDestmCherry-CALCOCO1	This study
pDONOR221-TAX1BP1	This study
pDONOR221-TAX1BP1ΔLIR	This study
pDONOR221-TAX1BP1mLIRΔ701-789	This study
pDest-MYC-TAX1BP1	This study
pDest-MYC-TAX1BP1ΔLIR	This study
pDest-MYC-TAX1BP1mLIRΔ701-789	This study

pDONOR221-NDP52	This study
pDONOR221-NDP52ΔLIR	This study
pDest-MYC-NDP52	This study
pDest-MYC-NDP52ΔLIR	This study
pDONOR221-VAPA	This study
pDONOR221-VAPA(K94D/M96D)	This study
pDest-MYC-VAPA	This study
pDest-FlpIn-EGFP-VAPA	This study
PDest15-VAPA	This study
PDest15-VAPA(K94D/M96D)	This study
pDONOR221-VAPB	This study
pDONOR221-VAPB(K87D/M89D)	This study
PDest15-VAPB	This study
pDest-MYC-VAPB	This study
pDest15-VAPB(K87D/M89D)	This study
pENTR-GABARAP	Pankiv et al., 2007
pENTR-GABARAPL1	Pankiv et al., 2007
pENTR-GABARAPL2	Pankiv et al., 2007
pENTR-LC3A	Pankiv et al., 2007
pENTR-LC3B	Pankiv et al., 2007
pENTR-LC3C	Kirkin et al., 2009
pENTR-GABARAP Y49A (mLDS)	Alemu et al., 2012

pENTR-GABARAPL1 Y49A (mLDS)	This study
pENTR-GABARAPL2 Y49A (mLDS)	This study
pENTR-LC3B F52A (mLDS)	Kirkin et al., 2009
pENTR-LC3C F58A (mLDS)	This study
pENTR-GABARAP ΔUDS	This study
pENTR-GABARAPL1 ΔUDS	This study
pENTR-GABARAPL2 ΔUDS	This study
pENTR-GABARAP Y49A/ΔUDS	This study
pENTR-GABARAPL1 Y49A/ΔUDS	This study
pENTR-GABARAPL2 Y49A/ΔUDS	This study
pENTR-LC3B F52A/ΔUDS	This study
pENTR-LC3C F58A/ΔUDS	This study
pDest15-GABARAP	Pankiv et al., 2007
pDest15-GABARAPL1	Pankiv et al., 2007
pDest15-GABARAPL2	Pankiv et al., 2007
pDest15-LC3A	Pankiv et al., 2007
pDest15-LC3B	Pankiv et al., 2007
pDest15-LC3C	Kirkin et al., 2009
pDest15-GABARAP Y49A	Alemu et al., 2012
pDest15-GABARAPL1 Y49A	This study
pDest15-GABARAPL2 Y49A	This study
pDest15-LC3B F52A	Kirkin et al., 2009

pDest15-LC3C F58A	This study
pDest15-GABARAP ΔUDS	This study
pDest15-GABARAPL1 ΔUDS	This study
pDest15-GABARAPL2 ΔUDS	This study
pDest15-GABARAP Y49A/ΔUDS	This study
pDest15-GABARAPL1 Y49A/ΔUDS	This study
pDest15-GABARAPL2 Y49A/ΔUDS	This study
pDest15-LC3B F52A/ΔUDS	This study
pDest15-LC3C F58A/ΔUDS	This study

References:

Alemu, E.A.,, Lamark, T., Torgersen, K.M., Birgisdottir, A.B., Bowitz Larsen, K., Jain, A., Olsvik, H., Øvervatn, A., Kirkin, V. and Johansen, T. 2012. ATG8 Family Proteins Act as Scaffolds for Assembly of the ULK Complex: Sequence Requirements for LC3-Interacting Region (LIR) Motifs. ***J. Biol. Chem.*** **287,** 39275-39290

Kirkin, V., Lamark, T., Sou, Y.S., Bjørkøy, G., Nunn, J.L., Bruun J-A., Shvets, E., McEwan, D.G., Clausen, T.H., Wild, P., Bilusic, I., Theurillat, J.P., Øvervatn, A., Ishii, T., Elazar, Z., Komatsu, M., Dikic, I. and Johansen, T. 2009. A role for NBR1 in autophagosomal degradation of ubiquitinated substrates. ***Mol. Cell*** **33,** 505-516.

Lamark, T., Perander, M., Outzen, H., Kristiansen, K., Øvervatn, A., Michaelsen, E., Bjørkøy, G. and Johansen, T. 2003. Interaction codes within the family of mammalian PB1 domain-containing proteins. ***Journal of Biological Chemistry,*** **278,** 34568-34581.

Pankiv, S., Høyvarde Clausen, T., Lamark, T., Brech, A., Bruun, J-A., Outzen, H., Øvervatn, A., Bjørkøy, G. and Johansen, T. 2007. p62/SQSTM1 binds directly to Atg8/LC3 to facilitate degradation of ubiquitinated protein aggregates by autophagy. ***Journal of Biological Chemistry,*** **282,** 24131-24145.

Regulation of Golgi turnover by CALCOCO1-mediated selective autophagy

Thaddaeus Mutugi Nthiga, Birendra Kumar Shrestha, Jack-Ansgar Bruun, Kenneth Bowitz Larsen, Terje Johansen* and Trond Lamark*

Molecular Cancer Research Group, Department of Medical Biology, University of Tromsø – The Arctic University of Norway, 9037 Tromsø, Norway.

*Corresponding authors: Tel: +47 77644720; Email: trond.lamark@uit.no and Tel: +47 77644720; Email: terje.johansen@uit.no

Running Title: CALCOCO1 is a Golgiphagy receptor

Keywords: Autophagy, CALCOCO1, Golgi, Golgiphagy, ZDHHC17, ZDHHC13, TAX1BP1

Abstract

The Golgi complex is essential for the processing, sorting and trafficking of newly synthesized proteins and lipids. Golgi turnover is regulated to meet different cellular physiological demands. The role of autophagy in the turnover of Golgi however, has not been clarified. Here we show that CALCOCO1 binds membrane-bound Golgi-resident palmitoyltransferases ZDHHC17 and ZDHHC13 to facilitate Golgi degradation by autophagy during starvation. Depletion of CALCOCO1 in cells causes an expansion of the Golgi and accumulation of its structural and membrane proteins. ZDHHC17 overexpression experiments show that ZDHHC17 is itself degraded by autophagy together with other Golgi membrane proteins such as TMEM165. Taken together, our data suggest a model where CALCOCO1 mediates selective Golgiphagy to control Golgi size and morphology in eukaryotic cells via its interaction with ZDHHC17.

Introduction

Degradation of protein aggregates, invading pathogens and damaged organelles is important for maintaining eukaryotic cell function, health and survival. The dedicated molecular mechanism for degrading these materials is macroautophagy (henceforth autophagy). It is an evolutionary conserved process, which shuttles cytoplasmic materials or foreign agents to the lysosome for degradation. The process of autophagy involves sequestration of the cytoplasmic material into double-membraned vesicles called autophagosomes, which then fuse with the lysosomes to degrade their contents. At basal level, autophagy facilitates constitutive turnover of cytoplasmic contents to maintain cellular homeostasis. During nutrients starvation, autophagy degrades cellular macromolecules such as lipids, carbohydrates and proteins to recycle nutrients and generate energy (Ohsumi, 2014, Dikic and Elazar, 2018, Feng et al., 2014).

Evolutionary conserved autophagy-related proteins (ATG) acting in temporal hierarchical complexes regulate the formation and expansion of phagophores to form autophagosomes. The autophagosome formation is initiated and nucleated at ER membranes by the ULK complex comprising of FIP200, ATG13, ATG101 and ULK1/2; and the PI3KC3 complex comprising of VPS34, BECN1, VPS15 and ATG14L. Their co-ordinated action at the phagophore formation site generate phosphatidylinositol-3-phopshate (PI3P) which in turn recruits lipid-binding proteins WIPI (WD Repeat Domain, Phosphoinositide-Interacting protein 2) and DFCP1. Phagophore expansion is initiated by WIPI-dependent recruitment of ATG2 and ATG12-ATG5:ATG16L1 complex. The ATG12-ATG5:ATG16L1 complex acting as an E3 ligase with the E1 enzyme ATG7 and the E2 enzyme ATG3, facilitate the lipidation of ATG8 proteins to phosphatidylethanolamine (PE) on the phagophore (Ohsumi, 2014, Zaffagnini and Martens, 2016, Kirkin and Rogov, 2019a). ATG2-WIPI complex transfers lipids or membrane material to the phagophore for the expansion (Maeda et al., 2019, Osawa et al., 2019, Valverde et al., 2019). The role of ATG9, the only transmembrane core autophagy protein, is thought to be the trafficking of membrane vesicles from various sources to the phagophore formation site (Dikic and Elazar, 2018, Yu et al., 2018). Lipidated ATG8s act as scaffolds for the recruitment of cargos and essential autophagy proteins for the phagophore growth and closure (Lystad and Simonsen, 2019, Johansen and Lamark, 2019a).

The autophagy process induced by starvation is non-selective and any part of the cytoplasm can be sequestered into the autophagosomes and shuttled to the lysosome for degradation.

However, autophagy also acts selectively in the degradation of organelles, protein aggregates or invading foreign agents (Johansen and Lamark, 2011). The selectivity is mediated by receptor proteins, which link the degradable cargo to the phagophore membranes by binding to the LC3/GABARAP proteins on the phagophore membrane via LC3-interacting region (LIR) and/or Ubiquitin-like interacting motif (UIM) (Birgisdottir et al., 2013, Johansen and Lamark, 2019b, Marshall et al., 2019, Pankiv et al., 2007, Rogov et al., 2014). The cell engages selective autophagy as a form of organelle autoregulation to control the capacity, number and integrity of organelles in accordance with cellular demands. This is achieved by selectively clearing surplus, damaged or portions of organelles as a counter to the stress response mechanisms, which typically increase the number or volume of organelles in an attempt to alleviate the vagaries of cellular stress. For instance, in response to physiological or pathological conditions such as nutrients deprivation, accumulation of unfolded proteins or exposure to chemicals, the ER engages unfolded protein response (UPR) as a form of stress response mechanism. UPR increases the ER volume and the expression of ER-resident proteins to augment the capacity of the ER in alleviating the stress. Subsequent to the UPR, the cell engages ER-phagy which selectively degrade the excess ER fragments and components to restore homeostasis (Wilkinson, 2019b, Hubner and Dikic, 2019).

Previous studies have established the involvement of autophagy in the degradation of most of the cellular organelles and at the same time, identified specific receptor proteins mediating those degradations (Johansen and Lamark, 2019b, Kirkin and Rogov, 2019b). The Golgi apparatus however, is the odd one out among organelles for not having been associated with any known autophagy degradation mechanism or selective autophagy receptors. The Golgi is involved in processing and sorting of secretory and membrane proteins through addition of various modifications such as glycosylation and sulphation, before the proteins are transported to their destinations via vesicular transport (Farquhar, 1985). Although the molecular mechanism of Golgi stress response is less studied compared to the ER stress response, it is already established that it involves increased synthesis of Golgi structural proteins, glycosylation enzymes and vesicular transport components (Oku et al., 2011). It is therefore tempting to speculate that a yet to be identified autophagy mechanism is involved in the degradation of the Golgi apparatus. The identification of this mechanism however, is hampered by the lack of known receptor proteins that could mediate the degradation.

Several selective autophagy receptors have been found to mediate degradation of the same type of organelles. For instance, in ER-phagy, six different receptors have been identified so

far (Wilkinson, 2019b). In addition to this repertoire, we recently identified CALCOCO1 as an ER-phagy receptor (Nthiga et al. submitted). CALCOCO1 mediate ER-phagy by interacting with VAP on the ER membrane via a FFAT motif and with LC3/GABARAP proteins via LIR and UIR motifs. We established that a fraction of CALCOCO1 is localized with the Golgi, suggesting a Golgi-related function. Previous studies have suggested CALCOCO1 function in transcriptional co-activation, glucose metabolism and calcium signalling and determined that CALCOCO1 mRNA is highly expressed in the rat brain (Kim et al., 2003, Takahashi et al., 2004).

In this study, we have identified CALCOCO1 as a receptor for the autophagic degradation of Golgi apparatus during starvation. This requires CALCOCO1 binding to the AR domain of ZDHHC17 and ZDHHC13 via a ZDHHC-AR-binding (zDABM) motif. ZDHHC17/13 are cis-Golgi-localized transmembrane S-acyltransferases (also called palmitoyltransferases) (Ernst et al., 2018b) and their known function is to catalyze S-acylation reactions, which is a reversible addition of palmitate on cysteine residues in proteins. Depletion of CALCOCO1 in cells causes an expansion of the Golgi and accumulation of Golgi-resident proteins. CALCOCO1 therefore mediates Golgiphagy to regulate Golgi remodelling during stress.

Results

Interaction of CALCOCO1 with ZDHHC17 via zDABM motif

We identified Golgi-localized ZDHHC17 and ZDHHC13 S-acyltransferases in an affinity purification mass spectrometry-based screen for CALCOCO1 interactors (**Figure 1A, Appendix Table S1**). S-acyltransferases catalyze protein S-acylation reactions (also called palmitoylation), a reversible addition of fatty acids, usually palmitate, to cysteines of proteins. Palmitoylation plays major roles in regulating membrane targeting, trafficking, stability and function of the modified proteins (Fukata and Fukata, 2010, Linder and Deschenes, 2007). There are 24 palmitoyltransferases in mammals, but only two members, ZDHHC17 and ZDHHC13, contain an Ankyrin repeats (AR) domain on their N-termini. Both ZDHHC17 and ZDHHC13 are localized in the Golgi (Ernst et al., 2018a), but a separate study reported localization of ZDHHC13 in the endoplasmic reticulum (Ohno et al., 2006). In humans, ZDHHC17 is highly expressed in the brain and knockout in mice significantly affected synaptic plasticity and produced Huntington-like symptoms (Ohno et al., 2006, Sanders et al., 2015).

The ankyrin repeats (AR) domains of ZDHHC17/13 function in both substrate recruitment and S-acylation-independent functions (Lemonidis et al., 2017, Verardi et al., 2017). The AR domain interacts with proteins bearing ZDHHC-AR-binding motif (zDABM) on their sequences (Lemonidis et al., 2015).

We have already reported CALCOCO1 is localized in the Golgi (Nthiga et al. submitted). To investigate whether CALCOCO1 and ZDHHC17/13 interact and colocalize on the Golgi structures in HeLa cells, we co-transfected EGFP-CALCOCO1 with Myc- ZDHHC17 into CALCOCO1 knockout HeLa cells. We used CALCCO1 KO cells in order to avoid interference by the endogenous CALCOCO1. Imaging of the cells revealed that a proportion of EGFP-CALCOCO1 colocalized completely with ZDHHC17 and cis-Golgi protein GM130 (**Figure 1B**). Similarly, we observed colocalization of EGFP-CALCOCO1 with Myc-ZDHHC13 at the Golgi (**Figure 2A**), suggesting that CALCOCO1 and ZDHHC17/13 interact in cells and are colocalized in the Golgi apparatus. To test whether CALCOCO1 and ZDHHC17 interacted directly, Myc-CALCOCO1 was in vitro-translated and tested for interaction with GST-ZDHHC17 that was produced in bacteria in an *in vitro* pull down assay. GST-ZDHHC17 pulled down the *in vitro*-translated Myc-CALCOCO1 (**Figure 1C**), suggesting direct interaction of CALCOCO1 with ZDHHC17 and possible presence of a zDABM motif in CALCOCO1.

The critical residues in the AR domain of ZDHHC17 for binding to the zDABM motif of an interacting protein are N100/W130 (Verardi et al., 2017). To clarify whether the interaction of ZDHHC17 with CALCOCO1 is mediated by AR-zDABM contact, we made point mutations at these critical residues and tested their effect on ZDHHC17 binding to CALCOCO1. Alanine substitutions at these sites (N100A/W130A) abolished the interaction of ZDHHC17 with CALCOCO1 **(Figure 1C**), indicating that the interaction was specifically mediated by the AR-zDABM interface. zDABM motif is characterised by VIAP)(VIT)XXQP core consensus sequence, where x is any amino acid (Lemonidis et al., 2015). Analysis of the primary structure of CALCOCO1 revealed a similar motif encompassing 574-VVISQP-580 core sequence at the C-terminal half of the protein. To test whether the motif was mediating the interaction with ZDHHC17, we made point mutations within the motif and tested binding to ZDHHC17. Mutation of the critical binding residues within the motif (Lemonidis et al., 2017) into alanines (574-AAISAA-580) abolished the interaction of CALCOCO1 with ZDHHC17 (**Figure 1C**), suggesting that the sequence is a zDABM motif (**Figure 1D**).

CALCOCO1 is a paralog to TAX1BP1 and NDP52. The three proteins function as selective autophagy receptors and belong to a small CALCOCO protein family, sharing substantial similarity and identity. Because of this similarity and identity, we analysed the primary structures of NDP52 and TAX1BP1 for the presence of potential zDABM motif. While no potential zDABM motif was identified in NDP52, we identified a motif in TAX1BP1 encompassing 673-VVCSQP-679 core sequence as a potential zDABM motif, suggesting that ZDHHC17 could interact with TAX1BP1 in a mechanism similar to the mechanism of interaction with CALCOCO1. To test this hypothesis, in vitro-translated Myc-TAX1BP1 was tested for interaction with GST-tagged ZDHHC17 and N100A/W130A mutant. While the wild type ZDHHC17 interacted with TAX1BP1, the N100A/W130A abolished the interaction (**Figure 1E**), suggesting that the ZDHHC17 interaction with TAX1BP1 was mediated by AR-zDABM motif interface. Conversely, we deleted the VVCSQP motif in TAX1BP1 and tested how the interaction with ZDHHC17 was affected, whereupon the interaction was completely abrogated (**Figure 1E),** suggesting that the VVCSQP sequence in TAX1BP1 is a zDABM motif. These results suggest that CALCOCO1 and TAX1BP1 share similar mechanism of interaction with ZDHHC17/13.

To clarify whether the absence of zDABM motif affected the localization and interaction of CALCOCO1 with ZDHHC17/13 in cells, we deleted the C-terminal portion of CALCOCO1 that contains the zDABM motif and analyzed its localization in cells. Either EGFP-CALCOCO1 or EGFP-CALCCO1Δ514-691 was co-transfected into HeLa cells with Myc-ZDHHC17/13 and the co-localization pattern was then analyzed by confocal microscopy. While EGFP-CALCOCO1 completely co-localized with Myc-ZDHHC17/13 on Golgi stacks and ribbons, EGFP-CALCOCO1Δ514-691 formed vesicular structures that did not colocalize with Myc-ZDHHC17/13 (**Figure 2A, B**) (upper panels).

Surprisingly, the Golgi in cells transfected with EGFP-CALCOCO1Δ514-691 had a fragmented phenotype of vesicular structures (**Figure 2A, B**) (lower panels). This suggested that the fragmented phenotype was caused by the lack of CALCOCO1 localization on the Golgi. If this is true, we postulated that it should be replicated in cells lacking CALCOCO1. To test this, EGFP-ZDHHC17 only was transfected into either HeLa wild type or HeLa-CALCOCO1 KO cells and the effect on Golgi morphology compared between the two cell types. In both cell types, there was no disassembly or fragmentation of the Golgi, implying that the Golgi fragmentation phenotype was not caused by the lack of CALCOCO1 Golgi localization. Previous studies have shown that expression of mutant forms of proteins involved in vesicular

trafficking between the ER to the Golgi cause disassembly of Golgi stacks into vesicular structures (Dascher and Balch, 1994, Wilson et al., 1994). The disassembly of the Golgi stacks by the expression of the mutant CALCOCO1 lacking the zDABM motif for Golgi localization therefore could suggest that CALCOCO1 plays some trafficking role to and from the Golgi and the fragmented phenotype observed was probably due to a dominant negative effect on trafficking pathway by the CALCOCO1 mutant. Taken together, these results suggest that localization of CALCOCO1 on the Golgi is mediated by the interaction with ZDHHC17/13 via ZDABM motif.

ZDHHC17 coated Golgi fragments co-localize with CALCOCO1 on autophagosomes

Previous studies have shown that the Golgi apparatus is fragmented in response to stress conditions such as viral infection and nutrient starvation (Campadelli et al., 1993, Takahashi et al., 2011). The Golgi fragments induced by starvation disperse to the cytoplasm and co-localize with autophagosomes (Takahashi et al., 2011). Because CALCOCO1 is localized on the Golgi and also binds LC3/GABARAP proteins, we speculated that starvation-induced Golgi fragments are colocalized with CALCOCO1 in the cytoplasm and autophagosomes. To clarify this, we transiently co-expressed Myc-ZDHHC17 with EGFP-CALCOCO1 in CALCOCO1 KO HeLa cells and then monitored the morphology of the Golgi under normal culture conditions and under starvation in the presence of bafilomycin $A_{1.}$ We used bafilomycin A_1 to inhibit lysosomal degradation of Golgi fragments and LC3-positive vesicles.

Under normal culture conditions, the Golgi, as visualized with Myc-ZDHHC17 and endogenous TMEM165, formed intact stacks with ribbon-like morphology (**Figure 3A, B**), and completely colocalized with EGFP-CALCOCO1 but not with autophagosome marker LC3 (**Figure 3B**). Upon nutrient starvation, Myc-ZDHHC17 and TMEM165 lost the characteristic ribbon-like morphology of the Golgi and instead, formed dispersed vesicular structures in the cytoplasm, suggesting disassembly and fragmentation of the Golgi (**Figure 3A, B, C**). This also occurred in CALCOCO1 KO cells, suggesting that CALCOCO1 is not required for the Golgi fragmentation observed upon starvation (**Figure 3C**). The colocalization of EGFP-ZDHHC17 with endogenous TMEM65 on the Golgi shows that the overexpressed EGFP-ZDHHC17 is not mislocalized (**Figure 3A**).The ZDHHC17-positive Golgi fragments co-localized not only with

EGFP-CALCOCO1, but also with endogenous LC3-positive vesicles (**Figure 3B**), suggesting recruitment of the fragments to the autophagosomes. We interpret these results to mean that a fraction of the starvation-induced Golgi fragments is recruited to LC3-positive autophagosomes via interaction of ZDHHC17 with CALCOCO1.

Golgi is degraded by autophagy

The Golgi apparatus is a highly dynamic organelle whose capacity is regulated by cellular physiological demands. It has been proposed that the Golgi is regulated by Golgi stress response akin to the regulation of the ER by the ER stress response. Golgi stress response augments the capacity of the Golgi function by increasing the synthesis of Golgi structural proteins such as GM130, GCP60 and giantin; glycosyltransferases and vesicular transport components (Sasaki and Yoshida, 2015, Oku et al., 2011). It is however not known whether autophagy is involved in the turnover of the excess Golgi membranes to remodel the Golgi back to physiological size. We postulated that the Golgi is remodelled back to physiological size by autophagy-mediated degradation of the excess membranes and proteins that are produced by the stress response.

To determine whether autophagy is involved in the turnover of Golgi, we monitored the turnover of Golgi structural and membrane proteins during nutrients starvation in autophagy deficient cells. In autophagy-deficient Atg5-knockout MEF cells, starvation-induced turnover of Golgi structural protein GM130 and membrane proteins TMEM165, ZDHHC13 and ZDHHC17 was impaired when compared to wild type MEF cells (**Figure 4A**). Similarly, in ATG7-deficient HeLa cells, starvation-induced decrease in the amount of GM130, TMEM165 and ZDHHC13 was impaired when compared to wild type HeLa cells (**Figure 4B**). The accumulation of the Golgi proteins in the two autophagy-deficient cell types during starvation was similar to the observed accumulation of autophagy receptors p62 and CALCOCO1 in the same cells, suggesting that the Golgi proteins are also autophagy substrates. Treatment of the wild type MEF and HeLa cells with the lysosomal inhibitor bafilomycin A_1 blocked the starvation-induced decrease in the amount of GM130, TMEM165, ZDHHC17 and ZDHHC13 in a similar manner as the blockage of p62 and CALCOCO1 in the same cells, further supporting that they are autophagy substrates (**Figure 4A, B**). We interpreted these results to mean that autophagy is involved in the degradation of Golgi structural and membrane proteins during starvation.

ZDHHC17/13 are cis-Golgi integral membrane proteins. Their degradation by autophagy and interaction with CALCOCO1, an autophagy receptor, prompted us to speculate whether they mediated the observed degradation of Golgi membranes. To test this, we made stable HeLa cells expressing EGFP-ZDHHC17 under the control of a tetracycline-inducible promoter and monitored how expression influenced the turnover of Golgi transmembrane protein TMEM165. Expression of EGFP-ZDHHC17 promoted starvation-induced decrease of TMEM165 compared to the non-induced cells (**Figure 4C**), suggesting that overexpression of ZDHHC17 promoted degradation of Golgi membranes. In the same cells, EGFP-ZDHHC17 was also degraded upon starvation, confirming the results in MEF cells (**Figure 4A**), that ZDHHC17 is an autophagy substrate under starvation conditions.

CALCOCO1 is a Golgi-phagy Receptor

The Golgi localization and the interaction with Golgi integral membrane proteins ZDHHC17/13 raised the possibility that CALCOCO1 could mediate degradation of Golgi membrane components and proteome. To test the possibility that CALCOCO1 has a role in the turnover of Golgi membranes, henceforth called Golgiphagy, we investigated how absence of CALCOCO1 affected the turnover of Golgi structural and membrane proteins. CALCOCO1 KO in HeLa cells impaired the starvation-induced decrease of Golgi structural protein GM130 and Golgi integral membrane proteins TMEM165 and ZDHHC13 but not p62, NDP52 or LC3B when compared to the starvation-induced decrease of the same proteins that was observed in wild type HeLa cells (**Figure 5A**). To test whether re-introduction of CALCOCO1 could rescue the degradation of GM130, TMEM165 and ZDHHC13, we reconstituted the CALCOCO1 KO HeLa cells with tetracycline-inducible EGFP-CALCOCO1. Induced expression of EGFP-CALCOCO1 restored the starvation-induced degradation of Golgi proteins GM130, TMEM165 and ZDHHC13 that was blocked when cells were treated with bafilomycin A_1 (**Figure 5B**), suggesting that CALCOCO1 was mediating their degradation by autophagy. In addition, we observed decreased basal amount of TMEM165 and ZDHHC13 in the reconstituted cells compared to the non-induced cells, suggesting that CALCOCO1also mediated basal turnover of Golgi membranes.

To corroborate our findings that CALCOCO1 mediated degradation of Golgi by autophagy, we monitored by immunofluorescence, the labelling intensity of GM130 in HeLa cells in the presence or absence of induced or non-induced EGFP-CALCOCO1. When EGFP-CALCOCO1

was induced for 24 hours under basal conditions, the average GM130 intensity was relatively lower than in the non-induced cells (**Figure 5C**), suggesting decreased amount of the protein due to CALCOCO1 expression. When the cells were starved for different time periods prior to intensity measurement, the average GM130 intensity was relatively lower in the induced cells than in the non-induced cells at both two hours and four hours starvation, suggesting that CALCOCO1 promoted starvation-induced turnover of GM130 during starvation. Immunoblotting of the same cells revealed that the amounts of GM130 and TMEM165 in the non-induced cells were higher at all the tested time points during starvation (**Figure 5D**). Taken together, these results suggest that CALCOCO1 was mediating selective degradation of Golgi membranes.

To clarify whether the observed turnover of Golgi membranes was mediated via CALCOCO1 interaction with ATG8 proteins, we investigated how CALCOCO1 lacking LIR and UIR motifs affected turnover of transmembrane protein TMEM165. HeLa CALCOCO1 KO cells were reconstituted with inducible EGFP-CALCOCO1ΔLIRΔUIR and then monitored for the degradation of TMEM165. Induced expression of EGFP-CALCOCO1ΔLIRΔUIR did not promote starvation-induced decrease in TMEM165 when compared to the non-induced cells (**Figure 5E**). This contrasted with starvation-induced decrease that was observed when the same cells were expressing wild type EGFP-CALCOCO1 (**Figure 5B**).

Discussion

The amount of each organelle in the cell is tightly regulated in accordance with cellular demands and physiological conditions. It is already established that autophagy regulates the amount and health of organelles by shuttling surplus and damaged organelles to the lysosome for degradation. Previous studies on the selective macroautophagy of organelles have identified receptors for the degradation of mitochondria, endoplasmic reticulum, lysosomes, and peroxisomes in which they act as molecular bridges between the cargo to be degraded and the autophagosomes (Johansen and Lamark, 2019b, Kirkin and Rogov, 2019b). The autophagic degradation of the Golgi however had not been defined. In this study, we have identified CALCOCO1 as a selective autophagy receptor for the degradation of Golgi membranes and proteins and demonstrated that autophagy is a Golgi remodelling mechanism in response to nutrient starvation, as demonstrated by the degradation of Golgi proteins GM130, TMEM165, ZDHHC17 and ZDHHC13. The interaction of CALCOCO1 (and its paralog TAX1BP1) with

the Golgi membrane is mediated through binding to the cytoplasmic AR domain of the Golgi transmembrane ZDHHC17 and ZDHHC13 proteins via an evolutionary conserved zDABM motif, a canonical ZDHHC17/13 substrate recognition motif, which in CALCOCO1 encompasses the 574-VVISQP-580 core sequence. Because recent large scale palmitoylation studies did not identify CALCOCO1 as a substrate (Blanc et al., 2015), the involvement of ZDHHC17/13 in mediating degradation of Golgi by autophagy could be a palmitoylation-independent function.

Our results suggest that under basal conditions, CALCOCO1 is anchored on the Golgi by ZDHHC17/13. Nutrients starvation induces disassembly and fragmentation of the Golgi and delivery of the fragments to autophagosomes in the cytoplasm. The delivery of the Golgi fragments to the autophagosomes, in our opinion, is mediated by ZDHHC17-anchored CALCOCO1 interaction with the autophagy machinery. In this case, CALCOCO1 bound to the ZDHHC17 on the Golgi membrane, recruits ATG8 family proteins via LIR and UIR motifs to initiate autophagosome biogenesis and eventual degradation of a sub-set of Golgi proteins in order to maintain Golgi proteostasis (**Figure 5F**). This is consistent with the notion that autophagy receptors act upstream of the core autophagy machinery (Turco et al., 2019). This is supported by our observation that mutant CALCOCO1 lacking both LIR and UIR motifs impaired the turnover of TMEM165.

Because zDABM motif has been identified in a large number of proteins (Lemonidis et al., 2017), it is expected that the interaction of CALCOCO1 or TAX1BP1 with ZDHHC17 is transient and the recruitment of the autophagy machinery therefore is what buttresses the interactions to form stable entities necessary for Golgi deformation, punctation and engulfment into autophagosomes. This is conceptually similar to the proposed ER-phagy mechanisms (Wilkinson, 2019a), and consistent with the established notion that many cellular multi-component complexes do not exist as strong, stable entities, but instead, are assembled in a more stochastic manner with transient encounter complexes being progressively buttressed by the combinatorial addition of further elements or ligands (Morriswood et al., 2007, Tang et al., 2006).

Overexpression of zDABM-deletion mutant of CALCOCO1 induced disassembly of the Golgi stacks into dispersed vesicular structures in the cytoplasm. Because the absence of CALCOCO1 did not cause a similar phenotype, we conclude that the fragmentation phenotype was caused by a dominant negative effect of the mutant CALCOCO1, probably due to lack of

Golgi localization. Because the Golgi structure is maintained by the efficient bidirectional vesicular transport with the ER (Nassif et al., 2010), the disruption of the Golgi structure by mutant CALCOCO1 could imply involvement of CALCLCO1 in trafficking to and from the Golgi. This notion is consistent with previous studies, which have shown that overexpression of mutant forms of proteins that are involved in trafficking to and from the Golgi cause disassembly of Golgi stacks into vesicular structures (Dascher and Balch, 1994, Wilson et al., 1994).

Our data suggest a direct link between starvation-induced Golgi stress response and the CALCOCO1-mediated degradation of the Golgi, Golgiphagy. Nutrients starvation induced upregulation of Golgi matrix and transmembrane proteins which were subsequently cleared by CALCOCO1-mediated autophagy. The upregulation of the proteins is consistent with previous studies which have shown that Golgi stress response due to nutrients starvation, viral infections or toxic insults caused upregulation of structural proteins, glycosylation enzymes and vesicular transport components (Oku et al., 2011, Taniguchi and Yoshida, 2017, Taniguchi et al., 2015). The conclusion to be drawn here is that CALCOCO1-mediated Golgiphagy is induced by the need to remove excess Golgi membranes generated during stress in order to restore the pre-stress state of the Golgi. It is possible that nutrient starvation is not the only trigger for CALCOCO1-mediated Golgiphagy. It has been shown that pathological and physiological conditions such as bacterial and viral infections and neurodegenerative diseases induce Golgi fragmentation (Campadelli et al., 1993, Gonatas et al., 2006). It is possible that CALCOCO1 is involved in autophagy-mediated removal of the damaged Golgi portions and fragments caused by these pathological conditions.

The discovery that ZDHHC17/13-CALCOCO1coupling is involved in the degradation of Golgi membranes by autophagy is an important step in understanding how autophagy may regulate Golgi homeostasis. Future investigations will determine whether CALCOCO1-ZDHHC17/13 interaction has functions other than autophagy, which may contribute to Golgi homeostasis.

Materials and Methods

Antibodies: Mouse monoclonal anti-CALCOCO1 (A-10) (Santa Cruz Biotech Cat#sc-515670), rabbit polyclonal anti-CALCOCO1 (Sigma-Aldrich Cat#HPA038314), rabbit polyclonal anti-ZDHHC13 (Proteintech Cat# 24759-1-AP), rabbit polyclonal anti-ZDHHC17 (Proteintech Cat# 15465-1-AP), rabbit polyclonal anti-TMEM165 (proteintech Cat# 20485-1-AP), rabbit polyclonal anti-GFP (Abcam Cat #ab290), mouse monoclonal anti-p62 (BD Biosciences Cat #610833), guinea pig polyclonal anti-p62 (Progen Cat #GP62-C), rabbit monoclonal anti-ATG7 (Cell Signaling Cat #D12B11), rabbit polyclonal anti-LC3B (Novus Bio Cat #NB100-2220), rabbit polyclonal anti-LC3B (Sigma-Aldrich Cat # L7543), mouse monoclonal anti-GABARAP(MBL Cat # M135-3), mouse monoclonal anti-Myc tag (9B11) cell signalling #2276), rabbit monoclonal anti-GM130 (Abcam Cat#52649), rabbit polyclonal anti-GAPDH (Sigma-Aldrich Cat#G9545), rabbit polyclonal anti-Actin (Sigma-Aldrich Cat #A2066), HRP-conjugated goat polyclonal anti-rabbit (BD Biosciences Cat #554021), HRP-conjugated goat polyclonal anti-mouse (BD Biosciences Cat #554002).

Reagents/Chemicals: Bafilomycin A1 (Santa Cruz Biotech sc-201550), MG132 (Sigma-Aldrich #C2211), [35S] methionine (PerkinElmer NEG709A500UC), T7 coupled reticulocyte lysate system (Promega #14610), Ponceau S (sigma #P3504), Dulbeco's modified Eagle's medium (DMEM) (Sigma-Aldrich #D6046), HBSS (Sigma-Aldrich #H9269), Hygromycin (Thermofisher #10687-010), Tetracycline (Sigma-Aldrich #87128), Pen/Strep (Sigma-Aldrich #P4333), Metafectene Pro (Biontex #T040), Fetal bovine serum (FBS) (Biochrom #S0615), Lipofectamine RNAiMAX (Thermofisher #13778), Complete EDTA-free Protease inhibitor (Roche #11836170001), Chemiluminescent HRP substrate (Sigma-Aldrich), Glutathione sepharose beads (GE Healthcare #17-5132-01).

Plasmid constructs

All the plasmid constructs used in this study are listed in Table 1 below. The constructs were made using conventional cloning techniques and the Gateway recombination system (Invitrogen). Mutagenesis was performed using the QuickChange site-directed mutagenesis kit (Stratagene). Oligonucleotides for mutagenesis and sequencing were from Invitrogen. All constructs were verified by sequencing (BigDye, Applied Biosystems). pDONR201-

CALCOCO1 (HSCD00081507), pENTR223-ZDHHC13 (HsCD00376338) and PENTR223-ZDHHC17 (HsCD00377094) were obtained from Harvard plasmid collection.

Table 1: plasmids used in the study

pDONOR221-CALCOCO1	This study
pDONOR221-CALCOCO1 ΔLIRΔ623-691	This study
pDONOR221-CALCOCO1 (1-513)	This study
pDONOR221-CALCOCO1 (574-VVISQP/574-AAISAA)	This study
pDest-MYC-CALCOCO1	This study
pDest-MYC-CALCOCO1 (574-VVISQP/574-AAISAA)	This study
pDest-EGFP-C1	Lamark et al., 2003
pDest-EGFP-CALCOCO1	This study
pDest-EGFP-CALCOCO1(1-513)	This study
pDest-FlpIn-EGFP-CALCOCO1	This study
pDONOR221-TAX1BP1	This study
pDONOR221-TAX1BP1Δ673-679)	This study
pDest-MYC-TAX1BP1	This study
pDest-MYC-TAX1BP1Δ673-679)	This study
pDONOR221-ZDHHC13	This study
pDest-EGFP-ZDHHC13	This study
pDONOR221-ZDHHC17	This study
pDONOR221-ZDHHC17 (N100A/W130A)	This study

pDest-EGFP-ZDHHC17	This study
pDest-FlpIn-EGFP-ZDHHC17	This study
pDest15-C1	This study
pDest15-ZDHHC17	This study
pDest15-ZDHHC17 (N100A/W130A)	This study

Mammalian cell culture and cell treatments

We used human HeLa cells (ATCC CCL-2), MEFs and Atg5 KO MEFs (Kuma et al., 2004), and HeLa KO for all six ATG8 family genes (Abudu et al., in preparation). All cells were cultured in DMEM (Sigma-Aldrich, D6046) supplemented with 10% fetal bovine serum (Biochrom, S 0615) and 1% streptomycin-penicillin (Sigma-Aldrich, P4333) and kept in a humidified incubator at 37^0C and 5% CO_2. Starvation experiments were conducted by incubating cells in Hanks' Balanced Salt solution (Sigma-Aldrich, H9269). Cells were treated with one µg/ml of tetracycline (Sigma-Aldrich), 200 ng/ml bafilomycin A1 (Santa Cruz Biotechnology, sc-201550), 25 µM MG132, for the indicated time periods. DNA transfection were done with metafectene Pro(Biontex #T040) according to manufacturers protocol. SiRNA transfections were done with RNAiMAX according to manufacturer's protocol

Generation and propagation of inducible stable cell lines

Flp-In Trex HeLa cells and Flp-In Trex HEK293 cells were used to create inducible stable cell lines and to produce CALCOCO1 knockout cells. Tagged constructs were cloned into pcDNA5/FRT/TO vector using the Gateway technology and then co-transfected with recombinase pOG44 into the Flp-In Trex cells. After 48 hours, colonies of cells with the gene of interest integrated into the FRT site were selected with 200 µg/ml of hygromycin (Calbiochem, 400051) and 7.5 µg/ml blasticidin. Polyclonal hygromycin-resistant cells were then expanded in the selection media and later tested for expression by immunoblotting and immunofluorescence. The expression of the gene was induced with 1µg/ml tetracycline for 24 hours.

Generation of knockout cell lines using CRISPR-Cas9

Specific RNA-guides were designed using the CHOPCHOP web tool (found at https://chopchop.cbu.uib.no) (Labun et al., 2019). The sequences of the sgRNA used are 5' CACCGGAAGAATCACCACTAAGCC 3', 5'- CACCGAGAAAGTTGACTCCACCAC-3'and 5'- CACCGTTCCGATATGTGAACCGCC-3' (see Fig EV3). The sense and antisense oligonucleotides were annealed and phosphorylated and then ligated into a BbsI linearized pSpCas9(BB)-2A-Puro (PX459) vector (Addgene #62988). To generate CALCOCO1 knockout Flp-In T-Rex HeLa cells were transfected with the PX459 vector containing sgRNA targeting exon 2 while to generate CALCOCO1 knockout Flp-In T-Rex HEK293 cells, cells were transfected with PX459 vector containing sgRNA targeting exon2 and 4 using Metafectene Pro (Biontex #T040). 24 hours post transfection, the cells were selected by treatment with puromycin at 1 µg/mL for 72 hours. Puromycin-resistant cells were then singly sorted into 96-well plates. The clones were then expanded and screened by immunoblotting. Once knockout were confirmed by immunoblotting, genomic DNA were extracted and the area of interest amplified by PCR. The amplified region was ligated into the PGEM vector (Promega #A3600) and sequenced to identify the indels.

Western blotting

Cells were directly lysed in 2x Laemli buffer (50 mM Tris pH 7.4, 2% SDS, 10% Glycerol, 200 mM dithiothreitol (DTT, Sigma, #D0632) and heated for 10 min. Protein concentrations were measured by Pierce BCA Protein Assay Kit (Thermofischer Scientific, #23227) and 30-40 µg protein of the sample were resolved by SDS-PAGE and transferred to nitrocellulose membrane. Membranes were blocked in PBS or TBS containing 0.1% Tween and 5% low fat milk and then incubated overnight at 4°C with the indicated primary antibodies in the blocking solution. Immuno-blot bands were quantified using ImageJ program.

Mass spectrometry

Gel pieces were subjected to in gel reduction, alkylation, and tryptic digestion using 6 ng/µl trypsin (V511A, Promega, Wisconsin, USA) . OMIX C18 tips (Varian, Inc., Palo Alto, CA, USA) was used for sample cleanup and concentration. Peptide mixtures containing 0.1% formic

acid were loaded onto a Thermo Fisher Scientific EASY-nLC1000 system and EASY-Spray column (C18, 2µm, 100 Å, 50µm, 50 cm). Peptides were fractionated using a 2-100% acetonitrile gradient in 0.1 % formic acid over 50 min at a flow rate of 200 nl/min. The separated peptides was analysed using a Thermo Scientific Q-Exactive mass spectrometer. Data was collected in data dependent mode using a Top10 method. The raw data were processes using the MaxQuant software v1.6.0.16 using label-free quantification (LFQ) method. MS/MS data was searched against a Uniprot human database. A FDR ratio of 0.01 were needed to give a protein identification. Perseus v1.6.0.7 was used for statistical analysis.

GST-pulldown assays

GST-fusion proteins (LC3s, GABARAPs, CALCOCO1, VAPs) were expressed in Escherichia coli SoluBL21 (DE3) (Genlantis, # C700200) in LB medium. Protein expression were induced by addition of 0.5 mM IPTG and cells were incubated with shaking at 37°C for 4 hours. Harvested cells were sonicated in the lysis buffer (20 mM Tris-HCl pH 7.5, 10 mM EDTA, 5 mM EGTA, 150 mM NaCl) and the GST-fused proteins then immobilized on Glutathione Sepharose 4 Fast Flow beads (GE Healthcare, #17-5132-01) by incubating in a rotator at 4^0C for one hour. Fusion protein-bound beads were then used directly in GST pull down assays with in vitro-translated proteins. In-vitro translation was done in the presence of radioactive ^{35}S-methionine using the TNT T7 Reticulocyte Lysate System (Promega, #l4610). 12 µL of the in-vitro translated protein were then pre-cleared by incubation with 10 µL of empty Glutathione sepharose beads in 100 µL of NETN buffer (50 mM Tris pH 8.0, 150 mM NaCl, 1 mM EDTA, 0.5% NP-40) supplemented with cOmplete Mini EDTA-free protease inhibitor for 30 min at 4 ^{0}C to remove non-specific binding. The precleared lysates were then incubated with the GST-fusion protein loaded beads for 1 hour at 4 ^{0}C. The beads were then washed five times with NETN buffer followed by resuspension in sample loading buffer (100 mM Tris pH 7.4, 4% SDS, 20% Glycerol, 0.2% Bromophenol blue and 200 mM dithiothreitol DTT (Sigma, # D0632) and boiled for 10 minutes and then resolution in SDS-PAGE. Gels were stained with Coomassie Brilliant Blue R-250 Dye (ThermoFisher Scientific, #20278) for 30 min to visualize the fusion proteins, washed and then vacuum-dried (in Saskia HochVakuum combined with BIO-RAD Gel dryer model 583, #1651746) for 30 min. Radioactive signals were analysed by Fujifilm bioimaging analyzer BAS-5000 (Fujifilm).

Immunofluorescence

Cells were plated on glass coverslips (VWR, #631-0150) or in Lab-Tek chambered coverglass (Thermo Scientific, #155411) and fixed in 4% (wt/vol) formaldehyde for 10 min at room temperature and then permeabilized with 0.1% Triton X-100 in PBS at room temperature for 5 min and blocked in PBS containing 3% goat serum for 1 hr at room temperature. Cells were then incubated overnight at 4° C with primary antibody diluted in PBS containing 2% goat serum. After five washes in PBS, they were incubated with AlexaFluor secondary antibodies in PBS containing 2% goat serum for 1 hr at room temperature followed by five washes in PBS. Nuclei were stained with 1 μg/ml DAPI in PBS for 10 min, followed by one final wash in PBS. Coverslips were mounted in 10 μl of Mowiol and placed on a glass microscope slide.

Light Microscopy

Cells were imaged on an Observer Z.1 inverted microscope, equipped either with an LSM780 scanner for confocal microscopy or an Axiocam 506 monochromatic camera for widefield microscopy followed by deconvolution (both systems Carl Zeiss Microscopy). Images were collected in ZEN software using a 63X NA1.4 oil immersion lens for coverslips, or a 40X NA1.2 water immersion lens for chambered coverglass. Optimal excitation and emission settings were determined using the Smart Setup function. For deconvolution microscopy, z-stacks were obtained with 0.1 μm step size and without camera binning, resulting in a lateral pixel spacing of 0.114 μm. Images were deconvolved in Huygens (Scientific Volume Imaging) ver. 19.04 using the Classic Maximum Likelihood Estimation (CMLE) algorithm with built-in theoretical point spread functions for each fluorophore. All fluorescence channels were recorded at non-saturating levels and settings were kept identical between all samples used for comparisons or quantifications.

Image Analysis

The abundance the Golgi apparatus was quantified from wide-field fluorescence images of endogenous GM130, acquired in random fashion using the Tiles & Positions module of ZEN. For each condition analysed, 25 regions of interest (typically containing 1,200 – 1,800 cells in total) were randomly distributed across each well. Cells were autofocussed in the DAPI channel

and images acquired with identical illumination and camera settings between wells. Images were analysed in Volocity (PerkinElmer) ver. 6.3 using a custom-made measurement protocol to segment images into populations of objects representing nuclei, total cell area, and Golgi. To quantify changes in Golgi abundance, the average fluorescence intensity of GM130-positive structures contained inside the total cell area population was measured for all images, and the average intensity reported for each treatment group.

Acknowledgements

We thank the Bioimaging core facility (KAM) and the proteomics core facility at the Institute of Medical Biology (UiT – The Arctic University of Norway) for the use of instrumentation and expert assistance. This work was funded by grants from the FRIBIOMED (grant number 214448) and the TOPPFORSK (grant number 249884) programs of the Research Council of Norway to T.J.

References

Birgisdottir, A. B., Lamark, T. & Johansen, T. 2013. The LIR motif - crucial for selective autophagy. *J Cell Sci,* 126**,** 3237-47.

Blanc, M., David, F., Abrami, L., Migliozzi, D., Armand, F., Bürgi, J. & Van Der Goot, F. 2015. SwissPalm: Protein Palmitoylation database [version 1; peer review: 3 approved]. *F1000Research,* 4.

Campadelli, G., Brandimarti, R., Di Lazzaro, C., Ward, P. L., Roizman, B. & Torrisi, M. R. 1993. Fragmentation and dispersal of Golgi proteins and redistribution of glycoproteins and glycolipids processed through the Golgi apparatus after infection with herpes simplex virus 1. *Proceedings of the National Academy of Sciences,* 90**,** 2798.

Dascher, C. & Balch, W. E. 1994. Dominant inhibitory mutants of ARF1 block endoplasmic reticulum to Golgi transport and trigger disassembly of the Golgi apparatus. *Journal of Biological Chemistry,* 269**,** 1437-48.

Dikic, I. & Elazar, Z. 2018. Mechanism and medical implications of mammalian autophagy. *Nat Rev Mol Cell Biol,* 19**,** 349-364.

Ernst, A. M., Syed, S. A., Zaki, O., Bottanelli, F., Zheng, H., Hacke, M., Xi, Z., Rivera-Molina, F., Graham, M., Rebane, A. A., Bjorkholm, P., Baddeley, D., Toomre, D., Pincet, F. & Rothman, J. E. 2018a. S-Palmitoylation Sorts Membrane Cargo for Anterograde Transport in the Golgi. *Dev Cell,* 47**,** 479-493.e7.

Ernst, A. M., Syed, S. A., Zaki, O., Bottanelli, F., Zheng, H., Hacke, M., Xi, Z., Rivera-Molina, F., Graham, M., Rebane, A. A., Björkholm, P., Baddeley, D., Toomre, D., Pincet, F. & Rothman, J. E. 2018b. S-Palmitoylation Sorts Membrane Cargo for Anterograde Transport in the Golgi. *Developmental Cell,* 47**,** 479-493.e7.

Farquhar, M. G. 1985. Progress in Unraveling Pathways of Golgi Traffic. *Annual Review of Cell Biology,* 1**,** 447-488.

Feng, Y., He, D., Yao, Z. & Klionsky, D. J. 2014. The machinery of macroautophagy. *Cell Research,* 24**,** 24-41.

Fukata, Y. & Fukata, M. 2010. Protein palmitoylation in neuronal development and synaptic plasticity. *Nature Reviews Neuroscience,* 11**,** 161.

Gonatas, N. K., Stieber, A. & Gonatas, J. O. 2006. Fragmentation of the Golgi apparatus in neurodegenerative diseases and cell death. *J Neurol Sci,* 246**,** 21-30.

Hubner, C. A. & Dikic, I. 2019. ER-phagy and human diseases. *Cell Death Differ*.

Johansen, T. & Lamark, T. 2011. Selective autophagy mediated by autophagic adapter proteins. *Autophagy,* 7**,** 279-296.

Johansen, T. & Lamark, T. 2019a. Selective Autophagy: ATG8 Family Proteins, LIR Motifs and Cargo Receptors. *J Mol Biol*.

Johansen, T. & Lamark, T. 2019b. Selective Autophagy: ATG8 Family Proteins, LIR Motifs and Cargo Receptors. *Journal of Molecular Biology*.

Kim, J. H., Li, H. & Stallcup, M. R. 2003. CoCoA, a nuclear receptor coactivator which acts through an N-terminal activation domain of p160 coactivators. *Mol Cell,* 12**,** 1537-49.

Kirkin, V. & Rogov, V. V. 2019a. A Diversity of Selective Autophagy Receptors Determines the Specificity of the Autophagy Pathway. *Molecular Cell,* 76**,** 268-285.

Kirkin, V. & Rogov, V. V. 2019b. A Diversity of Selective Autophagy Receptors Determines the Specificity of the Autophagy Pathway. *Mol Cell,* 76**,** 268-285.

Kuma, A., Hatano, M., Matsui, M., Yamamoto, A., Nakaya, H., Yoshimori, T., Ohsumi, Y., Tokuhisa, T. & Mizushima, N. 2004. The role of autophagy during the early neonatal starvation period. *Nature,* 432**,** 1032-6.

Labun, K., Montague, T. G., Krause, M., Torres cleuren, Y. N., Tjeldnes, H. & Valen, E. 2019. CHOPCHOP v3: expanding the CRISPR web toolbox beyond genome editing. *Nucleic Acids Research,* 47**,** W171-W174.

Lemonidis, K., Macleod, R., Baillie, G. S. & Chamberlain, L. H. 2017. Peptide array-based screening reveals a large number of proteins interacting with the ankyrin-repeat domain of the zDHHC17 S-acyltransferase. *Journal of Biological Chemistry,* 292**,** 17190-17202.

Lemonidis, K., Sanchez-Perez, M. C. & Chamberlain, L. H. 2015. Identification of a Novel Sequence Motif Recognized by the Ankyrin Repeat Domain of zDHHC17/13 S-Acyltransferases. *Journal of Biological Chemistry,* 290**,** 21939-21950.

Linder, M. E. & Deschenes, R. J. 2007. Palmitoylation: policing protein stability and traffic. *Nature Reviews Molecular Cell Biology,* 8**,** 74.

Lystad, A. H. & Simonsen, A. 2019. Mechanisms and Pathophysiological Roles of the ATG8 Conjugation Machinery. *Cells,* 8**,** 973.

Maeda, S., Otomo, C. & Otomo, T. 2019. The autophagic membrane tether ATG2A transfers lipids between membranes. *Elife,* 8.

Marshall, R. S., Hua, Z., Mali, S., Mcloughlin, F. & Vierstra, R. D. 2019. ATG8-Binding UIM Proteins Define a New Class of Autophagy Adaptors and Receptors. *Cell*.

Morriswood, B., Ryzhakov, G., Puri, C., Arden, S. D., Roberts, R., Dendrou, C., Kendrick-Jones, J. & Buss, F. 2007. T6BP and NDP52 are myosin VI binding partners with potential roles in cytokine signalling and cell adhesion. *J Cell Sci,* 120**,** 2574-85.

Nassif, M., Matus, S., Castillo, K. & Hetz, C. 2010. Amyotrophic Lateral Sclerosis Pathogenesis: A Journey Through the Secretory Pathway. *Antioxidants & Redox Signaling,* 13**,** 1955-1989.

Ohno, Y., Kihara, A., Sano, T. & Igarashi, Y. 2006. Intracellular localization and tissue-specific distribution of human and yeast DHHC cysteine-rich domain-containing proteins. *Biochimica et Biophysica Acta (BBA) - Molecular and Cell Biology of Lipids,* 1761**,** 474-483.

Ohsumi, Y. 2014. Historical landmarks of autophagy research. *Cell Res,* 24**,** 9-23.

Oku, M., Tanakura, S., Uemura, A., Sohda, M., Misumi, Y., Taniguchi, M., Wakabayashi, S. & Yoshida, H. 2011. Novel Cis-acting Element GASE Regulates Transcriptional Induction by the Golgi Stress Response. *Cell Structure and Function,* 36**,** 1-12.

Osawa, T., Kotani, T., Kawaoka, T., Hirata, E., Suzuki, K., Nakatogawa, H., Ohsumi, Y. & Noda, N. N. 2019. Atg2 mediates direct lipid transfer between membranes for autophagosome formation. *Nat Struct Mol Biol,* 26**,** 281-288.

Pankiv, S., Clausen, T. H., Lamark, T., Brech, A., Bruun, J. A., Outzen, H., Overvatn, A., Bjorkoy, G. & Johansen, T. 2007. p62/SQSTM1 binds directly to Atg8/LC3 to facilitate degradation of ubiquitinated protein aggregates by autophagy. *J Biol Chem,* 282**,** 24131-45.

Rogov, V., Dötsch, V., Johansen, T. & Kirkin, V. 2014. Interactions between Autophagy Receptors and Ubiquitin-like Proteins Form the Molecular Basis for Selective Autophagy. *Molecular Cell,* 53**,** 167-178.

Sanders, S. S., Hou, J., Sutton, L. M., Garside, V. C., Mui, K. K. N., Singaraja, R. R., Hayden, M. R. & Hoodless, P. A. 2015. Huntingtin interacting proteins 14 and 14-like are required for chorioallantoic fusion during early placental development. *Developmental Biology,* 397**,** 257-266.

Sasaki, K. & Yoshida, H. 2015. Organelle autoregulation—stress responses in the ER, Golgi, mitochondria and lysosome. *The Journal of Biochemistry,* 157**,** 185-195.

Takahashi, K., Inuzuka, M. & Ingi, T. 2004. Cellular signaling mediated by calphoglin-induced activation of IPP and PGM. *Biochemical and Biophysical Research Communications,* 325**,** 203-214.

Takahashi, Y., Meyerkord, C. L., Hori, T., Runkle, K., Fox, T. E., Kester, M., Loughran, T. P. & Wang, H.-G. 2011. Bif-1 regulates Atg9 trafficking by mediating the fission of Golgi membranes during autophagy. *Autophagy,* 7**,** 61-73.

Tang, C., Iwahara, J. & Clore, G. M. 2006. Visualization of transient encounter complexes in protein–protein association. *Nature,* 444**,** 383-386.

Taniguchi, M., Nadanaka, S., Tanakura, S., Sawaguchi, S., Midori, S., Kawai, Y., Yamaguchi, S., Shimada, Y., Nakamura, Y., Matsumura, Y., Fujita, N., Araki, N., Yamamoto, M., Oku, M., Wakabayashi, S., Kitagawa, H. & Yoshida, H. 2015. TFE3 Is a bHLH-ZIP-type Transcription Factor that Regulates the Mammalian Golgi Stress Response. *Cell Structure and Function,* 40**,** 13-30.

Taniguchi, M. & Yoshida, H. 2017. TFE3, HSP47, and CREB3 Pathways of the Mammalian Golgi Stress Response. *Cell Structure and Function,* 42**,** 27-36.

Turco, E., Fracchiolla, D. & Martens, S. 2019. Recruitment and Activation of the ULK1/Atg1 Kinase Complex in Selective Autophagy. *Journal of Molecular Biology*.

Valverde, D. P., Yu, S., Boggavarapu, V., Kumar, N., Lees, J. A., Walz, T., Reinisch, K. M. & Melia, T. J. 2019. ATG2 transports lipids to promote autophagosome biogenesis. *J Cell Biol,* 218**,** 1787-1798.

Verardi, R., Kim, J.-S., Ghirlando, R. & Banerjee, A. 2017. Structural Basis for Substrate Recognition by the Ankyrin Repeat Domain of Human DHHC17 Palmitoyltransferase. *Structure,* 25**,** 1337-1347.e6.

Wilkinson, S. 2019a. Emerging Principles of Selective ER Autophagy. *Journal of Molecular Biology*.

Wilkinson, S. 2019b. ER-phagy: shaping up and de-stressing the endoplasmic reticulum. *Febs j*.

Wilson, B. S., Nuoffer, C., Meinkoth, J. L., Mccaffery, M., Feramisco, J. R., Balch, W. E. & Farquhar, M. G. 1994. A Rab1 mutant affecting guanine nucleotide exchange promotes disassembly of the Golgi apparatus. *The Journal of Cell Biology,* 125**,** 557.

Yu, L., Chen, Y. & Tooze, S. A. 2018. Autophagy pathway: Cellular and molecular mechanisms. *Autophagy,* 14**,** 207-215.

Zaffagnini, G. & Martens, S. 2016. Mechanisms of Selective Autophagy. *Journal of Molecular Biology,* 428**,** 1714-1724.

FIGURE LEGENDS

Figure 1. CALCOCO1 interacts with ZDHHC17 via zDABM motif. (A) Volcano plot showing Golgi and ER localized proteins identified in the CALCOCO1 interactome screen. Three independent immunoprecipitations and MS analyses were conducted with EGFP-CALCOCO1 as bait. (**B**) HeLa CALCOCO1 KO cells were transiently co-transfected with Myc-ZDHHC17 and EGFP-CALCOCO1 cultured in full media and immunostained with anti-GM130 antibody. Scale bars represent 10 µm. (**C**) GST, GST-ZDHHC17 or GST-ZDHHC17(N100A/W130A) were used in pull down against in vitro translated Myc-CALCOCO1 or Myc-CALCOCO1-mutzDABM (mutzDABM, ZDHHC-AR-binding motif mutant). (**D**) Domain architecture of human CALCOCO1 showing the location of ZDABM motif relative to other domains. (**E**) GST, GST-ZDHHC17 or GST-ZDHHC17(N100A/W130A) were used in pull down against in vitro translated Myc-TAX1BP1 or Myc-TAX1BP1-ΔzDABM (ΔzDABM, ZDHHC-AR-binding motif deleted).

Figure 2. Mutation of zDABM motif of CALCOCO1 abolishes Golgi localization. **(A)** HeLa cells were co-transfected with Myc-ZDHHC17 and either EGFP-CALCOCO1 or EGFP-CALCOCO1 1-513 (lacking the zDABM motif), grown in full media and imaged by confocal microscopy. Bars represent 5 µm and 1 µm (insets). **(B)** HeLa cells were co-transfected with Myc-ZDHHC13 and either EGFP-CALCOCO1 or EGFP-CALCOCO1 1-513 (lacking the zDABM motif), grown in full media and imaged by confocal microscopy. Bars represent 5 µm and 1 µm (insets). **(C)** HeLa WT and HeLa-CALCOCO1 KO cells were transfected with EGFP-ZDHHC17 and immunostained with anti-GABARAP antibody.

Figure 3. CALCOCO1 co-localizes with Golgi fragments in autophagosomes. (A) HeLa WT cells transfected with EGFP-ZDHHC17 and 24 hours post-transfection they were left either untreated or starved (HBBS) for 4 hr with bafilomycin A_1 (BAFA1) treatment, then stained for endogenous TMEM165. **(B)** HeLa WT cells were co-transfected with Myc-ZDHHC17 and EGFP-CALCOCO1 and 24 hr post transfection, were left either untreated or starved for 4 hr with bafilomycin A_1 treatment and then immunostained for endogenous LC3B. **(C)** HeLa WT and HeLa-CALCOCO1 KO cells were transfected with EGFP-ZDHHC17 and 24 hr post transfection, they were either left untreated or they were starved for 6 hrs. The number of cells with fragmented Golgi phenotype was manually counted and weighted against total number of cells.

Figure 4. Starvation induces degradation of Golgi by autophagy. (A) MEF parental and Atg5 KO cells were left untreated or treated with either bafilomycin A_1 (Baf) for 6hrs, MG132 for 6hrs or starved for 6 hr with or without bafilomycin A_1. Cell lysates were analysed by immunoblotting with the indicated antibodies**. (B)** HeLa parental or ATG7 KO cells were treated as in (A) and the cell lysates analysed by immunoblotting with the indicated antibodies. **(C)** HeLa cells stably expressing inducible EGFP-ZDHHC17 were left uninduced or induced for 48 hrs and then treated as in (A). Cell lysate were analysed by immunoblotting with the indicated antibodies.

Figure 5. CALCOCO1 mediates degradation of Golgi by autophagy. (A) HeLa parental and CALCOCO1 KO cells were either left untreated or treated with bafilomycin A_1 (Baf) or starved with or without bafilomycin A_1 for the indicated time. The lysates were analysed by western blotting with the indicated antibodies. **(B)** HeLa-CALCOCO1 KO cells reconstituted with inducible EGFP-CALCOCO1 were left uninduced or induced for 48 hrs and then left untreated or treated with either bafilomycin A_1 for 6hrs, MG132 for 6hrs or starved (HBSS) for 6 hr with or without bafilomycin A_1. Cell lysates were analysed by immunoblotting with the indicated antibodies. **(C)** HeLa-CALCOCO1 KO cells reconstituted with inducible expression of EGFP-CALCOCO1 were induced for 24 hr and then left untreated or treated with bafilomycin A_1 or starved with or without bafilomycin A_1 for the indicated times. The abundance of the Golgi apparatus was then quantified from wide-field fluorescence images with immunostaining of endogenous GM130, acquired in random fashion. For each condition analysed, 25 regions of interest (typically containing 1,200 – 1,800 cells in total) were randomly chosen across each well and the average fluorescence intensity of GM130-positive structures contained inside the total cell area population of chosen regions were measured. Images were analysed in Volocity software using custom made measurement protocol to segment images into populations of objects representing nuclei, total cell area, and Golgi. **(D)** Reconstituted cells as in C were left uninduced or were induced for 24 hr and then left untreated or treated with bafilomycin A_1 or starved with or without bafilomycin A_1 for the indicated times. Cell lysates were analysed by immunoblotting using the indicated anti-bodies. (**E**) HeLa-CALCOCO1 KO cells reconstituted with EGFP-CALCOCO1-mutLIRΔUIR were left uninduced or were induced for 24 hr and then left either untreated or treated as indicated. Cell lysates were analysed by immunoblotting using the indicated antibodies. **(F)** A model of the CALCOCO1 bridging the gap between the Golgi and autophagic membrane.

Figure 1

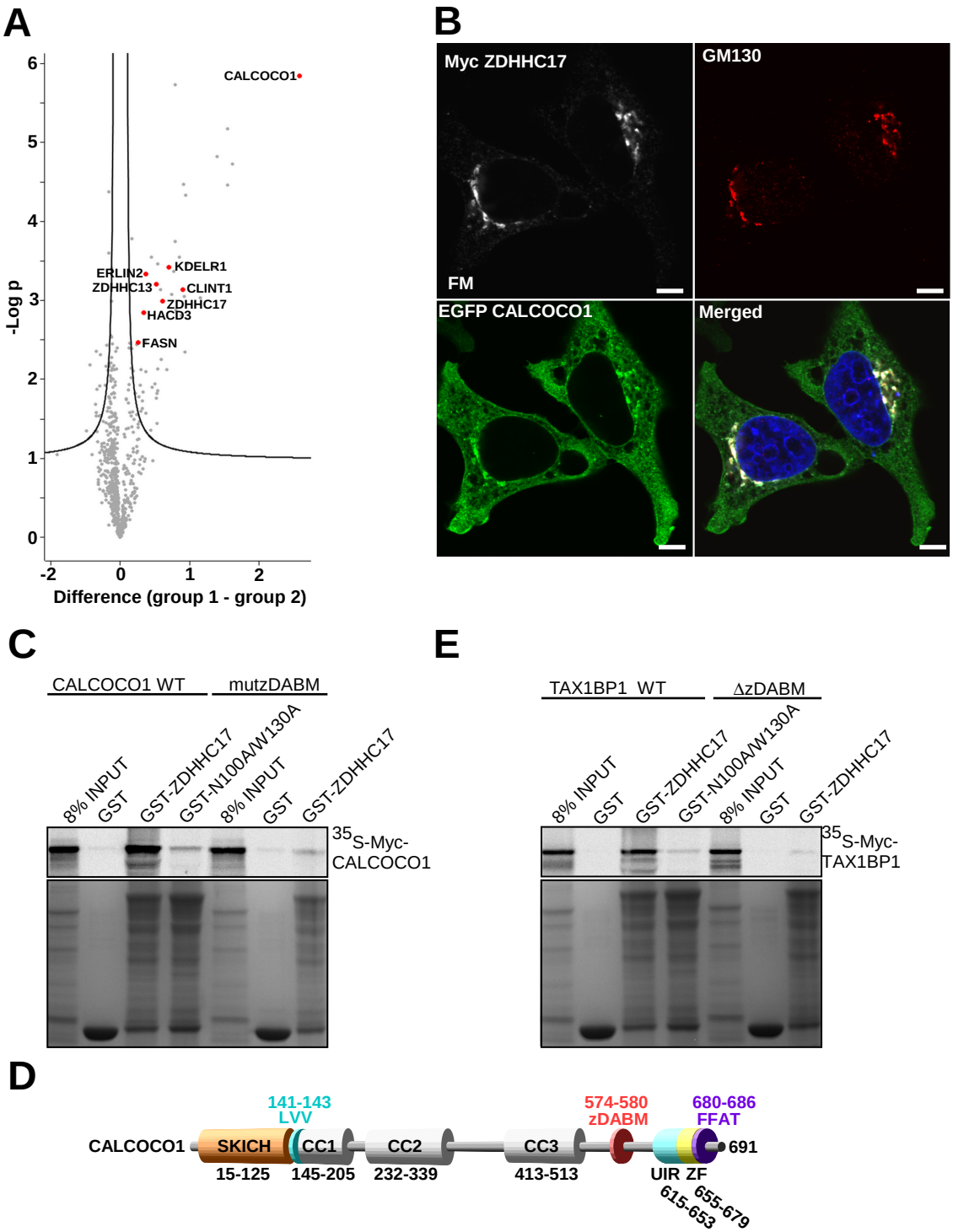
A
CALCOCO1
KDELR1
ERLIN2
ZDHHC13
CLINT1
ZDHHC17
HACD3
FASN
-Log p
Difference (group 1 - group 2)
B
Myc ZDHHC17
GM130
FM
EGFP CALCOCO1
Merged
C
CALCOCO1 WT
mutzDABM
8% INPUT
GST
GST-ZDHHC17
GST-N100A/W130A
35S-Myc-CALCOCO1
E
TAX1BP1 WT
ΔzDABM
35S-Myc-TAX1BP1
D
CALCOCO1
SKICH
CC1
CC2
CC3
691
141-143 LVV
574-580 zDABM
680-686 FFAT
15-125
145-205
232-339
413-513
UIR
ZF
615-653
655-679

Figure 2

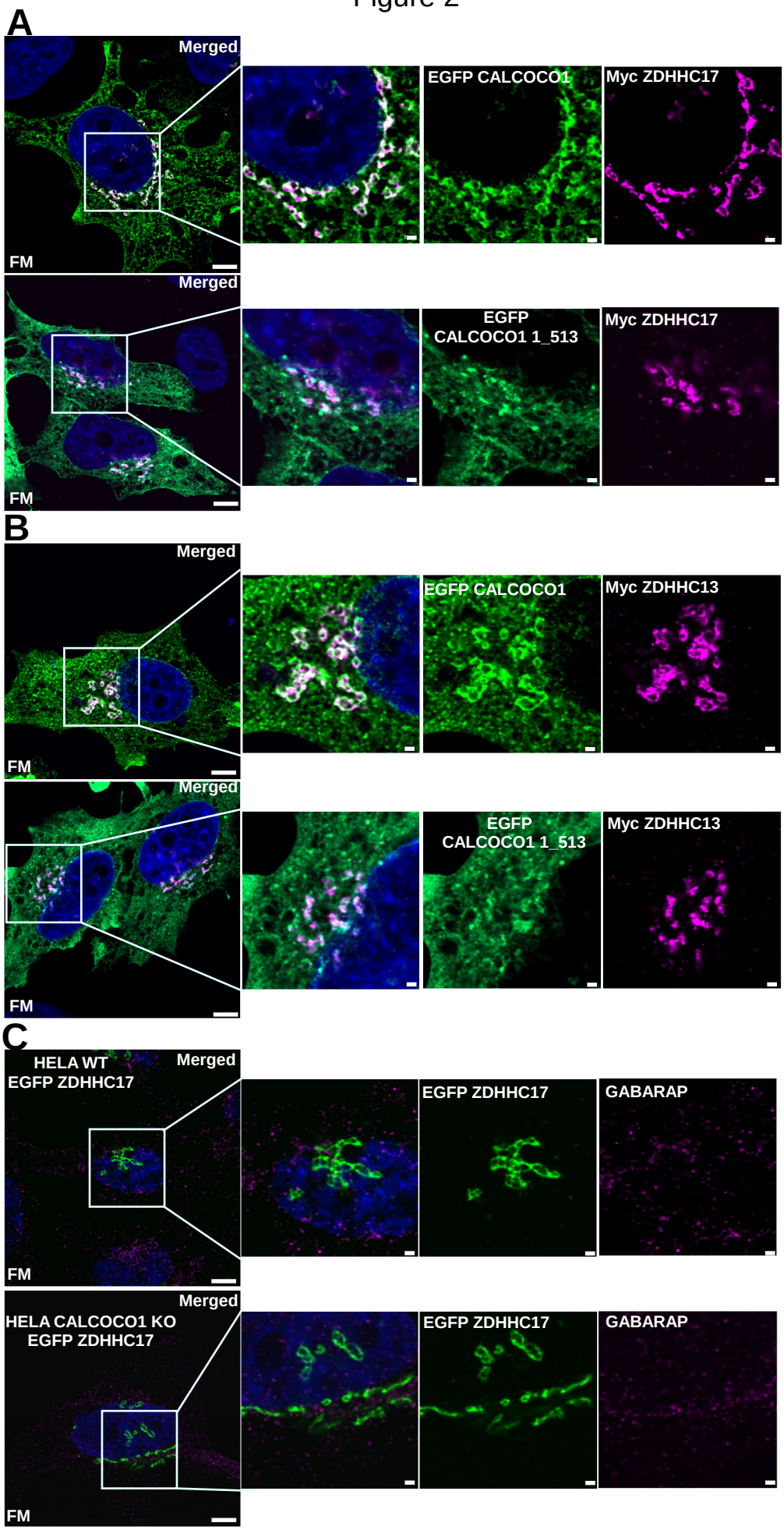
A
Merged
FM
EGFP CALCOCO1
Myc ZDHHC17
Merged
FM
EGFP
CALCOCO1 1_513
Myc ZDHHC17
B
Merged
FM
EGFP CALCOCO1
Myc ZDHHC13
Merged
FM
EGFP
CALCOCO1 1_513
Myc ZDHHC13
C
HELA WT
EGFP ZDHHC17
Merged
FM
EGFP ZDHHC17
GABARAP
Merged
HELA CALCOCO1 KO
EGFP ZDHHC17
FM
EGFP ZDHHC17
GABARAP

Figure 3

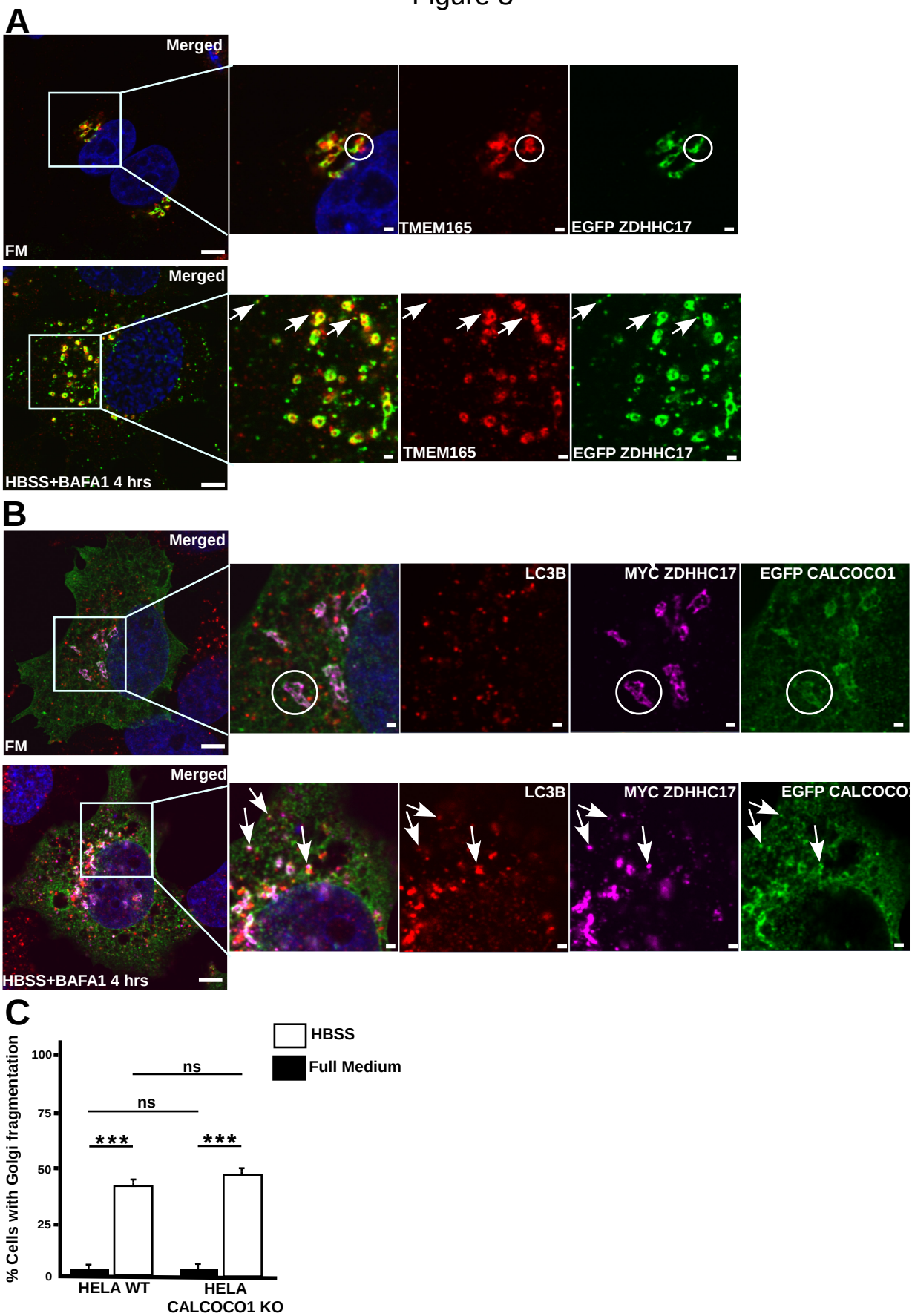
A
Merged
FM
TMEM165
EGFP ZDHHC17
Merged
HBSS+BAFA1 4 hrs
TMEM165
EGFP ZDHHC17
B
Merged
FM
LC3B
MYC ZDHHC17
EGFP CALCOCO1
Merged
HBSS+BAFA1 4 hrs
LC3B
MYC ZDHHC17
EGFP CALCOCO
C
HBSS
Full Medium
% Cells with Golgi fragmentation
100
75
50
25
0
ns
ns
***
***
HELA WT
HELA CALCOCO1 KO

Figure 4

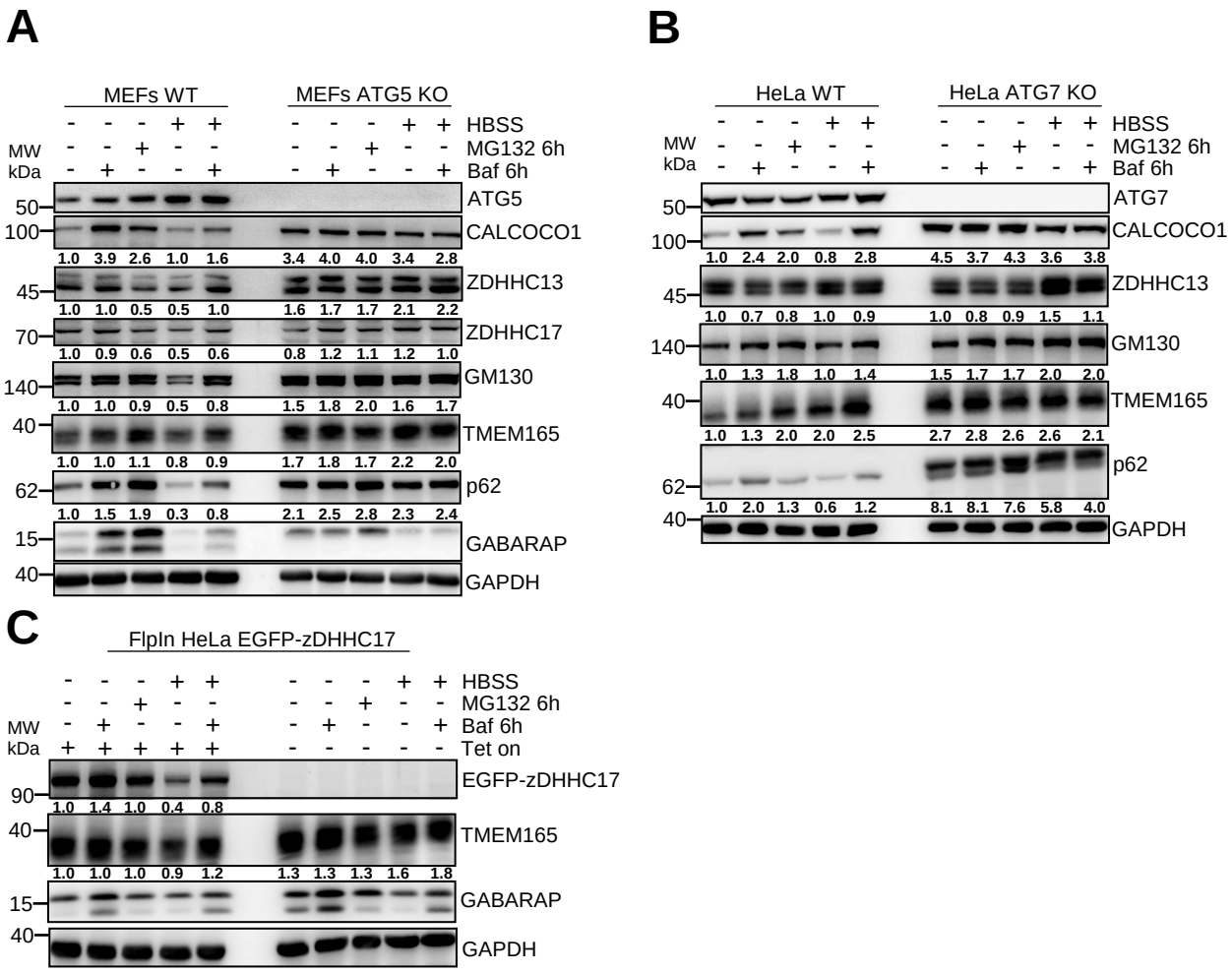
A
MEFs WT
MEFs ATG5 KO
HBSS
MG132 6h
Baf 6h
MW
kDa
ATG5
CALCOCO1
ZDHHC13
ZDHHC17
GM130
TMEM165
p62
GABARAP
GAPDH
B
HeLa WT
HeLa ATG7 KO
ATG7
C
FlpIn HeLa EGFP-zDHHC17
Tet on
EGFP-zDHHC17

Figure 5

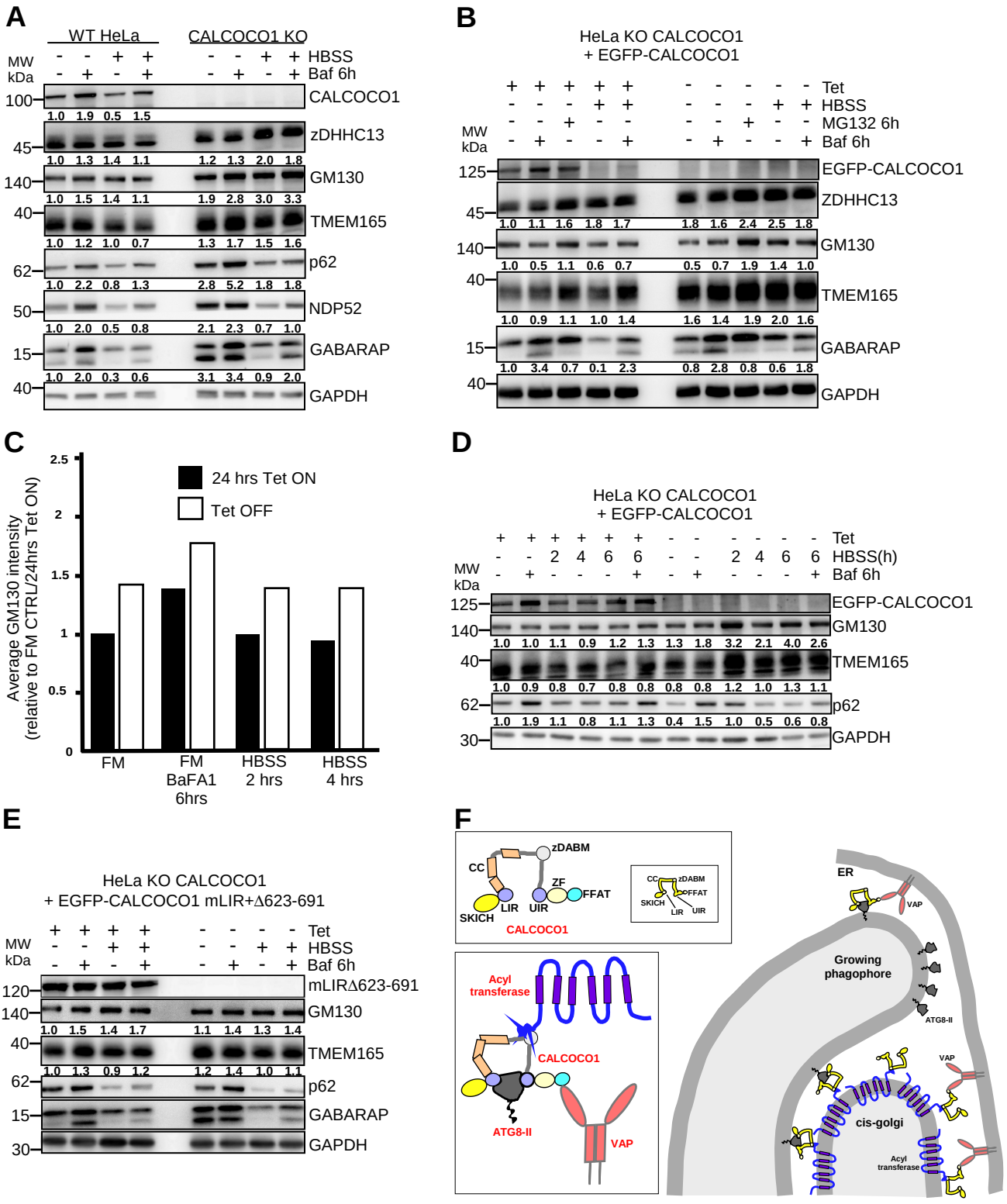
A
WT HeLa
CALCOCO1 KO
MW kDa
HBSS
Baf 6h
CALCOCO1
zDHHC13
GM130
TMEM165
p62
NDP52
GABARAP
GAPDH
B
HeLa KO CALCOCO1
+ EGFP-CALCOCO1
Tet
HBSS
MG132 6h
Baf 6h
EGFP-CALCOCO1
ZDHHC13
GM130
TMEM165
GABARAP
GAPDH
C
Average GM130 intensity (relative to FM CTRL/24hrs Tet ON)
24 hrs Tet ON
Tet OFF
FM
FM BaFA1 6hrs
HBSS 2 hrs
HBSS 4 hrs
D
HeLa KO CALCOCO1
+ EGFP-CALCOCO1
Tet
HBSS(h)
Baf 6h
EGFP-CALCOCO1
GM130
TMEM165
p62
GAPDH
E
HeLa KO CALCOCO1
+ EGFP-CALCOCO1 mLIR+Δ623-691
Tet
HBSS
Baf 6h
mLIRΔ623-691
GM130
TMEM165
p62
GABARAP
GAPDH
F
zDABM
CC
ZF
FFAT
SKICH
LIR
UIR
CALCOCO1
Acyl transferase
ATG8-II
VAP
ER
Growing phagophore
cis-golgi

Appendix Table S1: Interactors of CALCOCO1

Uniprot Accession	Gene	Description	Coverage[%]	# Peptides
Q9P1Z2	CALCOCO1	Calcium-binding and coiled-coil domain-containing protein 1	70	53
A0A087WVQ6	CLTC	Clathrin heavy chain OS=Homo sapiens GN=CLTC PE=1 SV=1	66	93
P10809	HSPD1	60 kDa heat shock protein, mitochondrial	73	39
Q5T9A4	ATAD3B	ATPase family AAA domain-containing protein 3B	66	35
P63010	AP2B1	AP-2 complex subunit beta OS=Homo sapiens	64	50
O95782	AP2A1	AP-2 complex subunit alpha-1	57	45
H0Y2W2	ATAD3A	ATPase family AAA domain-containing protein 3A	52	28
O94973	AP2A2	AP-2 complex subunit alpha-2	53	35
Q9NVV4	MTPAP	Poly(A) RNA polymerase, mitochondrial	46	22
P04350	TUBB4A	Tubulin beta-4A chain OS=Homo sapiens	62	19
E9PFW3	AP2M1	AP-2 complex subunit mu	53	21
Q10567	AP1B1	AP-1 complex subunit beta-1	26	24

O00443	PIK3C2A	Phosphatidylinositol 4-phosphate 3-kinase C2 domain-containing subunit alpha	20	29
Q16891	IMMT	MICOS complex subunit MIC60	56	33
C9J406	IMMT	MICOS complex subunit MIC60	50	28
Q14677	CLINT1	Clathrin interactor 1	31	17
P13646	KRT13	Keratin, type I cytoskeletal 13	15	9
Q9ULM3	YEATS2	YEATS domain-containing protein 2	17	18
P28288	ABCD3	ATP-binding cassette sub-family D member 3	30	16
Q96L58	B3GALT6	Beta-1,3-galactosyltransferase 6	36	11
P46060	RANGAP1	Ran GTPase-activating protein 1	29	12
Q9UBC2	EPS15L1	Epidermal growth factor receptor substrate 15-like 1	15	10
C9JRZ6	CHCHD3	MICOS complex subunit OS=Homo sapiens	31	8
M0QYZ2	AP2S1	AP-2 complex subunit sigma OS=Homo sapiens	32	5
P42704	LRPPRC	Leucine-rich PPR motif-containing protein, mitochondrial	12	13

Q16478	GRIK5	Glutamate receptor ionotropic, kainate 5	1	1
Q92830	KAT2A	Histone acetyltransferase KAT2A	14	10
Q9NS73	MBIP	MAP3K12-binding inhibitory protein 1	28	8
Q7LGA3	HS2ST1	Heparan sulfate 2-O-sulfotransferase 1	18	6
P24390	KDELR1	ER lumen protein-retaining receptor 1	14	2
Q8IUH5	ZDHHC17	Palmitoyltransferase ZDHHC17	10	5
Q9Y512	SAMM50	Sorting and assembly machinery component 50 homolog SV=3	14	5
Q12931	TRAP1	Heat shock protein 75 kDa, mitochondrial	3	2
Q9UJZ1	STOML2	Stomatin-like protein 2, mitochondrial	19	5
F8WF69	CLTA	Clathrin light chain A OS=Homo sapiens	10	3
J3KN01	MLLT4	Afadin OS=Homo sapiens	1	1
Q8IUH4	ZDHHC13	Palmitoyltransferase ZDHHC13	6	3
Q6NXT4	SLC30A6	Zinc transporter 6	12	4
P09497	CLTB	Clathrin light chain B	8	2

Q8TAD4	SLC30A5	Zinc transporter 5	6	3
Q9NQ32	C11orf16	Uncharacterized protein C11orf16	1	1
Q8NDV7	TNRC6A	Trinucleotide repeat-containing gene 6A protein	2	4
Q14145	KEAP1	Kelch-like ECH-associated protein 1	5	3
Q96ES7	SGF29	SAGA-associated factor 29	13	3
O14965	AURKA	Aurora kinase A	7	2
Q9P0L0	VAPA	Vesicle-associated membrane protein-associated protein A SV=3	10	2
Q8TC07	TBC1D15	TBC1 domain family member 15	4	3
H3BVG0	NUP93	Nuclear pore complex protein Nup93	3	2
Q8TB61	SLC35B2	Adenosine 3'-phospho 5'-phosphosulfate transporter 1	8	3
Q53H12	AGK	Acylglycerol kinase, mitochondrial	6	1
Q9P2E5	CHPF2	Chondroitin sulfate glucuronyltransferase	3	2
O75528	TADA3	Transcriptional adapter 3	7	2
Q8N0Z8	PUSL1	tRNA pseudouridine synthase-like 1	5	1

A0A024R0Y4	TADA2L	Transcriptional adapter 2-alpha	4	1
Q8IYS2	KIAA2013	Uncharacterized protein KIAA2013	4	2
Q15382	RHEB	GTP-binding protein Rheb	8	2
P02794	FTH1	Ferritin heavy chain	10	2
Q9HC07	TMEM165	Transmembrane protein 165	13	2
P49792	RANBP2	E3 SUMO-protein ligase RanBP2	1	2
P32780	GTF2H1	General transcription factor IIH subunit 1	2	1
Q53GS7	GLE1	Nucleoporin GLE1	2	1